Controller Design of a Robotic Orthosis using Sinusoidal-Input Describing Function Model

CHIN KAR MUN

THESIS SUBMITTED TO
THE UNIVERSITY OF NOTTINGHAM FOR THE
DEGREE OF DOCTOR OF PHILOSOPHY

JUNE 2020

Abstract

Stroke is one of top leading causes of death in the world and it happens to more than 15 million people yearly. According to the National Stroke Association of Malaysia (NASAM), stroke is the third leading cause of death in Malaysia with around 40,000 cases reported annually. Forty percent of stroke survivors suffer from movement impairments after stroke. My grandfather was one of the victims and he was unable to attend any rehabilitation sessions due to several reasons. Hence, he lost the golden time to regain his movement and freedom. There are a lot of similar cases that happen daily in Malaysia. Besides, as the number of stroke patients increases yearly, the need for physiotherapists or rehabilitation machines equally increases. Hence, a low-cost clinical rehabilitation device is essential to provide assistance for an effective rehabilitation program and substitute the conventional method, as well as to reduce the burden of physiotherapists. In future, the proposed rehabilitation device would benefit not only stroke patients, but any patients who lost their normal walking ability including post-accident patients or those who suffer from spinal cord injury. The rehabilitation device aims to provide training assistance to patients not only in rehabilitation centres but also at home for daily training.

The robotic orthosis is planned to be configured based on moving joint angles of human lower extremities. In the first stage of this research, angle-time characteristics for knee and hip swinging motion are utilised as a sagittal motion reference for the rehabilitation devices. The aim of following a proper gait cycle during rehabilitation training is to train patients to perform standing and swinging phases at proper timing and simultaneously provide the correct position reference to the patient during rehabilitation training. This can prevent patients from walking abnormally with an asymmetric gait cycle along or after the rehabilitation program. Besides, various limitations and the bulky structure of other rehabilitation devices lead to the design of the two-link lower limb rehabilitation device.

This project aims to develop an assistive robotic rehabilitation device that generates a human gait trajectory for hemiplegic stroke patient gait rehabilitation in future. The

shortcomings of other control applications due to environmental conditions and disturbances lead to the implementation of the describing function approach in the development of the devices. A sinusoidal-input describing function (SIDF) approach was implemented to linearize the nonlinear robotic orthosis with linear transfer function. The reason for utilising the SIDF approach is due to the nonlinear actual plant model with the present of load torque disturbances, discontinuous nonlinearities such as saturation and backlash, and also multivariable in the system. The nonlinear properties of the plant were proven in the preliminary stage of the research. A conventional controller, PID control combined with position and trajectory inputs were also applied to the system in the early stage of research. However, the experimental results were not satisfying. Finally, the SIDF approach was chosen to linearize the nonlinear system. Hence, generating a controller is much easier with a linear model of the nonlinear system.

A SIDF approach was implemented to generate a controller for the multivariable, nonlinear closed loop system. Firstly, the SIDF approach enables the determination of the linear function of the nonlinear model known as the SIDF model. By utilising the linear model to mimic the behaviour of the nonlinear rehabilitation system, the controller for the nonlinear plant was able to be generated. In this research a controller based on linear control theory technique was used. The MATLAB library was used to design the lead-lag controller for the rehabilitation device.

Various simulations such as step responses, tracking and decoupling of both links were performed on the generated controller with the nonlinear model to study the capability of the controller. Besides that, real life experiment testing was carried out to validate the feasibility of the controller designed via the SIDF approach. Simulation and experimental results were obtained, compared, and discussed. The highly accurate responses gained from experimental setup showed the robustness of the controller generated via SIDF approach. The implementation of the SIDF approach in a rehabilitation device (vertical two-link manipulator) is a first and hence, fulfils a novelty requirement for this research.

Acknowledgement

First and foremost, I must thank my research supervisor, Dr. Ho Jee Hou who has provided countless guidance and opportunity through every step in the process of my research journey. Without his assistance and support, I would never have reached the final stage of my research. Thank you for your patience and understanding of my personal health issues and many more along these past five years. I am truly appreciative and feel glad to have been under his supervision.

Next, I would like to show my gratitude to my co-supervisors, Dr Teh Sze Hong and Dr. Ng Hoon Kiat. Thank you for the support, help and advices given along my research progress. Thanks to Dr Teh who was willing to be my co-supervisor in the middle of the research process and thanks for providing me with a new method to continue my research. Lastly, I am really grateful to able to attend an international conference with the support from my supervisor and co-supervisors.

Furthermore, I would like to express my gratitude to Dr Woo Ko Choong who always spent his time to teach me lessons of life and was always willing to send help to me during my times of hardship. Thanks for the guidance for my project as well as research assistance duty for the past few years. I have learned a lot. Last but not least, I sincerely thank him for providing a workspace in the NB03 laboratory for me to facilitate my work in the Research Building.

I also take this opportunity to express my appreciation to the Faculty of Science and Engineering (FOSE) Research Office for dealing with all my issues and their assistance in handling my graduate school documents. Special thanks to Siti Zaharatul Asyiqin Mohammed Mokhtar and Galoh Munawwarah Osman. Besides that, a great thanks to the Graduate School staff who also organized training course and programmes for postgraduate students, to help us gain knowledge and respond to our doubt. Thank you to the staff who work in the Research Building and workshop who provided support, help and instruction in fabricating all the hardware and electrical components for my research project.

Getting through the research, I would like to thank the undergraduate students who helped out and participated in certain parts of the research. They are Chong Ser Lii, Wong Theam Chun, Lo Chi Hong, Alhasan Osamah Mohammed Alabd, Loo Soon Yuen, Ong Jun Yang, Tan Xue Ming, Cheong May Xin, Aravindaakumar Krishnan, Kee Mun Yan, Naveen Natarajan and Calvin Lit Kar Yin.

Additionally, I would like to express my gratitude towards my family, especially my parents. None of this could have happened without the support from them. Thank for the mental and financial support along my research journey. Thank you for the care and unconditional love when I was feeling up and down along this long journey. Thanks to my sister and brother who supported me financially and sometimes provided encouragement for to me to keep going.

Finally, I would like to thank my soulmate, Ong Meng Chung. Thanks for everything you gave to me, your unconditional love and motivation. Thanks to my best friends in University of Nottingham Malaysia, Elynn Tan, Esther Tiong, Tan Jing Yang and Chu Xue Ying who always give me support and advices no matter what.

Thank you.

Table of Contents

List of Figures

List of Tables

List of Abbreviations

ADL	Activities of Daily Living
ARM	Advanced Reduced Instruction Set Computer Machines
BWS	Body Weight Support
CAE	Computer-Aided Engineering
CPU	Central Processing Unit
DAC	Digital to Analog
DAQ	Data Acquisition Devices
DC	Direct Current
DOF	Degree-of-Freedom
EMG	Electromyography Signal
GND	Ground
GUI	Graphical User Interface
HDPE	High-Density Polyethylene
I/O	Input or Output
IC	Integrated Circuit
LABVIEW	Laboratory Virtual Instrument Engineering Workbench
MATLAB	Matrix Laboratory
NI	National Instruments
PID	Proportional Integral Derivative
PWM	Pulse-Width Modulation
RIDF	Random-Input Describing Function
SIDF	Sinusoidal-Input Describing Function
V_{cc}	Voltage at the Common Collector

Chapter 1 Introduction

1.1 Background

1.1.1 Stroke

Stroke (cerebrovascular accidents) is a kind of brain injury which is also known as a sudden defeat of brain function. It can happen to anyone at any time and can be categorized into ischemic stroke or hemiplegic stroke. Ischemic stroke happens due to the lack of blood flow to the brain while hemiplegic stroke occurs due to the damage of blood vessels in the brain [1]. Brain cells of the affected area will begin to die within minutes due to the lack of oxygen and nutrients supplied. This eventually leads to brain damage, losses of ability in performing activities of daily living (ADL) controlled by the particular region of brain, or it may also cause sudden death. However, the impact on the stroke patient is dependent on how severely the brain was damaged. For instance, a patient following a minor stroke might face problems such as short-term weakness of arm or leg. Meanwhile, a patient who had a major stroke might result in long-term paralysis on one side of the body or lose their speaking ability [2], [3].

1.1.1.1 Statistics of Stroke in Malaysia and Worldwide

According to the statistics published by the World Health Organization (WHO), there are approximately 15 million people who suffer from stroke every year. There are one third of stroke patients in the world who passed away and another one third who suffer from permanent disability [3]. Globally, stroke is the second leading cause of death and the third leading cause of disability [4]. In Malaysia, stroke is the third leading cause of death. According to the National Stroke Association of Malaysia (NASAM), there are about 40,000 patients suffering from stroke each year. Based on the analysis of collected data, the number of stroke patients increases by six every hour [3], [5].

1.1.2.1 Stroke Survival Rates in Malaysia

Table 1 shows the stroke survival rate published by Ramsay Sime Darby Health Care. As shown in the table, there are about 40% of survivors who recover with severe impairments that affects their daily life. Most of them are likely to suffer from motor impairment such as muscle weakness, gait impairment, long-term disability, or total paralysis following a stroke. Limitation of muscle movements of face, arm and leg of one side of the body bothered around 80% of stroke victims and lead to limitation in the activity of daily living (ADL) and mobility [3], [6]. Besides that, most of the victims are not able to walk with their original speed post stroke [7]. Impairment in mobility of patients would increase the family burden. As a result, physical therapy including rehabilitation mostly emphasise on recovery of motor impairment and the interrelated functions to help the victims to regain walking ability and muscle movements [6].

Table 1 Table of stroke survival rates [3]

Recovery State	**Percentage (%)**
Completely recover	10
Recover with minor impairments	25
Recover with moderate to severe impairments with special care required	40
Require long-term care facility or nursing home	10
Die shortly after stroke	15

1.1.2 Exoskeleton and Active Orthosis

An exoskeleton is defined as “an active mechanical device that is essentially anthropomorphic in nature”. It carries the meaning of a mechanical device which can be fitted nicely to the operator and provide them with strength or facilitate their movements to complete a task that is difficult to be done by normal human such as carrying a heavy load while running or climbing stairs. Generally, the term “exoskeleton” is defined as a device that enhance the performance of the operator, while the term “active orthosis” is usually used to describe devices that assist the ambulatory movements of a person who suffers from walking disability. Figure 1 shows the example of exoskeletons: general electric’s Hardiman and HAL-5 exoskeleton and the example of active orthosis: Michigan ankle orthoses and MIT active AFO. However, nowadays, the term “exoskeleton” is also used to describe certain assistive device for lower limbs [8]. Hence, both terms are applicable to describe assistive devices for lower extremities.

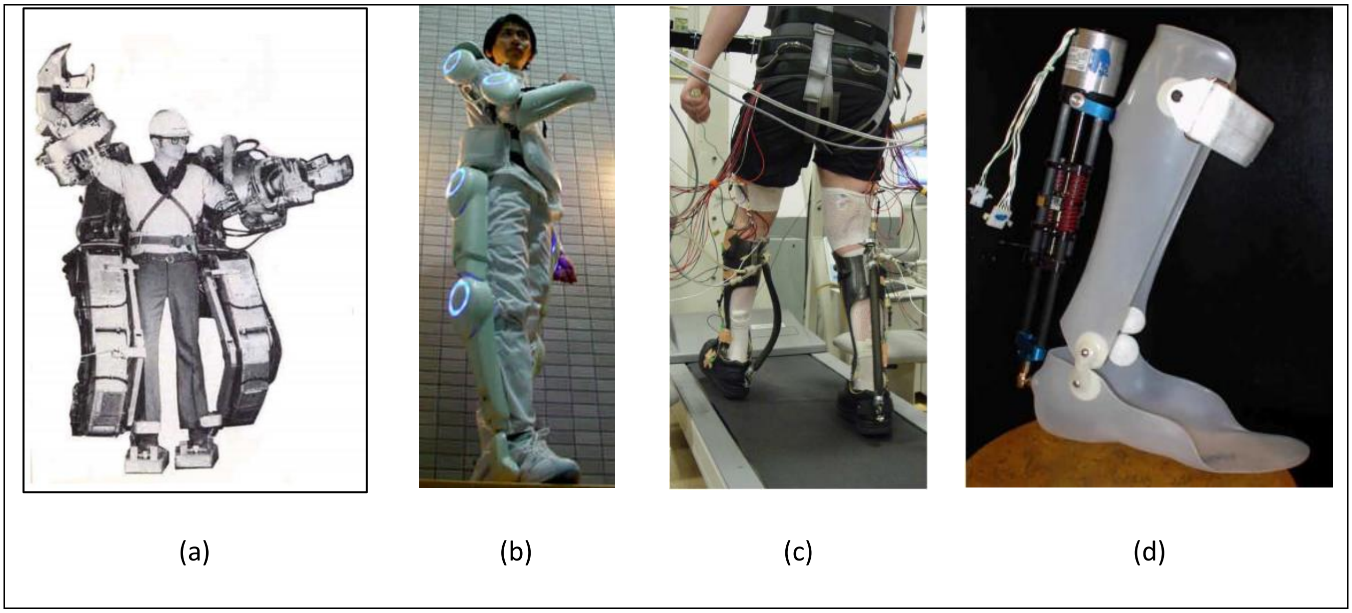

Figure 1 Exoskeleton: a) General Electric's Hardiman, b) HAL-5 exoskeleton and active orthosis: c) Michigan ankle orthoses, and d) MIT active AFO [8].

1.1.2.1 History of Exoskeleton and Robotic Orthosis

Early research on exoskeletons were mostly conceptual studies that never left a detailed record on the work done. The first recorded exoskeleton is Yagn's running aid (Figure 2(a)) developed by U.S. Patents in 1890. It was initially built to enhance the running and jumping of the Russian Army. However, there is no successful record found for this device [8], [9]. In the year of 1963, a detailed report of "powered orthopaedic supplement" was published by Zaroodny of the U.S. Army Exterior Ballistics Laboratory [10]. This pneumatic powered prototype device was aimed to perform as a load-carry exoskeleton for operators such as a soldier. However, due to some unknown difficulties faced by the researchers and funding issues, the research was later terminated [8].

After a few years, during the late 1960s, Hardiman (Human Augmentation Research and Development Investigation) [11], a full-body powered exoskeleton prototype was developed by the General Electric Research of Schenectady, New York in cooperation with Cornell University and the project was financially supported by the U.S. Office of Naval Research. Hardiman was aimed to increase an operator's performance by about 25 times. According to the record, a satisfactory result was obtained for arm-amplifying, but some problems were encountered for lower limb components and ware never resolved. In the middle of 1980s, a paper released by Jeffrey Moore introduced an exoskeleton, Pitman, with the purpose of augmenting the ability of soldiers during operations [12]. However, this paper did not provide details of practical implementation and other issues such as power supply. This project was also ended due to a failure to secure funding [8].

In the early 21st century, a DARPA exoskeleton program was established. The Exoskeleton for Human Performance Augmentation (EHPA) program aimed to increase the abilities of ground soldiers to complete tasks beyond human limitations. Three exoskeletons has been introduced over the period of the EHPA program which included the Berkeley Exoskeleton (BLEEX) (Figure 2(b)), Sarcos Exoskeleton, and MIT Exoskeleton [8], [13]. The end product of Sarcos Exoskeleton, called XOS Exoskeleton, could lift a weight of 91 kg without any human effort. This design was finally chosen by DARPA and was awarded with the name of "Iron man-like robot" as well as one of the 50 Best Inventions of 2010 by Time Magazine [14]–[16]. The famous exoskeleton named HAL, which operates with EMG-based system to enhance a wearer's bodily function, was also developed in the early 2000s by Prof. Yoshikuyi Sankai [17].

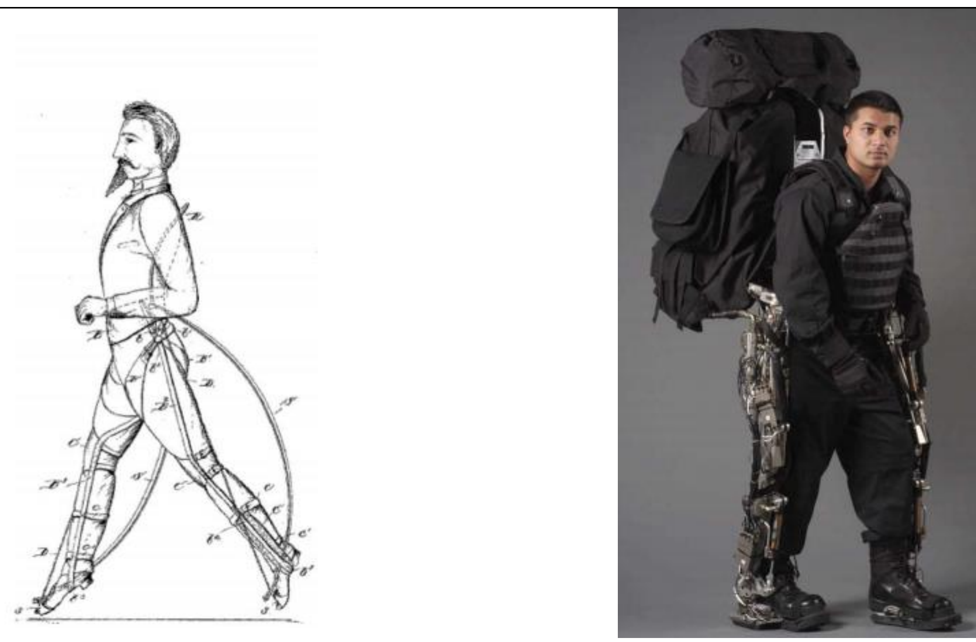

(a) (b)

Figure 2 Exoskeleton: a) Yagn's running aid develop by U.S. Patents in 1890 and b) Berkeley Exoskeleton (BLEEX) [8], [9] Apart from exoskeletons developed to enhance the full body function of humans, there were also researches done on developing active orthosis which only included the lower limb performance of a user or to provide certain active assistance. The very first lower limb active orthosis was a U.S. patent in 1930. This orthosis primarily focuses on the motion at the knee with a torsional spring connected to a crank at the hip and a set of cam and follower at the ankle joint. Following that, in 1942, the first controllable active orthosis was created with hydraulic actuators at the hip and knee joints. There was also an early invention of a lower limb passive device recorded in 1951 that utilized spring-loaded pins to lock and unlock the joint of the leg brace of the user in various gait patterns [8].

There is history recorded of lower limb exoskeleton works by the Mihailo Pupin Institute in the late 1960s until 1970s. A partial active exoskeleton was introduced and clinical experiments were done in 1970 to demonstrate the effectiveness of this device in helping patients with paraplegia to regain their walking ability [8]. Besides that, a device named Zero-Moment Point which focuses on the control of bipedal locomotion was first demonstrated in Japan in 1984. Continuous work was done on it by Prof. Vukobratovis and Devon Juricic and the concept of ZMP was finally publish in the year of 2004 [8], [18].

The University of Wisconsin had a similar research to work on lower limb robotic device since 1968. The university was actively working on an autonomous exoskeleton for paraplegia patient with a hydraulic power and pump that covers the movement of the hip, ankle, and knee. The Wisconsin exoskeleton aimed to support the ability of sitting down, standing up and walking in a slow pace for the user [8]. Since then, many other lower limb exoskeletons were developed, mostly for patients with various degrees of paralysis in lower limb to help them in mobilization or gait training [19]–[21]. Table 2 is the summarization of the discussed historical exoskeletons and active orthoses. Research contributions on exoskeleton and active orthosis provide a foundation for today's studies in rehabilitation devices.

Table 2 Main function of historical exoskeleton and active orthosis

Exoskeleton to enhance body function	
Name	**Main Function**
Yagn's running aid	Enhance running and jumping
Zaroodny powered orthopaedic supplement	load-carry exoskeleton
Hardiman	Increase an operator's performance by about 25 times
DARPA exoskeleton	Complete task that beyond human limitation
Berkeley exoskeleton (BLEEX)	Support a load of up to 75 kg while walking fast
Sarcos exoskeleton	Support heavy load, loading with one leg standing, walking on mud
MIT exoskeleton	Load carrying while walking
XOS exoskeleton (EHPA program)	Lift a weight of 91 kg without any human effort
HAL	Enhance wearer' bodily function
Active Orthosis for lower limb rehabilitation	
Name	Main Function
First lower limb orthosis (U.S. patent)	Focus on knee motion
Controllable active orthosis	Lower limb passive device
Partial active exoskeleton	Help patients regain walking ability
Zero-moment point	Control bipedal locomotion
Wisconsin exoskeleton	Support sitting down, standing up and walking in slow pace

1.1.2.2 Current Research on Exoskeleton

Based on the discussion about the history of exoskeleton and robotic orthosis as well as literature review sections, exoskeletons and active devices are mostly developed for several aims including: to magnify the ability of humans to complete certain tasks such as running and carrying loads which mostly serve military purpose; and to help immobilized users to carry out daily activities and to provide rehabilitation training for paralysed patients to regain walking ability, at the same time to reduce the burden of physiotherapists. These devices are classified into several types such as full body mobility devices, lower limb active devices, foot manipulators, devices with body support, treadmill training devices, and so on, as illustrated in Figure 3. However, some devices are even equipped with more than one design and characteristics. Detailed characterization can be found in Table 5.

(a) (b) (c) (d) (e)

Figure 3 Device classification: a) full body mobility device, b) lower limb active device, c) foot manipulator, d) device with body support, and e) treadmill training device[22]–[25]

In the past decade, countless lower limb robotic devices are established for the purpose of helping paralysed patients in their daily lives. Some of the devices were developed to ease patients in their daily activities such as standing and walking, and to reduce their body weight on the foot. Besides that, devices with various rehabilitation training functions were designed for stroke patients to help them regain the functions of their lower limb. Different trainings provided by these exoskeletons included training of muscle and strength, walking posture and stability, proper walking pattern and trajectory, adapting patients' walking speed, climbing stairs or walking on slopes and many more. Various studies have proven the values of rehabilitation active devices in activating the muscle pattern of bedridden stroke patients, retrain their normal gait cycle and ultimately to achieve free walking with assistance [25], [26].

The most significant active devices in rehabilitation training include, Lokomat, Gait Trainer, Gait Master, Hybrid Assistive Limb (HAL), KineAsist, and LOPES. The effectiveness of each device was confirmed in clinical reviews. Treadmill training devices such as Lokomat, Lokohelp, and ReoAmbulator are overall safe to be used because partial body support is provided during rehabilitation training. Besides, this mechanism provides stability to patients on the treadmill and at the same time reduces efforts from physiotherapists. Studies show positive impact in correcting patients' lower limb motions along each treatment session [25], [27], [28].

Active devices that make use of foot manipulators are able to a simulate proper walking pattern as a reference during rehabilitation sessions of patients. A synchronized swing phase and stand phase of gait cycle of both legs can be demonstrated without fault. Patients are also able to carry out training with various terrains simulations with the end effector of the foot manipulators such as stairs climbing or walking on slopes. Hence, foot manipulators can adjust distorted and desynchronized gait pattern during rehabilitation training. Many clinical studies have been conducted and effectiveness of these devices are proven [24], [25], [29], [30].

Mobile devices such as HAL, KIneAsist, and Rewalk are also popular for stroke rehabilitation and therapy. There are small and easy to carry. Subjects or patients can move freely with these mobile devices without assistance. Sensors were implemented to react with subjects' movement to help or to lead them in motion. The drawbacks of mobile devices are the limited power supply with a portable battery and the weight of suit acting on the user. However, studies prove that stroke patients experience improvement in walking with the assistance of these devices [31]–[33].

For the past decade, countless robotic control systems for rehabilitation devices have been established and are categorized as impedance-based control, EMG-based control, and adaptive-based control. The impedance-based control aids assistance force when the limb deviates from a normal gait trajectory. The EMG-based control provides feedback muscle signal of subjects to activate assistance from the device. The major drawbacks of this control are that the calibration has to be repeatedly done to suit different patients and the sensitivities of electrode signals are easily affected by neighbouring muscle signals. Finally, the adaptive-based control has the ability to adjust itself to handle uncertainties in the system [34].

Apart from control systems, various control strategies such as sliding mode control and neural network control are popular in robotic rehabilitation devices. Sliding mode control is proven to be especially suitable for the design of robust control for rehabilitation robots with nonlinearities, parameter uncertainties and bounded input disturbances while neural network has many advantages such as simple construction, parallel processing, and adaptive learning. Parameters of neural network could be estimated via learning algorithm with a data set to let it to deal with numerous uncertainties during actual execution.

1.2 Motivation

Surviving stroke patients often experience gait impairments after recovery. Almost all stroke survivor attend rehabilitation session to restore their motor performance. However, these approaches often lead to the fatigue of physiotherapists as they rely heavily on physiotherapist's support and guidance. In fact, a stroke patient usually needs the help from more than three therapists to complete a set of gait training [25]. Hence, the duration and progression of patients' recovery will be affected due to the physical limit of the therapists themselves [7]. The rapid increase of stroke patients also leads to the shortage of therapists in the country and causes a great economic impact to the country's healthcare system [35]. Due to the factors mentioned above, innovative ideas are needed to substitute the conventional rehabilitation therapies with robotic rehabilitation devices, to reduce the workload of physiotherapists [26].

In the past few decades, many rehabilitation devices were developed for stroke patients to regain their walking ability. Various control methods were established for robotic control of the devices. Although there are advantages to each of the control method stated in previous sections, Jimenez states that rehabilitation exercise with a desired trajectory is important in helping stroke patients to achieve full recovery of their lower limb motion and gesture. The trajectory approach is shown to be more effective in activating muscle recovery compared to the fully assistive device [36]. However, the contributions of robotic control methods to stroke rehabilitation are still imprecise [9]. Hence, there is still space for progression in improving the standard protocols and approaches toward utilizing human lower limb trajectory pattern to achieve a better outcome for lower limb rehabilitation.

The control system is commonly used for controlling a robot. For the lower limb robotic orthosis, an effective control system is important to perform precise function to provide the best rehabilitation for patients. However, such device is normally equipped with various manipulators, actuators and sensors that contribute to the presence of nonlinearities, parameter uncertainties, and input disturbances. Techniques such as neural network and sliding mode control are widely used in the recent decades for a nonlinear system. However, both approaches receive backlashes as the neural network require large memory and hard disk space during the design process while the sliding mode control must be combined with various control strategies to overcome the fundamental restriction of a nonlinear system. Thus, a new control scheme and robust control system that is able to improve the properties of an unstable system of the robotic orthosis is the future direction for current researchers.

1.3 Research Plan

1.3.1 Research Aim and Objectives

The aim of the research is to design a controller for a lower-limb robotic orthosis based on SIDF method.

The objectives of the proposed research include:

- To develop a rehabilitation system that facilitates an effective rehabilitation program
- To develop a lower limb two-link manipulator that generates human gait trajectory
- To implement sinusoidal-input describing function (SIDF) model to the robotic orthosis and generate system controller for the nonlinear two-link manipulator
- To generate a new scheme of controller to incorporate into the SIDF approach function library

1.3.1.1 Development of Rehabilitation System that Facilitates an Effective Rehabilitation Program

The main objective of this research is to develop a rehabilitation device for stroke patients. A more effective rehabilitation training program for stroke patients is aimed to be implemented with a rehabilitation system that provides appropriate lower limb walking training. Hence, the biomechanics of human walking is the key to the development of an effective rehabilitation program. The comparison of gait pattern data and gait cycle timing of a normal person and a stroke patient is important for the development of the orthosis' controller. Progression of stroke patients to regain their walking ability can be accelerated with a more suitable rehabilitation program. A better walking pattern and gait cycle timing of post stroke patients can be achieved.

1.3.1.2 Development of a Lower Limb Two-link Manipulator to Generate Human Gait Trajectory

This research also aims to create a two-link manipulator that generates human gait trajectories. The development of the rehabilitation orthosis focuses on the motion of hip and knee as both joint movements are in the major plane of human walking kinematic model. The development of ankle motion will be done in future. The different gait profiles between a normal human and a stroke patient will be computed. Additionally, the established device aims to generate accurate human gait trajectories of hip and knee during rehabilitation training, to guide patients with a proper walking manner.

1.3.1.3 Implementation of SIDF Model and Generate System Controller

Next, SIDF method is to be implemented to overcome system instability. The two-link manipulator holds the properties of nonlinearities, parameter uncertainties and input disturbance due to various manipulators, actuators and sensors executed in the system. These unknown variables turn into obstacles in the process of software simulation. Hence, this approach is used to build a SIDF model of the plant to ease the process of generating the system controller for the nonlinear device.

1.3.1.4 Establish of New Scheme of Controller to Incorporate to SIDF Approach Function Library

Lastly, a new scheme of controller is established to be incorporated with the MATLAB function library. A linear model of the unstable system is produced and utilized in the simulation with the support of the function library. Then, a new scheme of controller can be formed via repeated MATLAB simulations. By utilizing the human walking kinematic model, verification of the controller and plant is done in advance of testing the system on a stroke patient.

1.4 Research Scope

In this research, attention is paid to establish a lower limb robotic device that rotates in sagittal plane with human joint trajectories pattern. A new manipulator consists of hip joint and knee joint is developed. The manipulator provides single degree-of-freedom (DOF) in sagittal plane at the hip and knee joint in real time. The low-level motion is implemented by the servomotor and encoder, while the high-level trajectory planning function by controlling with a new controller scheme to perform gait movements. This new controller is generated based on SIDF approach with the MATLAB function library.

1.4.1 Research Project Scope

The first year of the research plan focuses on a basic understanding of lower limb muscle activities and gait trajectory. This is essential for the development of a compatible assistive robotic rehabilitation device. A robotic orthosis prototype is aimed to be fabricated and tested. Actuators and sensors are then setup with a data acquisition controller device for setting up a control interface. Finally, a Simulink model simulating the movement of the robotic orthosis is developed.

The second year of the research focuses on the development of the SIDF model to characterize the nonlinear system of the two-link manipulator. Then, the SIDF model is utilized to undergo controller design with the SIDF function library to suit the performance of two-link robotic orthosis. This controller would incorporate low level motion control via DC motors and encoders and high-level gait trajectory control system via the gait pattern in real time. Simulation responses of the controller with SIDF model are compared with responses of a conventional PID on the manipulator to prove stability to the controller.

Finally, testing is done with the experimental setup to verify the compatibility of the SIDF model and controller for a multivariable nonlinear two-link manipulator. New scheme of controller is developed to be incorporated into the SIDF approach. The controller is tested in simulation and experiment. Successful implementation of the new controller is then amended to the MATLAB function library for future application

Table 3 summarises the 3-year project plan:

Table 3 Research planning

Duration	**Activities**
First Year	• Develop a robotic orthosis prototype for the project • Setup control interface for actuators and sensors with controller device • Develop a Simulink model which can simulate the movement of the robotic orthosis
Second Year	• Develop a mathematical model to describe the gait symmetry index of human lower limb • Develop a SIDF model to characterize the movement of robotic orthosis • Generate a control system based on SIDF approach MATLAB library
Third Year	• Experimental verification of SIDF model and control system • Develop new controller scheme based in SIDF approach

1.4.2 Research Project Executions

First, an ideal structure design of the rehabilitation orthosis is built. This research focuses on hip and knee movement. The two-link manipulator design was chosen to provide training for hip and knee in sagittal plane as this is the major plane of motion in human walking kinematic model. Manipulator or hardware for ankle movement in coronal plane is not considered in the current stage of research. Besides that, gait pattern and gait timing play an important role in symmetric walking. The temporal relationship between the left and right legs is vital to achieve a symmetric walking manner. Hence, the two-link manipulator design was chosen to provide guidance for patients during lower limb rehabilitation.

A structural design of the device is done by designing the mechanism of the manipulator. A flexible length adjustment design of each link is introduced to match the length of the lower limb of each patient during each rehabilitation session. The prototype of the support frame is designed to hold the manipulator in position. The design allows it to be incorporated into a treadmill for patient training purposes in future. Electronic components are chosen for the rehabilitation orthosis. Arduino Due and USB-6341 multifunction input-output device are used to control the system. The DC servomotor attached with encoder is installed to provide movement control and position feedback of the manipulator.

Next, a simulation model of the two-link robotic orthosis is needed for simulation work and controller deign. Hence, the mathematical model of two-link manipulator is computed, and the gait profile of a healthy human is applied. MATLAB is utilized to build the simulation model of the plant that consists of components such as actuators, sensors, and manipulators. Various simulation models and control system are built to mimic the actual behaviour of the system. Simulations and experiments of position control, speed control and current control are carried out. The PID controller is implemented but complications have occurred due to the unstable and nonlinear characteristic of the system. However, defective outcomes are seen in both simulation and experimental results.

Hence, the SIDF approach is implemented to solve the simulation problem. The SIDF model of the device is built and the simulation model is stabilized. The nominal SIDF model is selected, and linear fitting is done to obtain system transfer functions. Then, linear control theory technique is applied for the controller design. A lead-lag compensator for the device is generated and optimum constant gain of the controller is determined. Finally, the optimum controller is generated and the SIDF model is verified via nonlinear simulation.

After the verification in a nonlinear simulation, the lead-lag compensator is executed as a controller for the rehabilitation device. Experimental setup is also completed for validation of SIDF model with controller. Then, normalized step response in simulation and experimental setup are drawn. IN addition, tracking and decoupling of axes in simulation and experimental setups are done and outcomes are plotted. Comparison of normalized step response of both experimental setup and simulation are carried out and satisfying results are obtained. In conclusion, the application of SIDF approach with MATLAB function library is successful in a two-link manipulator. Trajectory implementations and clinical tests are aimed to be done in future.

1.5 Research Contributions

This research will lead to the following contributions:

1. Provide a new design of lower limb rehabilitation device which is low cost to be accessed.

   Based on Table 3 in the literature review, the price of a commercialized rehabilitation device ranges from RM100,000 to RM1,480,000. There are more than 10 states in our country, and it is a huge sum to be allocated to each state with even one rehabilitation device, considering that the number of stroke survivals with impairment is around 16,000 people. Hence, the research aims to produce a high cost-performance ratio lower limb rehabilitation device with a minimum budget. With the low cost of production, the selling price of the device will eventually be lowered. Hence, consumers can purchase or access this device at a more affordable price as compared to other rehabilitation devices in the Malaysian market.

2. Development of a new design of lower limb exoskeleton that focuses on joint trajectories training for rehabilitation training purposes.

   Over the past few decades, most commercialized rehabilitation devices that are developed(refer to Table 3) focus on assisting the patients to regain walking ability by providing body weight support, treadmill training and end effector only without guiding the walking angle and timing of the patient. These devices are mostly unable to adapt their movements fully to the patient during the rehabilitation session [37]. Hence, a design of lower limb orthosis device which is able to assist the leg and joint movements is developed to guide patients towards correct gait trajectories to help them regain gait movement with correct hip and knee flex-extension angle with respect to their walking cycle.

3. Introduction of SIDF model with sliding mode control in modelling the robotics orthosis.

   This is the first design method for a lower limb rehabilitation system that is based on a SIDF model. As stated by Dr Amir Nassirharand in [38], the SIDF model is applied to tracking and decoupling of a multivariable nonlinear system, showing that a describing model is a good method to represent the input-output behaviour of a nonlinear plant; in this case, it is the robotic orthosis. Besides that, the sliding mode technique is also a well-known approach to control a nonlinear system. Hence, this research is aimed to apply both methods to generate a new controller for the robotic orthosis.

4. Propose a new controller to be incorporated to the MATLAB SIDF function library.

   The Sinusoidal-input describing-function MATLAB library is developed by Dr Amir Nassirharand [39]. It consists of a series of MATLAB codes that can synthesis the SIDF model for a nonlinear system by providing the information of the particular plant. To design the controller for the linearized model, different approaches such as factorization approach and classical linear compensators are applied. Hence in this research, the sliding mode control is aimed to be added to the MATLAB library to generate a new controller for the lower limb rehabilitation device.

1.6 Thesis Outline

The concepts of developing a control system robotic rehabilitation device with SIDF model are introduced in Chapter 1. A lead-lag control system is developed by incorporate SIDF approach function library to generate a robust control system for the nonlinear multivariable system. History and current research on Exoskeleton and Robotic Orthosis are reviewed. Motivations behind the research are explained with proposed aims and objectives. Executions and contributions of the research project are described. The overview of thesis chapters is included at the end.

Chapter 2 outlines the four major research areas of the project: the biomedical aspect, robotic aspect, control systems and the control strategies of robotic rehabilitation devices. The importance and summaries of biomedical aspect for a lower limb device are discussed. Current literature review shows the basic understanding and benefits of lower limb rehabilitation device. Various model of these devices and mechanism of the system are reviewed. Potential control strategies to generate a robust controller are also highlighted. Critical reflections on design approach and control architecture are presented.

Control systems with describing function approach used for exoskeletons and lower limb manipulators are discussed. Lastly, research motivations for the research are reviewed.

Chapter 3 recorded the setup of the rehabilitation device including the mechanical, electrical and electronics designs. Safety factors and various functions are considered for protection purpose and user-friendliness. Justifications of the mechanical design and safety measurement are presented. The dynamic model is derived for simulation and to be utilized to generate the control system.

Preliminary work on the development of simulation model of the system is discussed in Chapter 4. Simulation model is built to verify the parameters of motor. Trajectory control with conventional controller in simulation and experiment are tested and the result is presented and discussed.

The theories of describing function and lead-lag compensator will be discussed in Chapter 5. The used of method of sinusoidal input describing function to stimulate the nonlinear model is discussed. Controller design with lead-lag compensator is also depicted and the outcomes from simulation and experimental setup are recorded and studied.

Novelty of the research is reviewed in Chapter 6. The implementation and validation of SIDF model with controller are done via several steps to assure its reliability. Nominal model selection via linear fitting was done for the SIDF model. Performance of the nonlinear feedback control system was verified with various methods including step responses and tracking and decoupling test. Comparison of the SIDF model with experiment setup are also presented. Justification and conclusion of the SIDF approached is presented, hence, marked the academic contributions in control system study.

In Chapter 7, the main findings of the research are summarized. The advantages of SIDF approach are concluded. Limitation of current works and suggestion for future works in the related field are proposed and recommended.

Chapter 2 Literature Review

2.1 Introduction

This chapter outlines the research area of the project. It is divided into 4 main parts: the biomedical aspect, robotic aspect, control systems and the control strategies of robotic rehabilitation devices. The biomedical aspect summarizes the gait analysis that includes the biomechanics of human walking, human normal gait cycle and related topics. Terminologies of human gait analysis such as step and stride length, phase of gait and timing of gait cycle are reviewed. Studies on various types of robotic rehabilitation devices are reviewed in the robotic section to provide basic understanding on the current development trend. The lower limb rehabilitation devices are classified into passive and active types. Active devices are categorized into treadmill training devices, feet manipulators and mobile device, and they are common choices for the conventional rehabilitation method. A chart of commercialized and non-commercialized devices often used for stroke rehabilitation is presented. The control systems and control strategies for rehabilitation devices are also described in this chapter. Additionally, there is a section describing various control systems that are applied in the commercialized and non-commercialized rehabilitation devices, which comprises the impedance-based control, EMG-based control, adaptive-based control. Besides that, two common control techniques including the sliding mode control and neural network control for lower limb orthosis are reviewed in this chapter. Finally, the study of describing function approach which is applied in this research is presented.

2.2 Biomedical Aspect

A basic understanding of human walking is necessary to design a robotic orthosis. This section describes the biomechanics of human walking and the terminologies used in gait analysis. Also, joint torque and electromyography (EMG) signal used to measure muscle activity will be presented.

2.2.1 Biomechanics of Human Walking

Figure 4 shows the description of human anatomical planes and the direction of leg motion in sagittal plane. The sagittal plane is the major plane of motion in human walking kinematic model. Motion in sagittal plane is referred as flexion (positive direction) and extension (negative direction). Abduction (moving away from the body) and adduction (moving toward the body) are used to describe motion of hip in coronal plane. Finally, eversion (moving away from the body) and inversion (moving toward the body) are used to describe the motion of ankle in coronal plane [8].

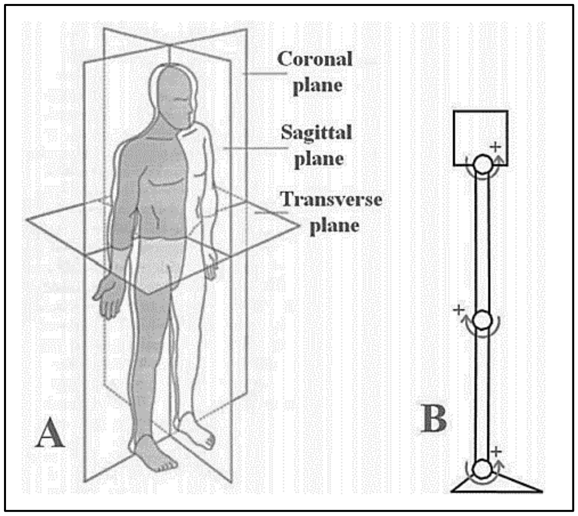

Figure 4 Description of human anatomical planes (A) and diagram of the leg shown in the rest position (0 degree at all joints) with the positive direction indicated (B) [8]

2.2.2 Human Normal Gait Cycle

Normal gait pattern can be utilized as a guidance on gait rehabilitation of stroke patients. However, there is not a particular standard for human walking pattern because people with different ages, sexes and different body geometries will result in different sets of gait pattern [40]. Hence in this section, a general gait pattern that represents a normal human walking trend will be discussed.

2.2.2.1 Terminology Used in Gait Analysis

Figure 5, Figure 6 and Figure 7 describe the gait parameters used to define the process of gait cycle. Figure 5 shows the comparison between a step and a stride. A step is the movement of either one foot to the front of the other, while a stride is referred to a step forward by the same foot. Therefore, a step length will be the distance travelled by one foot to the front of the other. However, stride length is measured by the displacement between the same foot from the instant that the foot contact with the ground and continue until the same action occurs. In order to walk in a straight line, the stride lengths of both sides of the feet should be equal even though the gait patterns might not be symmetrical to each other. Figure 6 and 7 describe the step length and stride length for a typical symmetrical and asymmetrical walking. As shown in Figure 6, step lengths of both sides of the symmetrical walking are equal. However, this might not apply to the asymmetrical walking as shown in Figure 7 [41].

Gait is a series of repeated patterns of lower limb movement that helps the body to move forward. Gait is normally referred to as walking. It can be divided into phases or periods [42]. Gait cycle is defined as the period of time between two successive occurrences of one of the repetitive events of walking [40], [43]. In this report, Rancho Los Amigos Observational Gait Analysis (OGA) system [44] is used to define the gait cycle.

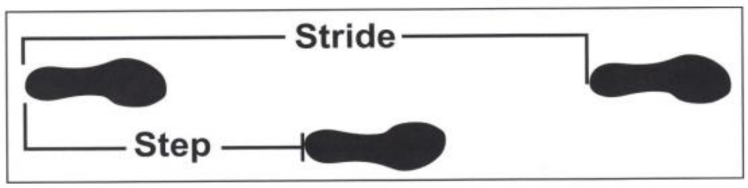

Figure 5 Gait cycle/step and stride [45]

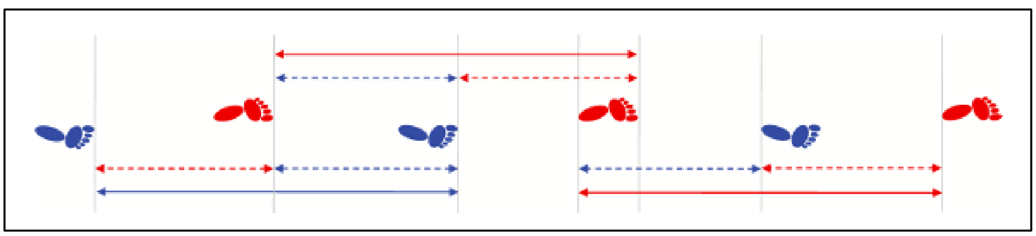

Figure 6 Step length (---) and stride length (-) for symmetrical walking [41]

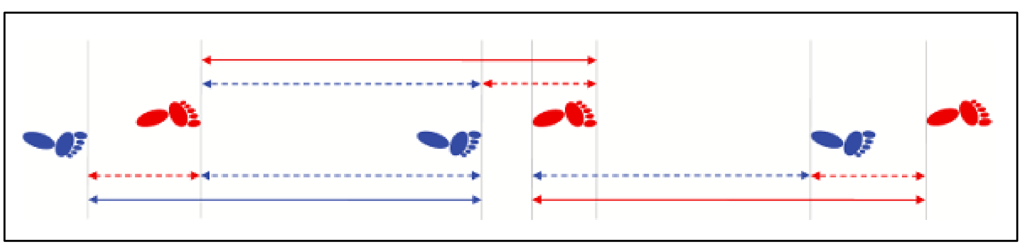

Figure 7 Step length (---) and stride length (-) for asymmetrical walking [41]

In the OGA method, gait pathology is defined as the deviation from normal function. Gait cycle is divided into 8 major events to accomplish 3 tasks as referred to Table 4. Figure 8 shows the details of a complete gait cycle. The gait cycle starts with initial contact of one foot and ends at the next initial contact of the same foot. The other foot will go through the exact same cycle but is displaced in time by half a cycle.

Both legs will undergo swing phase and stance phase. Swing phase refers to the instant when the foot is moving forward and hanging on the air while stance phase happens when the foot contacts the ground and acts as a support for the body to move over it [40], [46].

Table 4 Phase of gait [29]

Period	**Task**	**Phase/ Major Event**
Stance Phase	Weight Acceptance	Initial Contact
		Loading Response
	Single Limb Support	Mid-Stance
		Terminal Stance
	Swing Limb Advancement	Pre-Swing
Swing Phase		Initial Swing
		Mid-Swing
		Terminal Swing

<u>Task 1: Weight Acceptance</u>

The initial contact is not exactly a phase. It is the instant when the foot touches the ground. Usually the heel contacts the ground and continue by loading response until the other foot is lifted for swing. This two events are defined as weight acceptance because shock is absorbed by the outstretched limb when the body weight is rapidly transferred from one side of the body to the other [42].

<u>Task 2: Single Limb Support</u>

The gait cycle is continued with the mid-stance as the starting of single support period when the other foot is lifted up until the body weight is positioned over the forefoot. Terminal stance phase will then begin with the heel rise and continue until the other foot hits the ground. This task is named as single limb support as the total body weight is acting on one limb [42].

Task 3: Swing Limb Advancement

Pre-swing phase is the final stage of stance phase. It starts with the initial contact of the contralateral foot with the ground and end with ipsilateral toe-off. The body weight will then be transferred to the opposite limb. Therefore, this phase is often known as “weight release” or “weight transfer”. Then, the swing phase begins with initial swing when the foot is lifted up from the ground and swung while the opposite foot undergoes loading response. The main purpose of this phase is to allow the limb to move from its standing position to form a clearance between the foot and the ground. During the mid-swing phase, the swinging limb will move forward. Lastly, terminal swing occurs until the foot is in contact with the ground [42].

2.2.2.2 Gait Cycle Timing

In gait analysis, human gait pattern is often assumed to be symmetrical for both sides to ease data collection and analysis [47]. Figure 9 shows the timing of the heel contact and toe-off in a single gait cycle. When the initial heel contact of the right leg occurs, the left leg still rests on the ground. This phenomenon is called the “double support” where both legs are still in contact with the ground. Next, during the swing phase of the left leg, the right leg remains in stance phase and forms the “right single support” phase. After that, the same movements of both legs are repeated for the opposite limbs and hence result in “double support” again and followed by “left single support” [40].

Thus, two periods of single support and two periods of double support occur in one gait cycle. As shown in Figure 10, the stance phase usually occupies 60 percent of the cycle while the remaining 40 percent is the swing phase. Each period of double support occupies 10 percent of a single cycle. However, the timing of gait cycle is different with respect to the speed of walking. As the walking speed increases, the swing phase will be longer and the stance phase will eventually become shorter [40].

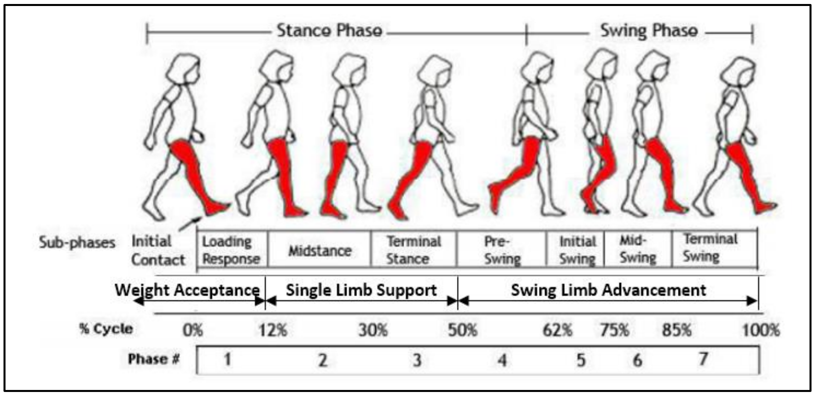

Figure 8 Phases of gait [43]

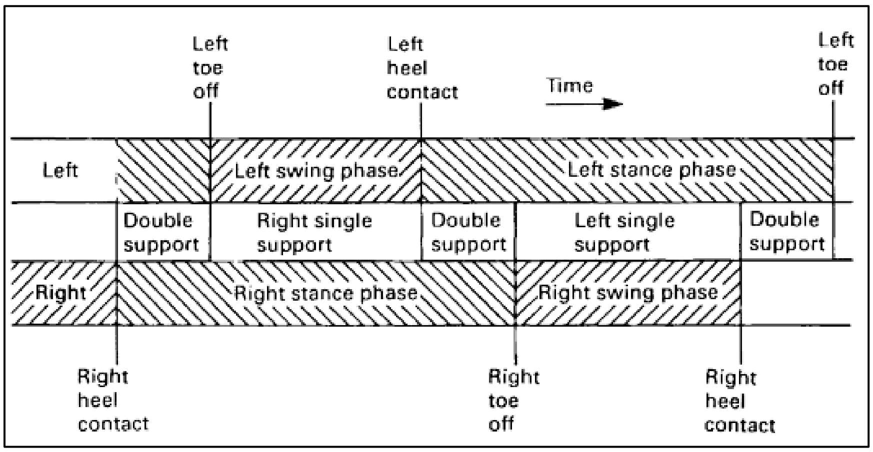

Figure 9 Timing of single and double support during a single gait cycle from right heel contact to right heel contact [40]

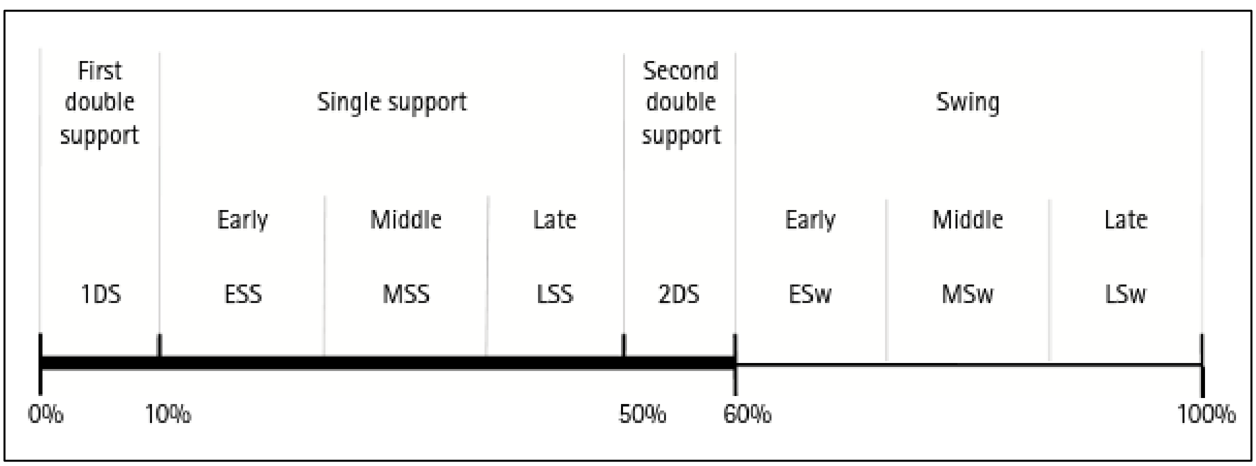

Figure 10 The timing and phase of the gait cycle based on equal subdivision of single support and swing into three phases [41]

2.2.2.3 Gait Graph

Joint angles are quantities that vary throughout the gait cycle, which is also one of the important aspects in gait rehabilitation of the lower limb. As the main objectives of rehabilitation training is to be able to restore a proper walking ability, accurate joint angles are able to provide a reference position for the patient at each time interval during rehabilitation. As it is impossible to feedback a patient's joint angle or to provide reference during a rehabilitation training, the best way to utilize joint angle is to implement it onto a rehabilitation device.

Database of joint angles need to be identified before the development of lower limb exoskeleton in order to compare the patient's real-time joint angles and provide support or lead the patient to walk in a proper manner. In this research, database of joint angles plotted in gait graphs is obtained from a study of human gait pattern by University School of Physical Education, Wrocław, Poland [48]. Kinematic pattern of adult gait for motion analysis system BTS Smart-E was established and used. Joint angles of a group of healthy adults were presented in three speed level. Two typical gait graphs of hip and knee from these studies are plotted in Figures 11 and 12 respectively with the percentage of gait cycle against the joint angle. Each graph shows three sets of average joint angles which represents the slow (1.16 m/s), preferred (1.36 m/s) and fast (1.86 m/s) speed. This data is obtained from 17 healthy male subjects between ages of 21 to 23 years old with average body mass of 76.3 kg and around 1.79 m tall [48].

Figure 11 shows that the hip flexes and extends once in a single gait cycle. The hip reaches its flexion limit at the middle of the swing phase and remain flexed until the start of the stance phase. Maximum extension occurs before the end of stance phase and the hip begins to flex again afterward.

Knee flex-extension graph plotted in Figure 12 shows that two flexions and two extensions happen in a single gait cycle. The knee is fully extended before initial contact with the floor, following by the flexion of muscle in the early stance phase. The knee muscle extends again during mid-stance and begins to flex again after it reaches a peak at the beginning of the swing phase.

Figure 13 illustrates the temporal relationship between the angles obtained from right (blue) and left (red) knees. The data is plotted for both sides with the same time scale. The peak knee flexion of left knee occurs during the swing phase of left limb and stance phase of right limb. The data from both sides are plotted in the same graph at the bottom of Figure 13. The blue and red dots are distanced from each other for about half a gait cycle. Hence, this indicates that the normal gait pattern of both limbs e basically correspond to each other by the interval of half a gait cycle [41].

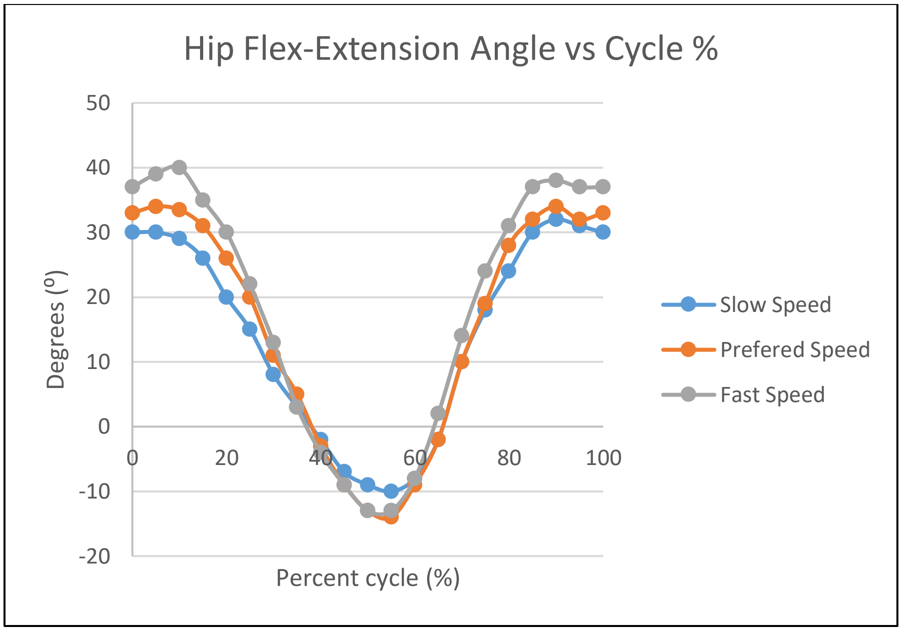

Figure 11 Angle-time characteristics for hip motion with different speed preference [48]

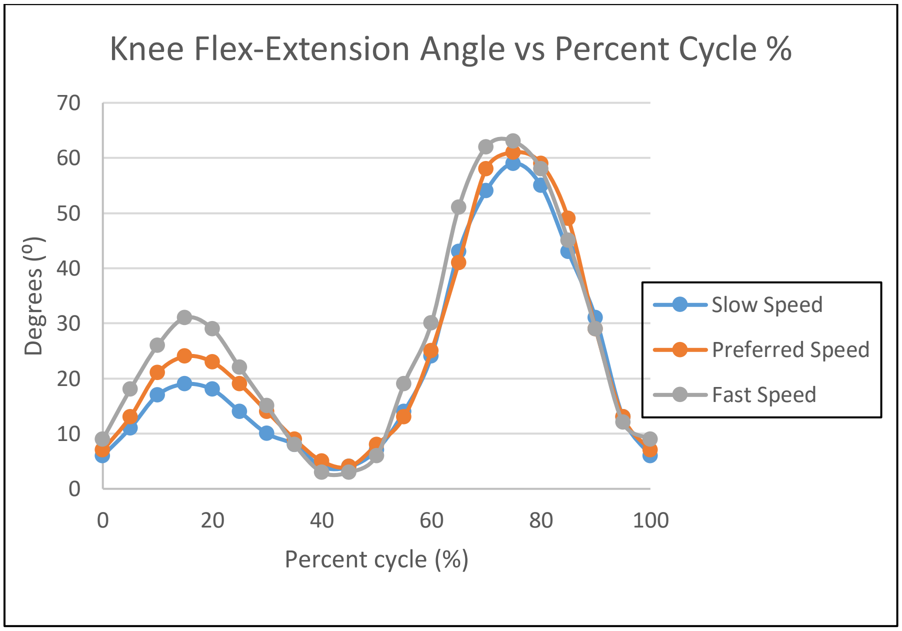

Figure 12 Angle-time characteristics for knee motion with different speed preference [48]

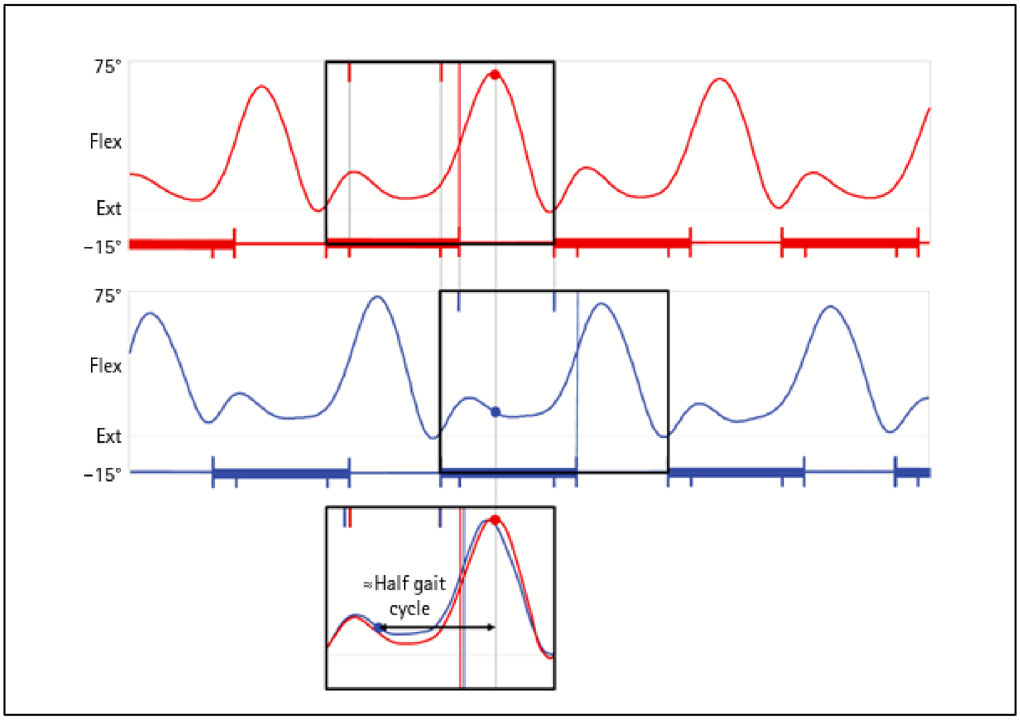

Figure 13 Temporal relationship between data for left and right knees [25]

2.2.3 Important of Biomedical Aspect

With the findings of gait analysis of human walking, a better control strategy can be designed to provide the best rehabilitation orthosis for the subject during rehabilitation process. The step and stride pattern of gait cycle provides timing information of the foot during asymmetric walking. Besides, gait phases such as swing phase and stand phase, as well as the 3 tasks of weight acceptance, single limb support and swing limb advancement, are concerns in designing the orthosis to allow the subject to carry out walking training in a proper rhythm and tempo with the correct amount of support in each side of the limb. Lastly, gait cycle timing and gait graph provides the average walking data of healthy human. These resources are important in programming the knee and hip movement of the rehabilitation device as the aim of the orthosis is to provide the best environment that mimics a normal walking pattern for subjects to exercise and regain their walking ability that is closest to their walking pattern before a stroke. Hence, the study of biomedical aspects is compulsory to design the structure and control strategies for the lower rehabilitation system.

2.2.3.1 Relationship of Gait Graph with Control System and Design of Robotic Orthosis

As shown in Figure 14, the gait pattern of a left-sided hemiplegic stroke patient is plotted and compared with normal gait cycle. Gait data of the right side of lower limb as shown in grey lines are slightly offset from the normal gait. However, the plots of the left leg (black lines) show a distorted pattern. The gaits of the left leg are abnormal and deviated from the normal gait. These can be seen where the peak of both graphs appears slightly earlier than the other leg. Also, a distorted gait pattern can be seen in the early stage (stand phase) of each gait graphs. These explain that a left-sided hemiplegic stroke patient could not control his left leg due to brain and nerve cell damage. Hence, the motion of the right leg (healthy side) will be slightly affected during walking.

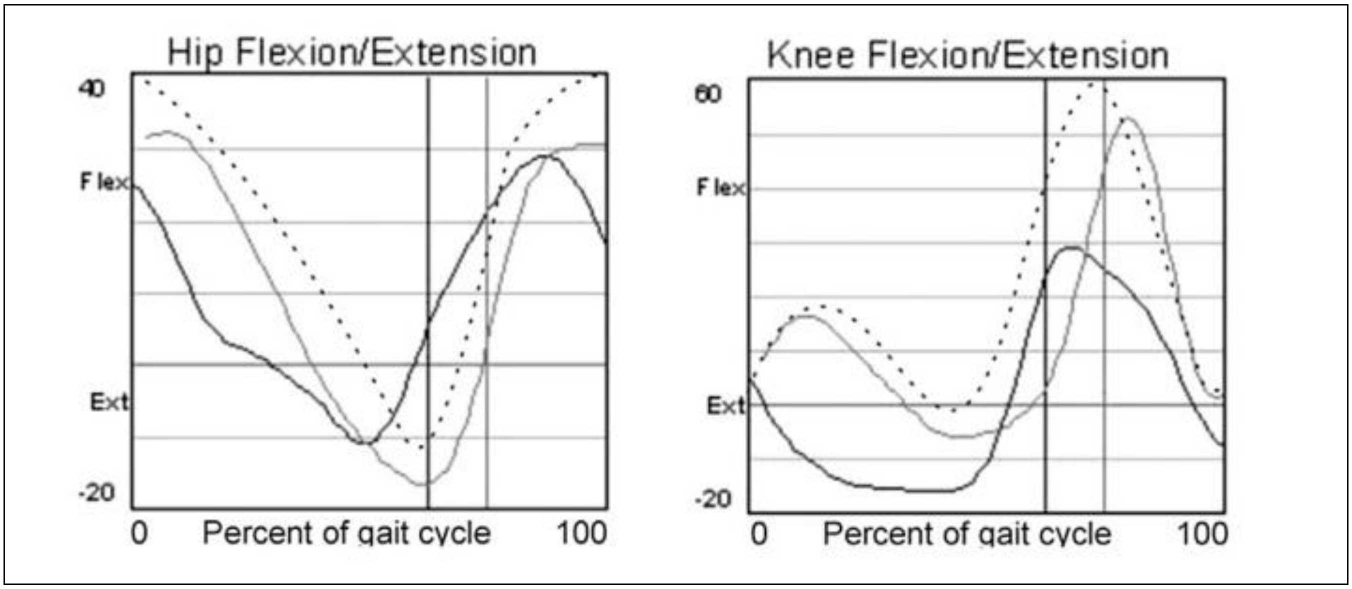

Figure 14 Kinematic graphs of the hip and knee of a left-sided hemiplegic stroke patient. (Dotted line: Normal data; Grey Line: Right side of body; Black line: Left side of body, distorted gait graph)[49].

To regain a balanced walking posture, both sides of the leg must walk with a normal gait cycle. Temporal relationships between both legs are aimed as the final outcomes of stroke rehabilitation. Therefore, the normal and asymmetric gait patterns must be utilized as a reference in the development of the rehabilitation device. The gap between these two values should be reduced with the rehabilitation program provided by the rehabilitation devices. The normal gait pattern acts as a tool in guiding stroke patients to walk with normal joint angles during rehabilitation training, while the distorted gait profile is the element to be fixed.

A normalized gait graph and the patient's gait profile are key points in the control system's development. The normalized gait graph represents the reference or desired input of a plant while the patient's gait pattern is the feedback signal in the system. Errors can be computed with the existence of these two values. Therefore, the control system will be able to compute the amount of strength or torque needed by patients during a rehabilitation training. The conceptual control system is illustrated in the block diagram (Figure 15).

To correct patients' gait patterns, the distorted gait profile of hip and knee must be obtained and compared with the normalized gait data. Moreover, the design of the rehabilitation devices should match with the objectives of the research to help patients regain a balance walking manner. Hence, the concept of two-link manipulator is proposed. The two links can be used to attach and guide the movement of hip and knee at real-time. DC servomotor and sensors can be implemented to control and feedback joint movements during rehabilitation training.

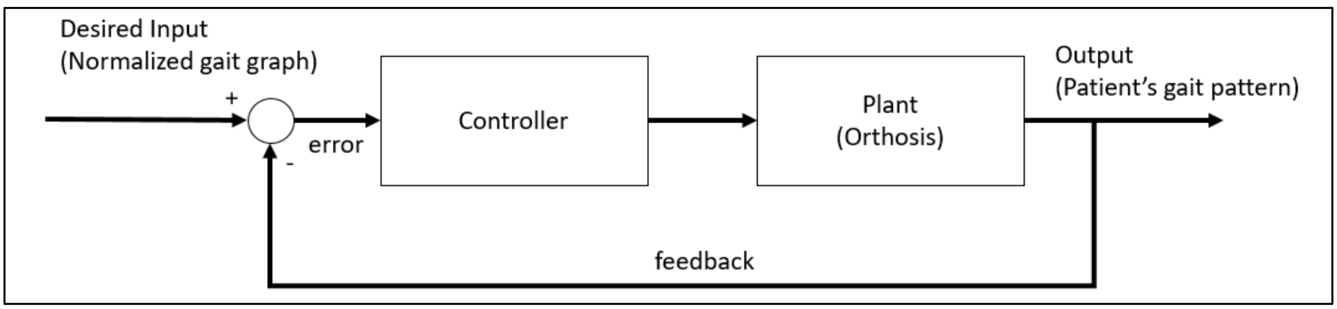

Figure 15 Conceptual block diagram of robotic orthosis

Referring to the angle-time characteristics of hip motion, as shown in Figure 11, the hip reaches a minimum value at the end of stance phase and starts to rise as a preparation to go into swing phase. Besides, Figure 12 shows two turning points at midstance and midswing positions. The changing directions of hip and knee during flexion and extension are observed. These show the dynamic characteristics of a human walking gait pattern. Hence, a controller needs to be instigated to the system to deal with the dynamics of the gait profile and multivariable of the two-link device. A stable model is required to deliver gait correction task, and at the same time manipulate the movement of two links. Hence, a robust control system is compulsory to be created for the rehabilitation devices.

2.3 Robotic Aspect

The number of stroke victims is increasing from year to year. A lack of physiotherapists lead to the development of assistive robotic devices for rehabilitation. With the existence of robotic rehabilitation, workload of physiotherapists can be replaced or reduced. At the same time, the patients can receive better post-stroke rehabilitation to overcome their disabilities and achieve the best training result. Massive research in rehabilitation devices result in robots providing different types of assistance for physiotherapists. Besides that, rehabilitation devices also provide various kinds of support and exercise for patients. Robotic devices can help patients in a passive or active way.

2.3.1 Passive Devices

Passive devices as shown in Figure 16 are usually attached with springs and links to provide patients with strength to move the lower limbs against the gravitational force [50]. These devices often contain simple interface with various kinds of geometry. Passive devices can aid with rehabilitation practice on stability, posture of walking, muscle control and strength. Passive devices are safe to be used and hence, it is preferable for patients to practice with them. The geometry and inertia of passive devices are also adjustable to suit the patients for optimum level of balance and practice. However, there are some drawbacks for the passive devices as they only provide little assistance for the movement of patients and hence result in slow rehabilitation progressions [27], [51].

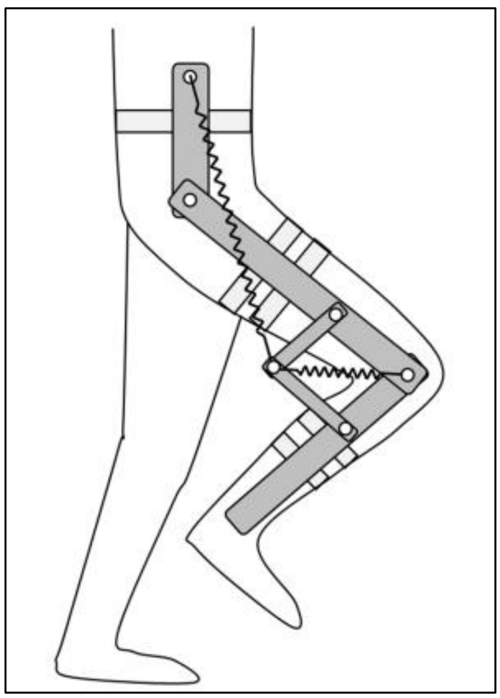

Figure 16 A Gravity Balancing Passive Exoskeleton for the human leg - basic component of gravity mechanism [52].

2.3.2 Active Devices

For active devices, patients have to provide the energy or to initiate certain motions to activate the device's movements. These devices are usually actuated with motors, actuators and sensors controlled by a controller or CPU. Sensors act as a receiver to notice patients' movement, while actuators and motors are connected to end effectors to provide support or guidance. Active devices are usually classified into three main approaches: treadmill training devices, feet manipulators, and mobile devices.

2.3.2.1 Treadmill Training Devices

Treadmill training is a common practice by physiotherapist to assist stroke patients to regain functional mobility. This method is also known as partial body weight support treadmill training (PBWSTT). In traditional practices, three physiotherapists are needed to help a patient by holding his legs and hips to walk on the treadmill to achieve posture stability. Since huge efforts from physiotherapists are required for this kind of training, the idea of robotic devices to assist patients on treadmill is established. Utilizing robotic devices to hold the patients during treadmill training can reduce the body weight acting on the human legs. Besides that, robotic devices can help patients to practice the correct walking pattern at ground level [25], [27]. Studies show that this method is safe, feasible and is able to provide a positive impact during stroke rehabilitation [53].

Lokomat

The Lokomat as shown in Figure 17 developed by Hocoma [54] is the most famous robotic system which provides body weight support for patients during treadmill training. There are two 2-DOF robotic orthosis in the Lokomat system to support the pelvic girdle of both limbs on the sagittal plane. Each orthosis is responsible for the hip and knee joints control of one limb. The size of the orthosis is adjustable to match the patients' legs. DC motors are used to control the joint movements while potentiometers are implemented to measure the joint angles. Reference trajectories are used to keep track of the joint angles [27]. The computer-controlled drive of Lokomat are programmed to synchronize the treadmill speed with the speed of the orthosis [25]. The speed and forces of the Lokomat are changeable to suit the patients' needs. The Lokomat is mounted to the treadmill with a four-bar mechanism in order to achieve planar lateral stabilization. Velcro straps are used to connect the patient's legs to the device [27]. Lokomat is the most evaluated system and it is one of the very first robotic orthosis for treadmill gait training [25].

<u>Lokohelp</u>

Lokohelp as displayed in Figure 18 is an eletromechanical device placed at the front-center of the treadmill surface which is parallel to the gait direction. Besides that, there is a mechanism to support the body weight and provide stability to the patients on the treadmill as shown in Figure 19. Lokohelp is able to guide the patients' legs to move according to the normal walking pattern without any slippage. Studies show the system's effectiveness on the recovery of gait ability of the patients. Lokohelp is able to ensure the correct rhythmic and continuous motion of patients' lower limbs along the treatment session [25], [27].

<u>ReoAmbulator/AutoAmbulator</u>

ReoAmbulator as shown in Figure 20 also known as AutoAmbulator. It is actuated with robotic arms to control the hip and knee joint angles. It consists of a body weight support (BWS) system as shown in Figure 14 to hold the patients in an upright position on the treadmill [7], [33]. This device is similar to Lokomat as the movement of both devices are limited to the sagittal plane. ReoAmbulator is more concerned with the walking trajectory and stepping pattern than balance training [7], [25]. The robotic arms required patients to generate a necessary amount of force to perform the gait motion during the rehabilitation. AutoAmbulator is effective in providing balance and gait training for stroke patients. Besides that, AutoAmbulator is widely used in research centers and hospitals for rehabilitation purposes and research studies [28].

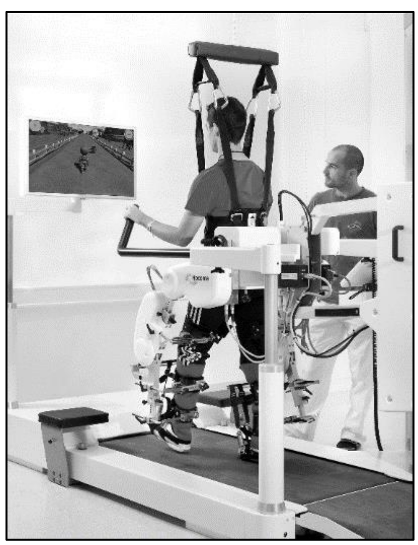

Figure 17 Lokomat [54]

Figure 18 Lokohelp on treadmill [55]

Figure 19 Lokohelp in use [55]

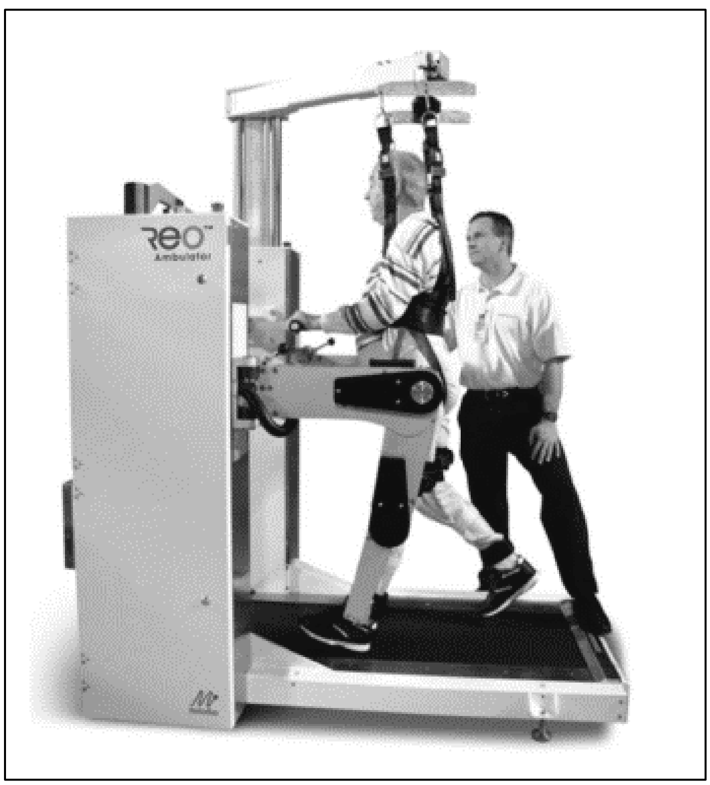

Figure 20 ReoAmbulator [25]

2.3.2.2 Foot Manipulators

Apart from BWS treadmill training devices, programmable foot manipulators are also a kind of active device for stroke rehabilitation. Patients' feet are placed and held on foot plates controlled by a robotic system that simulates walking patterns during swing phase and stance phase. In addition, the foot manipulators can simulate different terrains and human gait patterns for rehabilitation purpose. The aim of these devices are to provide platforms to correct patients' distorted and desynchronized gait patterns [25], [27].

<u>Gait Trainer GT I</u>

The Gait Trainer GT I as shown in Figure 21 is one of the most famous foot manipulator devices commercialized by Reha-Sim [23]. The concept of this device is to provide a task-specific platform for adequate therapy of stroke patients. This device can help to improve patients' walking ability by relieving their body weight and provide continuous training to patients by adapting to their walking speed. Patients' feet are secured onto the foot plates which stimulate the swing and stance phase. Cables are attached to the patients to keep track of the body's movements as demonstrated in Figure 21. The step length and gait speed are adjustable according to the preference of users. Many clinical studies had been conducted and the effectiveness of this device is justified. Furthermore, it is effortless to operate the Gait Trainer compared to the traditional treadmill training [25], [56].

<u>Haptic Walker</u>

Haptic Walker (Figure 22) is known as the improved version of GT I as it is able to generate different walking speeds and provide different modes of training for patients. Several modes of training provided by Haptic Walker include climbing up the stairs, walking on a rough grounds or slopes. Besides that, sensors are placed underneath the manipulators to measure the walking strength of patients and ease the physiotherapists to monitor the progression of patients [25], [30]. Clinical reviews on the Haptic Walker have been done on spinal cord patients and its effectiveness is confirmed [29].

<u>Gait Master 5</u>

Gait Master 5 is a non-commercialized device developed by University of Tsukuba [24]. It is a manipulator type of device actuated with two footplates that forms a virtual floor underneath the feet as shown in Figure 23. The repeating motion of the footplates enables users to experience walking on different kinds of terrain, and at the same time remain stationary on the device. Slider-crank mechanism is used as a linear guidance for the 2 DOFs motion footplates. Rotary encoders are attached to the servomotors for position feedback. The trajectories of the footplates are adjustable with the motion data inputted to the device to suit the needs of users. Flexi-force pressure sensors also implemented on the foot plates to measure the weight acted on the users' heel and toe during initial contact. This device has been evaluated and the outcomes show that it is capable to help hemiplegic patients to regain their stair climbing ability [24].

Figure 21 Gait Trainer GT I [56]

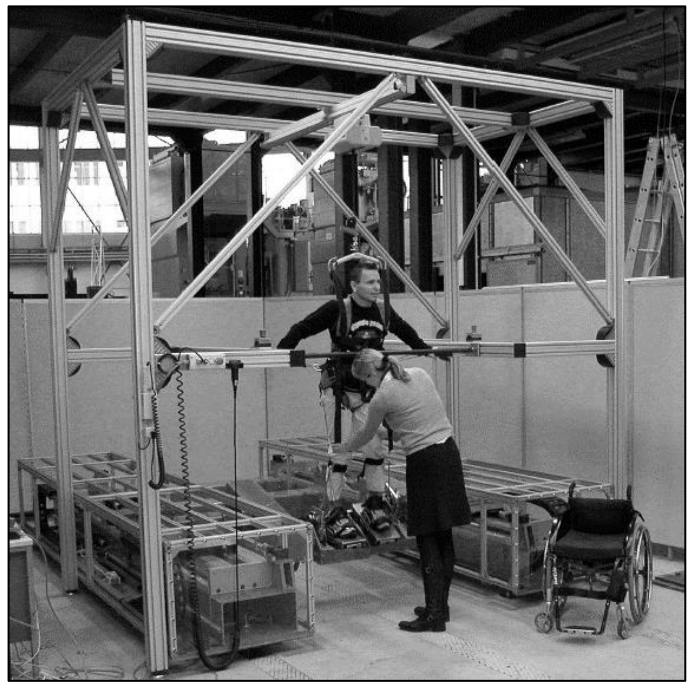

Figure 22 Haptic Walker [30]

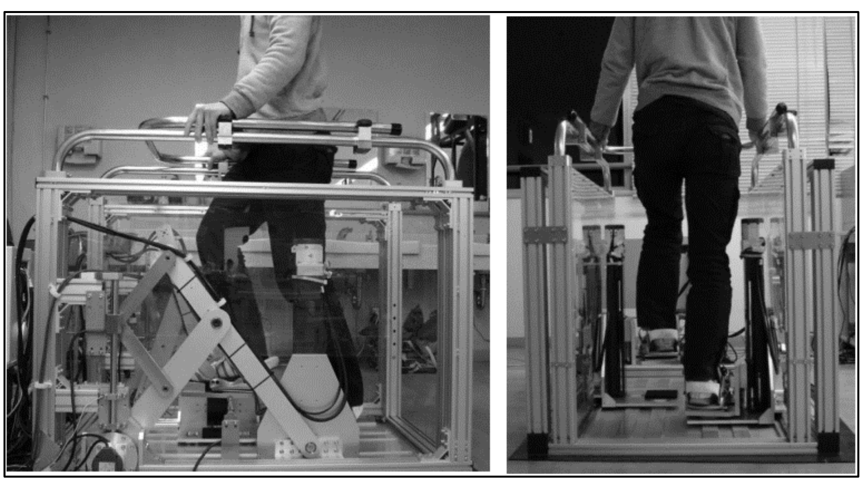

Figure 23 Gait Master 5 (Side view and back view) [24]

2.3.2.3 Mobile Devices

Overground gait training devices are also a kind of active device preferred by physiotherapists for gait rehabilitation. These mobile devices allow patients to retain their walking ability in a natural way. The patient can pre-set the device's movement and move freely on the ground without assistance from physiotherapists. These mobile devices often have a smaller size compared to treadmill training and foot manipulator devices. Thus, they allow patients to experience less visual impact during gait training. However, these devices might not be very effective as patients might be learning a compensatory gait. Besides that, there are some challenges faced by researchers to design such device due to various aspects such as balancing of devices, weight and size of devices, and weight and capacity of portable power supply [25], [27], [33].

<u>Hybrid Assistive Limb (HAL)</u>

Hybrid Assistive Limb (HAL), commercialized by Cyberdyne Tsukuba, Japan [31] is a wearable exoskeleton that provides a wide range of applications to users such as stroke rehabilitation and heavy works support [25]. The HAL as shown in Figure 24 is the first robotic invention that integrated human, mechanical and information technologies to provide assistance to the older with muscle weakness and people who suffered from motor function impairment [57]. HAL offers numerous versions including the full body version, lower limb version and single leg version. The single-leg version is a newly developed version of HAL specially designed for hemiplegia stroke patients. Each version is built to suit a specific task. HAL consists of a hybrid control system with two subsystems: cybernic voluntary control (CVC) mode and cybernic autonomous control (CAC) mode. The voluntary control mode allows activation of HAL with the bioelectrical signals of the patient for desired movements. However, the autonomous control mode works by providing physical support for the disabled people. DC motors are mounted to hip and knee joints to assist the flexion and extension of the limbs. Various sensors and components are installed to enhance the function of this exoskeleton. Force sensors are used to feedback on the ground reaction while waist belts are installed to secure the users. Furthermore, EMG electrodes are implemented to detect users' muscle signals on the surface of the skin, and potentiometers are installed for joint angle feedback. Finally, gyroscopes and accelerometers are used to predict the posture of users. The positions and EMG signals are used to control and determine the necessary torque required by patients to move the joints. The HAL is powered up by portable batteries which allows it to operate for more than 60 minutes for normal operation [25], [27], [58]. Several evaluations demonstrated the efficiency of HAL in rehabilitation training for stroke survivors [31], [57], [59].

KineAssist

KineAssist as shown in Figure 25 is a robotic device that can sense human movements. It is able to feedback on the motion of users and keep up with the direction of movements. A software-driven brace system is installed in the device to provide partial body weight support to the patients and hold them when they lose balance. There is a mobile base system actuated with passive sliders and force sensors placed at the lower part of the device. It is responsible to feedback on the patients' movement. Patients can walk freely without any turning constraint with the assist of this device and hence, achieve a natural walking pattern. Gait training parameter can be changed by the physiotherapist for a better clinical outcome [25], [60]. A study has determined that stroke patients can walk with a greater speed with the assistance from KineAssist [32].

ReWalk

AGRO Medical Technologies Ltd. has established a wearable robotic suit named ReWalk (Figure 26) for therapeutic activities. It is a light-weight robotic suit integrated with DC motors at each joint. Rechargeable batteries, sensors and a computer-based control system are installed in a backpack. Users can simply command the exoskeleton to perform various transition movements such as stair climbing, walking, sit-to-stand and vice versa motion. Sensors are integrated to detect upper body movements in order to predict users' intention and maintain their walking process [25], [33].

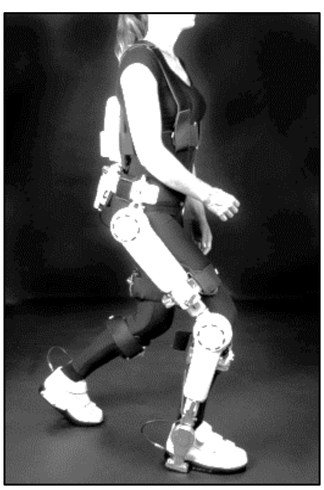

Figure 24 HAL [31]

Figure 25 KineAssist [32]

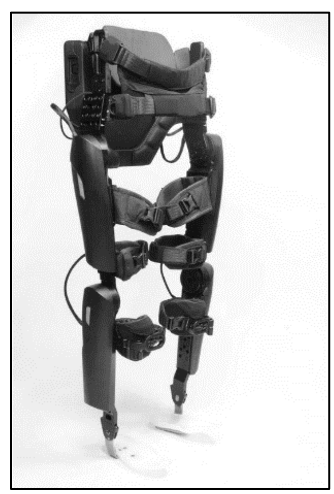

Figure 26 ReWalk [61]

2.3.2.4 Others

Anklebot

Anklebot as shown in Figure 27 is an impedance-controlled robot for ankle rehabilitation. It is composed of a seated paradigm to train the paretic ankle of chronic stroke patients. The Anklebot provide 3 DOFs in the normal range of foot motion for patients to overcome foot-drop problem. The kinematics design of Anklebot included two linear actuators to provide dorsi-plantarflexion and inversion-eversion torque. Two brushless DC motors are used to provide the relative amount of torque required by patients while encoders are implemented to feedback on the position of motions. Analog current sensors are applied to determine the motor torque. A preliminary test was conducted to evaluate the feasibility and safety of Anklebot [62].

Standing Biofeedback Trainer

Standing Biofeedback Trainer is a new training device modified from the Standing Training Table by Chang Gung Memorial Hospital, Taiwan [63]. This device consists of a height-adjustable worktable, a mirror for postural adjustment and a forearm suspension system to keep the upper trunk in a symmetric position. Moreover, a hip fixation system is installed to fix the pelvis and lower trunk in a proper position. Foot sensors are used to measure the weight distribution on the body. Feedbacks are shown with a real-time weight bearing biofeedback LED display and a balance scale on the correction mirror. Safety precaution was taken by introducing an auditory alarm system compatible with 3 most spoken languages in Taiwan to alert the patients [63].

LOPES

LOPES (lower extremity powered exoskeleton) shown in Figure 23 is designed to fully assist patients for lower limb movements. It allows a near-to normal free walking support which covers a wide range of possibilities in rehabilitation training and other actions. This device consists of several modes such as “patient-in-charge”, “robot-in-charge” as well as “therapist-in-charge” which allow the robot to follow or to guide patients. It is controlled by the therapist to apply corrective or supportive torques to the leg-joints and pelvis of the patient during free walking. This humanlike exoskeleton implemented impedance control with a combination of position and EMG sensors to help patients actively move their muscle in voluntary action. A clinical trial involving a small number of subjects was done and remarkable progression was observed from the range of knee angle, knee angular velocity, walking distance and gait speed and hence concluded the positive effect from gait rehabilitation training with LOPES [37], [64].

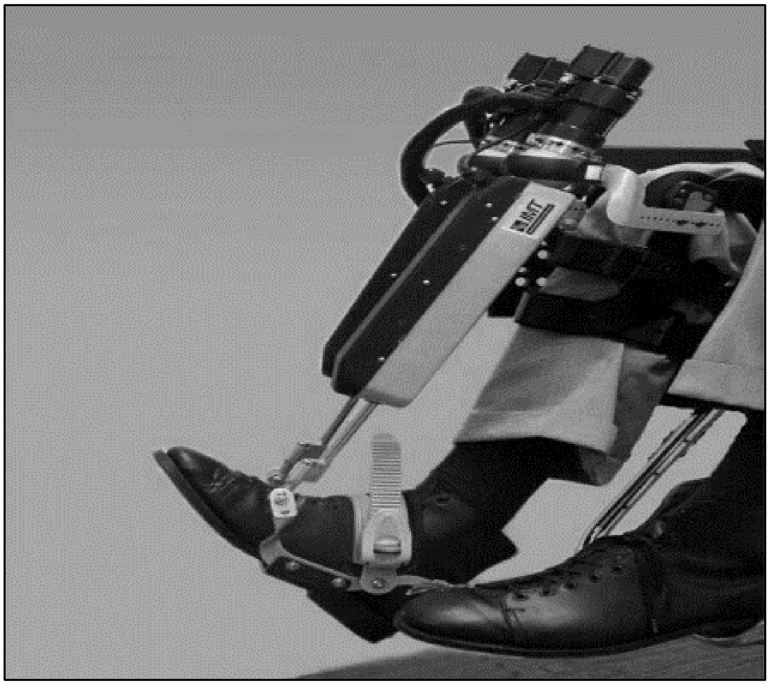

Figure 27 Anklebot [62]

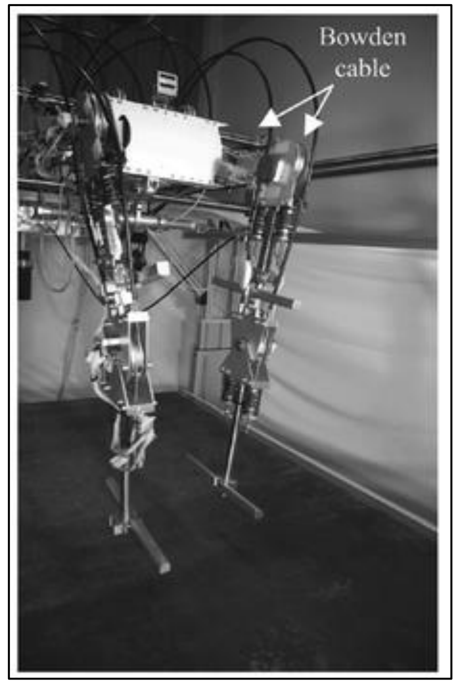

Figure 28 LOPES [37]

2.3.3 Commercialized Devices and Non-commercialized Devices

Most rehabilitation devices used in hospitals and rehabilitation centers are available in the market. However, there are some devices developed by research centers that are still under observation and further development. Table 5 summarizes the commercialized and non-commercialized devices often used for stroke rehabilitation.

Table 5 Table of commercialized and non-commercialized robotic rehabilitation devices

	Devices *(Approximate market price)*	**Year**	**Published/Produced by**	**Characteristics and Designs**				
				Body Weight Support	**Treadmill**	**End Effector**	**Mobile Devices**	**Others**
Commercialized Devices	Lokomat *(RM1480K)*	2001	Hocoma Inc. [54]	/	/			Trajectory control
	Lokohelp *(RM125K)*	2008	Woodway USA Inc. [65]	/		/		
	ReoAmbulator *(>RM42K)*	2002	Motorika USA Inc. [66]	/	/			
	Gait Trainer I *(RM135K)*	1999	Rehab-Sim Medtec Inc. [67]	/		/		
	KineAssist *(RM582K)*	2008	Woodway USA Inc. [60]	/			/	Actuated with force sensors
	Rewalk *(RM353K)*	2011	Rewalk Robotics Inc. [68]				/	
	HAL *(RM790K)*	2004	Cyberdyne Inc. [69]				/	Actuated with EMG sensors
Non-commercialized Devices	LOPES *(N/A)*	2007	Jan F. Veneman (University of Twente) [37]	*Partially	/			Joint trajectories training, actuated with EMG sensors
	ALEX *(N/A)*	2007	Sai K. Banala (Columbia University) [70]		/			Joint force training
	Haptic Walker *(N/A)*	2004	Schmidt, H. (Fraunhofer Institute) [71]	/		/		
	Gait Master 5 *(N/A)*	2010	Yano, H. (University of Ysukuba) [24]			/		
	Walkaround *(N/A)*	2008	Aleksandar Veg (Universtiy of Belgrade) [72]				/	Walk-assist with walking frame
	Standing Biofeedback Trainer *(N/A)*	1997	Alice M. K. Wong (Chang Gung Memorial Hospital, Taiwan) [63]	/				Standing postural training
	Anklebot *(N/A)*	2013	Massachusetts Institute of Technology [73]					Ankle rehabilitation

2.4 Control System and Control Strategies of Robotic Rehabilitation Devices

Active orthosis is worn on the subject with an impaired limb. The control system must deal with a possible lack of coordination between the user and the orthosis and with intrinsic limb dynamics. The primary objective of the control scheme for robotic rehabilitation therapies is the reproduction of motion sequences to facilitate patient recovery.

2.4.1 Control System of Robotic Rehabilitation Devices

Various control systems have been broadly implemented in the exoskeletons to keep track of the patient's gait trajectories during rehabilitation treatment. Figure 29 shows the simplified block diagram of a control system using a gait pattern generator. The structure of the control system usually involves a mid-level algorithm to detect the current gait sub-phase and different low-level controllers for each gait sub-phase. In several cases, finite-state machines are used for switching between the different dedicated or low-level controllers. Biomechanical signals such as Electromyography (EMG) signal obtained from the orthosis are fed back to both control levels to estimate the gait phase and to perform specific control tasks [36]. Furthermore, assistive control is also one of the most developed techniques for robotic devices. It uses external and physical assistance to help subjects achieve their desired movements, which stimulate brain plasticity. Besides that, these approaches can help patients to accomplish a correct gait pattern and improve their motor performance. Assistive strategies include impedance-based control, EMG-based control and adaptive-based control [34].

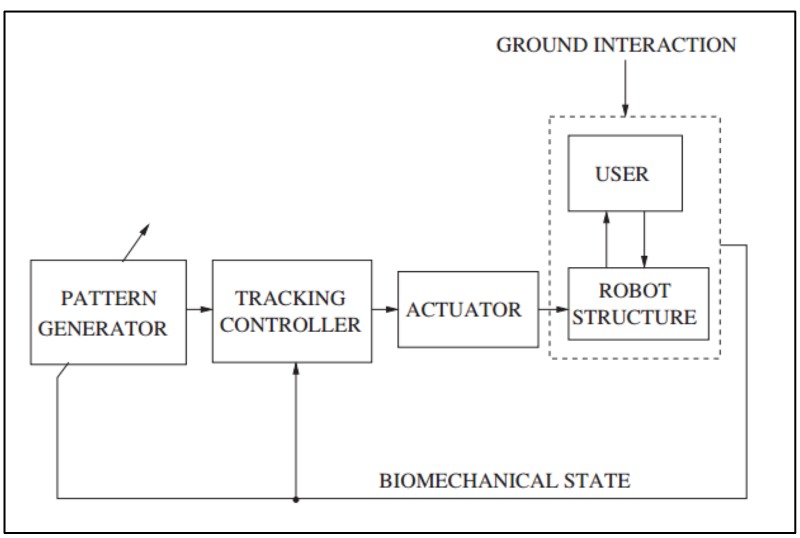

Figure 29 Main elements in a control system architecture with gait pattern generator [36]

2.4.1.1 Impedance-based Control

Impedance-based control is the implementation of assistive force when the human limb deviates from the normal gait trajectory. Strategies such as providing viscous force-fields, visual feedback in achieving the desired movement and pre-designed mechanical limits of the orthosis's movement are widely used. The assistive force is generated using an appropriately designed mechanical impedance. The mechanical impedance is the ratio of the force applied at a point to the resulting motion of that point. The greater the deviation of the movement from the desired trajectory, the greater the restoring force will be generated to overcome the overshoot of the movement. The controller provides a kind of assistive restoring force that increases as the participant deviates from the desire trajectory. It helps to provide forces for the limbs to achieve the correct gait. A few control systems were developed based on impedance control [34].

Active Leg Exoskeleton (ALEX) implements the force-field controller with visual feedback for lower limb rehabilitation training. The controller is used to apply desired force-field on the moving leg in the form of assisting or resisting the motion of the leg. Force-field controller provides low impedance when the subject moves in the desired trajectory and only offers high impedance when deviation is detected. A force-field is created around the foot with reference to the desired trajectory in the sagittal plane in addition to providing damping to it. The typical shape of the force-field "virtual wall" around the desired trajectory is shown in Figure 30. The red dotted lines around the desired trajectory (blue line) shows the width of the tunnel which represents the tolerance of the gait deviation [70], [74].

Since the virtual walls are used to guide the foot of the subjects, assistive and resistive forces are applied on the foot when gait deviation occurs. The device supplies both a combination of tangential, F_t and normal forces, F_n to the ankle joint with reference to the speed of desired trajectory. Normal force is applied to ensure that the foot is moving within the virtual tunnel while the tangential force act as a pushing force to move the foot along the tunnel in a forward direction. Let point P labelled in Figure 30 be the current position of the foot, N be the nearest point on the desired trajectory and d as the gait deviation. The controller is used to control the tangential forces to guide the ankle of the subject to move along the trajectory (blue line) and the normal forces to apply as an opposite reaction force to prevent the ankle from deviating from the desired trajectory. Hence, the assistive force varies for different subjects. This method can lead the subjects to gain more engagement in their training process [33], [34], [70], [74].

Besides that, the H2 robotic exoskeleton for gait rehabilitation was controlled by an impedance controller which created a force field around the desired joint trajectory to provide assistance to stroke patients. The assistance provided is based in their disability level. As shown in Figure 31, the input to the torque controller is converted from the output of the position controller fed with adapted trajectory. Then, the torque controller will estimate the output torque based on the motor's electrical current and the gearbox reduction rate with a value that is proportional to the trajectory deviation. Hence, this algorithm creates a force-field control that guide the subject's limb in a correct pattern. The controller only applies the sufficient amount of torque to move the joint when the subject is unable to complete their desired movement [75].

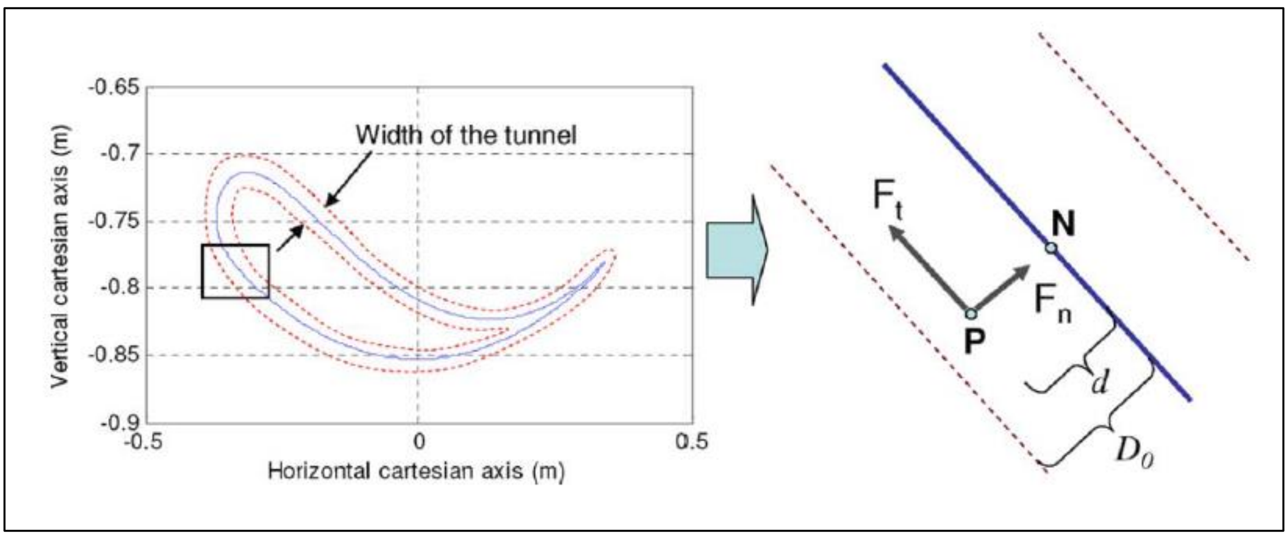

Figure 30 Cartesian plot of the ankle in the trunk reference frame, origin set at the hip joint. [74]

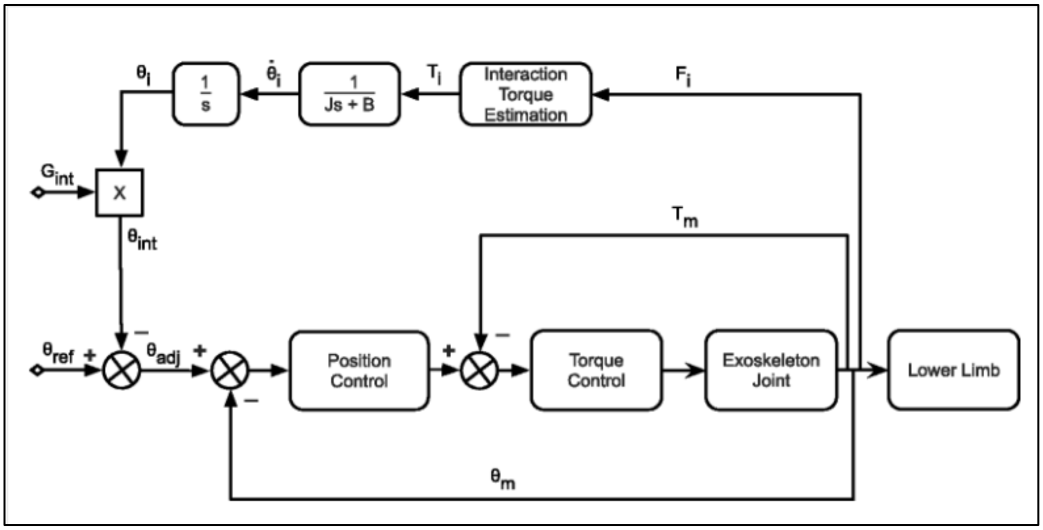

Figure 31 Force filed controller of the H2 robotic exoskeleton [75]

Besides, that, KineAssist also implementeds the impedance-based controller that can sense the lower limb movement. It is actuated with passive sliders and force sensors that are able to feedback on the pelvic motion of users and keep up with the direction of movements [25], [60]. Moreover, a variant of impedance-based assistance is triggered assistance which allows the user to attempt a movement without any robotic guidance. However, it can initiate some form of impedance-based assistance after some feedback variables reach a threshold. The triggered assistance encourages user to perform self-initiated movement which is beneficial for motor learning. The feedback variables could be force generated by the users, spatial tracking error, limb velocity or EMG signal [34].

The triggered method, also applied by the MIT-MANUS upper limb robotic therapy device, assisted users in moving along a minimum jerk trajectory when the participants exceed a movement error threshold, or move faster than the desired velocity [76]. A force-based trigger assistance was applied in MIME robotic device. This device consists of two force-based modes. For the active-assisted mode, the assistance is triggered when the participants apply force to move the robotic device. However, for the active-resisted mode, the robot provides viscous resistance in the direction of desired movement when the subject attempts to reach the target for strength training [26], [77]. However, there is a drawback of the triggered assistance as the assistive force is only produce when the trigger is activated; the weight of the resting robot becomes a burden to the users when the control system is not activated [34].

2.4.1.2 EMG-based Control

Some devices implemented the use of surface electromyography signals (EMG) to drive the assistance. The structure of EMG-based control is shown in Figure 32. EMG signals obtained from specific muscles can be treated as an indicator from the muscle to activate assistance [34]. An example of upper limb rehabilitation device, the MIT-MANUS robot, was proposed with EMG-based control. EMG signals are collected from different muscles on the elbow and shoulder. The signals are used to trigger assistance when they are above a threshold [76].

Some devices generate assisting force proportional to the amplitude of the processed EMG signal for arm movement or for walking. This approach help to control the users' movement according to their desired movement, while the robotic device compensates for generating a force proportional to the EMG signal needed to perform the movement [36].

HAL is one of the lower limb robotic devices that has implemented the EMG-based controller for assistive purposes. The relative amount of assistive force will be generated according to the amplitude of the EMG signals received from the relative muscles [36]. Recent study on Lower-Limb Exoskeleton System also applied the EMG control by reflecting the change of muscle strength and movement trends of the lower extremities to adjust the current status of the system to perform desired actions [78].

However, there are some limitations for this approach as the EMG signals are sensitive to electrode placement and easily affected by the neighbouring muscle signals. The controller needs to be calibrated for each subject in every experiment or treatment. Another issue with this approach is that if an unusual muscle signal is detected, the robot could move in an undesired way and cause danger to the user [34].

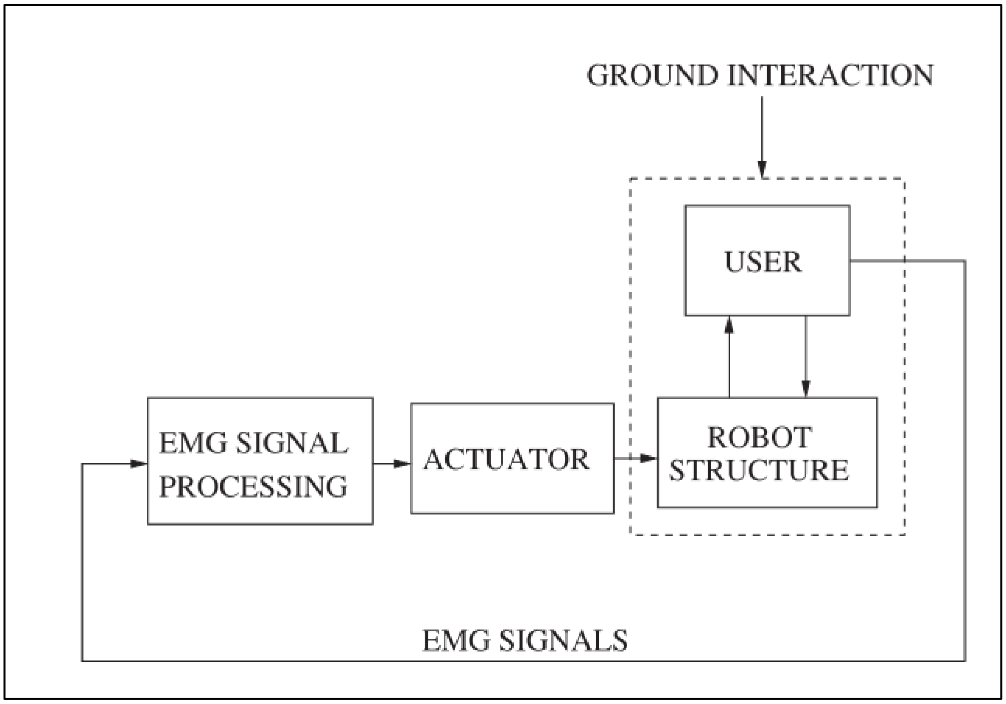

Figure 32 Structure of EMG-based control [36]

2.4.1.3 Adaptive-based Control

Adaptive control is popular for control system design to deal with uncertainties. An adaptive controller has the ability to adjust itself to handle unknown model uncertainties which makes its the key difference from linear controllers. This controller is generally divided into two groups: direct and indirect. Direct methods are able to estimate system parameters and directly apply then into in the adaptive control. However, indirect methods estimate system parameters in the plant and use the estimated model information to further adjust the controller [79].

The adaptive technique can also be applied to tune the trajectories of the subjects to match the desired gait of the exoskeleton. The need for the adaptive controller becomes more acute when it is needed to provide mechanically compliant assistance for movement. The system must calculate a suitable amount of force to cancel the effects of increased tone, weakness, or lack of coordinated control by the user. The variables vary broadly between the users, hence, suggests the use of adaptive controller. The adaptive-control parameters allow assistance to be tuned automatically to suit the subjects throughout the rehabilitation training [34].

Lokomat is the first device to implement this system. It is designed to take patient intention into account, instead of imposing an inflexible control system [80]. The adaptive control algorithm adapts the reference gait pattern by minimizing the interaction torques between the robot and subjects. This algorithm is implemented based on iterative learning control (ILC) to adjust the supportive torques. The controller functions as an assistance by providing the amount of additional supportive torque only when needed in order to keep the subjects continuously challenged [34], [81].

The block diagram of the control system is presented in Figure 33 where q_d is the reference trajectory, τ is the interaction torque estimated from the forces of knee and hip , and *F* and *q* is the output trajectory of the Lokomat. The dotted line with arrow as shown in Figure 33 is the representation of the impedance magnitude adaptation. The constant trajectory inputs are adapted to the impedance controller parameters. When there is a minimal force detected from the subject via the force sensors, the impedance controller will provide an extra force to the system to enable the motion of the Lokomat to reach a desired movement. The impedance parameter will be deducted when a desired force or effort is detected from the patient [80].

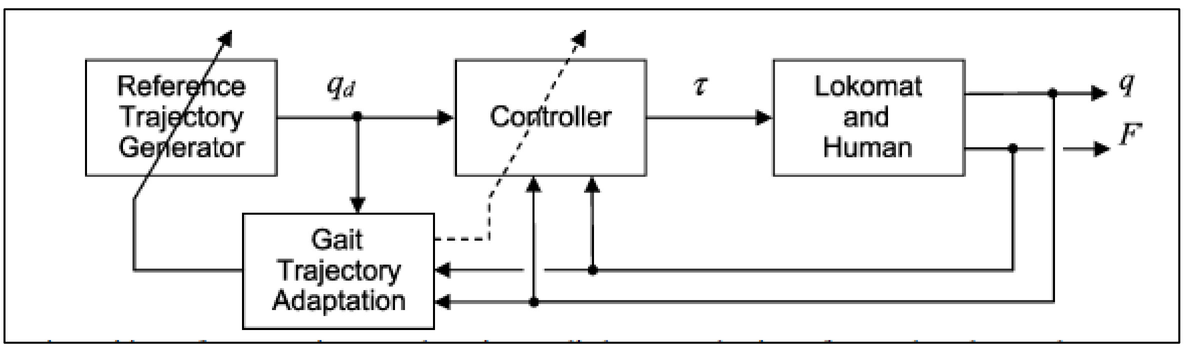

Figure 33 Adaptive-based control system of Lokomat [80]

The active ankle-foot orthoses (AAFO) has been proposed to assist drop-foot gait in hemi-paretic patients with impedance-based adaptive control system. Drop-foot patients often suffer foot slap during walking. Hence, the adaptive controller is used to control the stiffness of the orthotic torsional spring stiffness when substantial foot slap occurred. When a foot slap occurs, the differential of the forefoot force will be a negative value and the stiffness of the robot will increase. The robot's stiffness during controlled plantar flexion is adapted based on the number of foot slaps in the last 5 steps. The stiffness of robot reduces by a certain amount when no slaps are detected and increases proportionally to the number of slaps when more slaps are detected [82].

Lu et al. [83] implemented adaptive control and learning control techniques into the exoskeleton system for guidance of desired gait movement. Besides that, this controller is developed to solve periodic uncertainties with known periods. The adaptive control law mainly consists of three components -- the feedback law of tracking error, impedance parameters and also the estimated uncertainty. These components are adjustable to obtain a desired gait movement of the exoskeleton. This controller was proven to have the ability to track every single and periodic movement of the lower limb exoskeleton [83].

In another variation, adaptive Fuzzy controller is implemented for the 10 DOFs gait rehabilitation exoskeleton as presented in [84] to ensure proper trajectory control for patient to exercise according to a fixed reference gait pattern. The controller is implemented to regulate the lengths of the pneumatic actuators on the exoskeleton during rehabilitation training. As shown in Figure 34, the controller basically consists of a main Fuzzy controller and an additional Fuzzy controller. The controller input signals are the displacement error and error change rate of the pneumatic actuators, while the output signals are the control voltages of valves connected to the anterior and posterior cylinder chambers. The function of the controller is to control the adaptive parameter in order to cope with the dry friction of the pneumatic actuators which has a strong negative influence on system control accuracy. As the dry friction changes with the working conditions, the normalized controller parameter is tuned to change the controller's transform characteristics for both Fuzzy controllers. This controller was tested on the embedded real-time system and accurate trajectory control as well as the high robustness of the system are achieved [84].

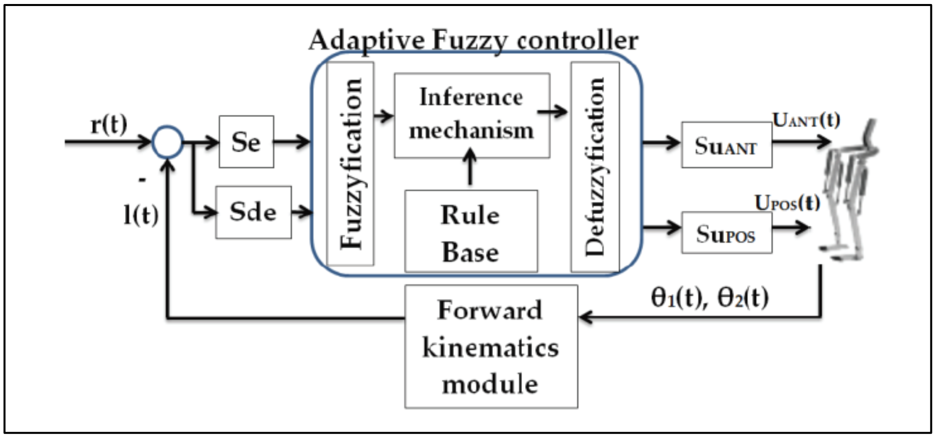

Figure 34 Architecture of adaptive Fuzzy control system [84]

2.4.2 Control Strategies of Robotic Rehabilitation Devices

2.4.2.1 Sliding mode Control

The Sliding Mode Control (SMC) is known as a robust control strategy which is well-known for positioning control in recent years. It is a nonlinear control technique with significant properties of accuracy, robustness, easy tuning, and implementation. The SMC system is designed to guide the system states onto a particular surface in the state space, called sliding surface, and to ensure that the states remains around the sliding surface. This controller mainly consists of two phases: design of siding surface based on the control application, and selection of appropriate control law. SMC has proven especially suitable for the design of robust control for rehabilitation robot with nonlinearities, parameter uncertainties and bounded input disturbance. It is widely used as the feedback control to counteract system uncertainties and is particularly useful for lower limb rehabilitation systems with friction [85]–[90].

The knee joint actuated orthosis is implemented with second order Sliding Mode controller (Figure 35), known as the "Super-twisting" algorithm to control the shank-foot-orthosis for desired position tracking. The sliding surface of the controller is formed based on the time derivatives of the differences between the current and the desired states of the system. Super-twisting algorithm is applied to overcome the chattering phenomenon that consists of sudden and fast variations of the control signal. Based on the proposed sliding mode control law, the controller can calculate in real time the necessary torque needed by the knee joint according to the subject's intention and hence, generate the corresponding torque for desired joint movement [91].

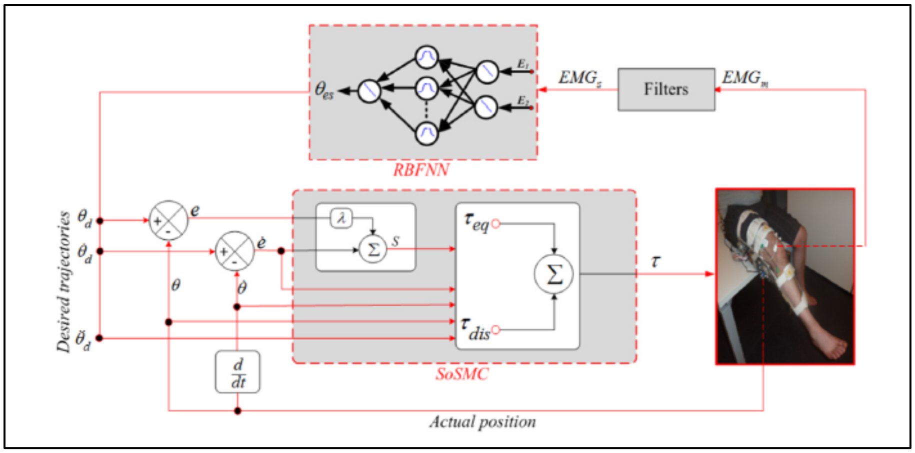

Figure 35 Block diagram of the knee joint actuated orthosis [91]

2.4.2.2 Neural Network Control

The neural network consists of simple elements operation in parallel. The form of simple elements (neurons) is inspired by the biological nervous system. Neural Network can be custom trained for a particular assignment by altering the connection parameter (the weight) between each element (the neuron) [91]. Neural Networks are famous learning models in process industry as a replacement of PID control. The parameters of neural network could be estimated through learning algorithm with data sets before any proper application, to allow it to cope with various uncertainties during actual implementation [92]. It can effectively estimate various nonlinear function under certain conditions and require minimum information from the system [93]. Neural Networks have been widely used in the control of robotic manipulators in recent years [92], [94]–[98].

The Radial Basic Function Neural Network (RBFNN), as shown in Figure 36, is a type of Artificial Neural Network that uses radial basis functions (RBFs) as activation functions. The characteristics feature of the RBF is that their response decrease monotonically with distance from a central point. Figure 37 illustrates a typical Gaussian Radial Basis Function with center c = 0 and radius r = 1 [99]. The output of the RBF neural network is a linear combination of radial basis functions of inputs and neuron parameters. RBF neural network has been shown to have a universal approximation ability, fast convergence and good approximation of system dynamic [91].

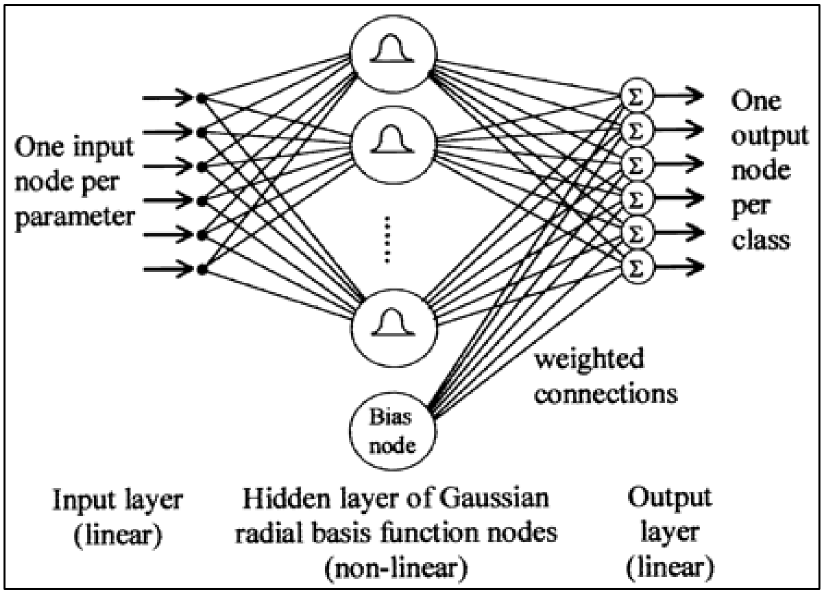

Figure 36 Schematic diagram radial basic function neural network (RBFNN) [100]

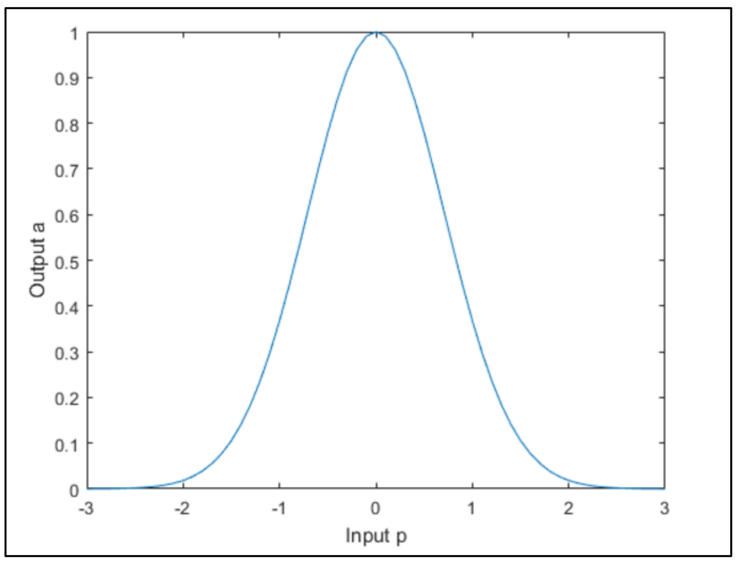

Figure 37 Gaussian radial basis function

The WHERE-II system consists of a mobile vehicle with a one-link robot arm, a pneumatic BWS mechanism, a user intention analysis system and a safety system. This mobile vehicle is developed for effective gait rehabilitation with body weight support (BWS) mechanism. A control algorithm based on Radial Basic Function Neural Network (RBFNN) was used to compensate dynamic interaction, not modelled dynamics and disturbance of the pneumatic actuators. The neural network was developed with adequate high number of hidden units in order to compensate the ground reaction force errors resulting from the system's mass, friction and strain. Besides that, another neural network-based methodology was developed for the velocity control of the system with dynamics and disturbances. Clinical and experimental trials have proven the effectiveness of the proposed control system for gait rehabilitation system [35].

The Radial Basic Function Neural Network (RBFNN) as shown in Figure 38 is implemented by the knee joint actuated orthosis as discussed in Section 1.1.2. This neural network can approximate the nonlinearities between the neural muscle excitation and the resulting knee joint position. The RBFNN is trained to estimate the subject's desired position based on the electromyography (EMG) signal produced by the quadriceps muscle [91].

Apart from the commonly used neural network control, SAGA University of Japan proposed the Neuro-fuzzy controller with more effective hierarchy for upper limb and wrist rehabilitation device [101]. Neural network is good at pattern reorganization but is poor in explaining how it reaches the decision. However, fuzzy logic can reason with imprecise information, good at decision explanation but cannot automatically obtain the rules for decisions making. The limitations of both system lead to the creation of the Neuro-fuzzy controller that combines the neural network control and fuzzy logic to overcome the limitation of individual techniques [102].

In later years, a motion controller based on Neuro-fuzzy network is established to predict human motion intention in advance and control the lower limb exoskeleton in real time. This controller integrates the EMG with joint information, angle and interaction force in real-time to perform human motion prediction and control the human-machine system. The functionality of the controller is validated with experimental results. As shown in Figure 39, the Neuro-fuzzy network based on Takagi Sugeno Kang model with five layers is implemented. Each layer of neural consists of fuzzy linguistic variables of fuzzy membership function to determine the angle of flexion and extension of muscles. With the integration of multi-sensors and information, the Neuro-fuzzy controller is able to decode human motion intention in advance and also to transmit control information in real-time [103].

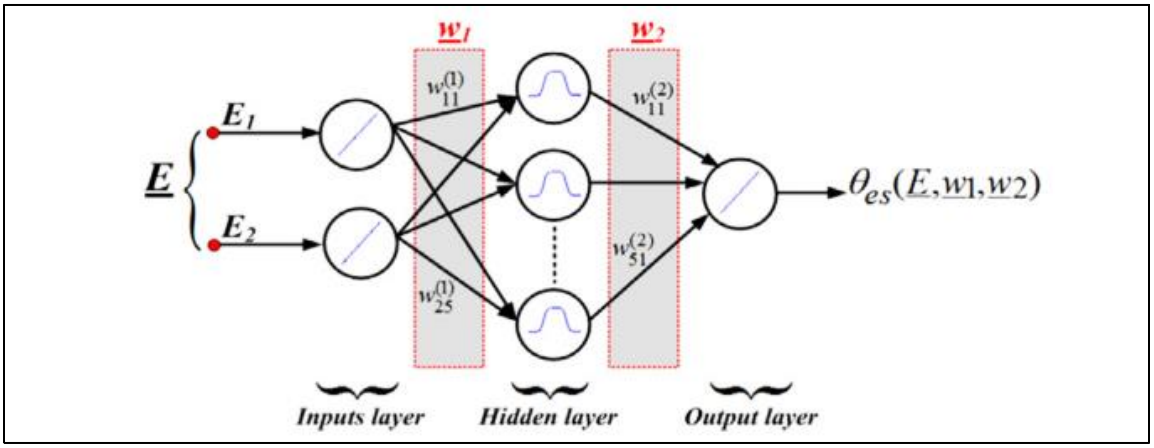

Figure 38 Radial basis function neural network of knee joint actuated orthosis [91]

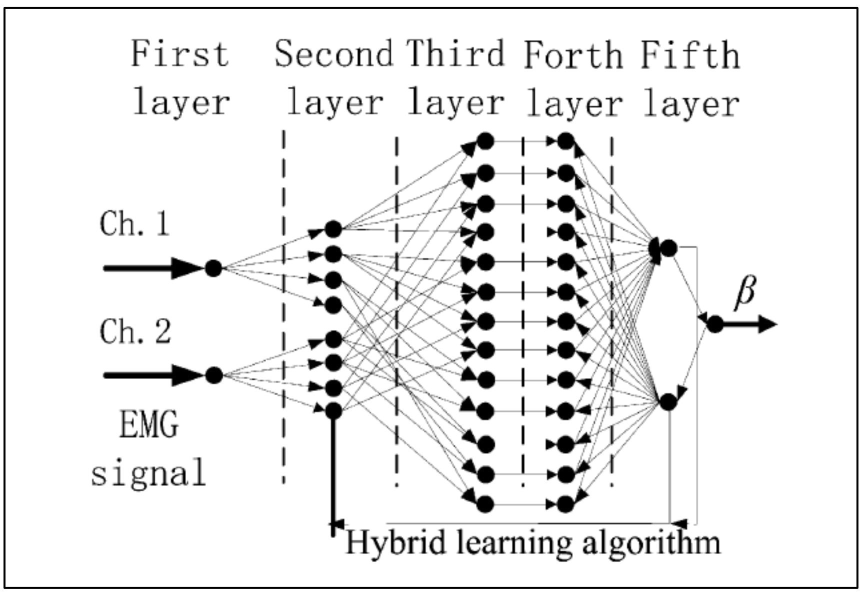

Figure 39 Neuro-fuzzy network [103]

2.4.2.3 Describing Function

Control systems are widely used in industrial and robotic control application. However, not every system can be represented with a mathematical model, especially a nonlinear system. A successful control system design must be performed by taking into account the nonlinear terms of the system. Describing function has been used to analyze and diagnose the nonlinear system. However, in the past two decade, there is rich literature that suggests that the describing function approach is a versatile tool for systematic design of nonlinear control system. [38], [39], [104].

Describing function is a linearization of a nonlinear element subjected to a sinusoidal input. It is an approximate method to characterize the nonlinear system. The aim of the use of the describing function is to reduce the gap between the control system analysis and design of nonlinear system with the rich theory of linear system [38], [104]. The most commonly used describing functions are the sinusoidal-input describing function (SIDF) and the random-input describing function (RIDF).

Sinusoidal Input Describing Function Approach

In 1983, a new platform for the design of classical nonlinear feedback control system based on one, two or more than two describing-function models of the plant was introduced. This platform had been applied to design robust nonlinear feedback system in position control of robotics and aerospace industries [105]–[107]. In the year of 1987, a computer-aided engineering (CAE) environment for input/output characterization of highly nonlinear systems is published. This approach is based on obtaining the SIDF models of the nonlinear plant. The SIDF modes are obtained by exciting the plant with a sinusoid of know amplitude and frequency, integrating the dynamic equations of motion to obtain system output, and finally evaluating whether Fourier integrals with system output is at a steady state. However, the software is limited to single-input single-output, nonlinear, time-invariant, deterministic and stable systems [108]. Figure 40 shows the flow chart of the developed software. The sinusoidal input signal is as follow.

$$u(t) = u_o + a\cos\omega t \qquad (1)$$

Where, u_o is the DC component of the input signal, $u(t)$, a is the amplitude level of the excitation signal, and ω is the frequency of excitation level.

In the year of 2002, a Fourier-based approach is used to obtain pseudo frequency response data known as SIDF model with a software developed in MATLAB environment with the *invfreqs.m* command. This command is capable of characterizing the input/output behaviour of the multivariable nonlinear process [39]. The study is then followed up by extending the previous design to a highly nonlinear multivariable system. A new software based on generating the SIDF models of a plant with nonlinear optimization technique is developed [109]. A recent application of this design platform is applied for idle speed control of uncertain automobile engines. The method is used to obtain the actual internal combustion engine model which includes discontinuous nonlinear terms. The describing function approach is implemented to handle the discontinuous models and a classical controller is designed using the algebraic approach via the computer-aided method. The designed controller is successfully applied to a real automobile engine and it is able to account for the time delay [110].

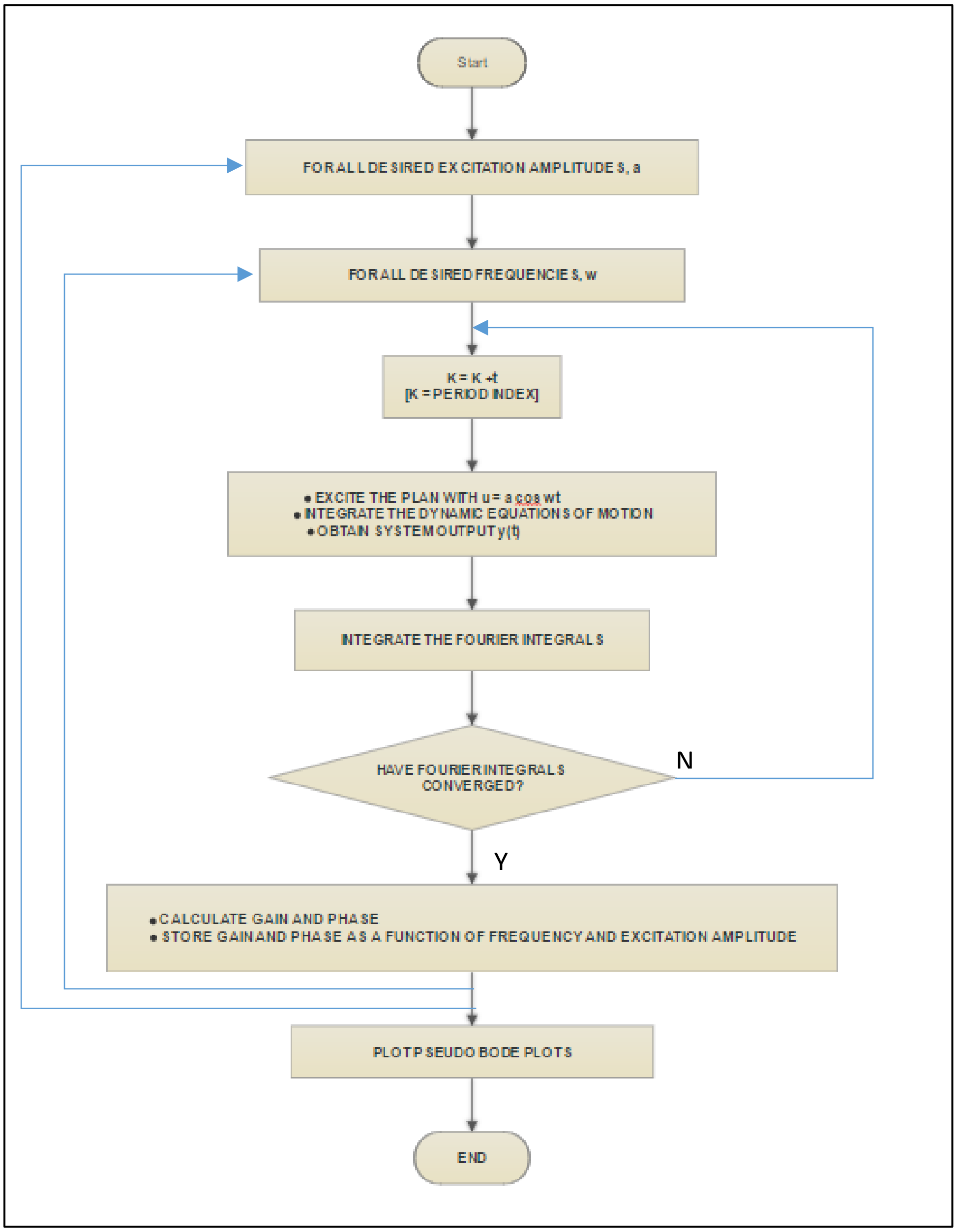

Figure 40 Flow chart of the computer-aided engineering (CAE) software [108]

2.5 Critical Reflection on Literature Review

Active assist practice is the primary control paradigm that has been widely explored in robotic therapy development. The active assist practice uses external, physical assistance to help subjects in accomplishing desired movements. Control systems including the impedance-based control, EMG-based control and adaptive-based control are reviewed. Besides that, sliding mode control, Fuzzy logic and neural network control are popular for lower limb rehabilitation device in the past decade.

2.5.1 Advantages and Disadvantages of Different Design Approach in Active Devices

Active devices often come with various design approach to fulfil the primary purpose. As mentioned in Section 2.3.3, commercialized and non-commercialized robotic rehabilitation devices usually consist of common features such as body weight support, treadmill, end effector, and mobility. Each feature plays its role in helping patients during rehabilitation training.

Devices such as Lokomat, Lokohelp, ReoAmbulator, Gait Trainer, KnieAsist, and Haptic Walker are actuated with body weight support features. This feature provides a safe environment for patients during rehabilitation as the safety belt will hold them in position whenever they lose balance or have no strength during training. The only drawback of this feature is that patients might tend to rely too much on the body weight support during the rehabilitation session. Patients might experience stagnation in training progression.

Apart from body weight support, some devices such as Lokomat, ReoAmbulator, LOPES, and ALEX are designed to work with a treadmill. The advantages of involving a treadmill in rehabilitation include allowing patients to get used to walking in different speeds and experiencing different steepness of slopes. Patients would easily discover their improvement when they are able to complete higher level tasks in each rehabilitation session. The downside of rehabilitation programs with treadmill is that patients easily fall from it when they lost control of balancing without body weight support.

Active devices utilizing end effector, such as Lokohelp, Gait Trainer, Haptic Walker and Gait Master can simulate symmetric walking pattern and provide training with various terrains via simulation during rehabilitation. However, there is a common disadvantage of devices discussed above where gait trajectory and angle of joint of lower limb are not concerned in the rehabilitation session. Patients might regain a walking ability after the training, but they might not be able to walk with a balanced posture or symmetric pattern if the joint movements of both legs are not trained to synchronize with each other.

Mobiles devices such as HAL, KineAsist, Walkaround and Rewalk are small and easy to carry. Patients can carry out their training at anytime and anyplace with these mobile devices without aid. The weaknesses of mobile devices are inadequate power supply from a transportable battery and the heavy weight of suit acting on user. Other devices designed with sensors to perform trajectory control, joint forces control, and ankle rehabilitation are also benefcial to patients as the performance of patients is always observed.

2.5.2 Advantages and Disadvantages of Control Architecture

Among the discussed control architecture for rehabilitation orthosis, all their advantages and disadvantages are seen. The impedance-based control systems generate assistive force for the robotic device when the human limb deviates from the normal trajectory during rehabilitation training. This control strategy does not intervene in the system until it is triggered, when the subject deviates from the reference trajectory. The main advantage of this control strategy is its inherent robustness to robotic device and environment modelling errors. However, this might lead to an ineffective gait rehabilitation training as the subject might experience false or distorted trajectory during rehabilitation since the controller is only triggered when errors are detected.

Furthermore, the EMG-based control is implemented to drive the assistance based on electrical signal obtained from muscle activities. The occurrence of electronic signal is earlier than the motion of human limbs. Hence, it is ideal in counteracting the delay of the control system and computing the output signal to regulate the robotic device. However, the wave form of EMG signal varies from subject to subject even though the same activity is performed. Besides, EMG signals are very sensitive to environment conditions and disturbance signals such as humidity and noise. Therefore, calibration needs to be done for each subject in every rehabilitation training or experiment which is very time consuming.

Adaptive control is common in control systems designed to deal with uncertainties. The main difference between adaptive controllers and linear controllers is that the adaptive controller can modify its behavior in response to the changes in dynamics of the processes and the disturbances acting on the process. However, the adaptive controller is an open-loop adaptation system without learning ability and intelligence. Furthermore, the design required for its implementation is enormous.

Apart from the control system discussed, various control strategies such as sliding mode and neural network are widely implemented in robotic rehabilitation devices. Sliding mode control has proven especially suitable for the design of robust control for rehabilitation robot with nonlinearities, parameter uncertainties and bounded input disturbances. However, a fundamental limitation was found in sliding mode control with fixed sliding mode gain, which is that it cannot handle large modelling uncertainties and external disturbances of the complex model. Hence, recently developed controllers often combine the sliding mode with various control strategies such as adaptive control and impedance control to overcome the fundamental restriction.

Besides that, the neural network control is broadly used for the control of robotic manipulators in recent decades. Artificial neural network has been widely employed to design controllers for nonlinear systems. It has many advantages such as simple construction, parallel processing, and adaptive learning. One of the major drawbacks of this controller is that the training of controller requires a large diversity of training data and the training is time consuming. Moreover, hardware issues often occur as vast amount of computer memory and hard disk space could be consumed during the process of neural network design.

2.5.3 Recent Trends of Control Scheme and Strategy of Rehabilitation Robotic Devices

Adaptive control, sliding mode control and neural network control are currently the most common controllers applied by developers for lower limb rehabilitation robotic devices. Besides that, the combination of various control strategies to form a new controller is popular in recent years [84], [86], [97], [103], [111], [112]. An adaptive control scheme by incorporating learning control approaches into the rehabilitation exoskeleton system is developed to adjust the subject's trajectory and deal with periodic uncertainties [83]. Gait trajectory adaptation control strategy was proposed to modify the gait trajectory of the 5-link model based gait rehabilitation exoskeleton prototype, based on the deviation of joint driving torques [113]. This strategy is also applied by Wu et al. [111] for a compliant gait trajectory planning.

Furthermore, a control architecture that contains a sliding mode adaptive controller is designed to perform trajectory tracking of a lower extremity exoskeleton [112]. Developers also combined the sliding mode control, impedance control and adaptive control to form a robust controller that is able to regulate both position and contact force of the lower rehabilitation robot [86]. Adaptive Fuzzy controller was successfully designed by Koceska et al. [84], and was successfully implemented and tested for accuracy and repeatability.

Moreover, fuzzy logic was employed in neural network by Yin [103] to predict human motion intention in advance and control the exoskeleton in real time. Neural network is also employed for the development of two mobile gait rehabilitation systems based on Radial Basis Function [114]. A knee joint actuated orthosis is driven by a Radial Basis Function neural network and a second order sliding mode control to assist the movements of dependent subjects [97]. Table 6 summarizes the recent trend of control strategies applied for lower limb rehabilitation system as discussed.

Table 6 Timeline of control strategies for lower limb rehabilitation devices

Year	**Controller**	**Reference**
2009	Radial Basis Function Neural Network (RBFNN)	[114]
2010	Gait trajectory adaptation control strategy	[113]
2011	Neuro-fuzzy network	[103]
2013	Adaptive fuzzy controller	[84]
2013	Adaptive Sliding Mode Impedance Control	[86]
2014	Adaptive control scheme	[83]
2014	Second order sliding mode control (SoSMC) and neural network control (NN)	[97]
2014	Adaptive control with PID controller	[111]
2015	Sliding Mode Adaptive Control	[112]
2015	Impedance-based force field control	[75]

2.5.4 Discussion and Motivation of Research

After reviewing several aspects and control scheme in this chapter, further understanding of each field is gained. Throughout the review, the biomedical aspect is essential for the development of rehabilitation devices. The proper human walking manner is studied, and various characteristics of walking are shown. The important of a balanced walking posture, symmetric walking pace, and timing of joint angle is highlighted. Thus, gait trajectory with angle-time characteristics is proposed for the development of the device. This study has a direct impact on the design focus of the orthosis to maximize the outcome of rehabilitation.

According to studies of various active devices, features such as body weight support, end effectors sensor and trajectory control play respectively important roles in a rehabilitation device and hence, a design that includes these features is recommended. Flexibility of each link with adjustable sizing is important to fit onto patients as their length of hip and knee may vary. A support frame is suggested to hold the orthosis in place to reduce weight burden on patients and to act as a handrail for patients to hold and balance themselves. Sensors can be implemented to feedback patients' movement and record their training data while actuators such as servomotor can provide position guidance and force support for patients to move their limb.

An effective control system is essential to provide precise control to the rehabilitation orthosis as it is equipped with numerous manipulators, actuators and sensors which lead to the presence of nonlinearities, parameters uncertainties and disturbances. Advantages and disadvantages of various approaches are discussed. Although a substantial research for recent developed control strategies is done, the field is rapidly evolving, and it is challenging to identify the most effective control algorithm. Besides that, there is still doubt on which robotic control approaches can bring the greatest benefits to the subject with a simple implementation. Hence, a few directions are suggested for future research.

The first direction is to focus on the development of a robust control system with a simpler technique during implementation. A complex control system should be avoided to reduce the simulation time and hardware issues for database and memory consumed during simulation. Meanwhile, the next focus is to develop an intelligent controller with learning ability for specific tasks. The learning algorithm of the controller can help to improve the system effectiveness over each training. Lastly, a combination of various strategies to overcome the limitations of each controller is recommended for the development of a novel control scheme. This method can help to enhance the function and effectiveness of the controller as each of them has its own benefits and drawbacks. Finally, SIDF method is suggested to linearize the system transfer function and make use of the outcome for controller development via MATLAB functions.

2.6 Conclusions

In this chapter, the biomedical aspect of lower limb such as biomechanics of human walking, gait cycle including the timing of gait cycle and gait graph are presented. Studies in the biomedical related aspect helped to review more on the human structure and mechanism of body movement which are important in the design of hardware and control strategies for the rehabilitation machine. Next, the robotic aspects are also discussed in this chapter. Various lower limb rehabilitation robots including treadmill training devices, foot manipulators, mobile and other non-categorized design are reviewed. Table 5 that summarizes commercialized and non-commercialized rehabilitation devices are presented. Moreover, various popular control strategies such as impedance-based controller, EMG-based controller and adaptive-based controller are discussed. Also, recent trends of control strategies for robotic devices include sliding mode control, neural network control and describing function with controller are reviewed. Lastly, a critical reflection of the chapter incorporated with motivations for future research is presented. Discussions and justifications of the final approach for the research in each aspect is conversed.

Chapter 3 Setup and Dynamic Model of Two-link Robotic Orthosis

3.1 Introduction

This chapter aims to explain the preliminary setup of the actuator model used in the proposed robotic orthosis by showing the mechanical setup, as well as the justifications for using a two-link model as the main structure. In addition to that, the circuit connections of all components are also presented alongside the electrical and electronic components of the system. Lastly, both the dynamic model and the mathematical model of the robotic orthosis using the Langrangian method is reviewed to provide further clarification.

3.2 Justification of Two-link Robotic Orthosis Design

The robotic rehabilitation devices are often categorized into 4 designs: body weight support, treadmill, end effector and mobile devices. Each design has a positive impact on its rehabilitation application. Hence, in this research, a robotic orthosis is developed with reference to these characteristics. Furthermore, the biomechanics of human walking involve leg movement in the sagittal plane and coronal plane by moving 3 major body parts, which are the hip, knee and ankle. Hip and knee are moving (leg bending) in the sagittal plane while ankle is moving in the coronal plane. Hemiplegic stroke patients are usually unable to balance their body and walk with an asymmetric pattern due to muscular weakness as seen in the gait graph plotted in Figure 14. Hence, a rehabilitation device with movement correction in these 3 major body parts is aimed to be developed to provide the best rehabilitation training environment for stroke patients.

The first stage of the research focuses on developing a two-link robotic orthosis to control the movement of hip and knee as the sagittal plane is the major plane of motion in the human walking kinematic model. The current stage of work will study to the knee and hip motion as these two parts dominate the movement of the lower limb. Motion of the ankle in another direction, the coronal plane, will be done in future work due to timing constraint for a three-year research. Symmetric movement of left and right legs are aimed to be developed in future research with high-level trajectory control.

Hemiplegic stroke patients often experience muscle weakness in one side of the body after stroke occurs. More than 80% of stroke survivors suffer from limitation in activity of daily living (ADL) and mobility. Impairment of patients causes their walking speed to be reduced, as compared to the original speed.

Hence, a rehabilitation orthosis is essential not only to train patients to walk, but to help them to regain a normal walking speed and symmetric gait pattern in order to perform ADL just like before they had stroke.

The newly ergonomic and lightweight design of two-link robotic orthosis is chosen to guide the moving angle of hip and knee joints. The reference moving angle for hip and knee at each instant obtained from [48] are applied. Figure 11 and 12 shows the plots of hip and knee motion. Each joint of the link is attached with servomotor and sensors. Servomotor is used to provide movement guidance at each instant and to support patients when they lack energy to move their limbs. Position sensors are utilized for motion feedback. The feedback signal will be compared to the desired trajectory of a normal gait, while the controller will compute an appropriate amount of torque to help patients in their rehabilitation training. A conceptual diagram of the application of robotic orthosis is shown in Figure 41.

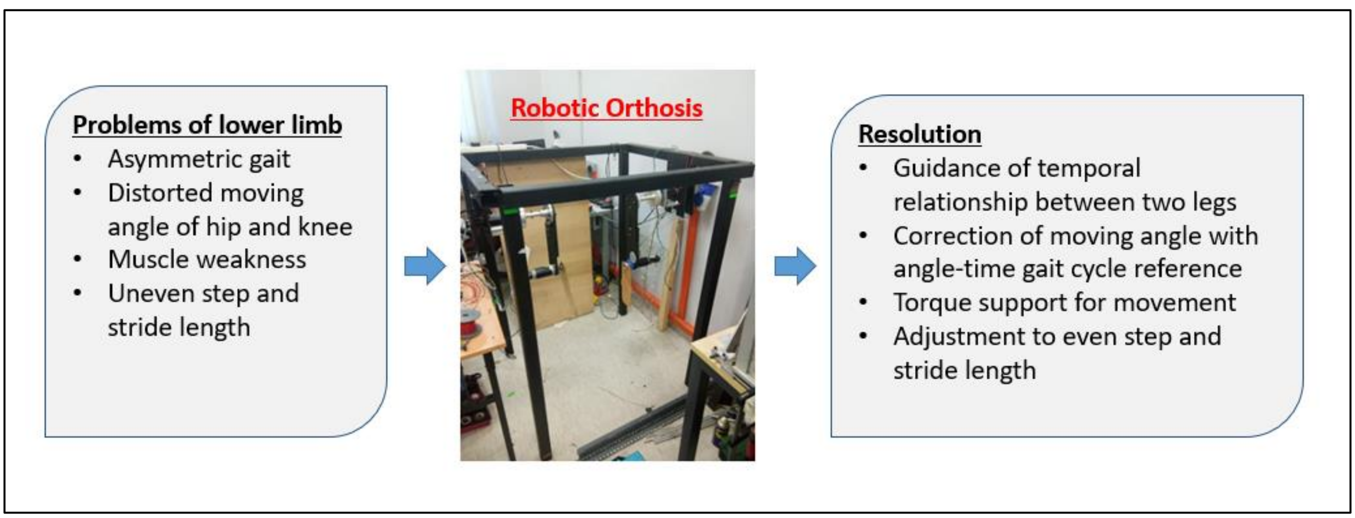

Figure 41 Conceptual diagram of robotic orthosis application

3.3 Mechanical Setup of Robotic Orthosis

The two-link robotic orthosis is designed at the first stage of the research. Various lower limb devices are reviewed, and information on human walking pattern is collected. Based on the findings, an ideal prototype with an ergonomic design and lightweight feature is developed. The major mechanical parts of the robotic orthosis consist of the support frame of the device, the assembly parts for DC servomotor, exoskeleton components (known as links of robotic devices in this thesis), and extendable parts. The detailed drawing and dimension of the parts are shown in Appendix A while the main assembly of the robotic orthosis and assembly parts are recorded in Appendix B.

3.3.1 Support Frame

A support frame to hold the robotic orthosis is built. It also serves the function as a handrail of support for subjects to balance their body during the training sessions. The support frame consists of a total of 20 steel bars, four extension motor plates, four motor plates, four square bars, four horizontal square bars and four vertical square bars. The used of the extension motor plates are to hold the DC servomotor in place using bolts and nuts on the motor plate. The motor plates are designed with two rows of holes at both side of the plate to allow the adjustment of position of the DC servomotor to suit the height of subjects. The square bars and horizontal square bars are designed with a wide space of 950 mm x 906 mm within the device to allow movement of subjects during rehabilitation training. Last but not least, there are four vertical square bars that act as the 'leg' of the device. These bars are made of rigid acrylic and HDPE to form a lightweight orthosis in order to reduce burden on the stroke patients.

3.3.2 Extendable Shaft and Motor Assembly

Next, a set of extendable shafts is designed. This part of the robotic device consists of an aluminium inner shaft, an aluminium outer shaft and a set of M5 bolt and nut. The major purpose of the extendable parts is to provide elongation and shortening of the motor shaft to allow adjustment of the position of the attached link to reach the thigh of the subject. With the adjustable shaft from both sides of the exoskeleton, the distance between left thigh and right thigh is free to be set according to the size of breech. Then, the extendable shaft is attached to the gearhead of the DC servomotor with a hub as shown in Figure 42.

3.3.3 Exoskeleton Assembly

The lightweight exoskeleton of the robotic orthosis consists of two major parts which are the link 1 and link 2 as shown in Figure 43, and are assembled as shown in Figure 44. Link 1 is the combination of exoskeleton thigh 1 and exoskeleton thigh 2. The purpose of separating the thigh into two components are to allow flexibility of the link to be adjusted according to the length of the subject's thigh. Both components are attached together using bolts and nuts. The top part of link 1 is attached to the hub as shown in Figure 42. Link 2 of the exoskeleton only consists of one component as no adjustment is needed in the current development of the robotic devices which focuses on the movement of thigh (hip) and calf (knee).

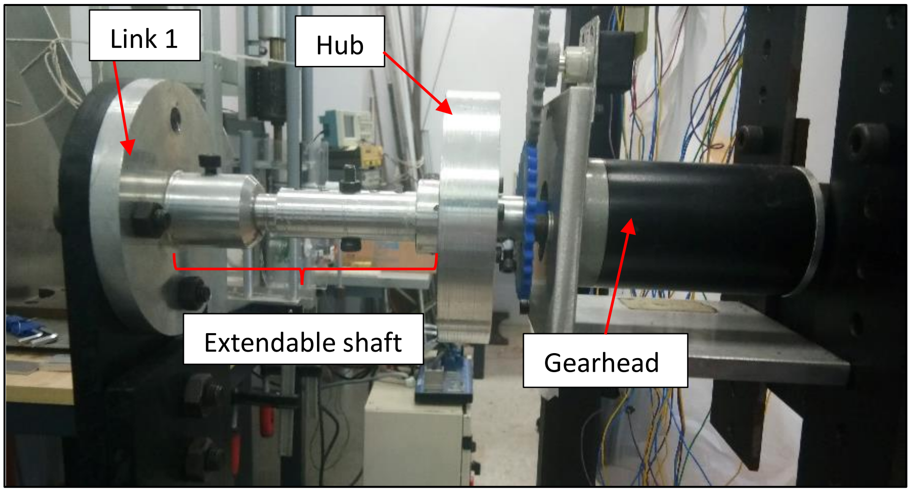

Figure 42 Extendable shaft and motor assembly

Figure 43 Hardware of link 1 and link 2

3.3.4 Main Assembly of Robotic Rehabilitation Device

Figure 45 shows the mechanical setup of the robotic orthosis including the support frame, extendable shaft, motor assembly and exoskeleton assembly. Four DC servomotors with gearbox and encoder are actuated at each joint (knee and hip) perpendicularly to the sagittal plane to allow joint movement. The total dimension of the system is 1205 mm x 1050 mm x 916 mm.

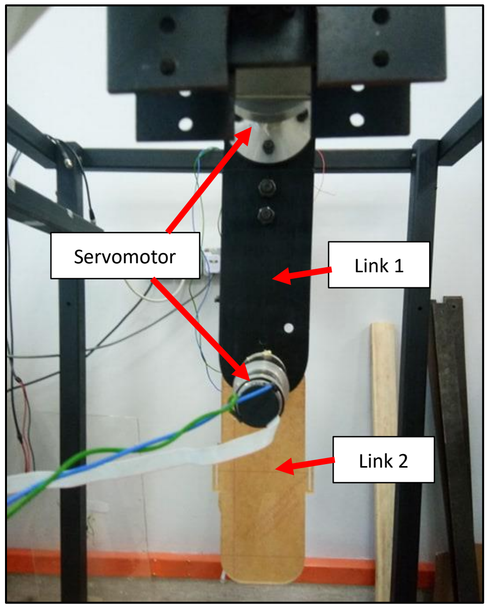

Figure 44 Exoskeleton assembly

Figure 45 Mechanical setup of the robotic orthosis

3.4 Electric and Electronic Design of Robotic Orthosis

Various electrical and electronic components are implemented in this system. In the first stage of the development of the robotic orthosis, Arduino Due is used to perform electronics components testing and low-level controller testing. In the final stage, Arduino is replaced by a multifunctional input-output device as Arduino could not provide a high feedback rate and performance qualities. Line receivers are applied to decode the encoder data. Besides that, major electrical components such as DC servomotors, servo controller, gearhead and encoder are reviewed in this section.

3.4.1 Arduino Due

The Arduino Due in Figure 46 is a microcontroller board manufactured by Arduino Italy, a world-leading open source hardware and software company. The Arduino Due board consist of various kinds of microprocessors and controllers. This board comes with the Atmel SAM3x8E ARM Cortex-M3 CPU built-in, and it is the first board to engage a 32-bit ARM core microcontroller. Besides that, the Arduino Due is equipped with many sets of digital and analog input/output (I/O) pins, a UARTs hardware serial port, 84 MHz bulid-in clock, digital to analog (DAC) pins and many cool features that allow the board to be interfaced to various circuits, actuators and sensors. The open-source Arduino Software (IDE) which runs on C programming languages is used to program the board.

Figure 46 Arduino Due

This low cost and easily accessible board is utilized in the primary stage of the research project. Primary testing of electronics devices such as DC servomotors with Servo controllers and rotary encoders are done using the Arduino Due. Program codes are written for each electronic device to test their functionality and to collect various data such as the torque limit of the DC servomotor. Later, a set of coding is written to perform the trajectory control of the robotic orthosis with a conventional PID controller. The collected results are recorded and will be further discussed in Chapter 4.

3.4.2 USB-6341 Multifunction Input-output Device

The USB-6341 Device, as shown in Figure 48 is one of the USB Data Acquisition Devices (DAQ) manufactured by National Instruments. This device is utilized in the second stage of the research project in developing GUI environment for the actuators and sensors used to setup the two-link lower limb manipulator for advanced controller application. This device provides analog and digital I/O, 32-bit counter for PWM, encoder and various functions. The onboard NI-STC3 timing and synchronization allows advanced timing functionality such as independent analog and digital timing trigger measurement tasks which suit the needs of the two-link manipulator control. The LABVIEW software provides a graphical programming method that eases the visualization of each application, measuring and collecting data, debugging to make it simple for users to customize the application and analysing the collected data.

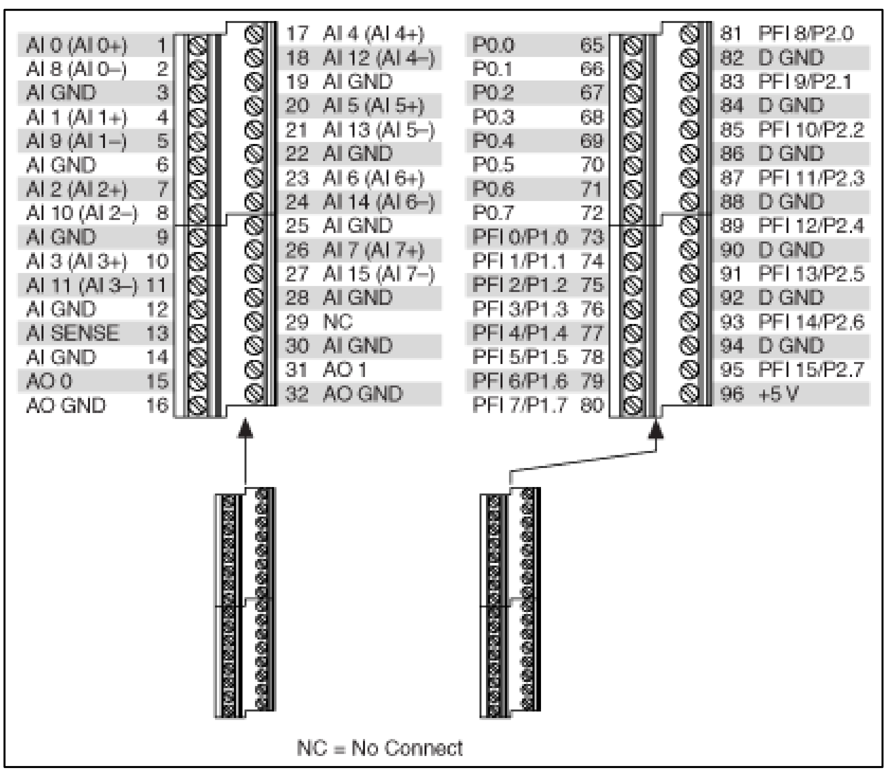

Figure 47 NI USB-6341 pin connection diagram

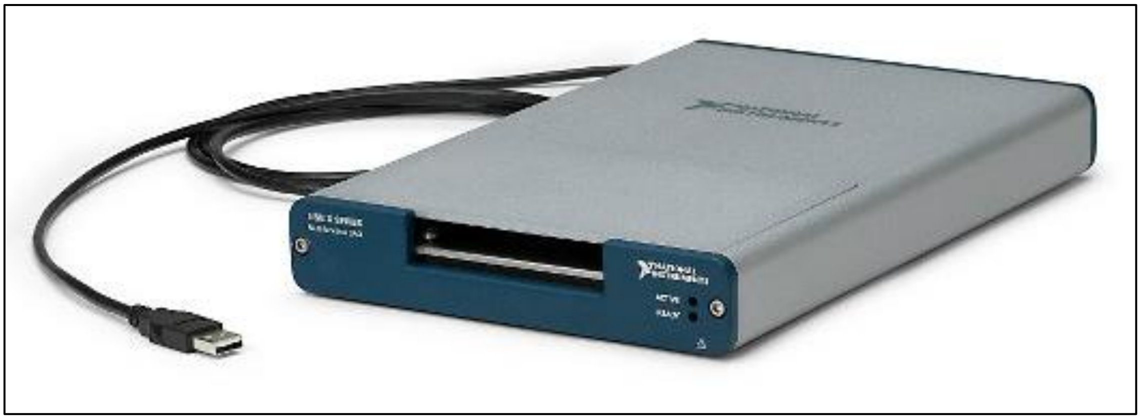

Figure 48 USB-6341 multifunction I/O device

3.4.3 Quadruple Differential Line Receiver

MC3486 quadruple differential line receiver as shown in Figure 49(a) is applied in this research project. The integrated circuit (IC) consists of four independent differential-input line receivers that provide 3-state TTL-compatible outputs. This IC with 16 pins which operates on a 5V voltage supply is suitable for reading data from the Maxon encoder that is connected to the back of the DC servomotor. This line receiver is able to decode the encoder data by sending position and direction data to the DAQ device for motor control. The aim of implementing the line receiver is to reduce the necessity of writing and decoding codes and to reduce the burden of the microcontroller or multifunctional DAQ device in running the decoding function.

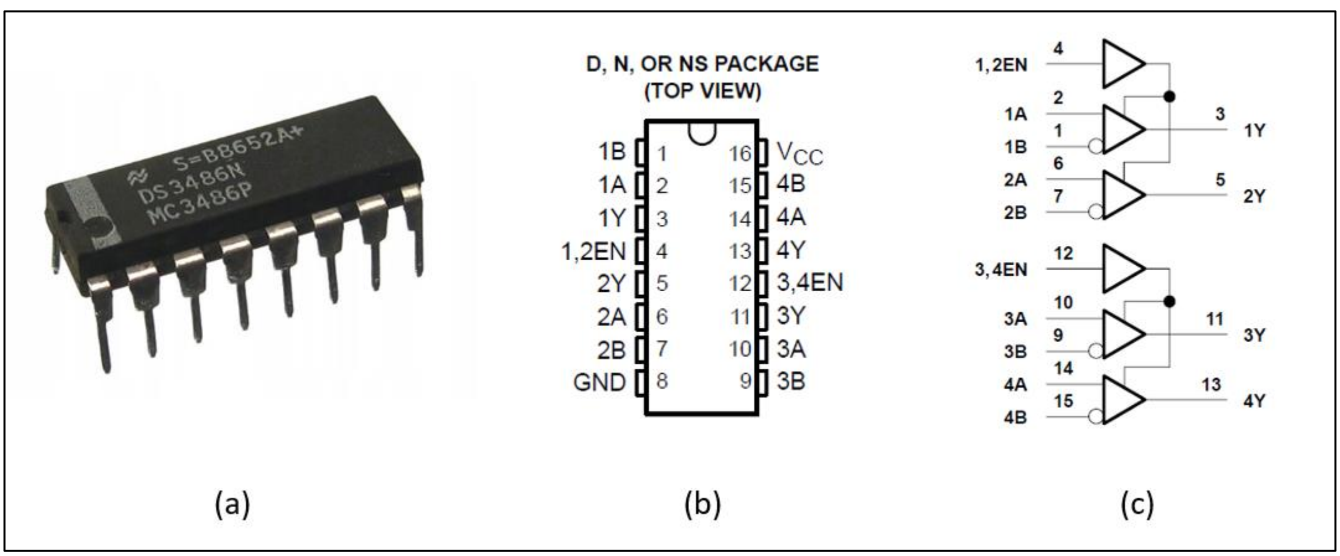

Figure 49 (a) MC3486 quadruple differential line receiver; (b) pins number and label of line receiver, (c) logic diagram of line receiver

Figure 49(b) shows the connection pin of the line receiver. This 16-pins IC is able to accommodate two 3-Channels encoders with the line driver at once. For example, as shown in Figure 49(c), Pin 1Y of the line receiver will output the actual channel data from one of the channels by combining the 1A and 1B input gained from the line driver of the encoder. The EN pin is the enable pin which allows the ID to send output to any microcontroller or devices. V_{cc} and GND are the voltage supply and the ground respectively.

3.4.4 Servo Controller for Maxon DC Servomotor

The chosen Maxon DC Servomotor is controlled by Escon 50/5 Servo Controller as shown in Figure 50. Escon 50/5 is a small-sized, powerful 4-quadrant PWM servo controller for highly efficient control of permanent magnet-activated brushed DC motors. This controller can operate in 3 different modes: speed control (closed loop control), speed control (open loop control), and current control, to cater for various application requirements. This controller processes commands from analogue input set values and features extensive analogue and digital I/O functionally. Besides that, this device could be configured via USB interface using the graphical user interface (GUI) window as shown in Figure 51, the ESCON Studio for Window PCs.

Figure 50 Escon 50/5 servo controller [115]

For this project application, the controller operates in open loop speed control mode. The encoder signal from the DC motor is fed to the microcontroller for signal processing. Detailed settings of the servo controller can be obtained from the GUI as shown in Figure 51. The speed controller is controlled by a main speed open loop and limited current control loop. Figure 52 shows the regulation tuning window while Figure 53 and Figure 54 show the dimensioning parameter for speed open loop and limiter current closed loop for of the Escon 50/5 servo controller. The AI1 port is the voltage input to the servo controller while DI2 and DI3 are the input ports for motor rotational directions. The offset speed, current limit, speed ramp and IxR factor of the controller can be varied to match the project requirements. Finally, the motor current and speed can be recorded from the GUI window in real time.

Analog set value, offset, speed ramp and the gain of the current controller are adjustable in the Simulink model. An Ideal Speed Closed-loop Controller block is included. The IxR compensator in the Ideal Speed Controller subsystem as shown in Figure 53 is a mathematical equation applied to compute the gain of the controller. The proportional (P) gain and integral time constant is obtained from the Dimensioning Parameter Window from the ESCON Studio as shown in Figure 54. The motor model in the system is built based on the basic equation of a DC Motor.

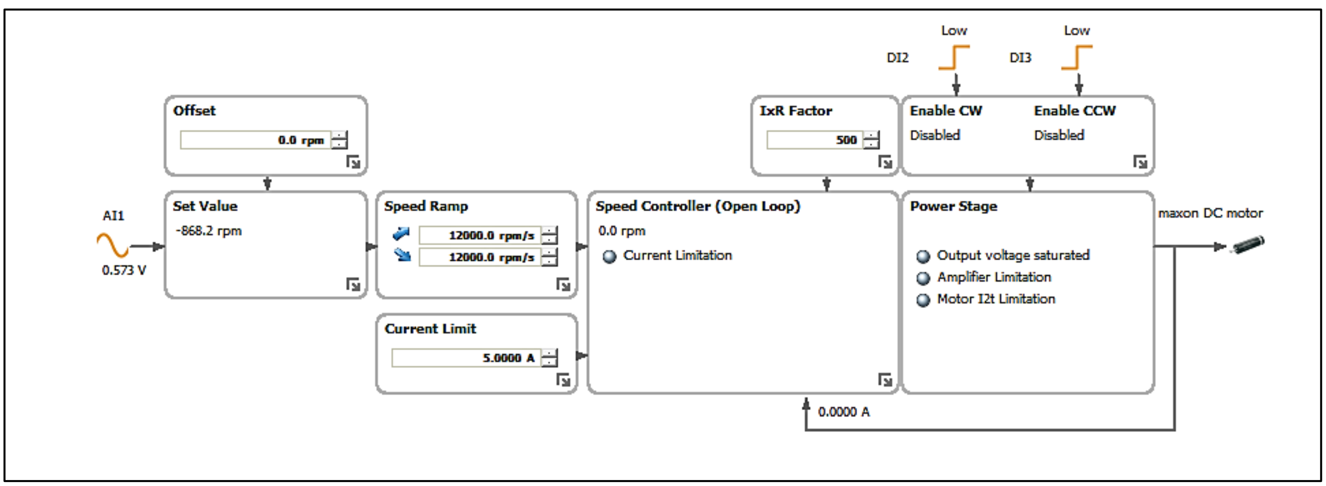

Figure 51 Graphical user interface (GUI) of Escon 50/5 servo controller

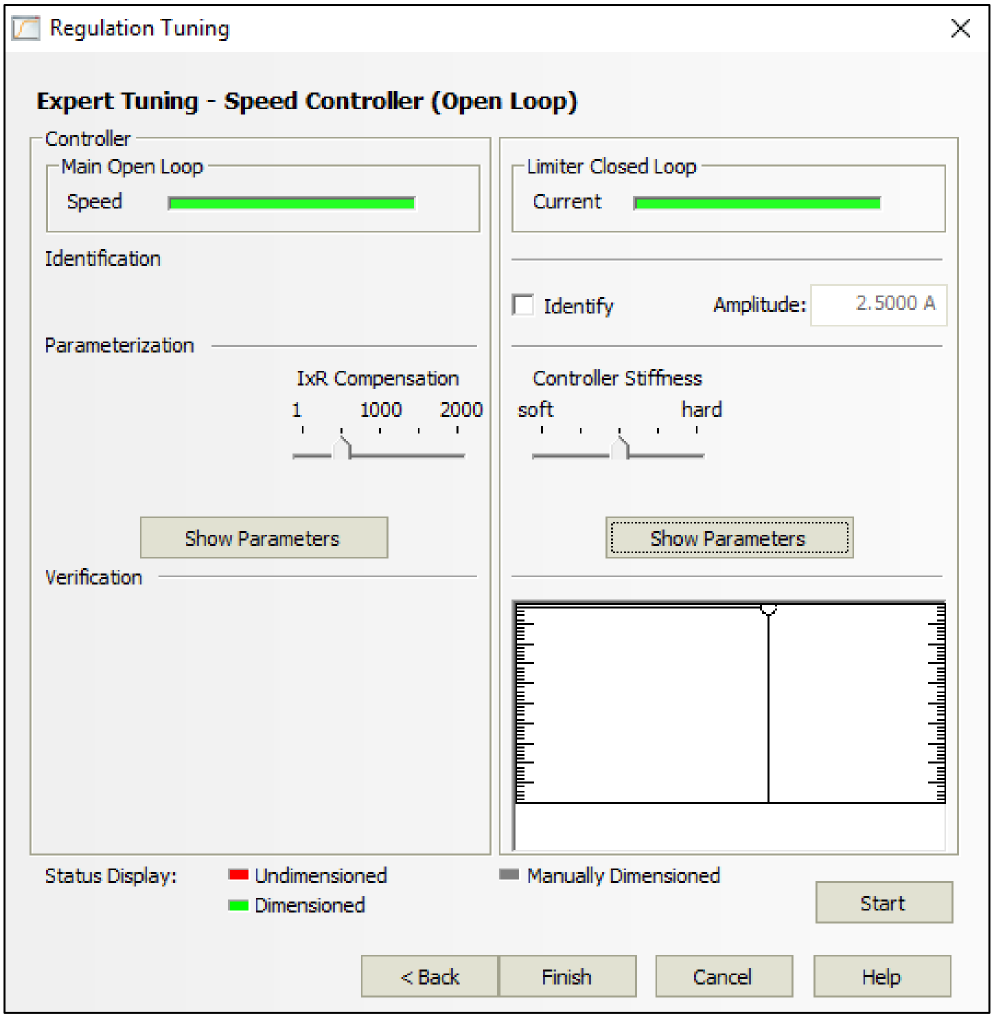

Figure 52 Regulation tuning parameter window

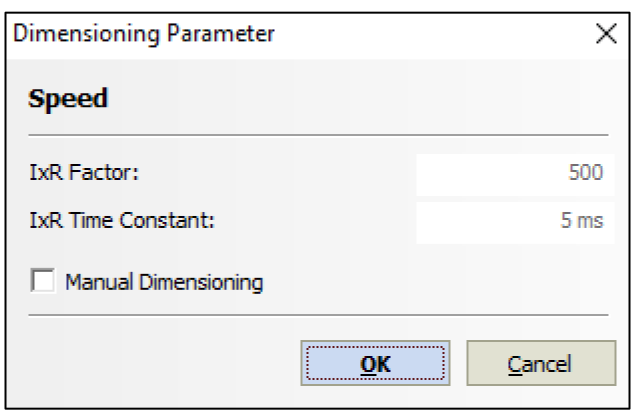

Figure 53 Speed open loop

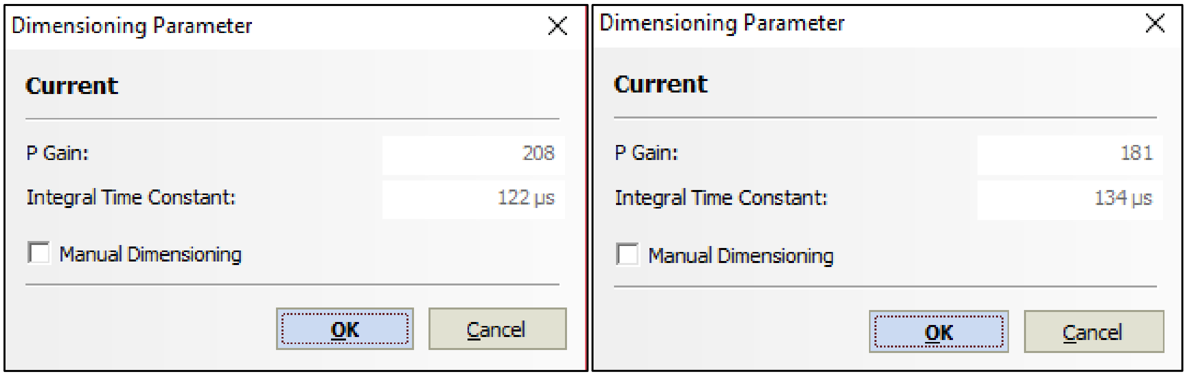

Figure 54 Dimensioning parameter window of limiter closed loop current control for knee and hip joints

3.4.5 Maxon DC Servomotor with Gearhead

Permanent magnet direct current servomotors are widely used for actuator applications. It is a device which transforms electrical power into mechanical power via magnetic coupling. Differential equations are developed for a linear approximation to the actual DC motor. The DC motor mainly consists of a rotor (armature) and a stator (field) as illustrated in Figure 55. A magnetic field arises from the stator coil when the current flows through the iron core. This occurrence transfers the electrical energy into rotational mechanical energy and hence, causes the motor to rotate. The major fraction of torque generated in the rotor (armature) of the motor is able to drive an external load. There are 4 DC permanent magnet servomotors (Maxon model no. 148867) with planetary gearhead (Maxon gearhead no. 223105) employed to actuate the lower limb of the robotic orthosis. The parameters in Table 7 are obtained from the Maxon Motor data sheet. The gear ratio for the motor is 1:353.

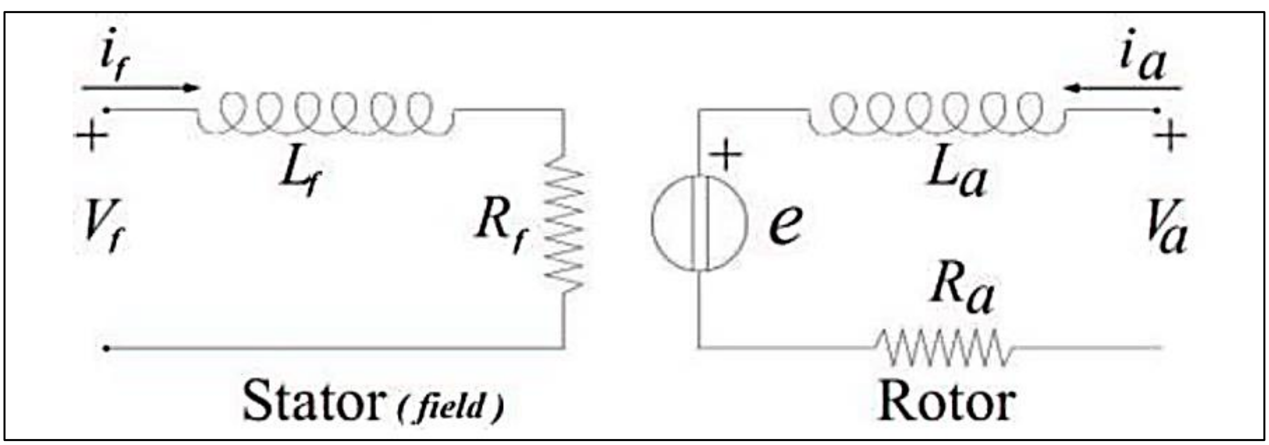

Figure 55 Electrical equivalent scheme of a DC motor [116]

Table 7 Table of constant parameters for DC servomotor

Parameters	**Value in SI unit**
Armature Resistance	0.299 Ω
Armature Inductance	0.0000823 H
Rotor Inertia	0.0000138 kgm^2
Motor torque constant	0.0302 Nm/A
Back EMF constant	0.0302 $rads^{-1}/V$
Gear ratio	1:353
Nominal voltage	24 V
No load speed	7580 rpm
No load current	137 mA

There is a 1:353 gear reduction of the DC servomotor. The gear ratio, *N* should be considered in the calculation as well. T_{Load} , is the load torque at the motor shaft before the gear reduction. $T_{load\ at\ the\ joint}$, is the torque after the gear reduction which drives the load. Equation (2) describes the relationship of T_{Load}, load torque at the motor shaft and $T_{load\ at\ the\ joint}$, load torque at the joint.

$$T_{load} = \frac{1}{N} T_{load\ at\ the\ joint} \tag{2}$$

3.4.6 Maxon Encoder

With the aim of trajectory control of a two-link manipulator, the quadrature encoder is the best sensor to capture the behaviour of the DC servomotor. The encoder implemented in the development of the robotic orthosis is a Maxon encoder attached to the Maxon DC servomotor. The Encoder with line driver (Maxon MR Type L no. 228452) provides a 3 channel feedback for the motor position and direction. This encoder offers a resolution of 500 counts per turn with a maximum speed of 24000rpm which is faster than the maximum speed of the DC servomotor and hence, this encoder is suitable to support the application of the project.

This Maxon encoder comes along with a line driver and the pin allocations are as shown in Figure 56. Channels A and B of the encoder are 90 degrees different in phase displacement and hence, it provides information to determine the rotating direction of the encoder when one channel is leading another.

The signal transitions of Channel A and B (low to high or high to low) produces counts in each electric cycle and hence provide the information of count per revolution, which allow the calculation of the position of the encoder.

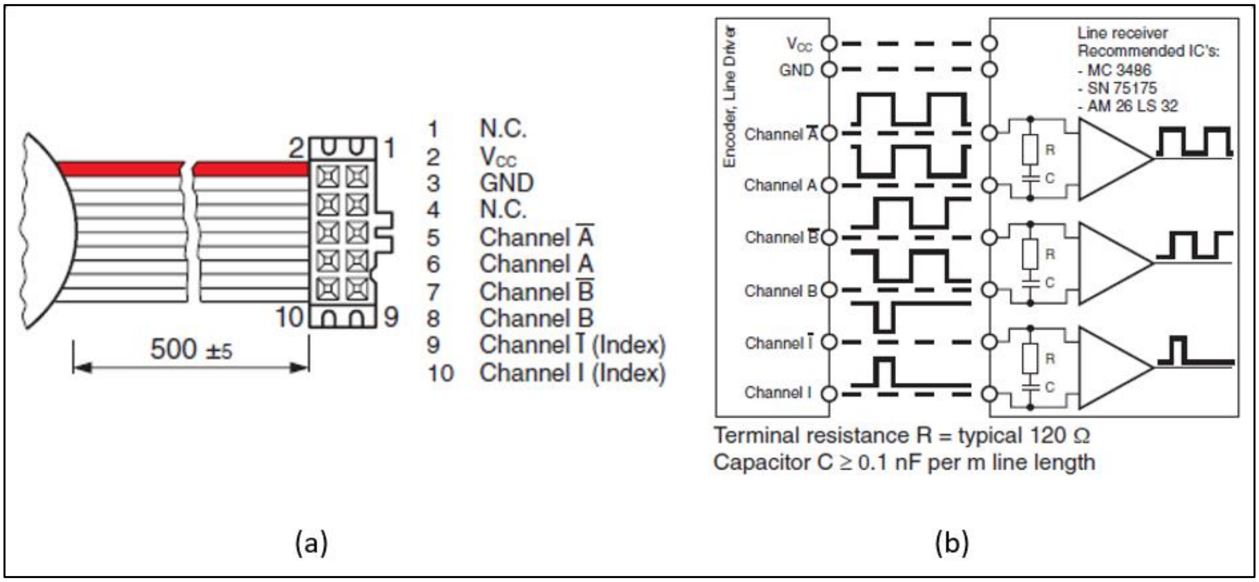

Figure 56 (a) Pin allocation of line driver of Maxon encoder; (b) connection example of Maxon encoder

3.4.7 Wiring Setup of the Electric and Electronic Components

In Figure 57, the wiring setup of major electronic components such as the USB-6341 multifunction input-output device, 24V AC power supply, ESCON 50/5 servo controller for the Maxon DC servomotor and MC3486 quadruple differential line receiver is shown. Figure 58 shows the circuit diagram of the wire connection (Appendix C). USB-6341 is the major component connected to the CPU for command and data transfer. The line receiver is implemented to decode the encoder data by merging both signals (A' and A) from the same channel of the encoder and send it to the CPU via USB 6341 for position tracking. A 24V analog power supply is connected to the servo controller. Three types of connections are connected to the servo controller. J2 is the connection port to the DC servomotor to provide voltage signal for rotational movement while J5 is the connection port to control the rotational direction of the servo motor in clockwise and counter-clockwise direction. Lastly, J6 is the connection port to receive voltage signals from the CPU via the USB-6341 device to control the rotational speed of the servomotor. The circuit diagram in Figure 58 shows the component connections of link 1 and link 2 respectively. Refer to Appendix C for a higher resolution of the circuit diagram.

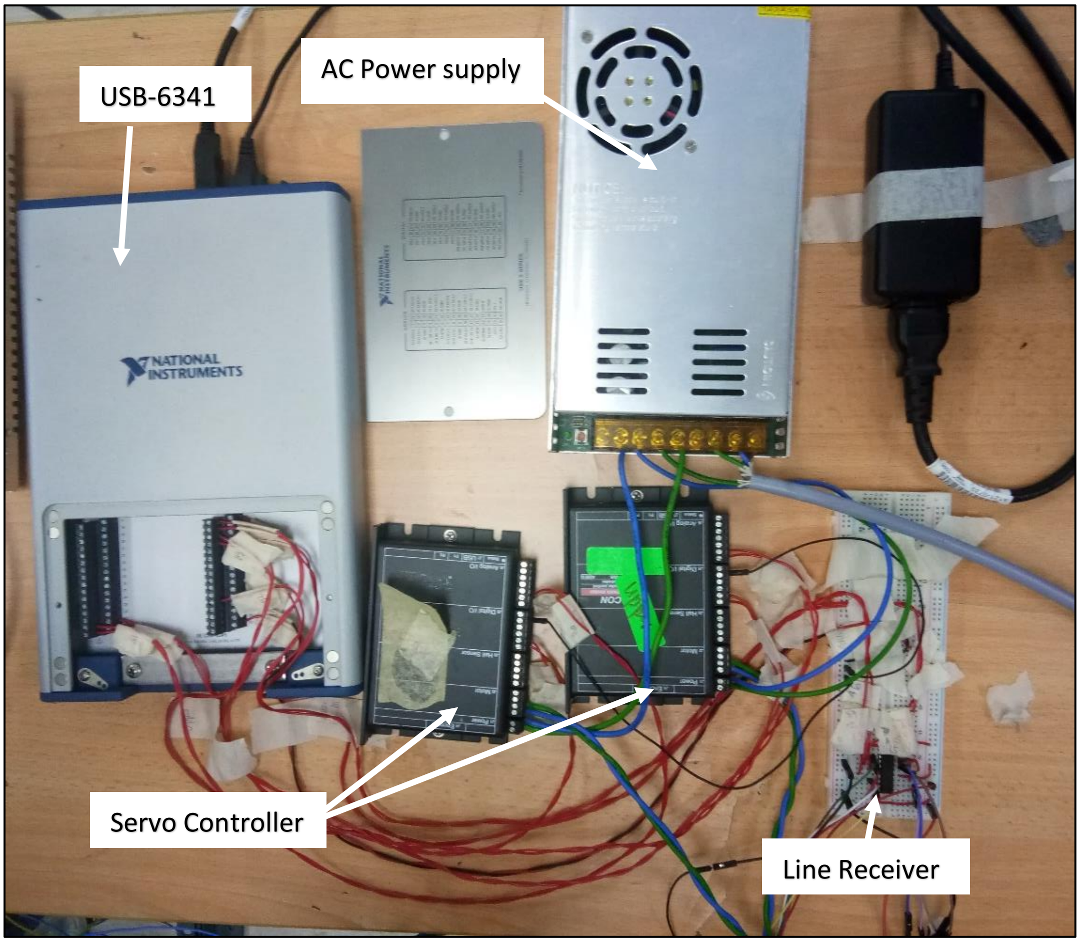

Figure 57 Wiring setup of robotic orthosis

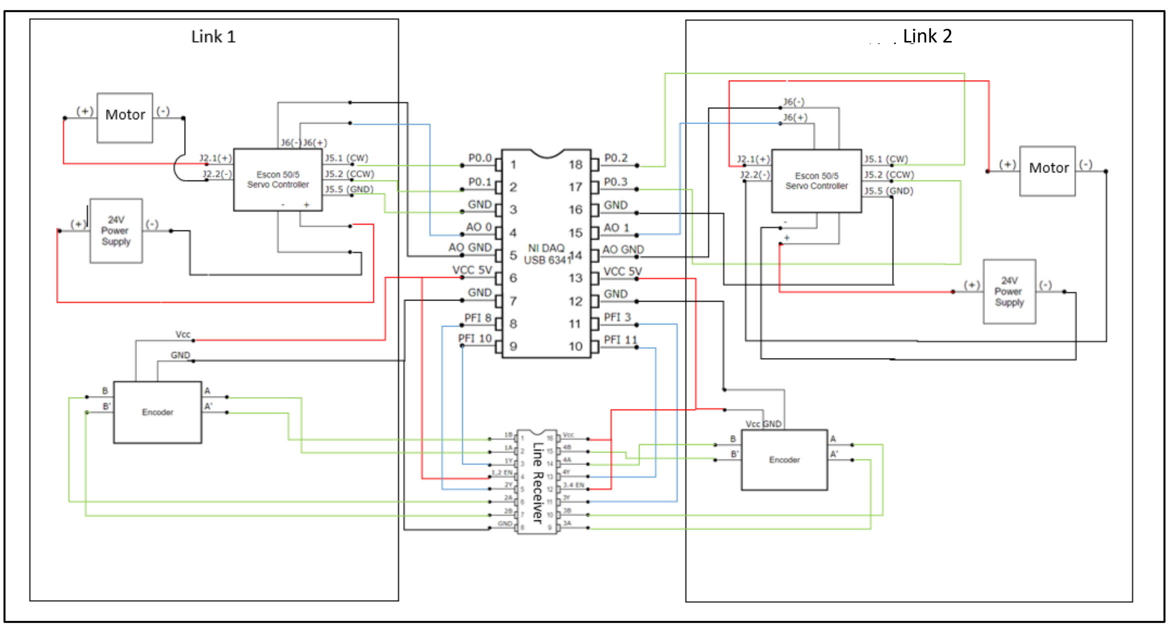

Figure 58 Circuit diagram of robotic orthosis

3.5 Dynamic Model of the Robotic Orthosis

As shown in Figure 59, the leg model has two joints: hip joint and knee joint. The two links are illustrated as two rigid bodies moving in a uniform gravitational field which are connected to joint O. Both links have their respective masses (M1, M2) and lengths (2L1, 2L2). The two joints can be represented by two generalized coordinates (θ1, θ2). Mass of the DC motor, M3 with attached gearbox, M4 are listed. Table 8 shows the constant of parameters for the leg model.

Equations (3) and (4) below are derived to represent the dynamic of motion of the human lower limbs. The Simulink model of the dynamic model is built for simulation purposes and is shown in Figure 60. $T_{L,1}$ and $T_{L,2}$ are the input torques provided by the DC motors.

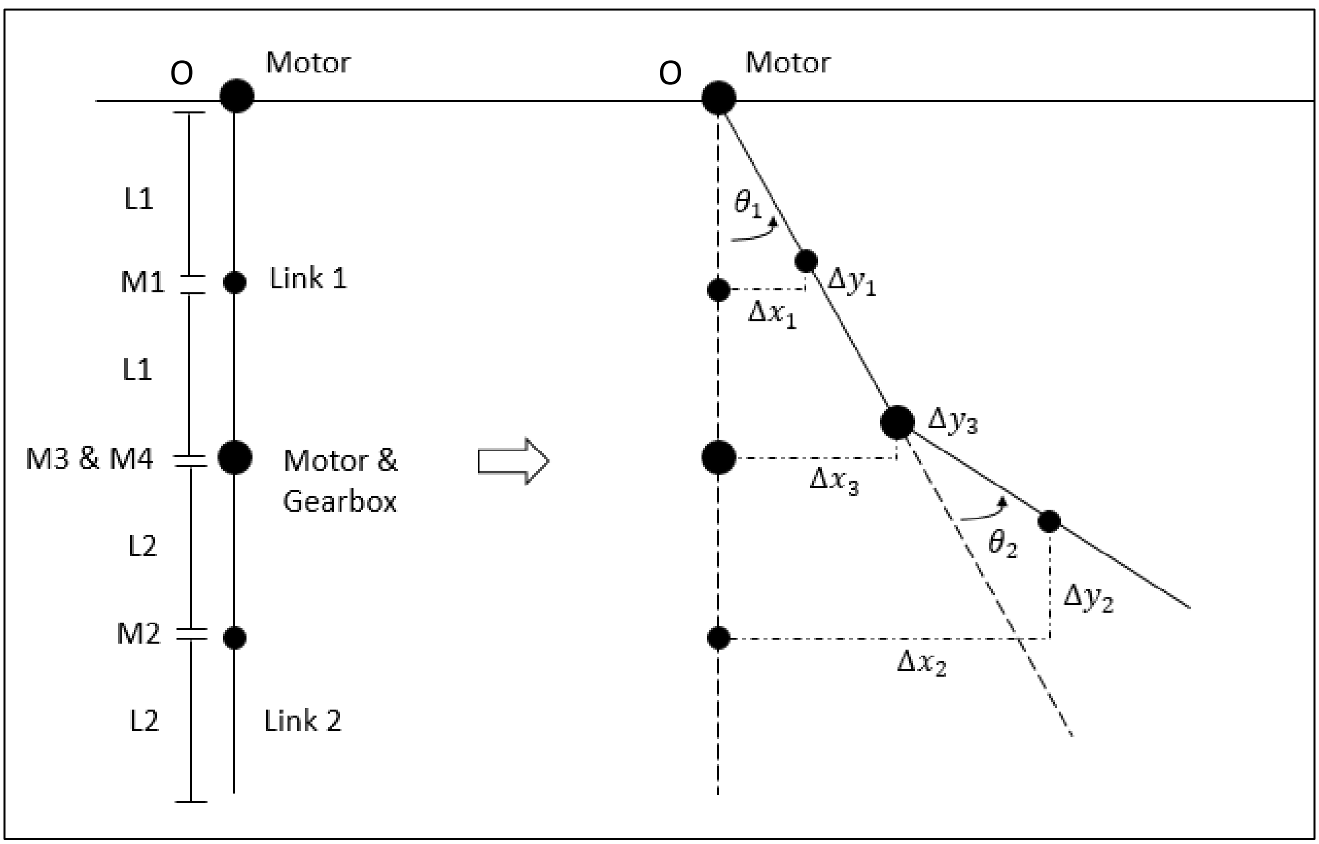

Figure 59 Lower limb exoskeleton free body diagram

Table 8 Table of constant parameters for leg model

Parameters	**Values**
Mass of link 1, $\boldsymbol{M_1}$	1.427 kg
Mass of link 2, $\boldsymbol{M_2}$	0.185 kg
Mass of motor, $\boldsymbol{M_3}$	0.400 kg
Mas of grearbox, $\boldsymbol{M_4}$	1.000 kg
Length of link 1, $\boldsymbol{2L_1}$	0.56 m
Length of link 2, $\boldsymbol{2L_2}$	0.50 m
Gravity of earth, $\boldsymbol{g}$	9.81 m/s^2

3.5.1 Derivation of Mathematical Model using Lagrangian Mechanics

The Cartesian coordinate system is used to analyse the kinematics of the two-degree-of-freedom lower link robotic orthosis. By referring to Figure 59, the magnitude of translation on the coordinate plane in *x* and *y* direction for each link and motor can be denoted as below:

$$\Delta x_1 = L_1 \sin\theta_1$$
$$\Delta y_1 = L_1 - L_1 \cos\theta_1$$
$$\Delta x_2 = 2L_1 \sin\theta_1 + L_2 \sin(\theta_1 + \theta_2)$$
$$\Delta y_2 = 2L_1 + L_2 - 2L_1 \cos\theta_1 - L_2 \cos(\theta_1 + \theta_2)$$
$$\Delta x_3 = 2L_1 \sin\theta_1$$
$$\Delta y_3 = 2L_1 - 2L_1 \cos\theta_1$$

Differentiation of the *x* and *y* components,

$$\Delta\dot{x}_1 = \frac{d\Delta x_1}{dt} = L_1\dot{\theta}_1 \cos\theta_1$$
$$\Delta\dot{y}_1 = \frac{d\Delta y_1}{dt} = L_1\dot{\theta}_1 \sin\theta_1$$
$$\Delta\dot{x}_2 = \frac{d\Delta x_2}{dt} = 2L_1\dot{\theta}_1 \cos\theta_1 + L_2\left(\dot{\theta}_1 + \dot{\theta}_2\right)\cos(\theta_1 + \theta_2)$$
$$= 2L_1\dot{\theta}_1 \cos\theta_1 + L_2\dot{\theta}_1 \cos(\theta_1 + \theta_2) + L_2\dot{\theta}_2 \cos(\theta_1 + \theta_2)$$
$$\Delta\dot{y}_2 = \frac{d\Delta y_2}{dt} = 2L_1\dot{\theta}_1 \sin\theta_1 + L_2\left(\dot{\theta}_1 + \dot{\theta}_2\right)\sin(\theta_1 + \theta_2)$$
$$= 2L_1\dot{\theta}_1 \sin\theta_1 + L_2\dot{\theta}_1 \sin(\theta_1 + \theta_2) + L_2\dot{\theta}_2 \sin(\theta_1 + \theta_2)$$
$$\Delta\dot{x}_3 = \frac{d\Delta x_3}{dt} = 2L_1\dot{\theta}_1 \cos\theta_1$$
$$\Delta\dot{y}_3 = \frac{d\Delta y_3}{dt} = 2L_1\dot{\theta}_1 \sin\theta_1$$

To obtain the Kinetic energy expression of the system, magnitude of velocity at each link is needed.

$$v_1{}^2 = \mathrm{L}_1{}^2\dot{\theta}_1{}^2$$
$$v_2{}^2 = 4\mathrm{L}_1{}^2\dot{\theta}_1{}^2 + \mathrm{L}_2{}^2\left(\dot{\theta}_1{}^2 + 2\dot{\theta}_1\dot{\theta}_2 + \dot{\theta}_2{}^2\right) + 4L_1L_2\left(\dot{\theta}_1{}^2 + \dot{\theta}_1\dot{\theta}_2\right)\cos\theta_2$$
$$v_3{}^2 = 4\mathrm{L}_1{}^2\dot{\theta}_1{}^2$$

The Lagrangian, $L = KE_1 + KE_2 + KE_3 - P_1 - P_2 - P_3 + RE_{1,1} + RE_{3,1} + RE_{2,1} + RE_{2.2}$

Where, KE_n is the kinetic energy of respective link or motor, P_n is the potential energy of respective link or motor and $RE_{n,\theta}$ is the rotational energy of the respective link or motor with reference to angle, θ.

$$L = \frac{1}{2}M_1L_1{}^2\dot{\theta}_1{}^2 + \frac{1}{2}M_2\left[4L_1{}^2\dot{\theta}_1{}^2 + L_2{}^2\left(\dot{\theta}_1{}^2 + 2\dot{\theta}_1\dot{\theta}_2 + \dot{\theta}_2{}^2\right) + 4L_1L_2\left(\dot{\theta}_1{}^2 + \dot{\theta}_1\dot{\theta}_2\right)\cos\theta_2\right]$$

$$+ \frac{1}{2}M_3\left[4\mathrm{L}_1{}^2\dot{\theta}_1{}^2\right] - M_1g(L_1 - L_1\cos\theta_1) - M_2g[2L_1 + L_2 - 2L_1\cos\theta_1 - L_2\cos(\theta_1+\theta_2)]$$

$$- M_3g(2L_1 - 2L_1\cos\theta_1) + \frac{1}{2}I_1\dot{\theta}_1{}^2 + \frac{1}{2}I_2\dot{\theta}_1{}^2 + \frac{1}{2}I_3\dot{\theta}_1{}^2 + \frac{1}{2}I_2\dot{\theta}_2{}^2 + \frac{1}{2}I_4\dot{\theta}_1{}^2$$

Derivation of Torque equation for link 1:

Differentiate L with respect to $\dot{\theta}_1$,

$$\frac{\partial L}{\partial\dot{\theta}_1} = M_1L_1{}^2\dot{\theta}_1 + 4M_2L_1{}^2\dot{\theta}_1 + M_2L_2{}^2\dot{\theta}_1 + M_2L_2{}^2\dot{\theta}_2 + 4M_2L_1L_2\dot{\theta}_1\cos\theta_2 + 4M_3L_1{}^2\dot{\theta}_1$$

$$+2M_2L_1L_2\dot{\theta}_2\cos\theta_2 + I_1\dot{\theta}_1 + I_2\dot{\theta}_1 + I_3\dot{\theta}_1 + I_4\dot{\theta}_1$$

Differentiate $\frac{\partial L}{\partial\dot{\theta}_1}$ with respect to time, t,

$$\frac{d}{dt}\left(\frac{\partial L}{\partial\dot{\theta}_1}\right) = M_1L_1{}^2\ddot{\theta}_1 + 4M_2L_1{}^2\ddot{\theta}_1 + M_2L_2{}^2\ddot{\theta}_1 + M_2L_2{}^2\ddot{\theta}_2 + 4M_2L_1L_2\ddot{\theta}_1\cos\theta_2$$

$$-4M_2L_1L_2\dot{\theta}_1\dot{\theta}_2\sin\theta_2 + 4M_3L_1{}^2\ddot{\theta}_1 + 2M_2L_1L_2\ddot{\theta}_2\cos\theta_2 - 2M_2L_1L_2\dot{\theta}_2{}^2\sin\theta_2 + I_1\ddot{\theta}_1$$

$$+I_2\ddot{\theta}_1 + I_3\ddot{\theta}_1 + I_4\ddot{\theta}_1$$

Differentiate L with respect to θ_1,

$$\frac{\partial L}{\partial\theta_1} = -M_1gL_1\sin\theta_1 - 2M_2gL_1\sin\theta_1 - M_2gL_2\sin(\theta_1+\theta_2) - 2M_3gL_1\sin\theta_1$$

Hence, the torque at pivot point for link 1 is

$$T_1 = \frac{d}{dt}\left(\frac{\partial L}{\partial \dot{\theta}_1}\right) - \frac{\partial L}{\partial \theta_1}$$

$$= \left(M_1{L_1}^2 + 4M_2{L_1}^2 + M_2{L_2}^2 + 4M_2L_1L_2\cos\theta_2 + 4M_3{L_1}^2 + I_1 + I_2 + I_3 + I_4\right)\ddot{\theta}_1 +$$
$$\left(M_2{L_2}^2 + 2M_2L_1L_2\cos\theta_2 + I_2\right)\ddot{\theta}_2 - 2M_2L_1L_2\left(2\dot{\theta}_1\dot{\theta}_2 + {\dot{\theta}_2}^2\right)\sin\theta_2 + (M_1gL_1 + 2M_2gL_1 +$$
$$2M_3gL_1)\sin\theta_1 + M_2gL_2\sin(\theta_1 + \theta_2)$$

Derivation of Torque equation for link 2:

Differentiate L with respect to $\dot{\theta}_2$,

$$\frac{\partial L}{\partial \dot{\theta}_2} = M_2{L_2}^2\dot{\theta}_1 + M_2{L_2}^2\dot{\theta}_2 + 2M_2L_1L_2\dot{\theta}_1\cos\theta_2 + I_2\dot{\theta}_2$$

Differentiate $\frac{\partial L}{\partial \dot{\theta}_2}$ with respect to time, t,

$$\frac{d}{dt}\left(\frac{\partial L}{\partial \dot{\theta}_2}\right) = M_2{L_2}^2\ddot{\theta}_1 + M_2{L_2}^2\ddot{\theta}_2 + 2M_2L_1L_2\ddot{\theta}_1\cos\theta_2 - 2M_2L_1L_2\dot{\theta}_1\dot{\theta}_2\sin\theta_2 + I_2\ddot{\theta}_2$$

Differentiate L with respect to θ_2,

$$\frac{\partial L}{\partial \theta_2} = -2M_2L_1L_2\left({\dot{\theta}_1}^2 + \dot{\theta}_1\dot{\theta}_2\right)\sin\theta_2 - M_2gL_2\sin(\theta_1 + \theta_2)$$

Hence, the torque at pivot point for link 2 is

$$T_2 = \frac{d}{dt}\left(\frac{\partial L}{\partial \dot{\theta}_2}\right) - \frac{\partial L}{\partial \theta_2}$$

$$= \left(M_2{L_2}^2 + 2M_2L_1L_2\cos\theta_2\right)\ddot{\theta}_1 + (M_2{L_2}^2 + I_2)\ddot{\theta}_2 + 2M_2L_1L_2{\dot{\theta}_1}^2\sin\theta_2 + M_2gL_2\sin(\theta_1 + \theta_2)$$

Link 1,

$$T_{L,1} = \frac{d}{dt}\left(\frac{\partial L}{\partial \dot{\theta}_1}\right) - \frac{\partial L}{\partial \theta_1}$$

$$= \left(M_1{L_1}^2 + 4M_2{L_1}^2 + M_2{L_2}^2 + 4M_2L_1L_2\cos\theta_2 + 4(M_3 + M_4)\,{L_1}^2 + I_1 + I_2 + I_3 + I_4\right)\ddot{\theta}_1$$
$$+\left(M_2{L_2}^2 + 2M_2L_1L_2\cos\theta_2 + I_2\right)\ddot{\theta}_2 - 2M_2L_1L_2\left(2\dot{\theta}_1\dot{\theta}_2 + {\dot{\theta}_2}^2\right)\sin\theta_2 + (M_1gL_1 + 2M_2gL_1$$
$$+2(M_3 + M_4)gL_1)\sin\theta_1 + M_2gL_2\sin(\theta_1 + \theta_2) \qquad (3)$$

Link 2,

$$T_{L,2} = \frac{d}{dt}\left(\frac{\partial L}{\partial \dot{\theta}_2}\right) - \frac{\partial L}{\partial \theta_2}$$

$$= \left(M_2 {L_2}^2 + 2M_2L_1L_2\cos\theta_2\right)\ddot{\theta}_1 + \left(M_2{L_2}^2 + I_2\right)\ddot{\theta}_2 + 2M_2L_1L_2{\dot{\theta}_1}^2 \sin\theta_2 + M_2gL_2\sin(\theta_1+\theta_2) \qquad (4)$$

3.6 Conclusions

In conclusion, a new lightweight and ergonomic design of two-link manipulator is justified. The mechanical setup of robotic orthosis is shown in this chapter. The descriptions and purposes of the support frame, extendable shaft, motor assembly parts and main assembly of the rehabilitation device are reviewed. Furthermore, the reason and purpose of each electric and electronic component is reviewed. In addition to that, specifications of all components are stated. Wiring setup and circuit diagram of the robotic orthosis are discussed. Then, the dynamic model of robotic orthosis is analysed, and the mathematical model of the exoskeleton is derived.

Chapter 4 Trajectory Control Using Conventional Controllers

In this chapter, the development of the conventional PID controller is discussed. In Stage 1, a Simulink model that mimics the DC servomotor and ESCON 50/5 servo controller is built and the output parameters of the simulation model such as motor speed and armature current are compared with the outcomes of the actual system recorded from the GUI of ESCON Studio. Besides, a position control with PID controller is implemented and is tested on both simulation and experiment with hip trajectory data. In stage 2, the simulation model of trajectory control for one side of the robotic orthosis includes both links is developed. This model is verified with output parameters measured from the robotic orthosis that such as actual motor current and motor speed. PID controllers are also implemented to the simulation model for trajectory control of the knee and hip joint and the desired PID values are chosen to be applied in the experimental setup of the robotic orthosis.

4.1 Verification of Simulation Model and Position Control of DC Servomotor

4.1.1 Verification of Simulation Model of DC Servomotor

After study on the GUI and functions of the Escon 50/5 Servomotor, a Simulink model of the servo controller and the motor model is developed with the MATLAB Software as shown in Figure 60. The motor model in the Simulink model is built based on the motor parameters recorded in Table 7. This Simulink model is aimed to provide the same features and perform similarly as the Escon50/5 Servo Controller. The Simulink model is built for future development of simulation models of real-time control system for robotic orthosis.

Analog set value, offset, speed ramp and the gain of speed controller are adjustable in the Simulink model. An Ideal type PI Speed Controller block is included in the model for speed control. The PI function in the subsystem is a mathematical Equation (5) applied to compute the integral (I) gain. The proportional (P) gain and integral time constant is obtained from the Dimensioning Parameter Window from the ESCON Studio. The motor model in the system is built based on the electrical equation of motion of the DC motor derived from the Kirchhoff voltage law.

$$Integral\ gain, I = \frac{Proportional\ gain,\ K_p}{integral\ time\ constant,\ t} \tag{5}$$

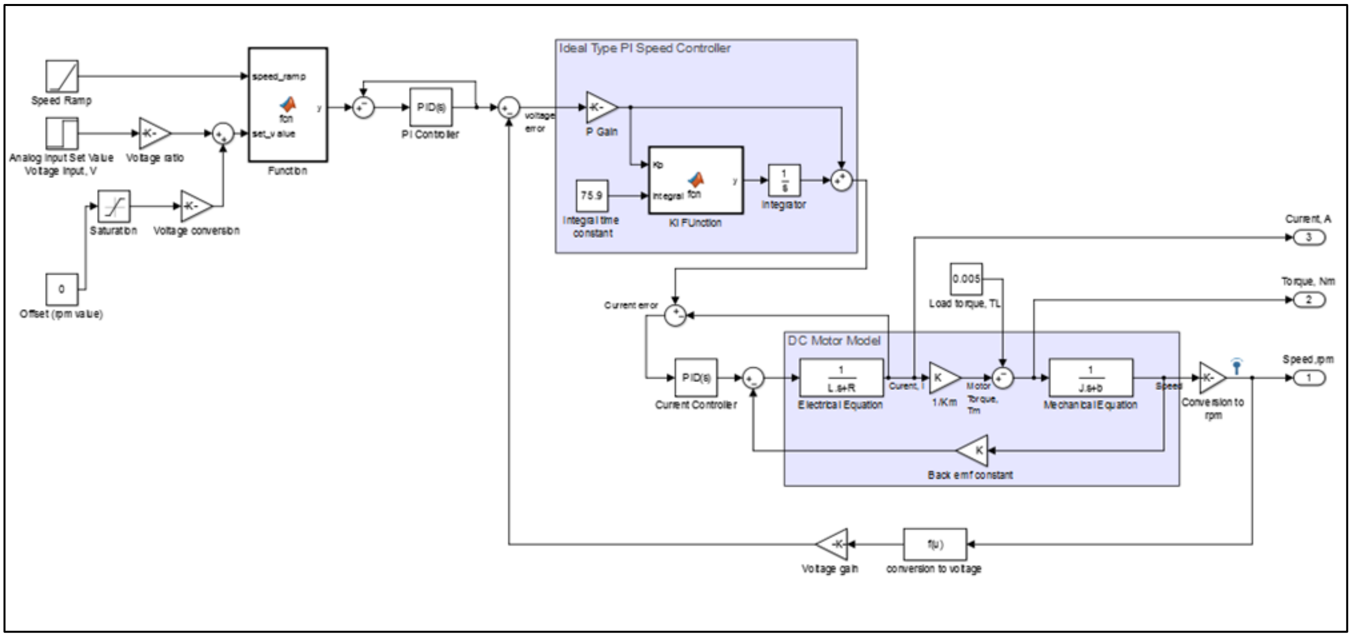

Figure 60 Simulink model of Escon 50/5 servo controller and DC servomotor

To verify the MATLAB Simulink model, the output parameters from ESCON Studio are recorded in Table 9, and simulation results from MATLAB under no load condition are compared. Both results are obtained from the respective system under no load condition based on the same setting of manipulated variables. The analog inputs (voltage input) to the Escon 50/5 servo controller are controlled by the PWM signals sent form Arduino controller. The PWM values are then computed to equivalent voltage values for the Simulink model simulation. The Conversion of PWM values to voltage values are listed in Table 10.

Table 9 Parameters setting for MATLAB simulation and experiment

Parameters	**Set Value**
Speed Ramp	10000 rpm/s
Offset	-
P Gain	1809
Integral Time Constant	69.5 ms

Table 10 Conversion of PWM value to equivalent voltage

PWM signal from Arduino Microcontroller	**Equivalent voltage to Simulink model (V)**
20	0.93
40	1.80
60	2.68
80	3.56
100	4.43
120	5.32
140	6.18
160	7.07
180	7.95

4.1.2 Verification of Motor Speed for Experimental and Simulation Model

Both experiment (DC Motor with Escon 50/5 Servo Controller) and simulation (Simulink model) are being run for 20 seconds to generate the motor speed. Nine PWM signals as shown in Table 10 are sent to the analogue port of the servo controller. The PWM signals indicate different desired speeds set to the motor. The speeds of the motor that form the 9 trials are captured with the GUI of the servo controller via encoder feedback. The motor speed obtained is then plotted in Figure 61. Same procedures are applied to the simulation of Simulink model with the equivalent voltage as listed in Table 10. The equivalent voltage fed to the system is treated as a step input. Then, the findings of motor speed is plotted in Figure 62. Both Figure 61 and Figure 62 show similar results for the motor speed at different levels of voltage input. In order to compare the motor speed from both experiment and simulation, 3 sets of data are chosen and plotted in Figure 63. As shown in Figure 63, simulation results and experimental results are comparable. Both results are similar in terms of transient response and settling time. However, the steady state value of motor speed for actual experiments is slightly lower than simulation results due to the disturbance from load torque received by the system when interacting with the environment. Hence, the design of the Ideal type PI Speed Controller and speed ramp feature in the Simulink model is satisfying.

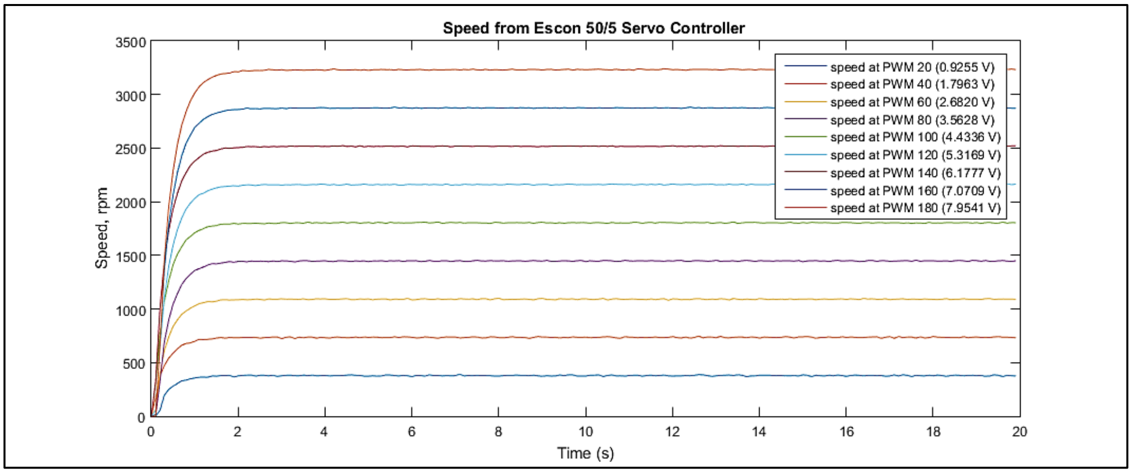

Figure 61 Speed from Escon 50/5 servo controller

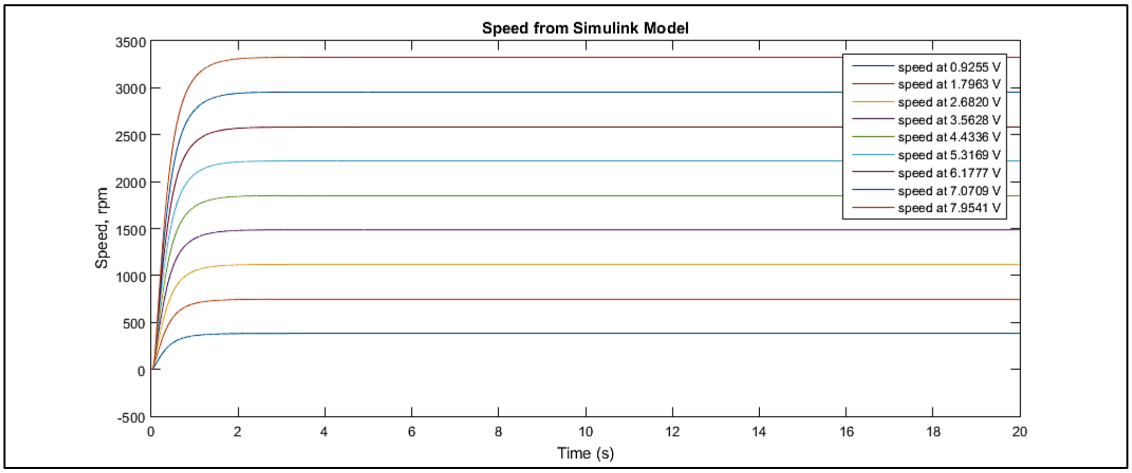

Figure 62 Speed from Simulink model

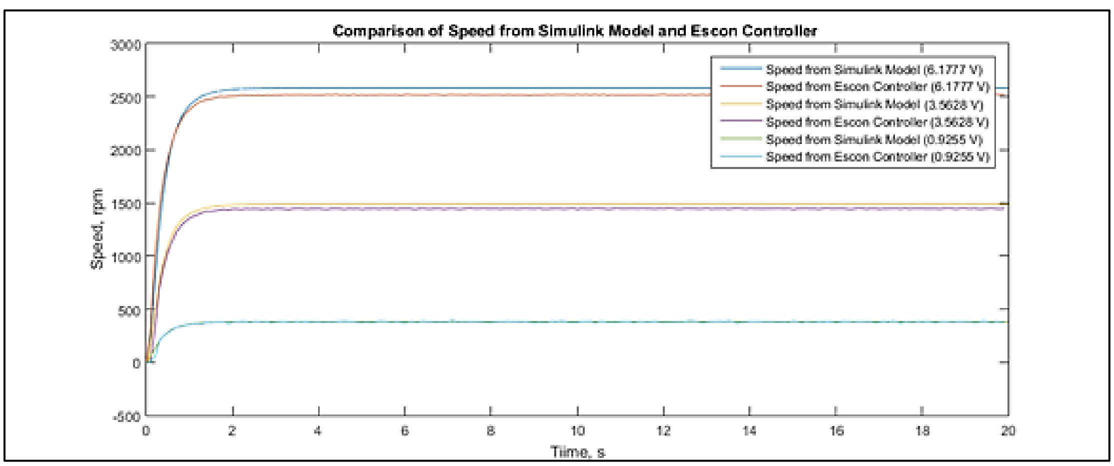

Figure 63 Comparison of speed from Simulink model and Escon servo controller

4.1.3 Verification of Motor Current for Experimental and Simulation Model

The current generated from different levels of voltage input of both systems are also recorded and plotted into Figure 64 and Figure 65 respectively. Figure 64 is plotted based on the actual motor current obtained from the Escon servo controller, whereas Figure 65 is plotted with current simulated from the MATLAB Simulink model. By comparing both figures, a huge difference between the peak values of each current responses is observed. Hence, Figure 66, Figure 67 and Figure 68 are plotted to compare the current response from both systems at 0.9255 V, 3.5628 V and 7.9541 V correspondingly. All 3 figures show that the steady states of the current responses are very close to each other. The only difference between the simulation result and experimental result is the peak value of the current response. A significantly higher peak value is obtained from the simulation result. Hence, it leads to a longer settling time for all 3 cases. A current controller should be implemented to prevent overshoot for the current response. However, no information for the current controller is found in the GUI of the servo controller. Hence, further investigation and more testing need to be done to obtain the current response that corresponds to the actual experimental value.

Based on the discussion above, the Ideal type PI Speed Controller and Speed Ramp setting are valid after comparing the transient responses and steady states of motor speed obtained from the experiment and simulation. However, the current responses of the simulation model experienced overshoot before they settled down to the steady state. Hence, a more precise current controller needs to be developed in the simulation model to reduce the overshoot of the system in the Simulink model.

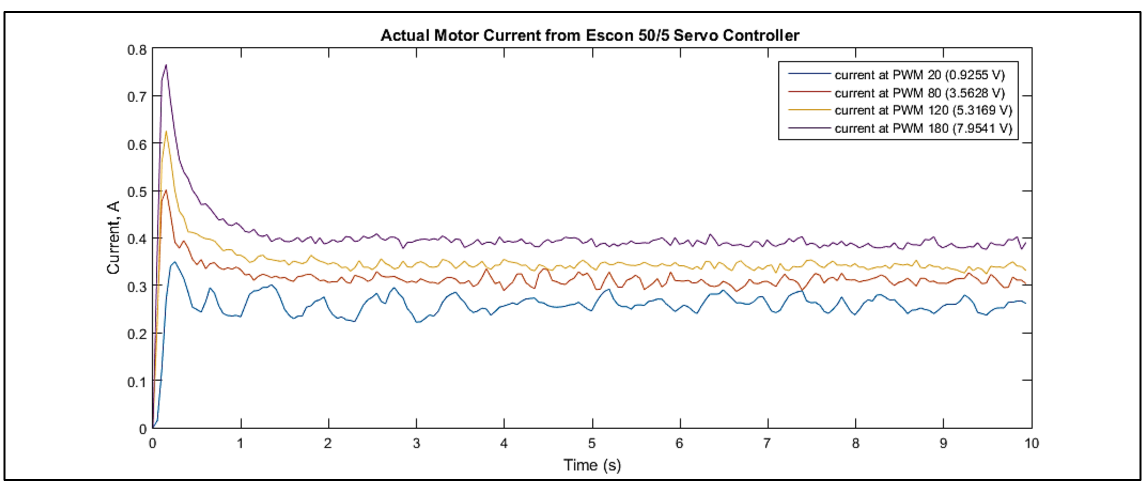

Figure 64 Actual Motor Current from Escon 50/5 servo controller

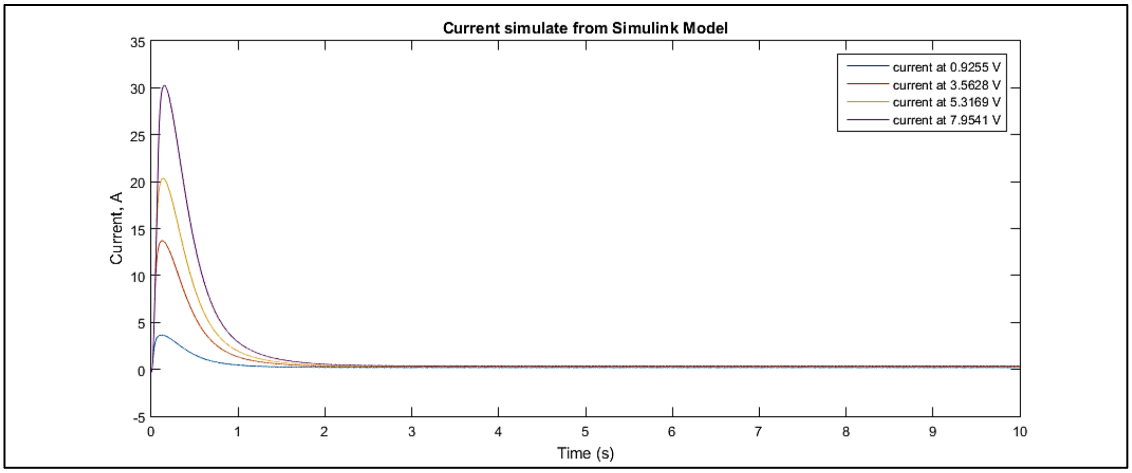

Figure 65 Current simulate from Simulink model

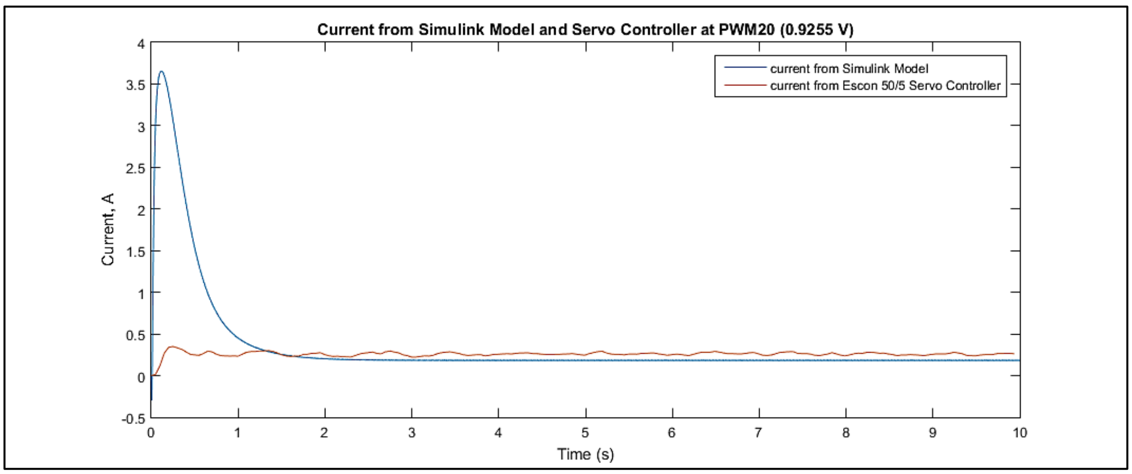

Figure 66 Current from Simulink model and servo controller at PWM20 (0.9255 V)

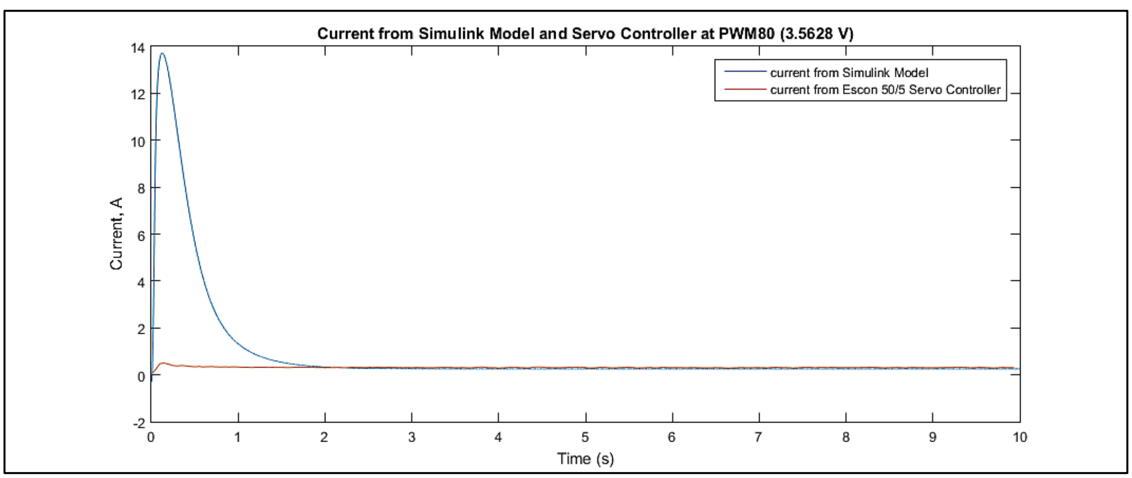

Figure 67 Current from Simulink model and servo controller at PWM80 (3.5628 V)

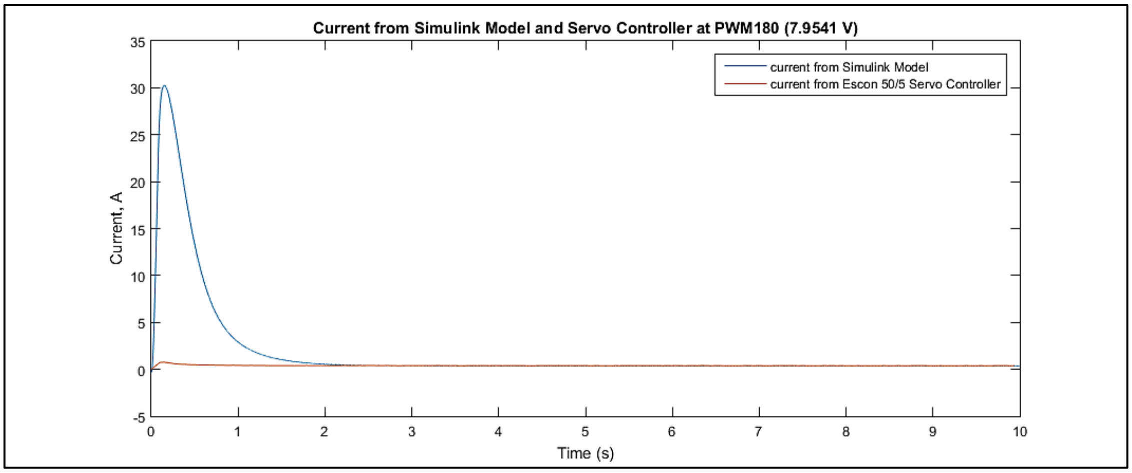

Figure 68 Current from Simulink model and servo controller at PWM180 (7.9541 V)

4.1.4 Position Control of DC Servomotor in Experiment

Position control of the robotic orthosis is important in this project to guide patients with the correct gait trajectory. In order to control the desired positions or angle movements of the motor, a PID controller is implemented. The gain of each parameter of the PID controller is shown in Table 11. The parameters are gained from repeated testing of different values, and the best performance parameters are recorded. In the experiment setup, the trajectory of the hip movement as shown in Figure 69 in a normal gait cycle is broken down in to 21 setpoints as the input of the position control to the Arduino controller. Each cycle of trajectory is set to be completed in 4s. Angle-time data of trajectory is utilized in this research can help to guide patients using a proper walking profile as each interval of the reference data is able to provide accurate position and moving angle for impaired hip and knee. The link rotational angle (output of the experimental) is recorded with the encoder attached to the motor shaft and the data is transferred to Arduino via the serial communication with maximum speed at 115200 baud rates. The data is then extracted and plotted in MATLAB to be compared with the desired hip trajectory.

A desired trajectory of hip movement (angle) of a complete gait cycle obtained from a study of human gait pattern by University School of Physical Education, Wrocław, Poland as plotted in Figure 69 is employed as a reference trajectory for the system [48]. The Arduino microcontroller is programmed to rotate the link by following the desired trajectory with the PID controller as shown in Figure 70. Various PID constants are tested on the motor with one link. The outcomes of trajectory are recorded and compared. The desired parameter of the PID controller is obtained and presented in Table 11. The actual angle displaced by the motor is recorded with the GUI of the Escon 50/5 servo controller via the encoder attached to the DC servomotor. The experimental result and desired angle are plotted in Figure 71. The DC servomotor is programmed to complete each gait cycle in 4 minutes. The two red dotted lines in Figure 71 marks the range of a complete gait cycle.

As shown in Figure 71, the experimental result has a similar pattern as the desired trajectory. A little delay of the experimental trajectory which is within the acceptable range is observed from the graph. However, a slights jerk is seen from the experimental trajectory before it reaches the maximum and minimum angles. This is because, in a normal gait cycle, when the hip is about to change the direction of movement, the moving speed decreases. However, for a moving DC motor, there will be rotational inertia when it is slowing down and about to change its direction of rotation. Hence, the rotational inertia is the cause of the jerk in the experimental trajectory. Thus, the PID controller needs to be refined to obtain a more satisfactory result with a minimal deviation from the desired trajectory.

Table 11 PID Controller for experimental testing with Escon 50/5 servo controller

Parameters of PID Controller	**Value**
Proportional Gain	45
Integral Gain	3
Derivative Gain	10

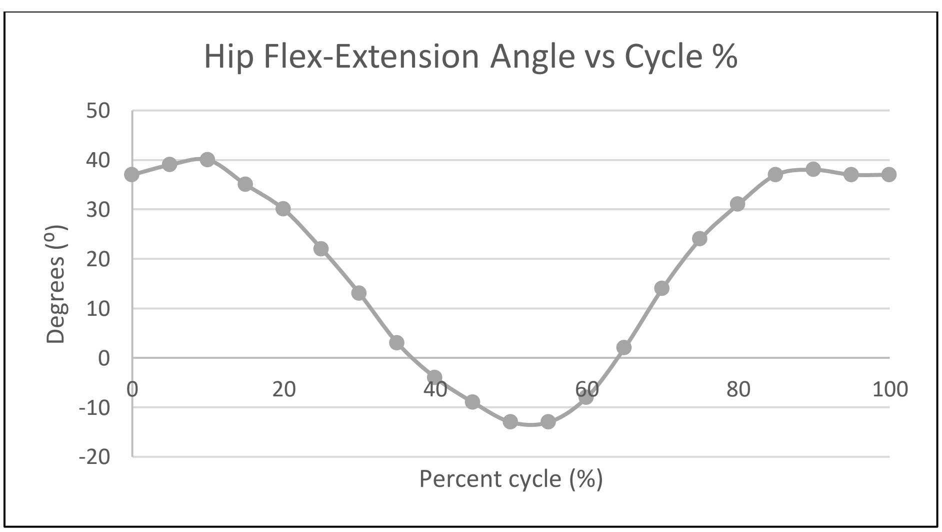

Figure 69 Trajectory of hip movement in a gait cycle [48]

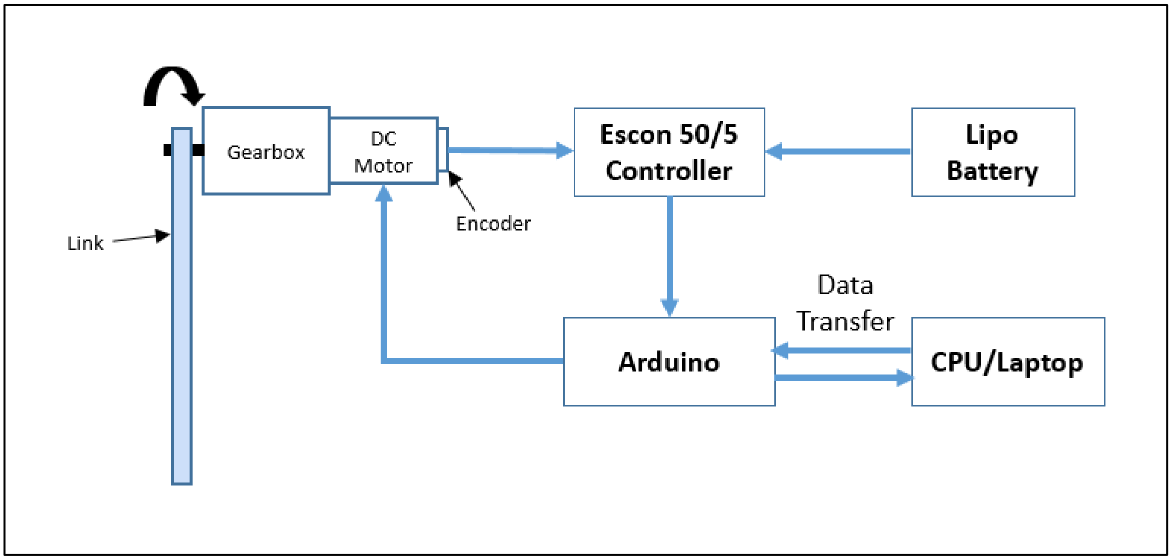

Figure 70 Schematic Diagram of position control of DC servomotor

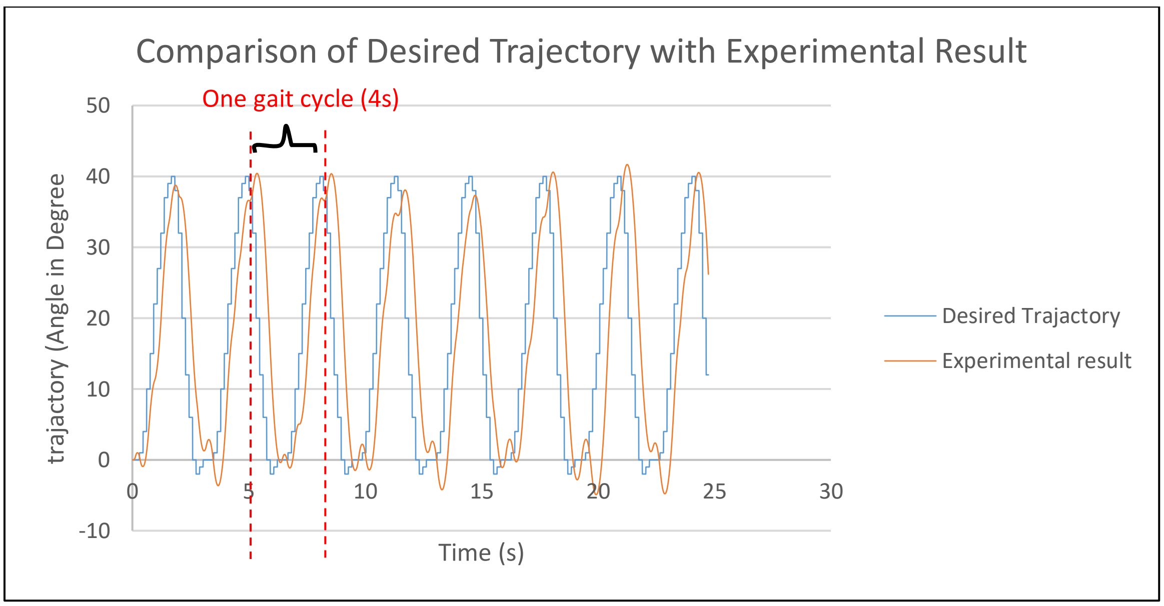

Figure 71 Comparison of desired trajectory with experimental result

4.1.5 Position Control of DC Servomotor in Simulation

A PI controller is also implemented to the Simulink model for position control as shown in Figure 73.The PI controller is used instead of a PID controller because the derivative gain of the controller causes an infinite damping to the system and the desired output could not be obtained. The PI parameter obtained from the experiment is used in the Simulink model. The reference trajectory and result from simulation with PI controller are plotted in Figure 72. The red dotted lines indicate that each gait cycle is completed in 2 seconds as shown in the Figure 72. The simulated trajectory experienced a slight delay compared to the reference trajectory. However, the overall result is close to the desired trajectory. In short, the PI controller is able to track the trajectory with satisfactory results from the reference trajectory.

In conclusion, both PI and PID controllers are suitable to be used for position control as seen from the results demonstrated above. However, further refinement of the controller in the experimental trial is needed in order to obtain a simulation model which can represent the actual experiment. Moreover, a stiffer position controller should be developed to accomplish a higher accuracy of desired output.

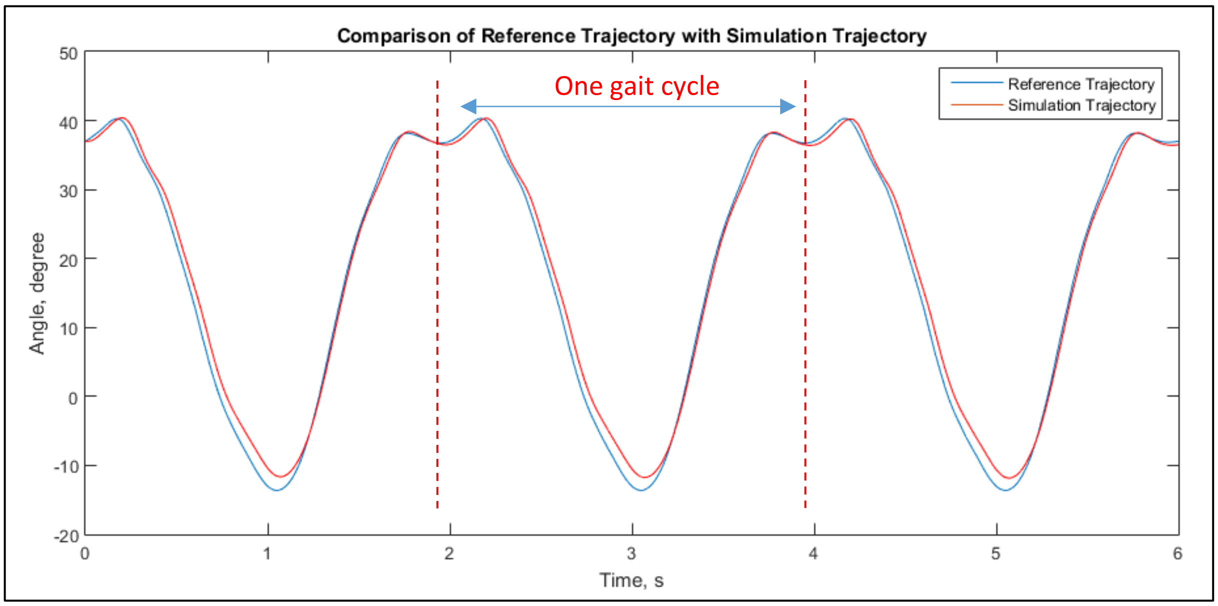

Figure 72 Comparison of reference trajectory with simulation trajectory

Table 12 PI controller for simulation with Simulink model

Parameters of PID Controller	**Value**
Proportional Gain	45
Integral Gain	3

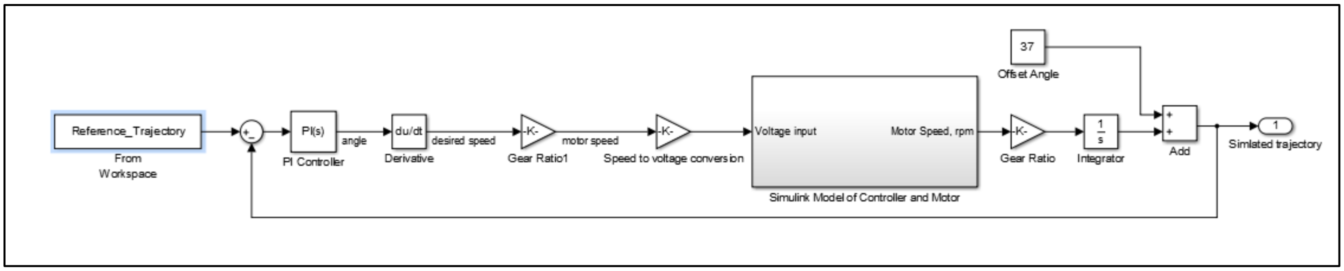

Figure 73 Simulink model with PI controller for position control

4.2 Verification of Simulation Model and Trajectory Control of Two-link Robotic Orthosis

The simulation of the trajectory control for one side of the robotic orthosis is developed to simulate the actual movement of the robotic orthosis. The Simulink model as shown in Figure 74 is built based on the actual setup of the robotic orthosis. The model consists of several major blocks that represent the system including the PID controller for both joints, DC motor model for both joints, and the dynamic model of the robotic orthosis. Desired input trajectories of knee and hip joints as shown in Figure 75 and Figure 76 obtained from a study of human gait pattern by University School of Physical Education, Wrocław, Poland are fed into the system and PID controllers are implemented at each joint to control the rotational angle of the link [48]. Parameters of both servo controllers (current limiter loop) are shown in Table 13. These parameters are obtained from the GUI of the Escon 50/5 servo controller after tuning with the Maxon Servomotor. A simulation of 12 seconds is conducted to obtain results for 3 gait cycles. Both experiment and simulation results are compared in the following section.

Table 13 Table of PI current controller parameters

Parameters	**Proportional Gain**	**Integral Time Constant**
Hip	181	134µs
Knee	208	122µs

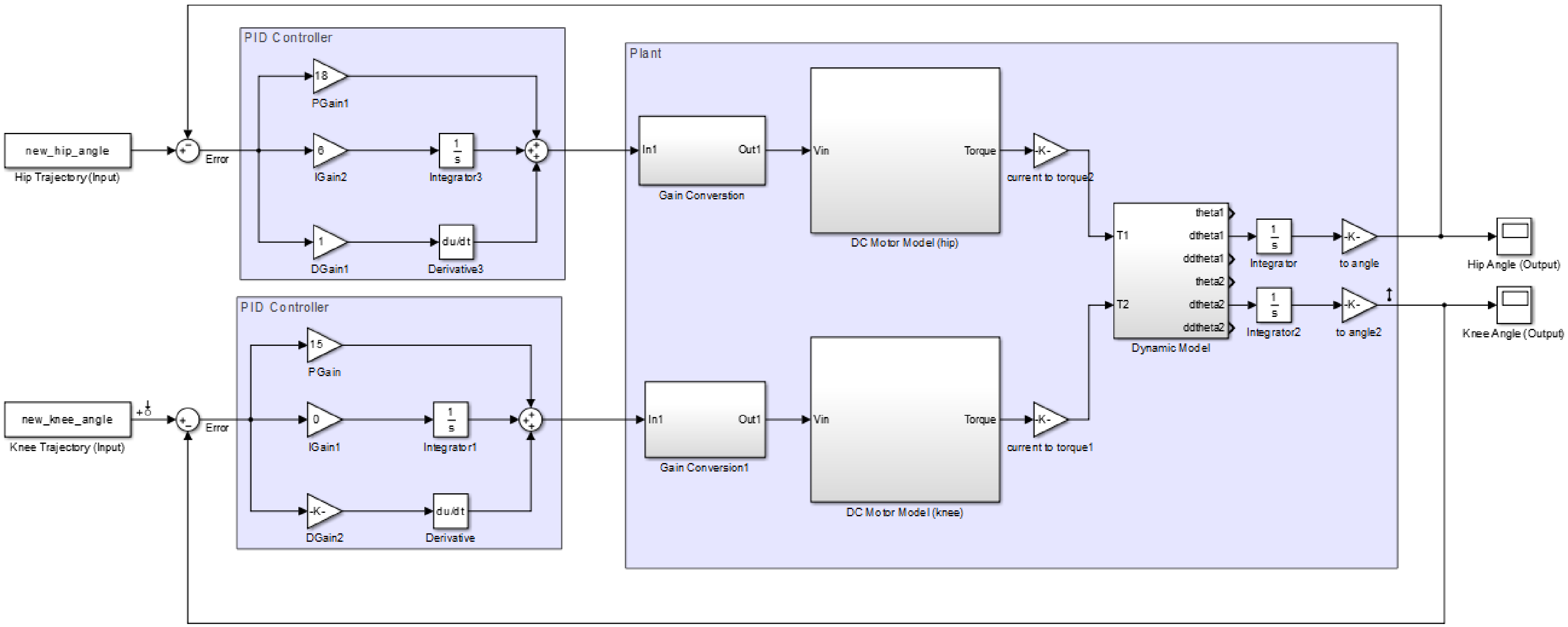

Figure 74 Simulation model for robotic orthosis (Escon 50/5 servo controller and DC motor)

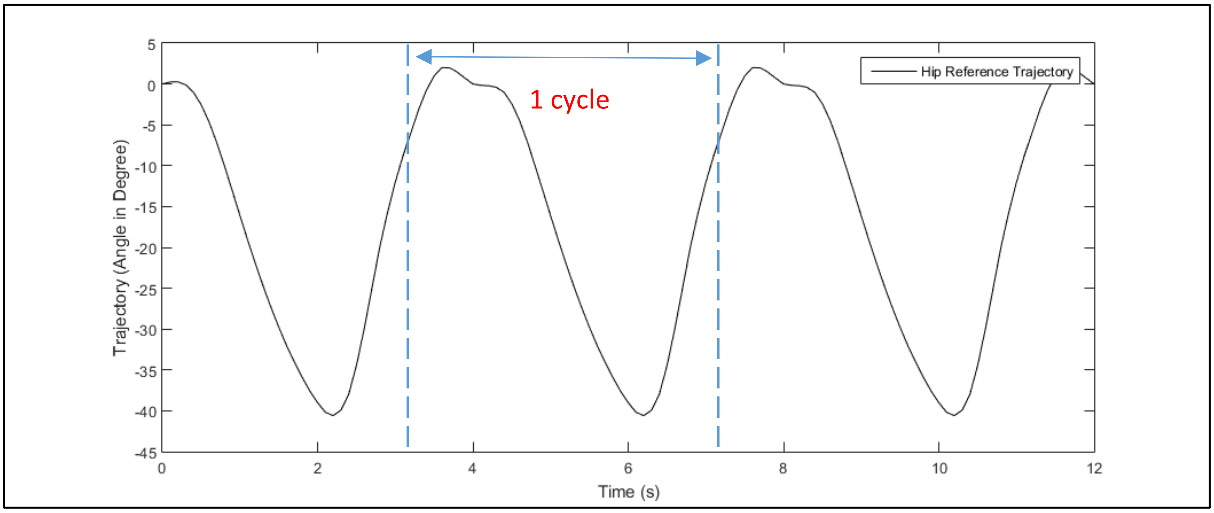

Figure 75 Reference trajectory for knee joint [48]

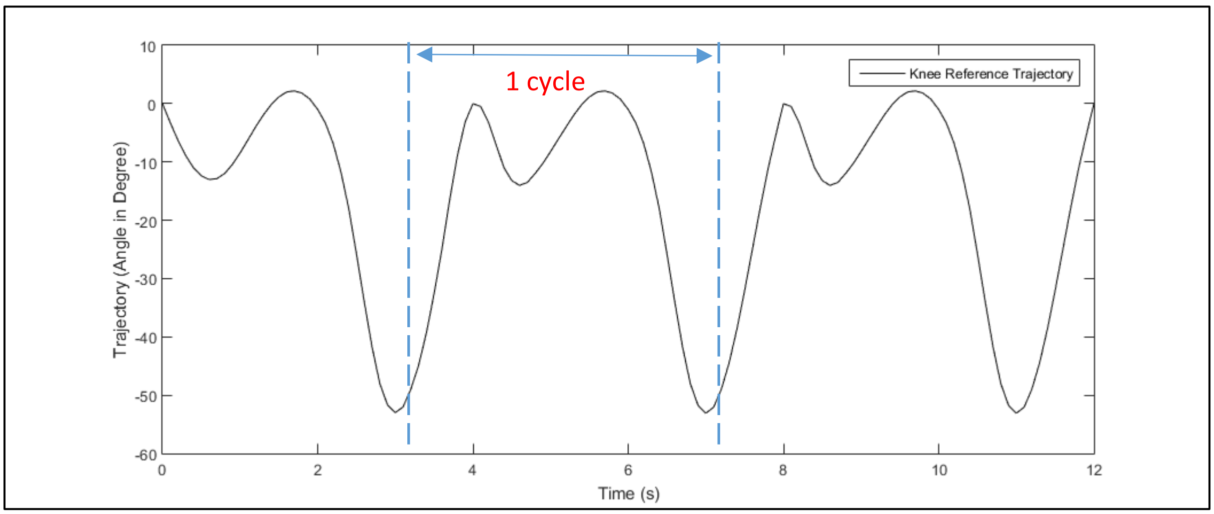

Figure 76 Reference trajectory for hip joint [48]

4.2.1 Verification of Motor Current and Speed for Experimental and Simulation Model

To verify the two-link robotic orthosis simulation model, step inputs with different voltage are applied to the actual system in order to record the motor current and speed output of each DC motor. Next, similar step inputs are applied to the Simulink motor model. The generated current and speed are recorded and compared to the experimental result. Table 14 shows the parameters of input and output of the DC motor recorded from the GUI of the Escon 50/5 servo controller.

In order to obtain a wide range of data for simulation verification, a series of step input is applied to the DC motor. The Arduino Due microcontroller is used to provide 5 different voltages to the DC motor by varying the PWM values. The experiment (DC Motor with Escon 50/5 Servo Controller) is being run for 5 seconds to generate the motor speed and current. The generated motor current and speed are captured with the GUI of the servo controller via encoder feedback. The average motor current and speed are then calculated and shown in Table 14. Next, the same procedures are repeated onto the simulation of Simulink model with the equivalent voltage as listed in Table 14. The equivalent voltage fed to the system is treated as a step input. Then, the findings of motor current and speed are recorded and plotted in Figure 77 to 82 to be compared with the experiment result.

Table 14 Parameters of input and output of the DC servomotor

PWM	**Equivalent Voltage input (V)**	**Average Motor Current (A)**	**Average Motor speed (RPM)**
20	0.737	0.2945	1078
60	1.082	0.3130	1595
100	1.423	0.3679	2110
140	1.767	0.3942	2626
180	2.112	0.4197	3182

4.2.2 Current Verification for Experimental and Simulation Result

Both simulated motor current and experimental motor current showed similar steady state results at different levels of voltage input, as recorded in Table 14. The maximum difference between both sets of values is only 0.0102A which is insignificant. However, there is slight overshoot during the transient response of the actual motor current signal as shown in Figure 77 to 81. The overshoot is due to the stationary condition of the DC motor before the voltage is applied to it, hence, a higher value of current is needed to overcome the friction and to turn the DC motor. This condition can be omitted in the simulation model as the motor will be turning continuously according to the reference trajectory in the actual simulation model of the robotic orthosis and overshoot of current will be prevented.

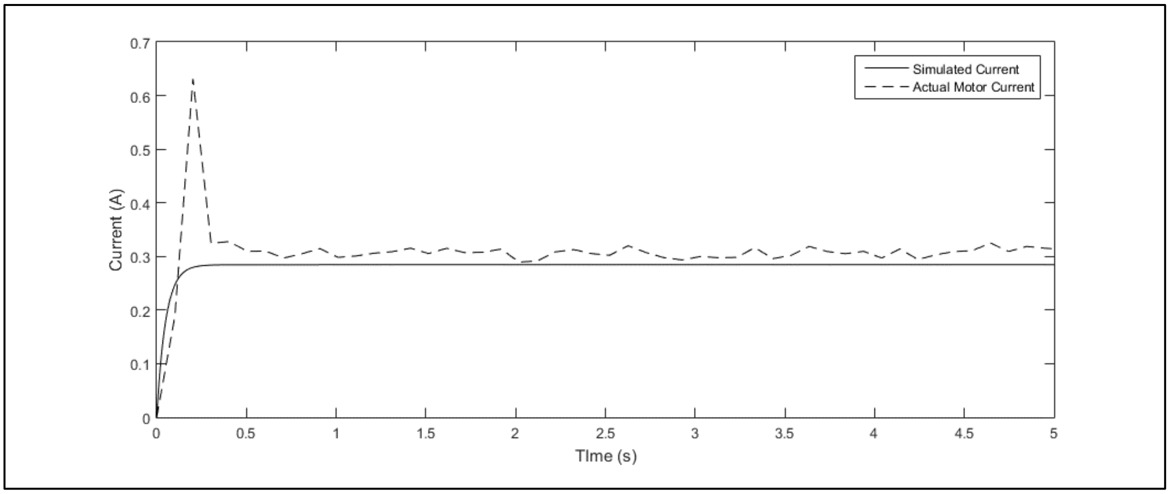

Figure 77 Current output of 20 PWM step input

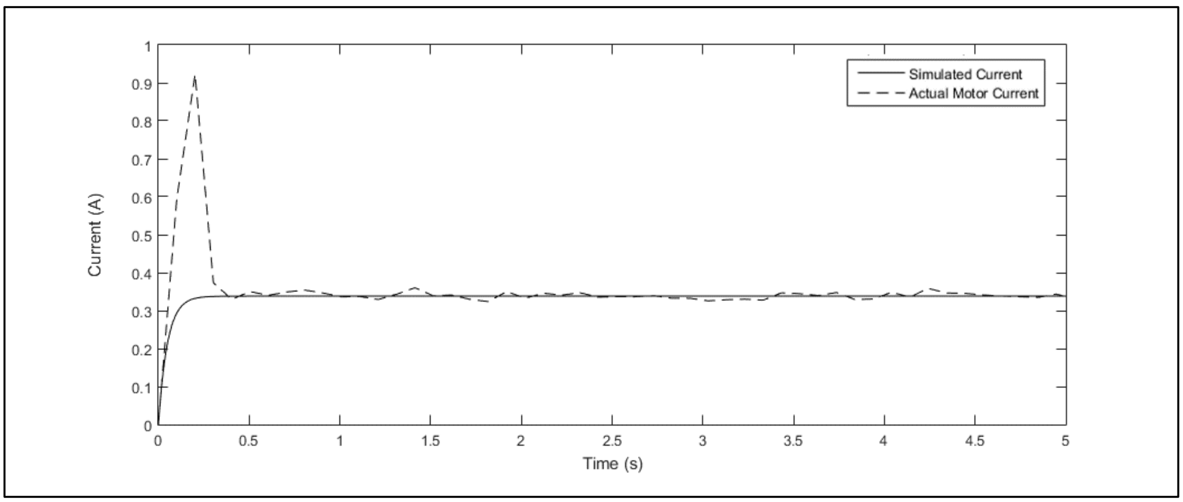

Figure 78 Current output of 60 PWM step input

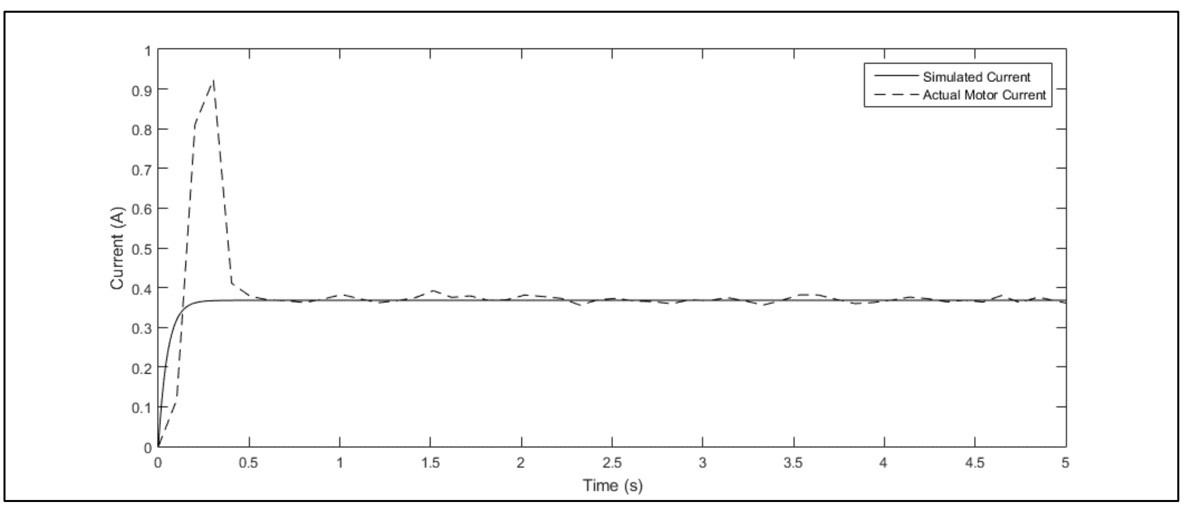

Figure 79 Current output of 100 PWM step input

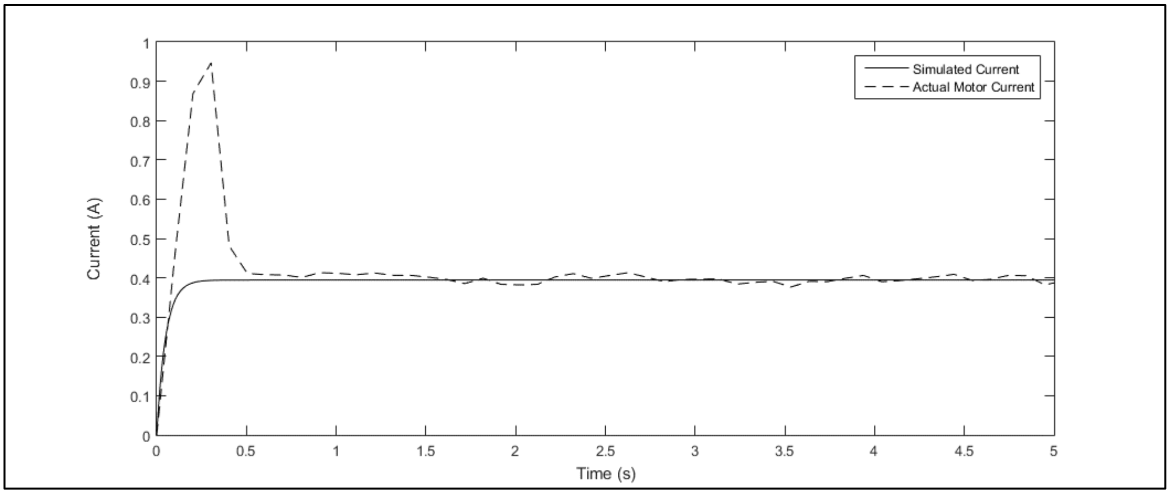

Figure 80 Current output of 140 PWM step input

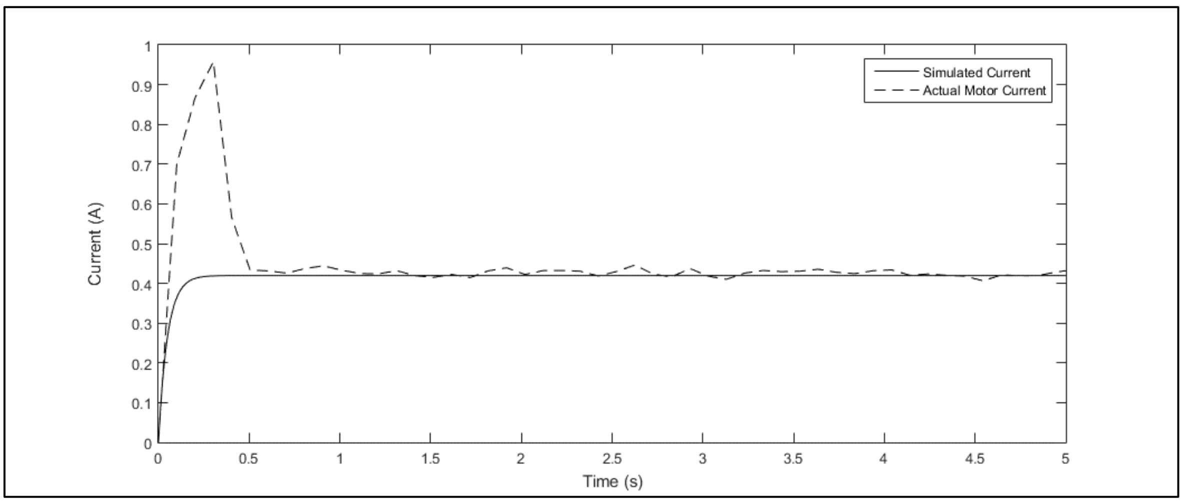

Figure 81 Current Output of 180 PWM step input

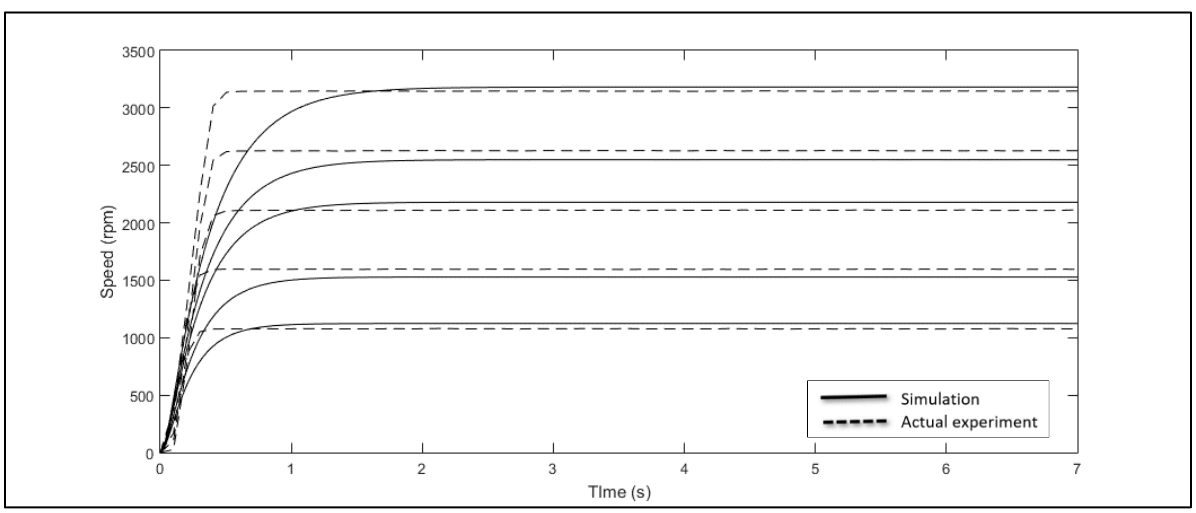

Figure 82 Compare motor speed of simulation (solid line) and actual experiment (dashed line)

4.2.3 Speed Verification for Experimental and Simulation Result

The motor speed generated from different levels of voltage input of both systems are also recorded and plotted respectively into Figure 82. The solid lines represent the simulation result while the dashed lines represent the experimental result. Both average motor speed at steady state obtained from simulation and experiment are calculated and recorded in Table 15. As shown in Figure 82, both simulated motor speed and experimental motor speed are comparable. The transient response of the motor speed of the simulation is slightly slower than experimental result. However, both results are similar in terms of steady state value as shown in Table 15. The maximum difference between the simulation and experiment values is 79 rpm. Since there is a gearbox attached to the motor with a ratio of 1:353, the difference of the final speed of the motor is only 0.22rpm, which is negligible. Hence, the design of the Simulink motor model is satisfying.

Table 15 Comparison of experiment and simulation result

Average Motor Current (A)	**Simulated Motor Current (A)**	**Average Motor speed (RPM)**	**Simulated Motor speed (RPM)**
0.2947	0.2845	1078	1123
0.3380	0.3381	1595	1528
0.3679	0.3678	2110	2179
0.3942	0.3941	2626	2549
0.4197	0.4149	3182	3181

4.2.4 Simulation Result of PID Trajectory Control for Knee Joint

The simulation model of robotic orthosis as shown in Figure 74 is used to perform the simulation of PID trajectory control for knee joint. In the process of obtaining the trajectory control result, the input of the hip joint is set to zero. A desired trajectory of knee movement (angle) of 3 complete gait cycles, as shown in Figure 75, is employed as a reference trajectory for the knee joint in the simulation model. Each gait cycle is set to be completed in 4 seconds. The simulation model is run with the desired trajectory input and a PID controller. Various PID constants are tested on the simulation model. The outcomes of the trajectory are recorded and compared. The desired parameters of PID control for knee joint movement are obtained after numerous analyses and are presented in Table 16.

Both simulation and experiment results are plotted in Figure 83. As shown in Figure 83, the simulation result has a similar pattern as the desired trajectory. The controller for the hip joint is able to generate an output trajectory that follows the reference trajectory. A slight overshoot is observed when the motor is about to change the rotational direction. However, the amount of overshoot is very little and hence is negligible. In conclusion, this shows that the PID constant is suitable to be implemented in the experiment to control the motor and link of hip joint.

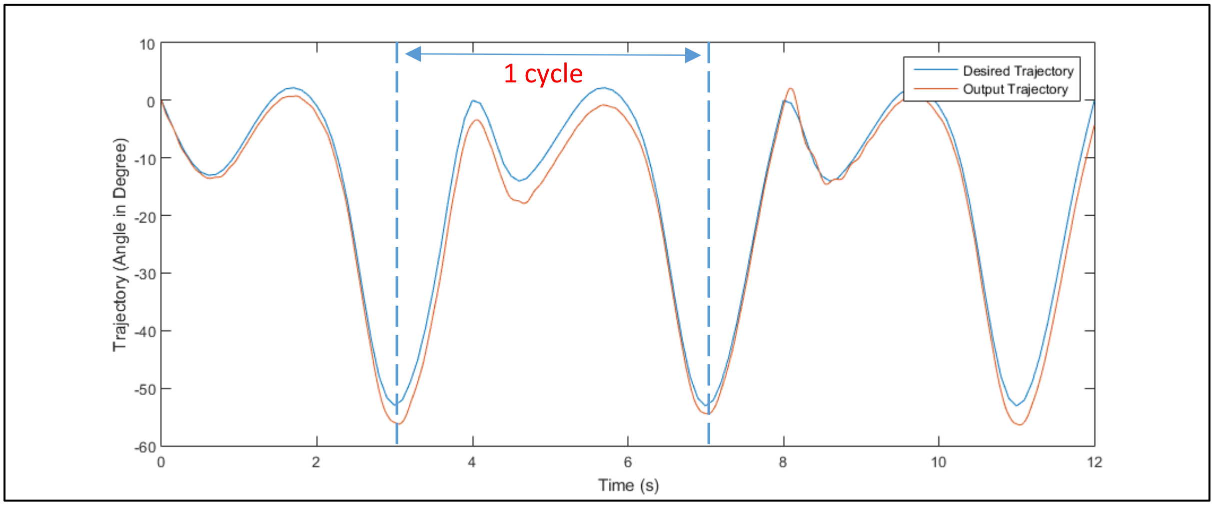

Figure 83 Comparison of desired trajectory with simulation output trajectory for knee joint

Table 16 PID Controller for simulation with Escon 50/5 servo controller for knee joint

Parameters of PID Controller	**Value**
Proportional Gain	15
Integral Gain	0
Derivative Gain	0.01

4.2.5 Simulation Result of PID Trajectory Control for Hip Joint

Desired trajectory of hip movement (angle) of 3 complete gait cycles as shown in Figure 76 is used as a reference trajectory for the hip joint for the simulation model. Similar to the knee joint, each gait cycle is set to be completed in 4 seconds and the simulation model is conducted with the desired trajectory input and a PID controller. The simulation model as shown in Figure 74 is applied and the input of the knee joint is set to zero. Various PID constants are tested on the simulation model. The results of the trajectory are recorded and compared. The best parameters of PID control for hip joint movement are obtained and presented in Table 17.

The desired trajectory input and simulation output of the hip joint are plotted in the same graph as shown in Figure 84. The output trajectory of the hip joint matched with the reference trajectory in an acceptable range, but the errors of the feedback signal of the knee jointincreased with time. In conclusion, this set of PID constants is not the best value for the controller. However, it can be applied to the experimental system for verification since both trajectories matched each other within an acceptable range. Besides that, each gait cycle was completed within 4 seconds.

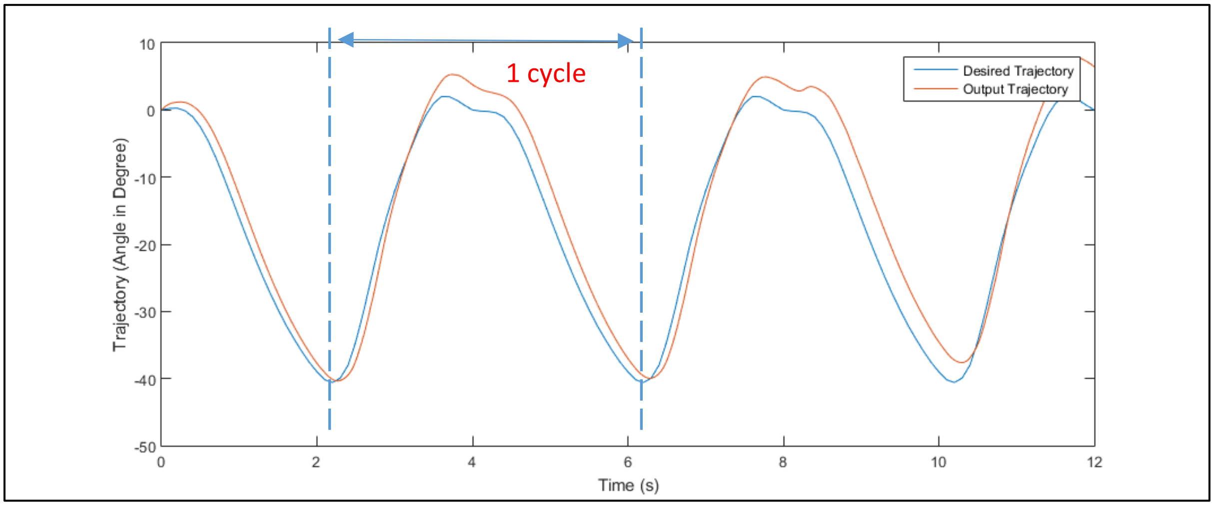

Figure 84 Comparison of desired trajectory with simulation output trajectory for hip joint

Table 17 PID Controller for simulation with Escon 50/5 servo controller for hip joint

Parameters of PID Controller	**Value**
Proportional Gain	18
Integral Gain	6
Derivative Gain	1

4.2.6 Experimental Result of PID Trajectory Control for Knee Joint and Hip Joint

The 4-DOFs lower limb exoskeleton, set up with Arduino Due and PID controller, is implemented to the trajectory control. Each side of the orthosis is controlled by one Arduino Due as shown in Figure 85. Figure 86 and Figure 87 as shown below present the comparison of desired input trajectories and experimental output trajectories for both joints of one side of the orthosis. The PID values gained from the simulation are applied in the experiment model for verification.

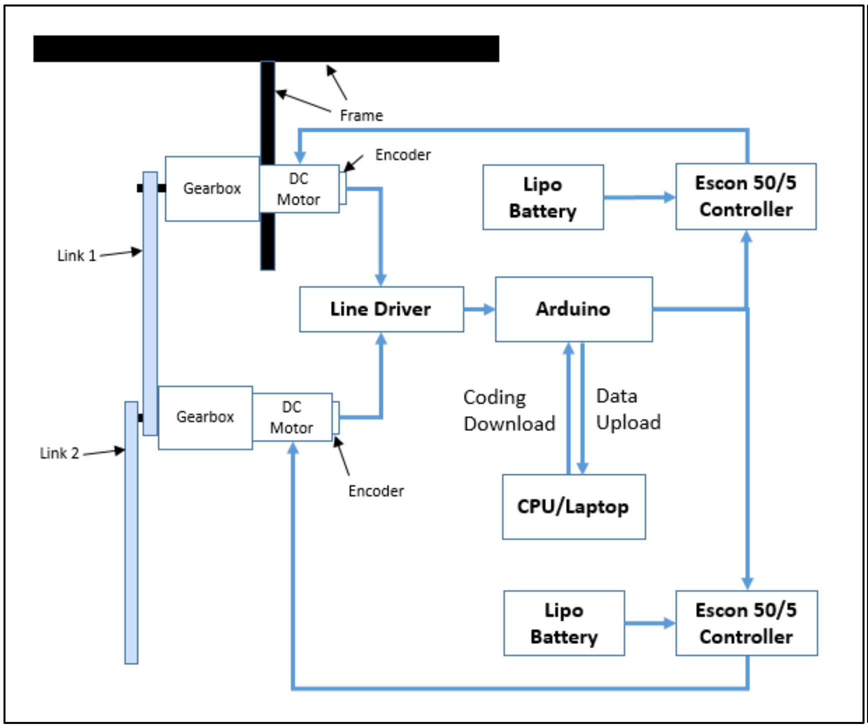

Figure 85 Schematic diagram and experiment setup of two-link robotic orthosis

For the experimental setting of the knee joint, PID controller is implemented with the PID parameters obtained from the simulation model run in MATLAB. As shown in Figure 86, there is a slight delay of 0.5 second at the start of both reference trajectory and experimental output trajectory caused by the debounce of the push start button. The time required for the knee joint to finish one gait cycle is 4.4 seconds. The 0.4 second delay is due to time consumed for system calculation and complexity of the system, which involved sensors, integrated circuits and massive wires. Although the experimental output has a slight delay as compared to the simulation result, it is able to present a similar pattern as the input reference trajectory. Hence, the PID constants for knee joint (as shown in Table 18) obtained from the simulation is proven to be applicable and the simulation model is verified.

Similar experimental procedure for the knee joint is applied to the hip joint to verify the PID constants (Table 19) obtained in the simulation. Each gait cycle is finished within 4.4 seconds which is similar to the experimental result of knee joint as shown in Figure 86. A 0.5 second delay is also observed at the starting of the system due to the debounce of the push start button. In Figure 87, a slight delay of 0.2 second is observed between the desired trajectory and the experimental output. Besides that, a jerk is observed at 5.2 seconds during the change in motor rotation direction. The jerk in experimental trajectory response is caused by the rotational inertia of the DC motor when it is slowing down and about to change its direction of rotation. Thus, the PID controller needs to be refined to obtain a more satisfactory result with a minimal deviation from the desired trajectory. Besides that, more experiments need to be carried out to ensure the delay time of each joint is the same for desired movement of a gait cycle.

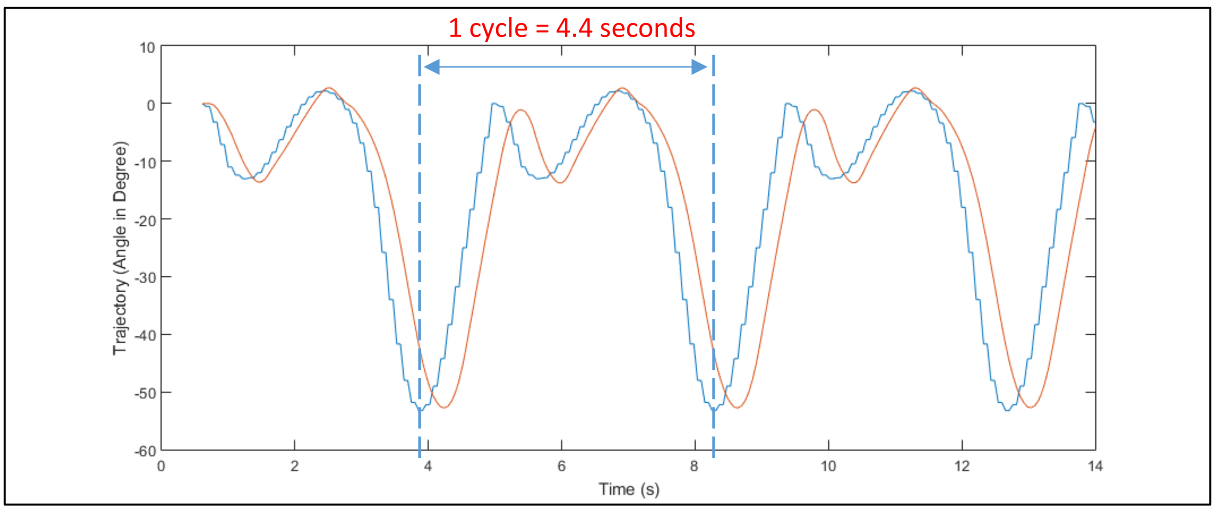

Figure 86 Comparison of desired trajectory (red line) with experimental output trajectory (blue line) for knee joint

Table 18 PID Controller for experimental testing with Escon 50/5 servo controller for knee joint

Parameters of PID Controller	**Value**
Proportional Gain	15
Integral Gain	0
Derivative Gain	0.01

In conclusion, the motor model is being verified by comparing the motor speed and current with the outcome data recorded from the Escon 50/5. The motor model is combined with the PID controller and dynamic model to simulate the actual model of robotic orthosis. Desired PID values are obtained from the simulation model and applied to the actual system for verification. Both PID values for the hip and knee joints show satisfied results during actual implementation with the robotic orthosis. It shows that the PID controller is suitable for the robotic orthosis to provide a trajectory control. However, slight delay is observed for both joints in the actual implementation. Besides that, there is a jerk observed from the experimental output of the hip joint with the tuned PID values. Hence, the PID controller needs to be refined or substituted with a more advanced controller in order to obtain a more satisfactory result with a minimal deviation from the desired trajectory.

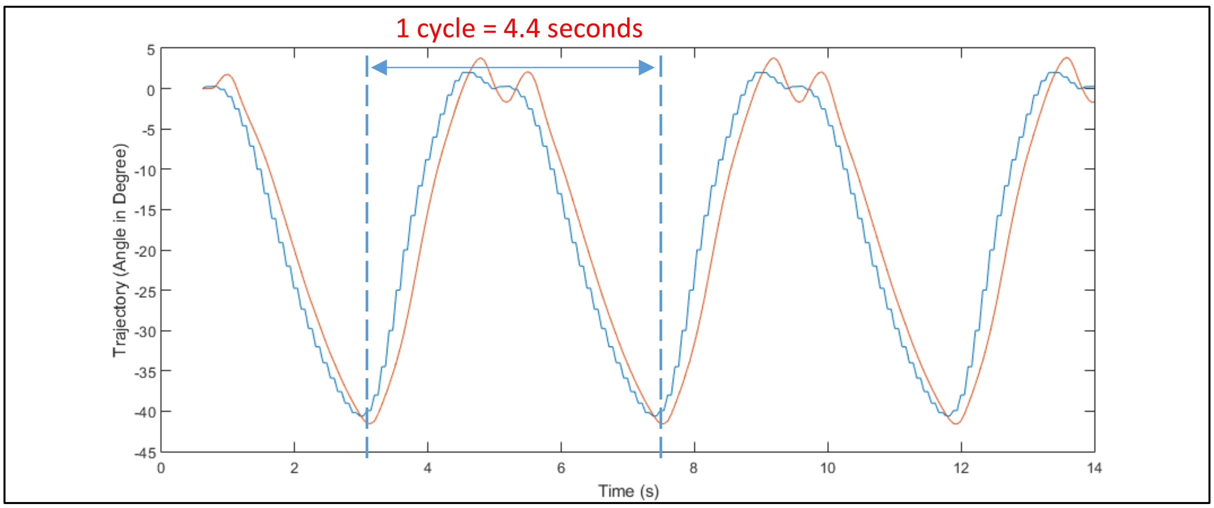

Figure 87 Comparison of desired trajectory (red line) with experimental output trajectory (blue line) for hip joint

Table 19 PID Controller for experimental testing with Escon 50/5 servo controller for hip joint

Parameters of PID Controller	**Value**
Proportional Gain	18
Integral Gain	6
Derivative Gain	1

4.3 Conventional Controller Design

A conventional control design is done with the two-link manipulator (one side of the leg) after the setup and verification of the simulation of the robotic orthosis. In order to control the desired positions and angle movement of the DC servomotor, a faster PID control system to perform a correct gait trajectory is developed in this section. The Arduino Due is used to perform the conventional control of the two-link manipulator. The Arduino coding used in Section 4.2.6 is modified to perform the trajectory control with a cycle time of 2 seconds. The schematic diagram is shown in Figure 88 while the circuit connections of the system is attached in Appendix D.

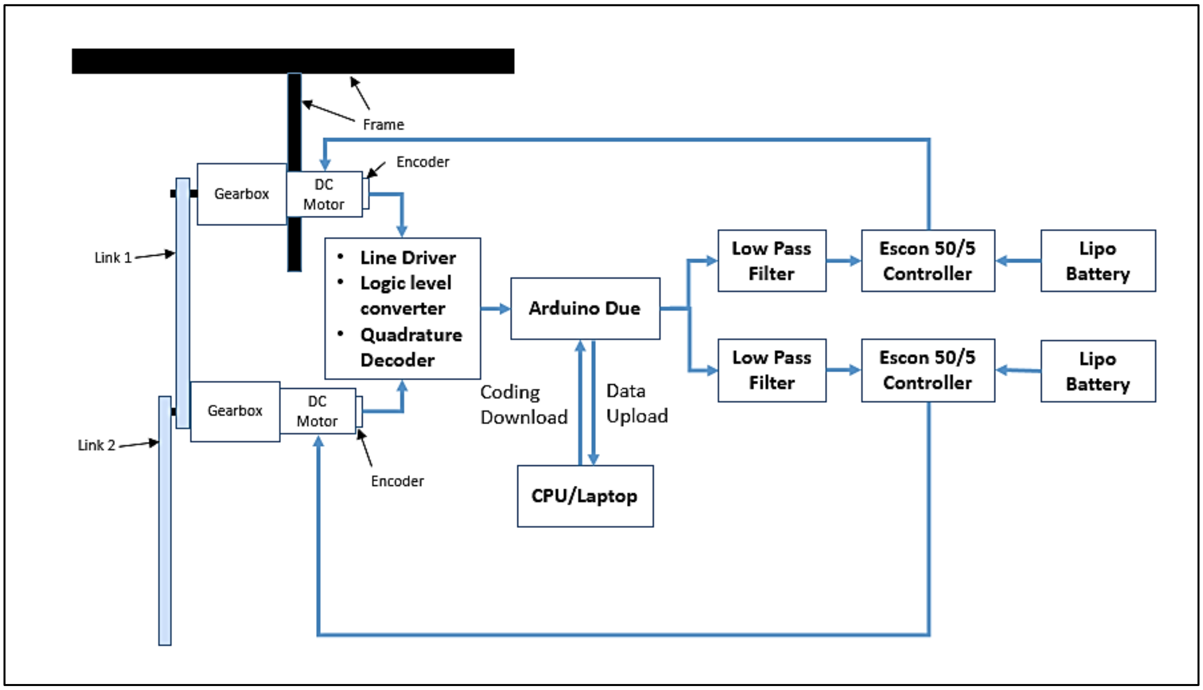

Figure 88 Schematic Diagram of two-link manipulator with conventional controller

Firstly, the hip and knee gait reference trajectories of a complete gait cycle as shown in Figures 75 and 76 are pre-set in the Arduino microcontroller with the discrete number method. Each gait cycle is set to be completed in 2 seconds with 22 setpoints. The PID controller used in the code is applied to compute the output to the DC motor by multiplying the error with the controller gains. Next, the PID output is saturated with the range from -255 to 255 of PWM, and the PWM signal is then converted to a voltage to activate the DC servomotor and drive it to the desired position. The block diagram and flow chat are shown in Figure 89 and 90 respectively.

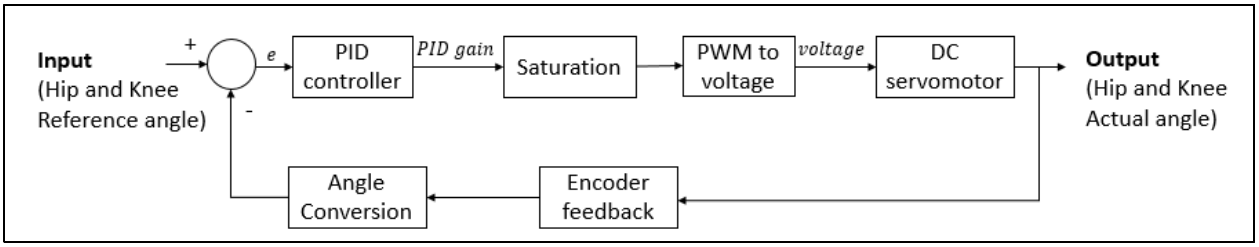

Figure 89 Bock diagram of PID control system

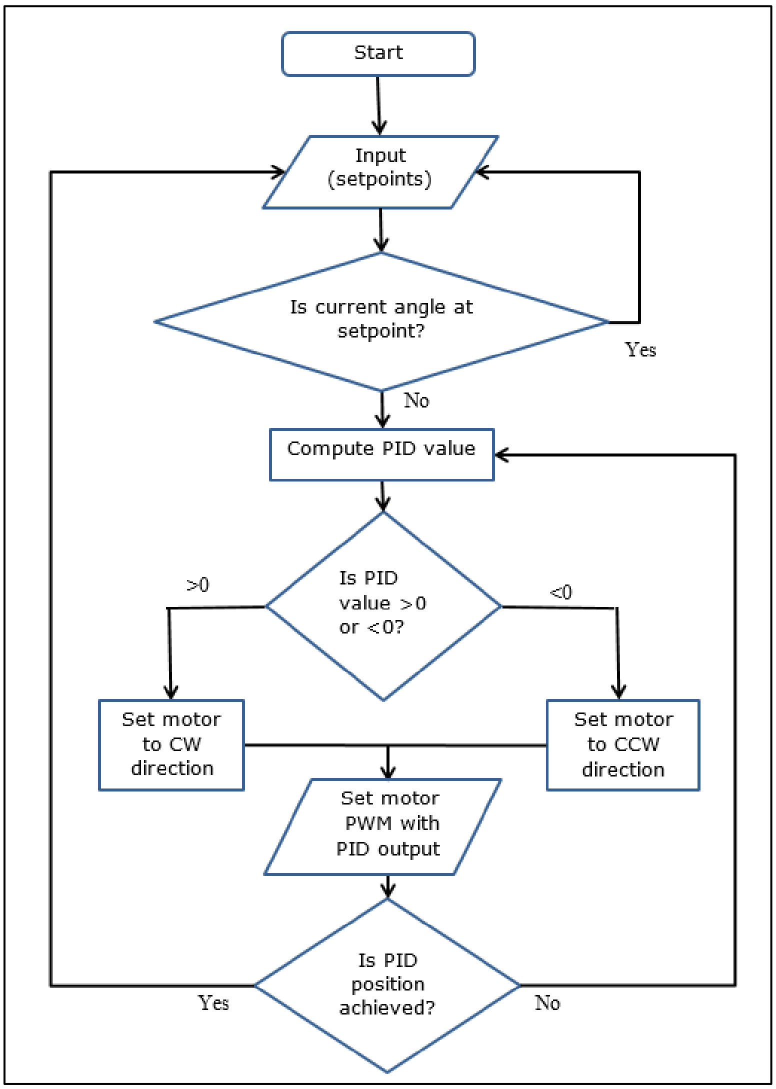

Figure 90 Flowchart of PID control system

Various PID constants are tested on the motor with both links after having setup the two-link manipulator and the Arduino code. All the outcomes of trajectories for both knee and hip joint are recorded and compared. The desired parameters of the PID controller are obtained and recorded in

Table 20. The PID controller results are plotted with the desired trajectories in Figure 91 for hip joint and Figure 92 for knee joint respectively.

Table 20 Parameter for PID control system

Parameters of PID Controller (link 1)	**Value**	**Parameters of PID Controller (link 2)**	**Value**
Proportional Gain	45	Proportional Gain	47
Integral Gain	2	Integral Gain	3
Derivative Gain	5	Derivative Gain	11

As shown in Figure 91, the output trajectory from the PID controlled setup has a 0.2 second delay from the desired trajectory. Besides that, there is an overshoot of 7 degrees at the minimum angle when rotating link 1 is about to change the direction of turning. A slight jerk is seen from the experimental trajectory output at 2.4 seconds after the maximum angle is reached. The overshoots and jerks observed from the outcomes are due to the rotational inertia of the DC servomotor, formed when it is slowing down and about to change its direction of rotation. Furthermore, the response for the hip joint is oscillates quite frequently and the disturbance generated from link 2 might have contributed to the jerks. This showed the insensitivity of the PID controller in the trajectory tracking of the hip joint of the two-link manipulator. The controller for link 1 needs to be refined to obtain a more satisfactory result with a minimum deviation from the desired trajectory.

The output trajectory of link 2 with PID controller (as shown in Figure 92) shows that the knee joint did not experience any delay in the output. Slight overshoots are seen every time when the DC servomotor is about to change its rotation direction. The overall response of link 2 is very close to the reference trajectory as compared to link 1. The reason for a stable outcome is because there is nothing much attached to the motor except link 2 with a smaller weight. The DC servomotor of link 2 does not experience disturbance as much as DC servomotor of link 1. Hence, the PID controller is sufficient for the trajectory control of link 2. In short, the PID controller is not suitable for a two-link robotic orthosis even though effective controller result is shown in link 2, as the PID controller is unable to cope with the disturbance and decoupling effect from the other link.

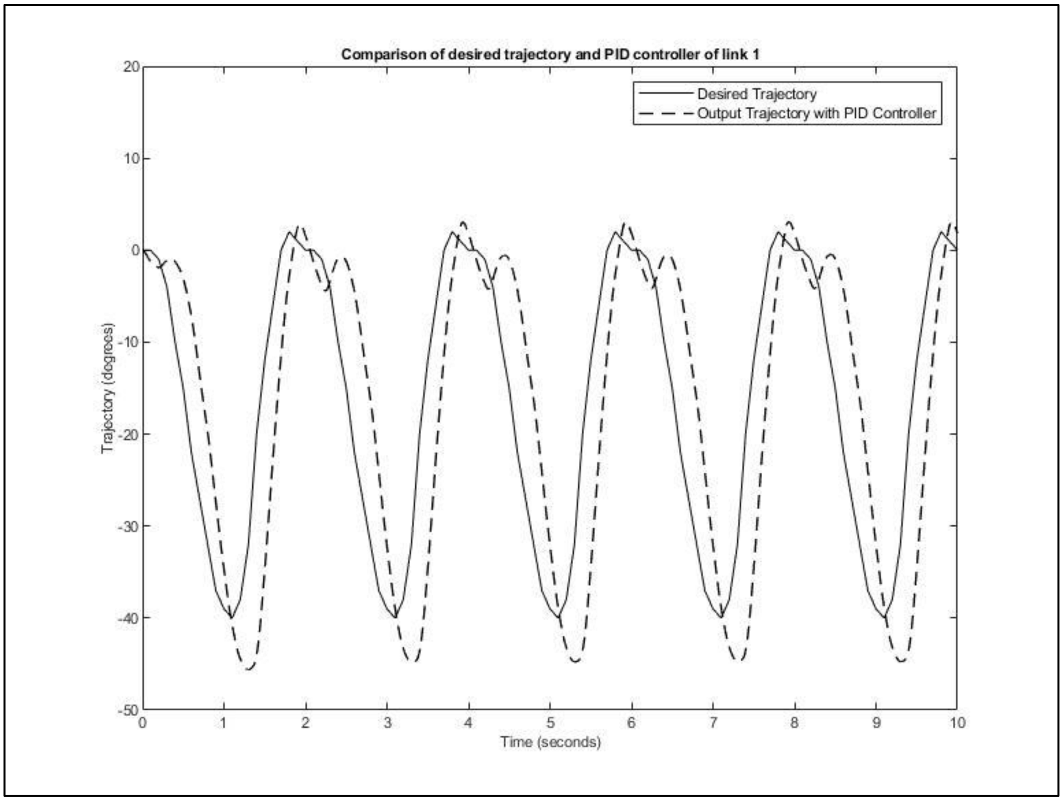

Figure 91 Comparison of desired trajectory and PID controller of link 1

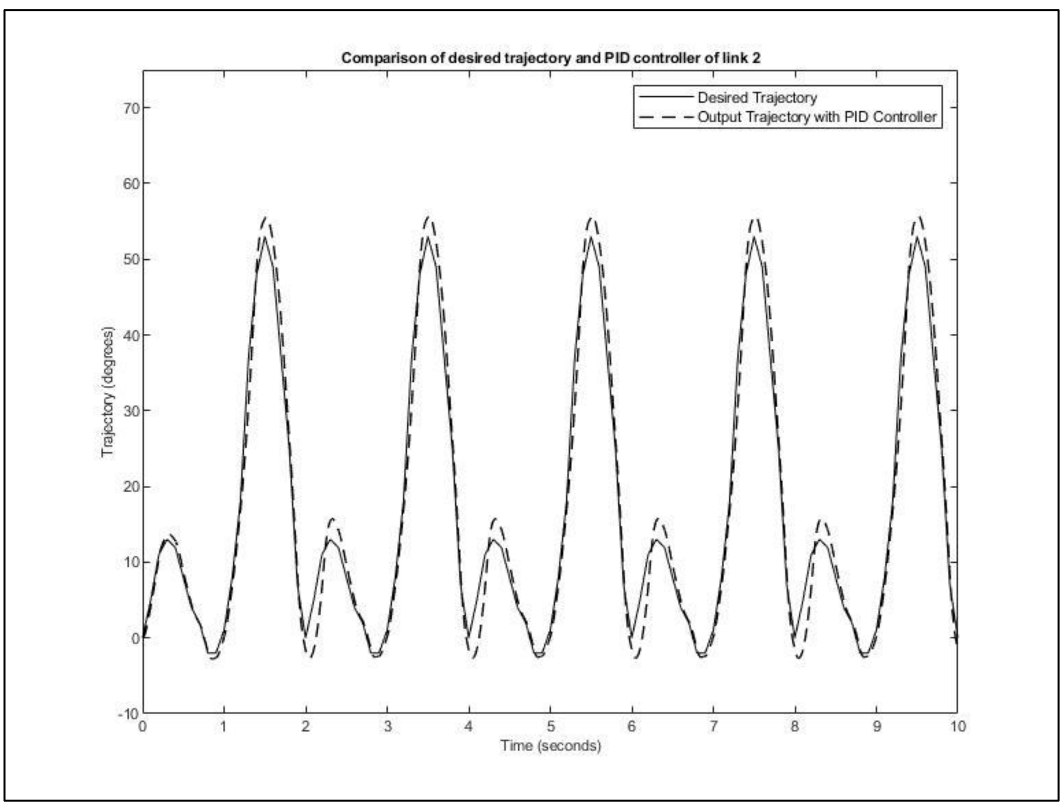

Figure 92 Comparison of desired trajectory and PID controller of link 2

4.4 Conclusions

In this chapter, preliminary work on the development of a simulation model of the DC servomotor with Ecson 50/5 servomotor controller is done. To verify the simulation model, motor current and motor speed in simulation and experiment are compared. Desired trajectory of hip and knee joint are input to the experimental setup. Limitations are observed in the system during the changing in rotational direction of the motor. Angle-time data of trajectory utilized in this research can help to build up a proper walking manner for patients as each instance from the data is able to provide accurate position and moving angle for impaired hip and knee.

Then, a simulation model of the two-link robotic orthosis is developed and verified with experimental data. Exploration of controller to track gait profile is done. A PID controller is implemented to each joint for trajectories control in simulation and experiment. Best PID parameters combination for experiments and simulations are obtained based on repeated testing and comparison between the outcomes of each test. However, the outcomes of the experimental results are not satisfying and further adjustment of the PID controller is done to obtain an outcome with minimal deviation from the desired trajectories. The Arduino coding of the experiment setup with the PID controller is improved and a shorter cycle time compared to the previous experiment is achieved in the new setting. In the improved system, there are still slight delays and overshoots observed from the outputs due to limitation in representing the full system with mathematical equations or component simulations. Further investigation needs to be done to cope with the disturbance and decoupling effect from the respective links. However, simulation and experiment done with PID controller for the rehabilitation orthosis is a benchmark for the development of control strategy for a robotic orthosis.

Chapter 5 Describing Function (DF) and Controller Synthesis Procedure

5.1 Introduction

As discussed in the previous chapter, both the Simulink model and experimental setup control with PID controller are assessed with step inputs and trajectory inputs. The results from both systems are compared, and it does not provide an adequate outcome as the classical system model transfer function is unable to fully mimic the actual plant model. Hence, representing the nonlinear plant only from the dynamic model of the plant is not an ideal solution or even impossible with the presence of load torque disturbances, discontinuous nonlinearities such as saturation and backlash as well as multivariable in the system. Thus, a linearized approximation for the nonlinear plant at its nominal operation condition, as known as describing function approach, is required. Implementation of describing function is expected to solve the problems stated in the previous chapter.

In this chapter, the describing function approach will be discussed. Sinusoidal-input describing function approach with lead-lag compensator will be introduced. Next, procedures of generating the new SIDF model with controller for the rehabilitation orthosis are presented. In the final section, the actual implementation of SIDF model and controller is reviewed. The benefits of the SIDF approach in this research are discussed.

5.2 Describing Function and Controller

Various problems such as delays, and overshoot of signal are detected in the exploration of a PID controller to track the trajectory profile. Multivariable and nonlinearities of the robotic orthosis are the factors of these problems. To improve the control system design of the orthosis, SIDF approach is introduced. This approach aims to reduce the gap between a control system analysis and the design of a nonlinear system with linearization theory, hence, provides a novel contribution to the control systems and strategies for a robotic rehabilitation system.

Besides that, for a lower limb device with rehabilitation purpose, it is important for the controller to control the manipulator and at the same time be able to correct the gait motion of a hemiplegic stroke patient. Abnormal gait pattern signal of the patient is obtained and fed to the system, and a robust controller is responsible to send out appropriate commands to tune the moving angle of the rehabilitation orthosis. Hence, a precise controller in tracking the gait profile at each instant is needed.

The controller of the rehabilitation device is able to be generated via simulation in MATLAB after the SIDF model of the nonlinear system is formed.

5.2.1 Introduction of Describing Function

The describing function approach is gaining attention in recent research to develop controllers for nonlinear systems as it is a robust tool to approximate the nonlinear plant model with a linear mathematical function that is usable of controller designs in simulations. Difficulties in representing the multivariable, discontinuous nonlinearities and disturbances of the system are overcome with the linear approximation properties of the describing function. In the past two decades, the describing function approach method has been implemented in a few applications and the design of nonlinear control systems such as liquid propellant engine [39], space robots [104] and two-link robot in horizontal plane [38], [117]. Hence, the describing function-based system approach which has no restriction on the nonlinearities mentioned is required for the controller design to represent the nonlinear plant at its nominal operation condition.

Describing function (DF) is a frequency domain approach established to represent a nonlinear system with a linear time-invariant system approximately with an equivalent transfer function. This approach is suitable to predict the behaviour of a feedback system within a limited operating period. This method is applied based on quansi-linearization by generating a linear time-invariant transfer function based on the amplitude of the input signal to mimic the behaviour of a nonlinear system. The aim of the use of the describing function is to reduce the gap between the control system analysis and design of nonlinear system with the rich theory of linear system [38], [104].

The describing function method based on cases of nonlinear systems with single nonlinearity had been discussed and written in text by Gelb and Vander Velde [118] in 1968 and Athertone [119] in 1975. Later, cases of RIDF were discussed by Kazakov [120], Gelb and Warren [121] in 1965 and 1973 respectively; cases of SIDF were discussed by Talyor [122] and Hannebrink et al. [123] in 1977 for systems with various nonlinearities. The SIDF approach is mainly applied to systems with limited period of cycles to characterize the input and output characteristic of a nonlinear system in frequency domain, while RIDF method is widely used for nonlinear system analysis and design with random input signals. However, SIDF is by far the most widely used of the numerous describing functions, and is also the best of the numerous kinds of model to design a robust nonlinear feedback system.

5.2.2 Basic Describing Function

In many practical problems, the feedback system consists of two major parts, the linear part and nonlinear parts. In most circumstances, the linear part of the plant is known, while uncertainties of the system response are due to the effect of nonlinearity in the feedback loop. As shown in Figure 93 *f(u)* represented the nonlinearities in the system while *G(jω)* represented the linear section of a plant. The nonlinear phenomenon included saturation of actuators, backlash of gears, hysteresis in magnetic materials, Coulomb friction, relay control and dead zone in the electromechanical system etc. [124], [125].

In order to identify the basic describing function of the nonlinear system, a limit cycle prediction had to be done with the assumption that there is only single nonlinearity in the system. Limit cycle is a periodic oscillation around a constant working point. However, limit cycle analysis has a few drawbacks in the control system. The limit cycle can cause instability of the equilibrium point and hence lead to loss of accuracy in regulation. Mechanical failure and wear off might happen in the hardware due to constant oscillations [124], [126].

As shown in Figure 93, if the nonlinear term is a time-invariant constant, the stability of the feedback system can be found via the Nyquist condition, which provides the number of roots with positive real roots of the Harmonic Balance Equation (6).

$$1 + G(j\omega)\frac{1}{k} = 0\,, \tag{6}$$

where k is the nonlinear term

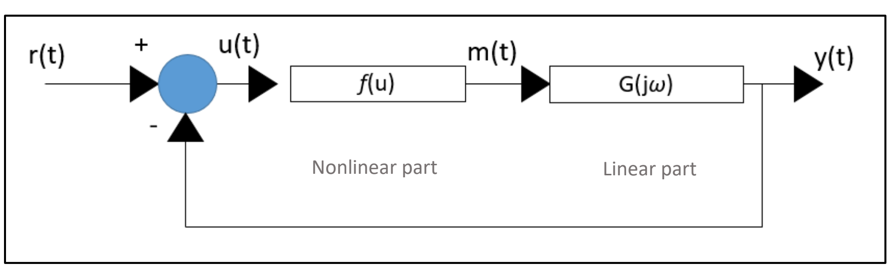

Figure 93 Block diagram of nonlinear system

With the use of limit cycle, the output, *y(t)* of the nonlinear system is mostly a sinusoidal signal with the lowest harmonic oscillation, as the linear component are usually has low-pass filter properties as shown in Equation (7), and it can be decomposed as the sum of many harmonic oscillation. Hence, the higher harmonics of the nonlinear element is neglected where only the first harmonic is considered in the output *y(t).*

$$|G(i \cdot \omega)| \gg |G(n \cdot i \cdot \omega)| \text{ , for n= 2, 3, …} \tag{7}$$

Furthermore, in order to perform the basic describing function analysis, the nonlinear properties in the system must be symmetric with respect to the origin. This assumption is introduced for simplicity as it assures that the static term in the Fourier expansion of the output of the nonlinearity can be neglected.

5.2.3 Sinusoidal-Input Describing Function (SIDF)

The SIDF is by far the most widely used of the numerous describing functions, also the best of numerous kinds of models to design a robust nonlinear feedback system. This method is applicable to nonlinear plants which have discontinuous or multivalued nonlinearities. It can deal with a highly nonlinear system without limitations on the number of nonlinear terms, nonlinearity kind and arrangement of the plant. The input and output behaviour of a nonlinear plant is dependent on the amplitude of the excitation signal and it can be captured with the SIDF model.

With this SIDF approach, there is no limitation on the system order as well as the number of inputs and outputs. This model is also capable of characterizing the dependency of the nonlinear plant on the expected range of frequencies of interest. The design of the robust nonlinear closed-loop system based on SIDF model can contribute to a solid basis for a robust design as the range of excitation amplitude levels are bounded. Furthermore, a robust closed-loop system without sacrificing performance can be achieved. The SIDF model is able to characterize the behaviour of the nonlinear plant with only one parameter which is the amplitude of excitation, hence, simplified the system model design. It is able to hold the amplitude sensitivity characteristics of the nonlinear system and represent the model in standard state-variable equations. Also, this model allows the controller design for nonlinear plants with discontinuous or multi-valued nonlinear terms [108], [110], [117].

An introduction of the describing function method utilised in conventional nonlinear system controller design based on one or more operating range was presented in the year of 1983 [127]. This technique had been applied in a nonlinear feedback system in position servo design problem from robotics and the liquid propellant engine in aerospace industries [105]–[107]. In the year of 1987, a great milestone was achieved by gaining the SIDF model of the highly nonlinear plant with a computer-aided engineering (CAE) environment designed based on the input/output characterisation of the plant as discussed in the literature review section [108]. Further software development was done in MATLAB in 2002 by upgrading the characterisation method to support multivariable nonlinear systems [39]. New systematic procedure to perform tracking and decoupling of the nonlinear multivariable system via stabilisation of the unstable system was introduced in 2009 [117]. A new software for controller design of the nonlinear system was then developed to replenish the controller synthesis procedure [109]. The software was then further developed with new, easy and well organised steps, including the method to obtain the describing function model and to design the idle speed controller for a nonlinear automobile engine with time delay [110].

5.2.4 Describing Function and Lead-lag Controller

Lead-lag controller is one of the most common classical control theories and can be found in various sources, for example in [128]. It is a control scheme consisting of phase lead compensator and phase lag compensator. It is often known as a component in a linear control system to improve the frequency response of a feedback control system. This compensator works by adding different numbers of poles and zeros to alter the transfer function in order to improve the transient response, stability and steady state error in a feedback loop. This controller has better performance in controlling the servo system compared to PID controller [129]. The lead controller is commonly used to reduce the percentage overshoot, while the lag controller improves the accuracy of steady state. However, the performance of a linear lead-lag controller is limited with a wider operating range. In 2004, a closed-form solution for lead-lag compensator with describing function based approach was developed [130]. The design technique allows the user to generate the lead-lag compensator based on a defined desired transfer function of the controller.

In the CAE [131], a series of MATLAB tools for SIDF model and controller design were developed. This integrated tool with a set of MATLAB routines allowed users to perform analyses for nonlinear control systems without restrictions on the system order to generate a characteristic equation and to design different types of compensator including lead-lag, Proportional-integral-derivative (PID), proportional and rate feedback, and n-th order linear compensator. A SIDF model of the nonlinear system needs to be generated beforehand and a desired closed-loop behaviour in terms of the desired order of transfer function is required in order to run the tool. A unified approach which minimizes the mean-squared error of the objective function is applied to generate a set of linear simultaneous algebraic equations. These final products will be the desired compensator generated for the nonlinear system.

5.3 Design Procedure of Sinusoidal Input Describing Function (SIDF) Model

The synthesis of the SIDF model and the lead lag controller for this nonlinear 2-input-2-output system is methodical. Direct optimization approach is used to tune the controller. This method consist of four major steps as follows:

Step 1: Generate of SIDF model and stabilize the model.

Step 2: Controller design using any linear control theory technique.

Step 3: Determine the optimum constant gain of the controller.

Step 4: Verify design via nonlinear simulation.

5.3.1 Generate of SIDF Model and Stabilize the Model

The simulation model as illustrated in Figure 94 is built in the Simulink environment based on the dynamic model of the nonlinear two-link system as shown in Figure 59. The actual simulation model of the closed-loop two-link devices is shown in Appendix E. A feedback system with proportional, K_p and integral, K_i gain is used for unity velocity feedback for both links to achieve system stability. A torque limiter based on the analysis on the motor current data recorded from the DC motor testing is included to mimic the behaviour of the DC motor.

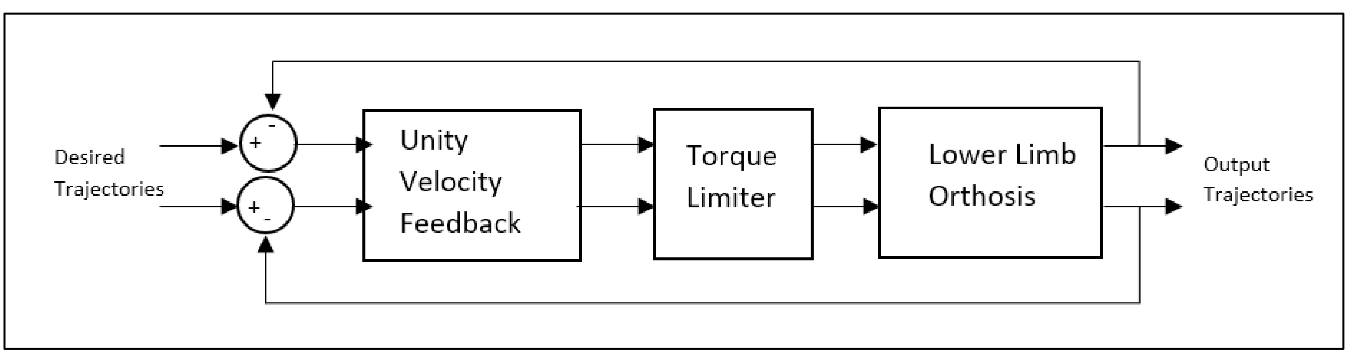

Figure 94 Block diagram of closed-loop two degree-of-freedom lower limb exoskeleton control system

To generate the SIDF model, sinusoidal signal in Equation (9) is excited on the system:

$$u_v(t) = u_{0,v} + a_v \cos(\omega_v t)\,, v = 1,2,3, \dots, m \qquad (8)$$

where, u_v is the input, v is the input channel index, $u_{o,v}$ is the DC term of the input signal, a_v is the amplitude of the excitation signal and ω_v is the excitation frequency. Both links are excited cocurrently with two similar sinusoidal signals of different frequency values to obtain the outputs of the system in the time domain. The purpose of using different frequencies is to separate effects of the inputs from the outputs of both links because the responses will be undefined if the excitation frequencies of inputs are the same.

Then, the Fourier integrals are evaluated with the steady state of outputs, y_q which is obtained by integrating dynamic equations of motion.

$$I_{q,p}^{h,k} = \int_{(k-1)T}^{kT} y_q(t) \exp\left[-jh\left(\omega_p t + \theta_p\right)\right] dt \qquad (9)$$

where k is the period index, h is the index for the measured harmonics, and T is the total period. For this two-inputs-two-outputs system, $T \frac{2\pi}{\omega_1 - \omega_2}$.

Then, the multivariable SIDF model at discrete frequencies are achieved with the relation given as follow:

$$G_{q,p}^{h,k}(j\omega; u_o, a, \theta) = {}^{2}/_{a_p T}\, I_{q,p}^{h,k} \qquad (10)$$

The MATLAB software developed in [117] was utilised for tracking and decoupling purposes, to characterize the unstable behaviour of the plant at the desired operating condition. Then, the SIDF model of the lower link robotic orthosis is generated and linear model, $G(s)$ is obtained with linear fitting method. Finally, the SIDF model is concluded to be stable when convergence of the Fourier integrals occurred where the ε_m, magnitude error and $\varepsilon_\emptyset$, phase error are bounded as demonstrated in Equation (11) and (12).

$$\left|\frac{M_{q,p}^{k} - M_{q,p}^{k-1}}{M_{q,p}^{k}}\right| < \varepsilon_m \qquad (11)$$

$$\left|\emptyset_{q,p}^{k} - \emptyset_{q,p}^{k-1}\right| < \varepsilon_\emptyset \qquad (12)$$

$$G(s) = \begin{bmatrix} g_{11} & g_{12} \\ g_{21} & g_{22} \end{bmatrix} \tag{13}$$

5.3.2 Controller Design of Lead-lag Compensator

The SIDF model generated is applied for the controller design. The algebraic technique [132] is utilised in this work. The following properties hold for the classical unity feedback system.

$$y = e_i\left(g_{ii}c_{ii} + g_{ij}c_{ji}\right) + e_j\left(g_{ii}c_{ij} + g_{ij}c_{jj}\right), i = 1,2; j = 1,2;\ i \neq j \tag{14}$$

where y is the output, e is the error signal, g is the matrix I/O model of the system, c is the matrix I/O model of the controller to be calculated. Equation (15) must be compiled to achieve decoupling.

$$c_{ij} = -\frac{g_{ij}c_{jj}}{g_{ii}},\ \ i = 1,2; j = 1,2;\ i \neq j \tag{15}$$

Then, Equation (14) and (15) are compared to attain tracking of the system to satisfy the following relation.

$$\frac{y_i}{r_i} = \frac{c_{ii}k_i}{1+c_{ii}k_i}, i = 1,2 \tag{16}$$

$$k_i = g_{ii} - \frac{g_{ij}g_{ji}}{g_{jj}},\ i = 1,2; j = 1,2;\ i \neq j \tag{17}$$

Next, the unified approach in cad_controller MATLAB function developed in [133] is implemented to design the lead-lag compensator c_{11} and c_{12}:

Step 1. The desired transfer function as shown in Equation (19) is determined. The second order system is implemented as it is the fundamental system that characterise the oscillation and overshoot of the system. Furthermore, the parameters such as the undamped natural frequency, ωn and damping ratio ζ are able to exhibit properties of various kinds of responses such as the settling time with Equation (18).

$$h_d = \frac{\omega_n^2}{s^2+2\zeta\omega_n + \omega_n^2} = \frac{Z_1}{Z_2} \tag{18}$$

$$t_s = \frac{4}{\zeta\omega_n} \tag{19}$$

Step 2. The actual closed-loop transfer function in the form of compensator parameters is derived in Equation (21).

$$h_a = \frac{Y_1}{Y_2} \tag{20}$$

Step 3. The objective function as shown in Equation (21) is obtained by applying Equation (18) and Equation (20). To obtain a desired outcome, the objective function is minimized with compensator parameters as the independent variables. To determine the compensator parameters, the simultaneous nonlinear numerical in Equation (22) must be solved. But, $Z_1Y_2 \approx Z_2Y_1$ is found under optimal condition, hence, the alternative objective function in Equation (23) is minimized instead of the objective function.

$$J = \int_{\omega_1}^{\omega_2} \left| \frac{Z_1}{Z_2} - \frac{Y_1}{Y_2} \right| \, d\omega \tag{21}$$

$$\frac{Z_1}{Z_2} = \frac{Y_1}{Y_2} => Z_1Y_2 - Z_2Y_1 = 0 \tag{22}$$

$$J = \int_{\omega_1}^{\omega_2} |Z_1Y_2 - Z_2Y_1|^2 \, d\omega \tag{23}$$

Step 4. The previous step in minimizing the objective function will result in the computing of the value of compensator parameters.

$$C(s) = \begin{bmatrix} c_{11} & c_{12} \\ c_{21} & c_{22} \end{bmatrix} \tag{24}$$

Then, optimum gain of the controller will be adjusted based on optimization approach if the dynamic behaviour of the unstable system is not satisfactory. The four gain, $K_{ij}$for each controller in the matrix as shown in Equation (24) are optimized by solving the objective function as below.

$$E = \left[\theta_{1,1}(t) - \theta_{1,d}(t)\right]^2 + \left[\theta_{1,2}(t)\right]^2 + \left[\theta_{2,1}(t) - \theta_{2,d}(t)\right]^2 + \left[\theta_{2,2}(t)\right]^2 \tag{25}$$

where,

$\theta_{n,1}(t)$ is the actual response of n^{th} angle where n=1,2 when the command angle n is a unit step and the command of the other angle is zero (rad/s).

$\theta_{n,2}(t)$ is the actual response of the n^{th} angle where n=1,2 when the command motor speed is zero and the command of the other angle is a unit step (rad/s).

$\theta_{n,d}(t)$ is the desired decoupled response of the n^{th} angle where n=1,2.

At last, the following form of controller is obtained and a further verification of its sensitivity in simulation and experimental setup are performed and discussed.

$$C(s) = \begin{bmatrix} K_{11}c_{11} & K_{12}c_{12} \\ K_{21}c_{21} & K_{22}c_{22} \end{bmatrix} \tag{26}$$

5.3.3 Determine the Optimum Constant Gain of the Controller

This step will be performed if the dynamic behaviour of the nonlinear system is not satisfactory. Then, optimum gain of the controller will be adjusted based on optimization approach if the dynamic behaviour of the unstable system is not satisfactory. The four gains, K_{ij} for each controller in the matrix, as shown in (26), are optimized by solving the objective function as shown in Equation (25).

At last, the final form of the controller, Equation (26) is obtained and its further verification with Simulink and experimental setup can be performed.

5.3.4 Verification of Controller via Nonlinear Simulation

The final step for this design approach is to verify the controller using a digital simulation. The system is concluded as stable when the closed loop describing functions are successfully obtained, because the Fourier integrals would not converge unless the outputs are constrained. The results are recorded and further discussed in Chapter 6.

5.4 Discussion on Sinusoidal-Input Describing Function (SIDF) Implementation

As mentioned in previous chapters, a robust control system is essential for a lower limb rehabilitation orthosis to provide the best rehabilitation for patients. Various simulations had to be done to simulate the best control system for the orthosis before any experimental implementations. However, rehabilitation devices are usually actuated with numerous parts including manipulators, sensors or actuator that contribute to the nonlinear characteristics of the system. A mathematical model that represents the system is hard to be formed when the nonlinear terms of the system need to be considered.

Hence, the SIDF approach is introduced to form the linear equations of the system. The approximate method is used to characterize the nonlinear system. Sinusoidal inputs are excited to the plant to obtain system outputs, and outputs at steady state are evaluated to obtain the SIDF model in linear form. Thus, the SIDF functions are utilized in controller simulation. This linearization process eases the development of the controller for the robotic orthosis to track the patient's lower limb gait pattern and control the movement of the manipulator, as the linearized functions are able to mimic the behaviour of the plant, and at the same time cope with nonlinearities, uncertainties and disturbances to the system.

The SIDF approach with the MATLAB library is first established in the year of 2002 and has been utilized in various nonlinear plants. However, it is the first for the implementation of this approach in a vertical two-link manipulator, and this marked the novelty of the research. A set of linearized transfer function of the highly nonlinear plant is generated, and the SIDF model is verified via simulation with the nonlinear system and experimental setup. Also, the proven SIDF function is utilized to generate a control system for the rehabilitation device using a classical control theory, lead-lag controller in the MATLAB environment. The controller of the orthosis is tested on the device with various inputs. Satisfying results are gained and discussed in the next chapter. Hence, this research proves that the novel implementation of SIDF method with the computer-aided design (CAE) MATLAB tool in a rehabilitation orthosis is successful.

5.5 Conclusions

In this section of the report, characteristics of describing function and the procedures of implementation are discussed, and the development of describing function approach is conversed. The development of MATLAB tools generated to simulate a controller with SIDF model for a rehabilitation device for the first time are discussed. Lastly, the design producer of the SIDF model is shown. The best results along the progression of the controller simulation and implementation of the SIDF model with lead-lag compensator in experimental setup are recorded and shown. This shows the academic contributions of implementation of the SIDF approach in a vertical two-link manipulator, which is also known as a rehabilitation device. Validation of the SIDF model and controller transfer function are recorded in Chapter 6.

Chapter 6 Validation of SIDF Model with Controller via Simulation and Experiment

6.1 Introduction

Novelty of the research is reviewed in this chapter. The first implementation of the SIDF model for the vertical two-link manipulator is shown and the parameters of the model are obtained. Selection of the optimum model via linear fitting is reviewed. Besides, this chapter shows the simulation result of the developed Sinusoidal-Input Describing Function Model. The generated controller for the rehabilitation orthosis, a nonlinear feedback closed-loop system for the first time, is then tested with various methods including step responses and tracking and decoupling test. The performance of the SIDF model and controller are obtained, compared and discussed. Lastly, the contribution of SIDF approach is justified.

6.2 Implementation of SIDF Model and Lead-lag Compensator

The steps of implementation of the MATLAB routines in computer-aided environment (CAE) to obtain the SIDF model and controller are described as follows:

Step 1. A Simulink model as shown in Figure 94 (details figure refer Appendix E) is built based on Equation (3) and (4). The proportional and integral gain used for the unity velocity feedback for both links are $K_{\mathrm{p},1}$ = 14.48, $K_{\mathrm{I},1}$ = 3.7 $K_{\mathrm{p},2}$ = 0.891, $K_{\mathrm{I},2}$ = 0.192 with torque limiter at range of -59.35 Nm < $T_{\mathrm{L},1}$ < 59.35 Nm and -65.72 Nm < $T_{\mathrm{L},2}$ < 65.72 Nm for link 1 and link 2 respectively.

Step 2. The set of outputs of the Simulink nonlinear model are generated with the sinusoidal input excited to the system simultaneously with a_1 = 2 rad/s, a_2 = 4 rad/s, ω_1 = [13, 17, 24, 32, 44, 60, 82, 112, 153, 210, 287, 392, 535, 732, 1000], ω_2 = [14, 18, 25, 33, 45, 61, 83, 117, 154, 211, 288, 393, 536, 733, 1001], θ_1 = θ_2 = 0° and u_{01}, u_{02} vary from 5° to 40°.

Step 3. The *invfreqs.m* function from the MATLAB software [39] is utilised to generate the sinusoidal-input describing function model of the lower limb exoskeleton at nominal condition.

$$G(s) = \begin{bmatrix} g_{11} & g_{12} \\ g_{21} & g_{22} \end{bmatrix} \tag{27}$$

$$g_{11}(s) = \frac{104.112s + 5.313e^4}{s^3 + 856.675s^2 + 1.273e^5 s + 1.565e^4}$$

$$g_{12}(s) = -\frac{16.817}{s^2+803.853s+1.233e^5}$$

$$g_{21}(s) = -\frac{0.112s-239.776}{s^2+772.872s+1.199e^5}$$

$$g_{22}(s) = \frac{0.00967s^2+255.3s+1.935e^4}{s^3+650.721s^2+4.117e^4+1.490e^4}$$

Step 4. To obtain the lead-lag compensator, c_{11} and c_{22}, the cad_controller MATLAB function is executed. Then, the off-diagonal terms of 2x2 matrix, c_{12} and c_{21} are calculated with Equation (15) and Equation (25).

$$C(s) = \begin{bmatrix} c_{11} & c_{12} \\ c_{21} & c_{22} \end{bmatrix} \tag{28}$$

$$c_{11}(s) = \frac{0.202s+2.743}{0.000.000666s^2+0.0853+1}$$

$$c_{12}(s) = \frac{0.00278s^5+188.130s^4+1.596e^5s^3+2.373s^2+1.647e^7s+1.667e^6}{5.963s^5+8334.640s^4+3.836e^6s^3+6.411e^8s^2+3.138e^{10}s+6.553e^9}$$

$$c_{21}(s) = \frac{0.00227s^5+49.842s^4+3.222e^4s^3+2.419e^6s^2+2.780e^7s+9.799e^6}{6.44e^{-6}s^6+0.176s^5+167.462s^4+4.918e^4s^3+5.648e^6s^2+2.434e^8s+2.320e^9}$$

$$c_{22}(s) = \frac{0.000165s^2+11.046s+6.337}{0.05728s^2+4.781s+1}$$

Step 5. Lastly, the gains of the controllers are tuned as the following:

$K_{11} = 0.6$, $K_{12} = 0.13$, $K_{21} = 0.35$, $K_{22} = 1$.

6.2.1 Obtaining Sinusoidal-Input Describing Function (SIDF) for the Multivariable Nonlinear System

The MATLAB simulation tool to obtain the SIDF model is used and the outputs of the system with various sinusoidal input signals are obtained and saved into a MATLAB data file. A set of frequencies ranged within the operating region of the nonlinear system are chosen. The developed MATLAB command is executed for various inputs with different amplitudes as shown in Table 21, and the pseudo-frequency responses are obtained and plotted in Figure 95 and Figure 96.

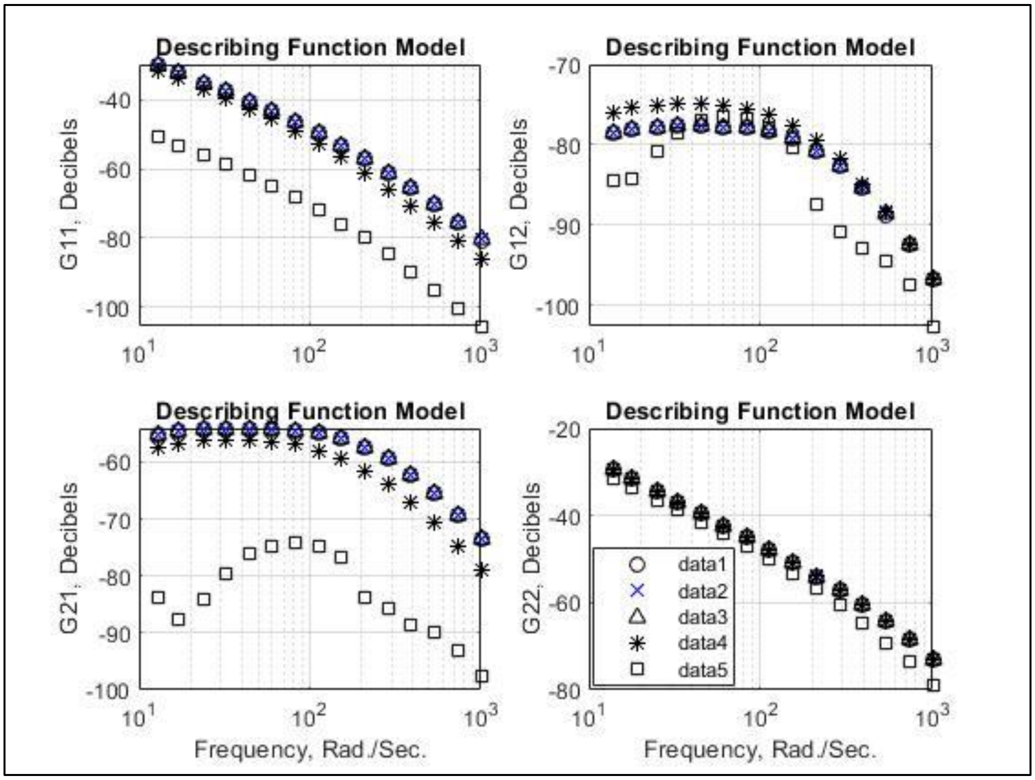

Figure 95 SIDF gain plot with different amplitudes

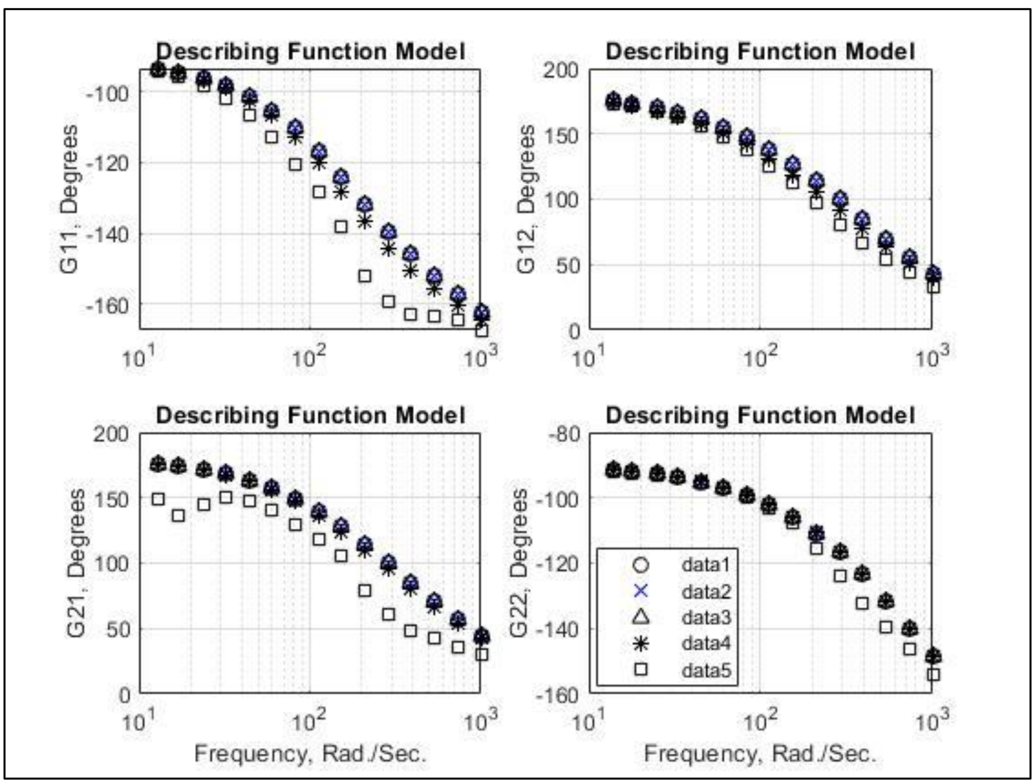

Figure 96 SIDF phase plot with different amplitudes

Table 21 Table of input amplitudes

Data	Amplitude 1	Amplitude 2
Data 1	0.01	0.02
Data 2	0.1	0.2
Data 3	2	4
Data 4	10	20
Data 5	100	200

6.2.2 Nominal Model Selection and Linear Fitting

Next, the model with input amplitude of 2 and 4 is selected as the nominal model and linear fit are obtained. In order to achieve the best fitting, the last two inputs in the *invfreqs.m* command which represent the order of the numerator and denominator of the linear transfer functions are adjusted. Finally, the best linear fitting graph is achieved as shown in Figure 97 and Figure 98. Hence the SIDF model transfer functions as shown in Equation (27) at nominal condition are obtained.

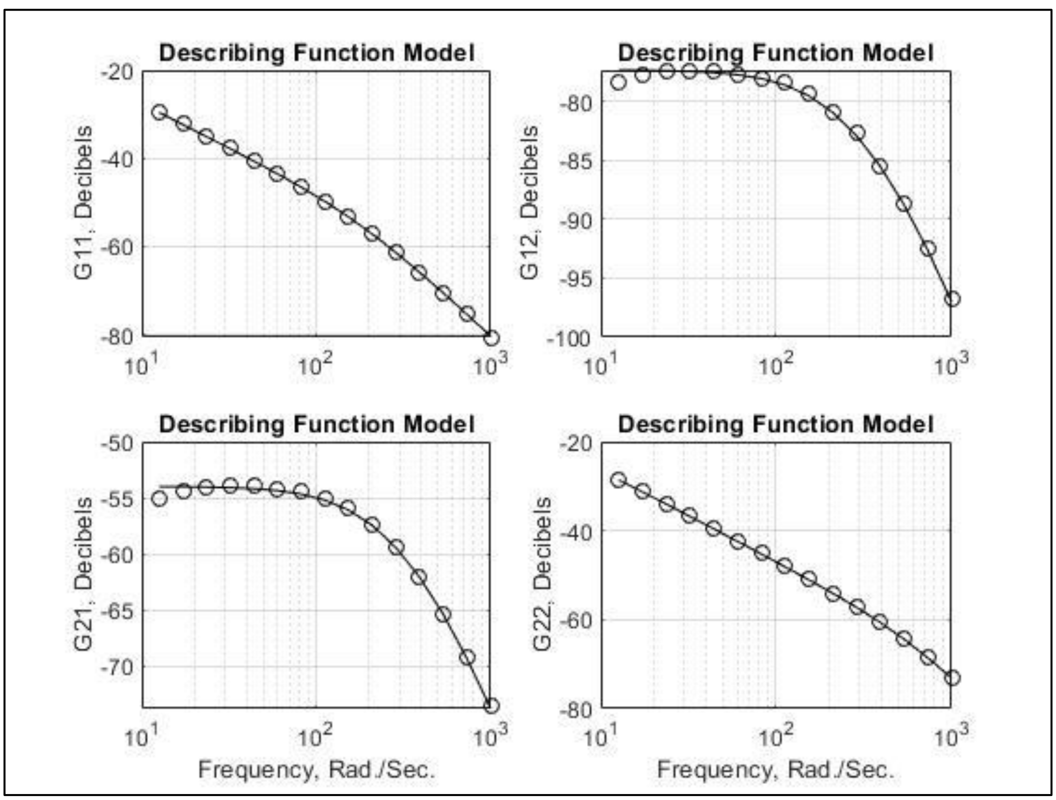

Figure 97 Gain matrix of the SIDF model at nominal condition

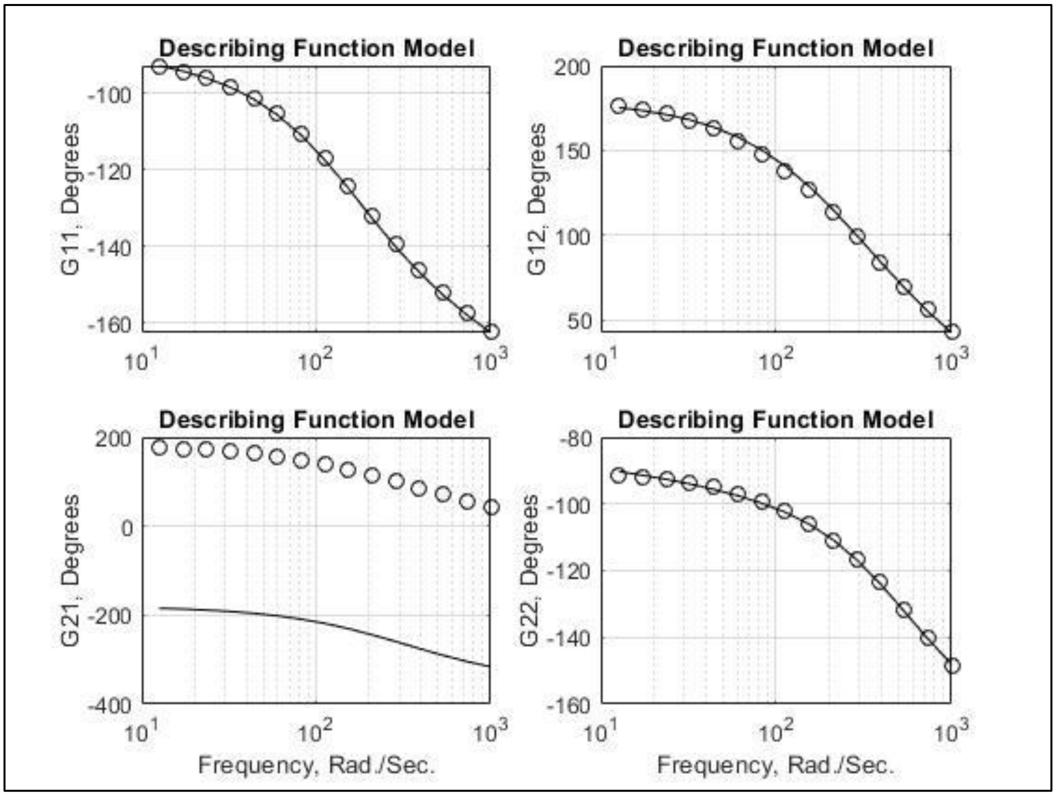

Figure 98 Phase matrix of the SIDF model at nominal condition

6.3 Experimental Setup of the Two-link Robotic Orthosis and Lead-lag Compensator

The experimental setup is as shown in the schematic diagram (Figure 99). The two-link robotic orthosis is actuated with a DC servomotor (Maxon Model no 148865) with a planetary gearhead (Macon gearhead no. 223105) and an encoder with line driver (Maxon no 228452). The actuators and sensors are connected and controlled with a multifunction I/O device. The graphical programming interface is built in the LABVIEW environment. In order to apply the controller in LABVIEW, $C(s)$ in the experiment setup, the controller transfer function has to present in discrete form. In this case, the sample time applied for the discrete-time transfer function is 0.01 second. The discrete form of lead-lag compensator is as shown.

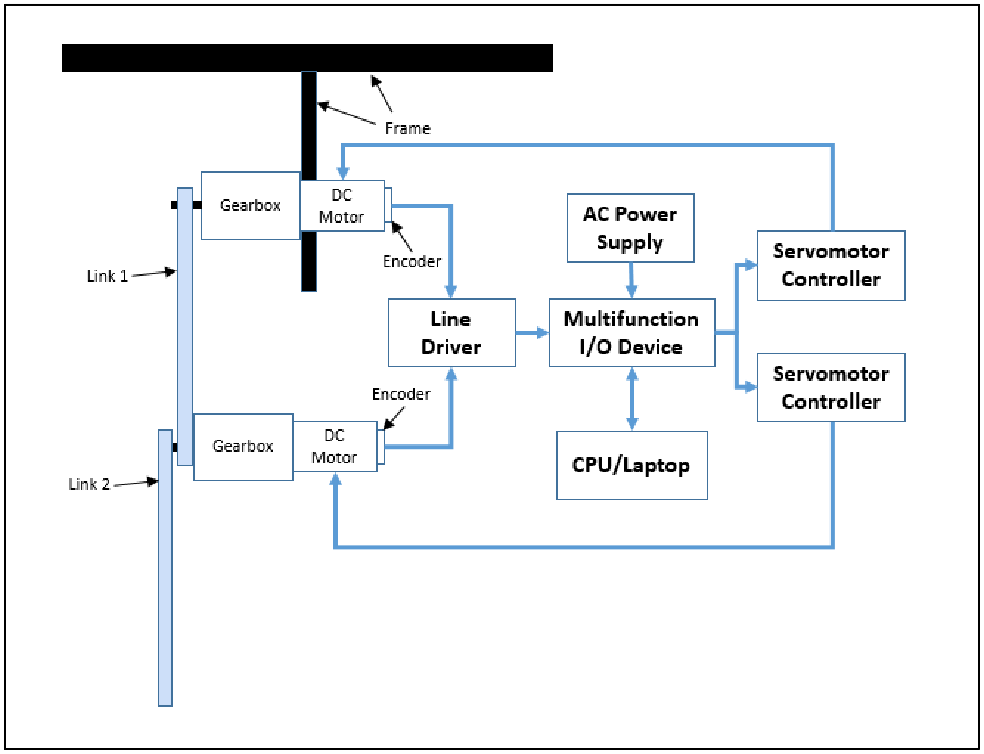

Figure 99 Schematic diagram of experimental setup with multifunction I/O devices (USB-6431)

$$D(z) = \begin{bmatrix} d_{11} & d_{12} \\ d_{21} & d_{22} \end{bmatrix} \tag{29}$$

$$d_{11}(z) = \frac{1.805z - 1.575}{z^2 - 1.194 + 0.278}$$

$$d_{12}(z) = \frac{0.000466z^5 + 0.0316z^4 - 0.0690z^3 + 0.0416z^2 - 0.00467z + 2.409e^{-6}}{z^5 - 1.568z^4 + 0.629z^3 - 0.0604z^2 + 0.000484 - 8.515e^{-7}}$$

$$d_{21}(z) = \frac{0.577z^5 - 1.365z^4 + 1.037z^3 - 0.250z^2 + 0.000381z - 1.466e^{-7}}{z^6 - 1.782z^5 + 1.037z^4 - 0.231z^3 + 0.0160z^2 - 5.718e^{-5}z + 9.277e^{-22}}$$

$$d_{22}(z) = \frac{0.0029z^2 + 1.306z - 1.301}{z^2 - 1.433z + 0.434}$$

Then, a LABVIEW function is developed with this discrete-time lead-lag controller configuration for the DC servomotor and encoder. Lastly, the gains of the controllers are tuned as following:

K_{11}= 0.3, K_{12} = 0.001, K_{21} = 0.02, K_{22} = 85.

6.4 Performance of Nonlinear Feedback Control System

Simulation and experiment are done in order to assess the quality of the SIDF model and functionality of the lead-lag compensator. The designed SIDF model is tested in MATLAB Simulink with the tuned lead-lag controller while the nonlinear two-link lower limb robotic orthosis model is tested in experiment setup with the lead-lag controller via the multifunction I/O device. Besides, the lead-lag compensator is tested in the real-life experiment. Both tests are conducted with step inputs as well as tracking and decoupling testing. The outputs are normalized to show the property of each response. The tracking qualities and decoupling qualities of the system are as shown in the following section. In this section, all step responses as well as tracking and decoupling test are carried out with step input of 5°, 10°, 20° and 30°.

6.4.1 Normalized Step Response in Simulation

In this test, both link 1 and link 2 are tested separately with a set of step input angles. The Simulink model as shown in Figure 94 is utilized in the simulation test. When the step response is carried out for one of the links, the input of the other link will remain zero in the whole process. The normalized step responses of the MATLAB Simulink model are then recorded and plotted in Figure 100. The output of step input of 5°, 10°, 20° and 30° for link 1 and link 2 are plotted respectively.

6.4.1.1 Normalized Step Response in Simulation for link 1

The response of the 5° input to link 1 rises gradually with a settling time of 0.1110s which is a 2% steady state error of the final value. Behaviour of the output of 10° step input to link 1 is similar but slightly slower than the previous response with a settling time of 0.1140s. For the response of 20° and 30° step inputs for link 1, the responses rise at a constant rate of 8.35°/s and 5.54°/s respectively and with settling time at 0.1490s and 0.1980s respectively.

6.4.1.2 Normalized Step Response in Simulation for link 2

Meanwhile, the output responses of four different step inputs to the SImulink model of link 2 are similar with slightly different settling time. All the output responses of 5°, 10°, 20° and 30° step inputs are rising slowly and reach the steady state at 0.3316s, 0.3319s 0.3321s and 0.3323s respectively.

6.4.1.3 Discussion of Normalized Step Response in Simulation

Hence, the system responses plotted in Figure 100 showed optimal static and dynamic behaviour using the tuned controller. The settling time of responses from both link 1 and link 2 with input angles of 5°, 10°, 20°, and 30° are very small which ranged from 0.1110s to 0.1980s and 0.3316s to 0.3323s. This proved the sensitivity of the tuned controller. The responses of link 1 had slight delay when the input angles increased while the second axis obtained a similar response for all input tested. No significant overshoot and oscillation are obtained for both responses. This satisfied the aim of low sensitivity of nonlinear feedback system with respect to the range of input command.

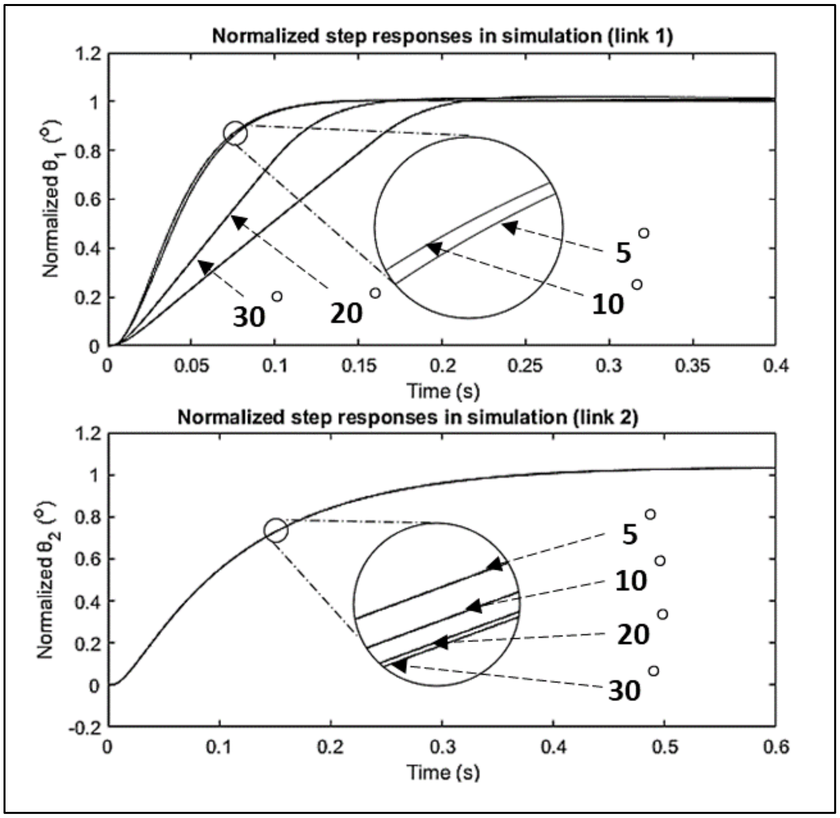

Figure 100 Normalized step response in simulation of first and second axis

6.4.2 Tracking and Decoupling of Axes in Simulation

In this simulation, the tracking quality test of the chosen link is performed by providing a set of input to the link while at the same time the input to the other link remains as zero. The output of the chosen link will be the tracking quality result and at the same time, the output from the other link without any input will be the decoupling result. The tracking and decoupling qualities of the nonlinear closed-loop system in MATLAB Simulink are obtained as shown in Figure 101 and Figure 102. In Figure 101, the first graph showed the tracking quality of link 1 with step inputs of 5°, 10°, 20° and 30° while the second graph showed the decoupling quality from link 2 with zero input and vice versa for the plots in Figure 102. The tracking qualities are plotted with normalized degree while the decoupling qualities are plotted without normalizing.

6.4.2.1 Tracking and Decoupling of Axes in Simulation for Link 1

As shown in Figure 101, the normalized tracking qualities of 5°, 10°, 20° and 30° step input in simulation showed that each of the responses rise gradually and reaches the final value at 0.1110s, 0.1140s, 0.1490s and 0.1980s respectively. For the decoupling qualities as shown in Figure 101, oscillation is observed from all the responses. Range of oscillation of each response increases when the step input value increases. Maximum overshoot of each decoupling response is 0. 2679°, 0.6534°, 2.200° and 3.800° accordingly. Although oscillation and overshoot are shown in all the decoupling responses from link 2, the system settled down after the first oscillation and gradually reduced to zero in a short while.

6.4.2.2 Tracking and Decoupling of Axes in Simulation for Link 2

Figure 102 presented the tracking qualities of link 2 and decoupling qualities from link 1 in the simulation model. As shown in the graph of tracking qualities, all responses have the same behaviour. The transient responses of 5°, 10°, 20° and 30° step input to link 1 rise gradually and settled down at 0.3316s, 0.3319s 0.3321s and 0.3323s respectively. The oscillation of decoupling qualities from link 1 in simulation is very small where the greatest oscillation range is less than 0.5°. The maximum overshoot for each decoupling plot is 0.05496°, 0.1099°, 0.2199° and 0.3298° correspondingly. All decoupling qualities reach a steady state within 0.5s.

6.4.2.3 Discussion of Tracking and decoupling of Axes in Simulation

Satisfying results of tracking and decoupling qualities in the simulation model are obtained based on Figure 101 and Figure 102. The tracking responses are within desired level as the maximum settling time for both links are only 0.1980s for link 1 and 0.3323s for link 2. No significant overshoot is detected from both tracking qualities. According to the decoupling responses, the degree of decoupling is small compared to the input of the system. The maximum degree of coupling is 3.800° and 0.3298° which are within the acceptable range. Thus, the outcomes showed the ability of the SIDF method to design a linear controller for the multivariable system which is able to support a concurrent signal tracking and decoupling with the two-link lower limb robotic orthosis.

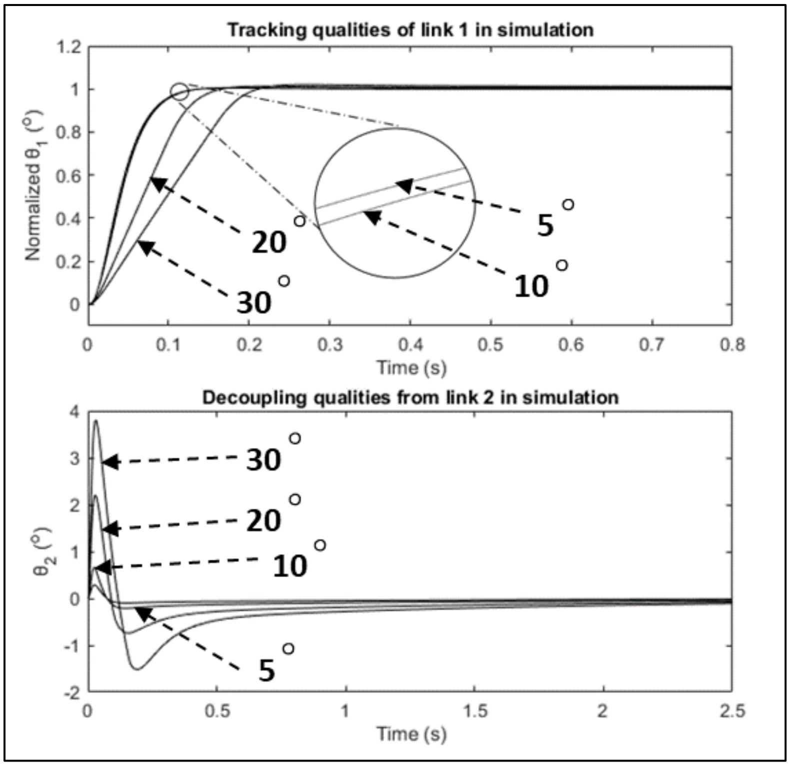

Figure 101 Tracking quality of first axis and decoupling from the second axis (simulation)

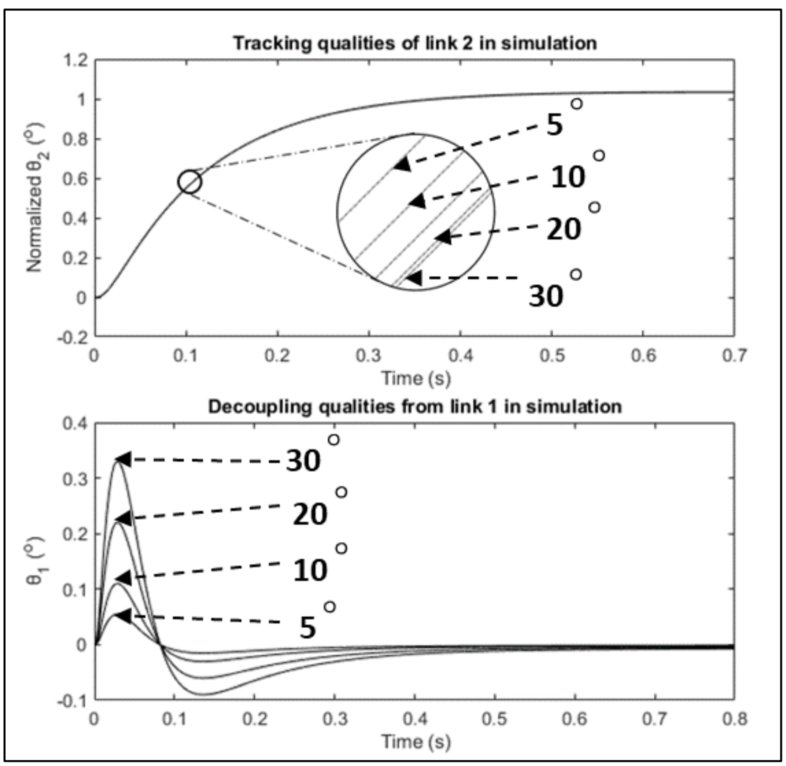

Figure 102 Tracking quality of second axis and decoupling from the first axis (simulation)

6.4.3 Normalized step responses in Experiment Setup

Similar to the testing of normalized step responses in simulation, both link 1 and link 2 are examined with a set of step input respectively. The experimental setup is shown in Figure 99. When the step response is carried out for one of the links, the input of the other link remained as zero in the whole process. The normalized step responses of the experiment are then recorded and plotted in Figure 103. The output of step input of 5°, 10°, 20° and 30° for link 1 and link 2 are plotted respectively.

6.4.2.1 Normalized Step Responses in Experiment Setup of Link 1

The normalized step responses of the experimental setup are also recorded and shown in Figure 103. According to the normalized step responses in the experiment setup of link 1, the settling time is 0.193s, 0.227s, 0.296s and 0.357s respectively for step input of 5°, 10°, 20° and 30°. Slight delays of 0.0331s, 0.0333, 0.0470s and 0.0480s are observed at the starting point of each response plot.

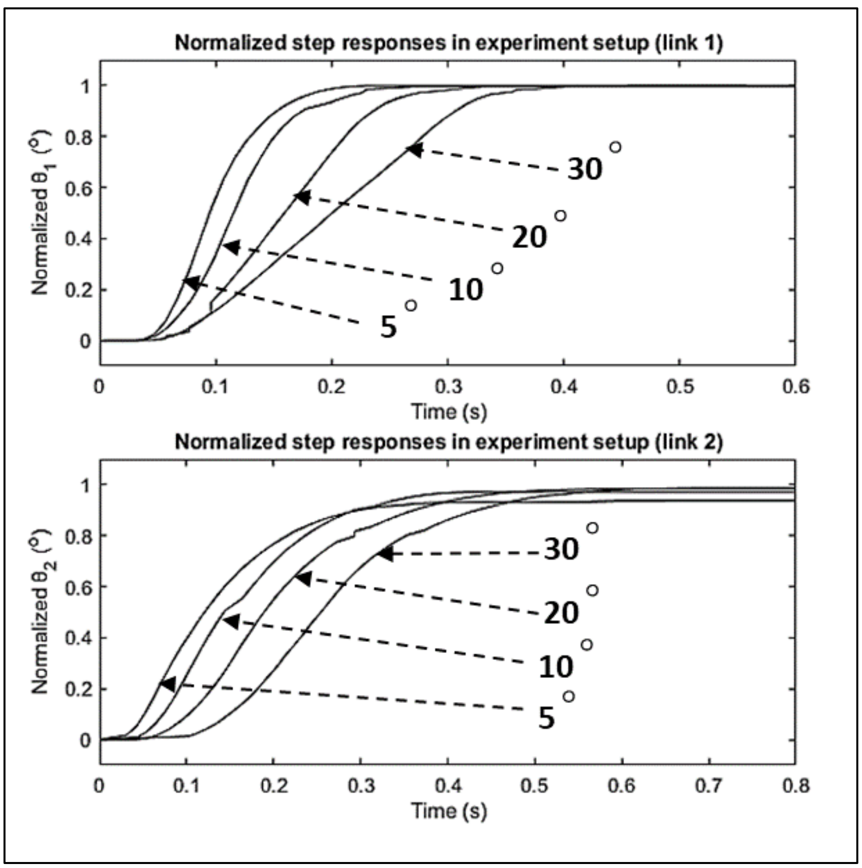

Figure 103 Normalized step response in experiment of first and second axis

6.4.2.2 Normalized Step Responses in Experiment Setup of link 2

In the normalized step responses of link 2 in Figure 103, output response of 5° and 10° step input reached a final value at 0.3730s and 0.4140s with normalized degree of 0.9351° and 0.9710° respectively which is equivalent to a steady state error of 6.49% and 2.91%. However, the steady state errors are acceptable as the error does not exceed a 10% of the desired input. For the 20° and 30° step input, the settling time of the responses fall on 0.543s and 0.603s respectively. There are also slight delays found in the starting point of each response with time of 0.0310s, 0.0400s, 0.0530s and 0.103s respectively.

6.4.2.3 Discussion of Normalized Step Responses in Experiment

The reason for this phenomenon to occur is the inertia that the control system needs to overcome at the joint of each link. However, no overshoot and oscillation are found in both normalized step responses of experiment setup in Figure 103. The settling time of all responses became larger when the degree of input value increased. Hence, the results fulfilled the objective of low sensitivity of the nonlinear feedback system with response to the desired inputs.

6.4.4 Tracking and Decoupling of Axes in Experiment Setup

The procedure to perform the tracking and decoupling test are discussed in Section 6.4.2 and the similar steps are applied in the experiment setup. In the tracking and decoupling experiment, link 1 is executed with step input ranged from 5°, 10°, 20° and 30° to obtain the tracking qualities, while link 2 is executed with zero input to acquire the decoupling qualities. The results are plotted in Figure 104 and vice versa results are recorded in Figure 105.

6.4.4.1 Tracking and Decoupling of Axes in Experiment Setup of Link 1

The tracking qualities of link 1 rose slowly and reached the desired value at 0.1930s, 0.2270s, 0.2960s and 0.3570s accordingly as shown in Figure 104. Referring to the second graph, step inputs of 5°and 10° to link 1 do not result in a rotational angle in decoupling qualities from link 2. The decoupling quality of link 2 with a 20° step input in link 1 has an output angle of 0.2943°. Lastly, for the decoupling quality by 30° step input, an overshoot with maximum value of 0.6628° occurred and settle down to 0.3038° at around 1s.

6.4.4.1 Tracking and decoupling of Axes in Experiment Setup of Link 2

Next, Figure 105 showed the tracking quality of link 2 and decoupling quality from link 1. A slightly delay is shown at the beginning of each response. The tracking qualities arrive at steady state at time 0.3730s, 0.4140s, 0.5430s and 0.6030s respectively for step input of 5°, 10°, 20° and 30°. The decoupling responses from link 1 for all inputs are zero as shown in the second plot in Figure 105.

6.4.4.1 Discussion Tracking and Decoupling of Axes in Experiment Setup

According to the plotted responses, the result of tracking and decoupling qualities in experiment setup for both axes are within a high satisfactory level. The tracking response for both links are within an optimal range which are 0.193s to 0.357s for link 1 and 0.3730s to 0.6030s for link 2. No overshoot is observed for tracking qualities of both links. The maximum degree of decoupling is very low with a final value of 0.3038° from link 2 and 0° from link 1.

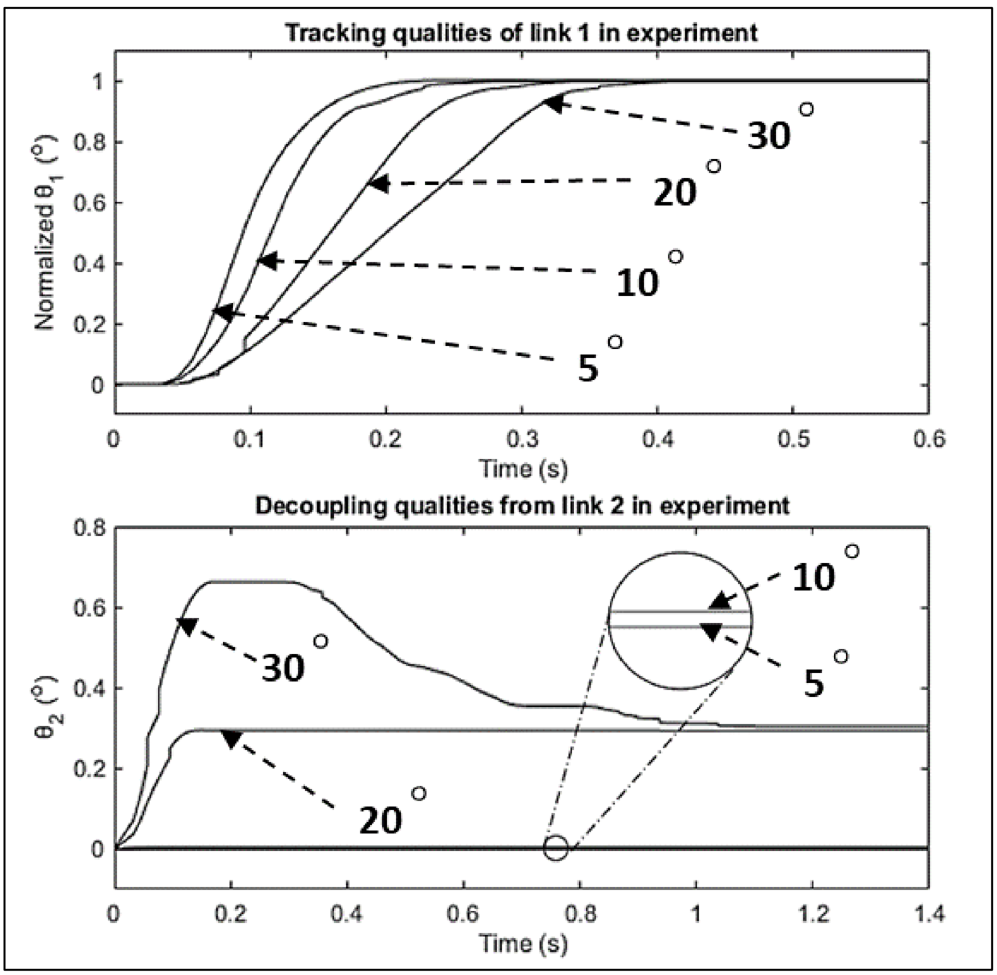

Figure 104 Tracking quality of first axis and decoupling from the second axis (experiment)

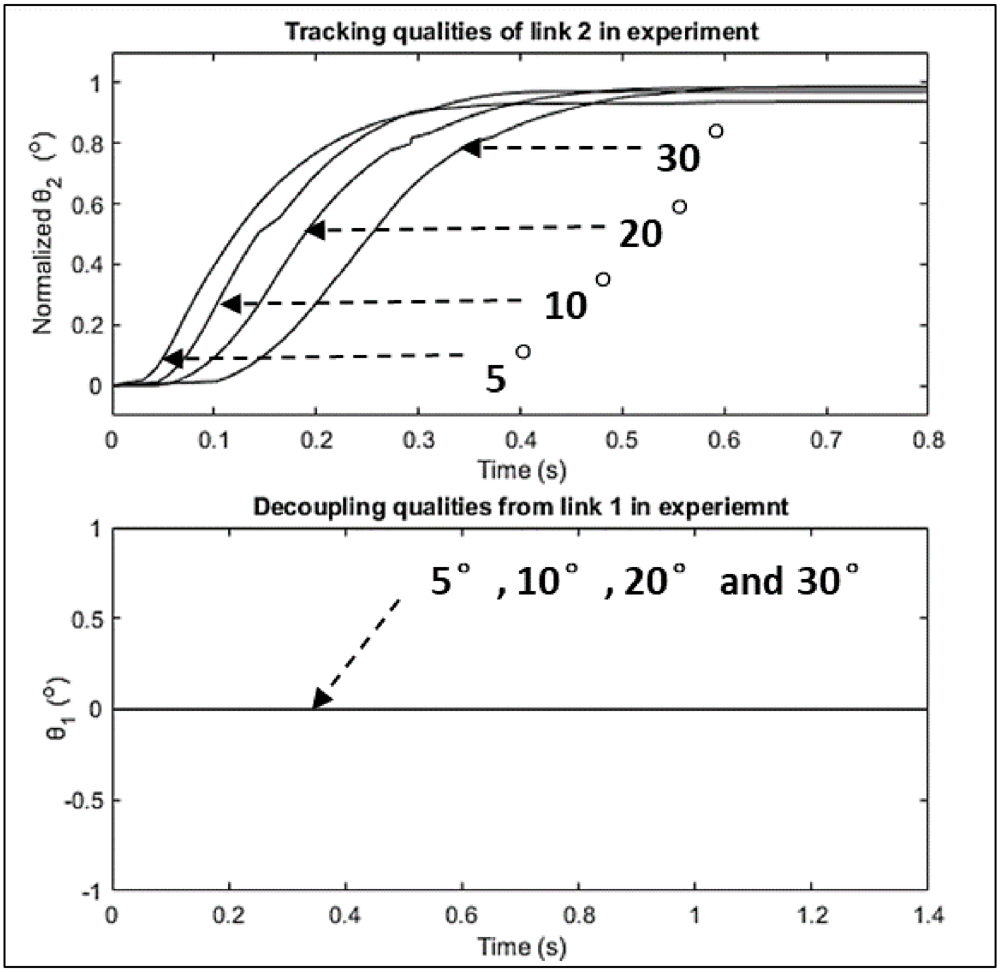

Figure 105 Tracking quality of second axis and decoupling from the first axis (experiment)

6.4.5 Comparison of Normalized Step Responses of Simulation and Experiment

The step responses obtained from the simulation and experiment are compared in Figure 106 and Figure 107. The response of step input in both simulation and experiment testing with inputs of 5°, 10°, 20° and 30° are plotted for both axes. By referring to the responses in Figure 106 and Figure 107, the settling time of the experimental setup is slightly larger than the settling time obtained from the MATLAB simulation model. The difference of settling time for link 1 between the simulation and experiment are 0.082s, 0.113s, 0.147s and 0.159s. However, the differences in settling time observed from link 2 are 0.0414s, 0.0821s, 0.2109s and 0.2707s respectively for step inputs of 5°, 10°, 20° and 30°. However, the amount of delay is negligible as the difference of time between both simulation and experiment is less than 0.3s which is negligible in this case. Furthermore, the delay of NI USB-6341 multifunction I/O device in sending the digital signal to the motor controller and the time consumed by the motor driver to process the digital signal from the monitor are also factors for the delay observed in the real-time experiment.

Besides that, the final value of the simulation result of link 2 is overall slightly higher than the experimental result. However, according to the comparison of both responses as shown in Figure 107, output responses from the experimental setup has a closer final value than the simulation result. The steady state errors of all the responses are all within 6.5% of the desired value which is within the acceptable range.

Based on the similar result of step input as shown in Figure 106 and Figure 107, the SIDF model generated successfully represents the multivariable nonlinear manipulator. In short, the lead-lag compensator generated with the SIDF model is suitable to control the two-link manipulator as the recorded decoupling qualities via experimental setup have a smaller value than the predicted value.

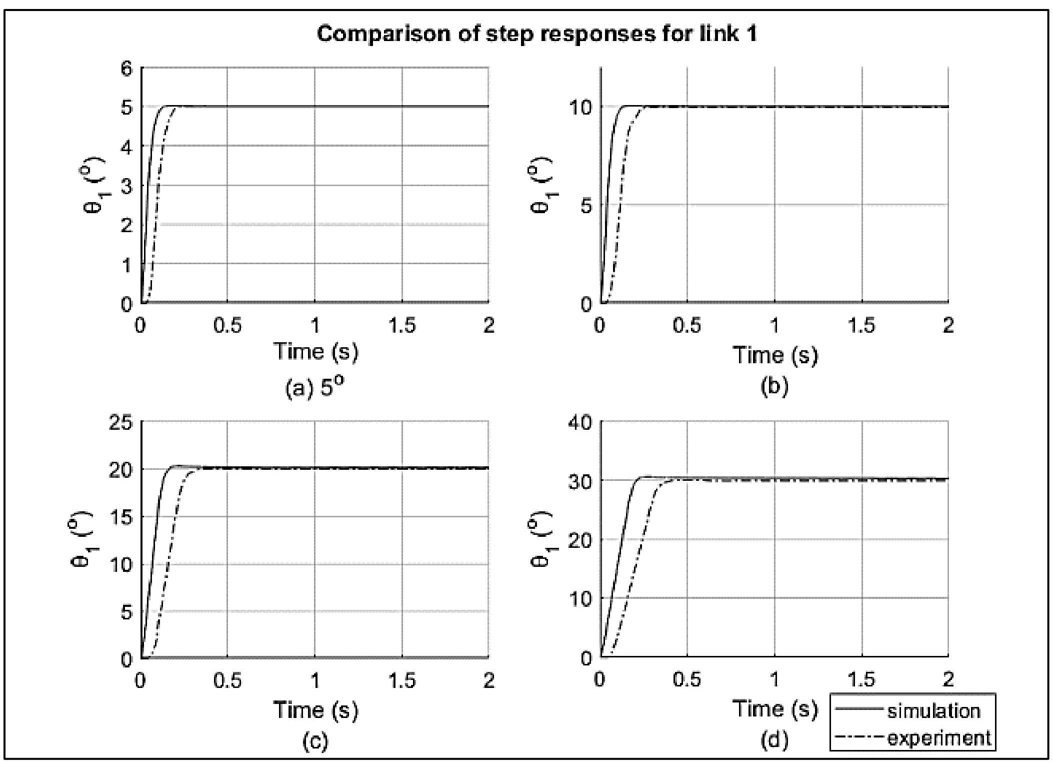

Figure 106 Comparison of simulation and experiment response of first axis with step input: a) 5°, b) 10°, c) 20°, and d) 30°

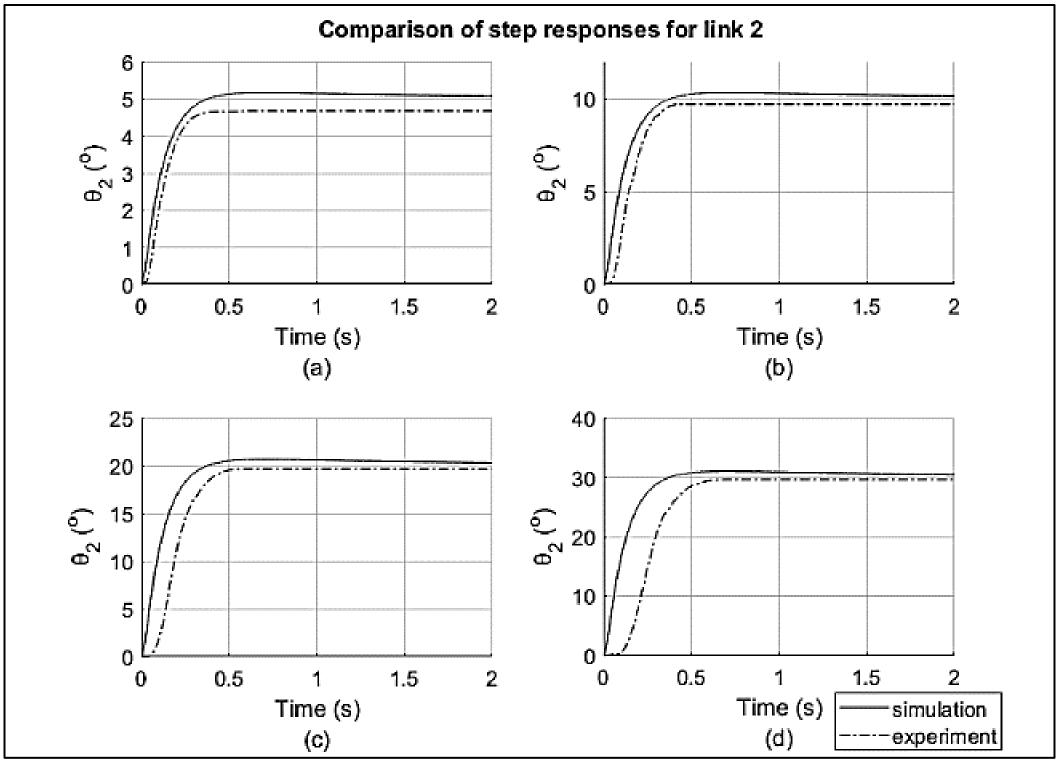

Figure 107 Comparison of simulation and experiment response of second axis with step input: a) 5°, b) 10°, c) 20°, and d) 30°

6.5 Justification and Discussion of the SIDF Model and Lead-lag Compensator

In this chapter, the SIDF approach is applied to linearize the highly nonlinear system and to generate a set of SIDF transfer functions that carry the characteristics of the two-link manipulator. Next, a lead-lag controller is generated to control the robotic orthosis movement and provide guidance for hemiplegic stroke patients in correcting their abnormal walking pattern. Utilizing the SIDF approach to generate SIDF model and lead-lag controller is first done in a vertical two-link manipulator for stroke rehabilitation.

As the major objective of the research is to build a rehabilitation orthosis for hemiplegic stroke patients, the mechanism of the robot is designed based on the hemiplegic stroke condition. Stroke survivors often experience muscle weakness and impairment. Most of them could not regain a proper walking ability due to the aftereffect of stroke. They cannot perform a proper gait cycle when walking and hence, asymmetric walking patterns or abnormal walking postures are seen. The distorted gait graphs are illustrated in Figure 14 in Chapter 2.

Hence, the controller tailored for the robotic orthosis plays an important role in fixing the gait pattern. To choose a suitable controller for the plant, study of the form of desired signal input to the plant is required. The desired input signals as illustrated in Figures 75 and 76 are the combination of various sinusoidal waveforms. Moreover, the gait patterns of both hip and knee are bounded signals within a fixed range.

One the other hand, the SIDF approach is to excite the plant with a sinusoidal-input to obtain the outputs of the system. The signal is then evaluated with Fourier integrals to obtain the dynamic equation of motion or the orthosis. Lastly, the SIDF model is chosen after the linear fitting process. Due to the similar aspect of the sinusoidal input waveforms to the plant and the proposed approach, the SIDF approach in MATLAB tool is chosen to generate the controller for the rehabilitation orthosis. The generated controller is customized to control the nonlinear rehabilitation plant to achieve the desired gait signal.

Besides, the SIDF approach is chosen to solve the problem of nonlinearities of the plant during the simulation process. Building a simulation model for the unstable two-linked device is challenging and various problems are seen along the development. However, the SIDF approach incorporated in the MATLAB tool is able to resolve the simulation problems and generate a set of linearized transfer function that mimics the actual behaviour of the system. The method eased the process of simulation with a SIDF model and the development of lead-lag controller with the MATLAB function that is able to fine tune the gain of the controller along the simulation process.

Validation of the SIDF model with controller is done in this chapter via simulation and experiment setup. The satisfying results proved the potential of this approach in forming the SIDF model and controller for a highly unstable plant. Besides, the highly effective controller is able to monitor the nonlinear system and produce an output close to the desired input. Hence, the precise results generated via SIDF approach proved that the SIDF approach is suitable to be used for the application of rehabilitation orthosis. The highly sensitive controller is able to provide support and correction to stroke patients at each instant of the rehabilitation training. However, limitation in synchronizing both sides of the lower limb orthosis still exists in this current research. Hence, the next level of development is aimed to be done in future in order to allow the rehabilitation orthosis to function in correspondence to each other.

6.6 Conclusions

In this chapter, the methodology in getting the SIDF model for the multivariable nonlinear system is shown. The first SIDF model of a multivariable nonlinear lower limb robotic device is obtained. The steps to obtain the SIDF model including the nominal selection and linear fitting of the generated result are shown. Next, the lead-lag controller for this orthosis is generated with the SIDF approach in MATLAB library for the first time. Conversion of continuous transfer function of the controller to discrete form for experimental proposed are reviewed. Then, the performance of the nonlinear feedback controller system is tested with a step input test together with a tracking and decoupling test. The results shown are within expectation and satisfaction. Besides that, satisfactory responses are obtained in the comparison of normalized step response in simulation and experiment. These show that the SIDF model and lead-lag compensator is suitable to be implemented for the lower limb orthosis. Hence, the originality in the formulation and implementation of the SIDF approach in a vertical two-linked robotic orthosis are shown and discussed. This research successfully introduces a new control strategy for a robotic rehabilitation system that had not been done in other researches and triumphantly marks the academic contributions in control system study.

Chapter 7: Conclusions and Future Work

7.1 Conclusions

This study has reported the new application of SIDF model for a two-link rehabilitation device for controller design. Application of the SIDF approach is implemented in a rehabilitation device for the first time. The study shows that the SIDF approach is capable to characterize the multivariable, unstable and nonlinear system with a linear second order transfer function and hence, is suitable for the control design application.

At the beginning of the study, rehabilitations devices are studied. The pros and cons of each device are discussed. Thus, an ideal design for the rehabilitation orthosis is proposed. Besides that, popular control schemes for rehabilitation devices are reviewed and the advantages and disadvantages of each approach are listed. Finally, the SIDF approach is suggested to form the SIDF model and to design a controller for the rehabilitation device.

The vertical two-link manipulator is suggested as the structure of the rehabilitation device. Lightweight materials such as acrylic and HDPE are used for the links. Extendable links are designed for the hip to allow adjustments according to each patient. Extendable shafts are implemented at both side of the thigh position to tune the distance between left and right thigh according to the size of breech. The novel ergonomic and lightweight design of the orthosis allow patients to perform their rehabilitation training in a comfortable environment. Electric and electronic components for the robotic orthosis are reviewed. The mathematical model of the two-link manipulator is denoted for system calculation and simulation purpose.

Besides that, a few applications are proposed to generate the simulation model of the nonlinear two-link manipulator. However, most of the outcomes are not satisfying. The best simulation model among all the applications is reviewed in the thesis. However, there is still a big gap toward the best model. Conventional PID controller is implemented on the two-link manipulator with Arduino Due. However due to the constraint of the processor power, Arduino could not provide a good feedback when both links of one side of the robotic orthosis are moving. Hence, the multifunction I/O device is utilised to solve the issue.

Then, the application of the MATLAB toolbox for SIDF model generation reduces the hardship to generate a simulation model of the two-link nonlinear system during simulation and preliminary testing as compared to various conventional approaches. By implementing the SIDF approach, the nonlinear system could be stabilized with proportional and integral gain. This toolbox allows users to provide a suitable frequency range to generate the SIDF model by considering the lowest and highest operating frequencies of the plant.

Furthermore, the tracking and decoupling procedure by applying two algebraic approaches with the describing function theory improves the system sensitivity. This application is important in the study of building a rehabilitation device for stroke patients. A highly sensitive and accurate position control system is the principal aim of this device. Besides, a lead-lag compensator characterized in transfer function for the nonlinear manipulator is generated and tested in simulations as well as experiments and the outcomes are validated. Faster responses are obtained in the simulation; however better decoupling qualities are achieved in real-time experiment. Overall implementation of the lead-lag compensator via SIDF model has been successfully demonstrated. The first implementation of SIDF approach to a rehabilitation device is done and the suitability of this approach is proven.

In conclusion, the first few stages of developing a rehabilitation orthosis are done. The ergonomic and lightweight structural design of the new rehabilitation orthosis is proposed and discussed. The novel implementation of SIDF approach in a vertical two-link manipulator is done. The new simulation model of the robotic orthosis is generated via SIDF method. A robust lead-lag controller for the orthosis is formed by utilizing the MATLAB tool of SIDF approach. The SIDF model and lead-lag controller are verified in simulation with non-linear model. Then, the generated controller is utilized for the orthosis. Various simulation and experiment are done to test the robustness of the newly designed controllers, and the outcomes are compared. Finally, the robustness of the controller is proven and satisfactory results suggest that the rehabilitation device build with the novel implementation is capable to correct the abnormal gait of hemiplegic stroke patients in future. The limitations of the current research are discussed in the next section.

7.2 Current Limitations and Future Works

The first stage of the research is carried out successfully. However, there are still limitations in the current work. As the SIDF approach is proven suitable for the controller design of the nonlinear two-link manipulator, there are several possibilities for further exploration with this approach. Some recommendations for future works are as follow:

a. **Trajectory control with designed controller via SIDF approach**

   Studies on the step response testing show positive results with the lead-lag controller to control the nonlinear orthosis. Better tracking and decoupling results with SIDF approach and controller are achieved. This proves that the application of the SIDF model for the controller design is feasible. Hence, trajectory control of the two-link manipulator is recommended.

b. **New scheme of controller design for the two-link manipulator**

   Various common linear controllers were developed In the MATLAB toolbox of the SIDF approach. With the help of the toolbox, the characterization and linearization of the nonlinear system becomes handy. Hence, expansion of the toolbox library is recommended. Advanced controllers such as neural network and sliding mode control are proposed to be inserted into the MATLAB toolbox. Hence, more selections will be provided for users to develop the two-link manipulator or even any other nonlinear system.

c. **High level trajectory control of the robotic orthosis by controlling both sides of the manipulator.**

   With the positive result obtained from the two-link manipulator control, the next target of the research should be carried out. A high-level trajectory control planning which involve both sides of the manipulator is suggested. It is important to synchronize and stabilize both limbs in the trajectory control to provide patients with a best symmetric walking training in the future.

d. **Implementation of sensors to the orthosis**

   Implementation of biomedical sensor or force sensor are recommended to collect subjects' walking data in order to provide the best help during rehabilitation training. With the instant feedback information from the subject, the rehabilitation device is able to determine the best support or movement to provide help on time. Once the subject lacks strength to move the leg, information will be collected by the device and it can provide instant help to allow automated movement of the link to reduce the subject's burden and avoid any accidents.

e. Implementation of ankle position control in coronal plane

Implementation of the third major part of lower limb which is the ankle is recommended to provide a full rehabilitation guidance for hemiplegic stroke patients. This part of rehabilitation orthosis is not developed due to limitation of time in this research. However, feature of ankle rehabilitation is essential in a prefect rehabilitation system. Patients will be able to regain a symmetric walking manner via a customized training for these 3 major parts of lower limb.

References

[1] “Stroke - what is stroke? - heart and stroke foundation of canada,” *Heart and Stroke Foundation*, 2014. http://www.heartandstroke.com/site/c.ikIQLcMWJtE/b.3483935/k.736A/Stroke__What_is_Stroke.htm (accessed Nov. 29, 2015).

[2] “What is stroke?,” *National Stroke Association*, 2015. http://www.stroke.org/understand-stroke/what-stroke (accessed Nov. 29, 2015).

[3] “Facts about stroke,” *Ramsay Sime Darby Health Care*, 2015. http://www.caringforstroke.com.my/understanding-stroke/facts-about-stroke/.

[4] W. Johnson, O. Onuma, M. Owolabi, and S. Sachdev, “Stroke: a global response is needed,” *Bull. World Health Organ.*, vol. 94, no. 9, pp. 634-634A, Sep. 2016, doi: 10.2471/BLT.16.181636.

[5] “National stroke association of malaysia (NASAM),” *National Stroke Association of Malaysia (NASAM)*. http://www.nasam.org/ (accessed Nov. 29, 2015).

[6] P. Langhorne, F. Coupar, and A. Pollock, “Motor recovery after stroke: a systematic review,” *Lancet Neurol.*, vol. 8, no. 8, pp. 741–54, Aug. 2009, doi: 10.1016/S1474-4422(09)70150-4.

[7] A. Pennycott, D. Wyss, H. Vallery, V. Klamroth-Marganska, and R. Riener, “Towards more effective robotic gait training for stroke rehabilitation: a review,” *J. Neuroeng. Rehabil.*, vol. 9, no. 1, p. 65, 2012, doi: 10.1186/1743-0003-9-65.

[8] A. M. Dollar and H. Herr, “Lower extremity exoskeletons and active orthoses: challenges and state-of-the-art,” *IEEE Trans. Robot.*, vol. 24, no. 1, pp. 144–158, Feb. 2008, doi: 10.1109/TRO.2008.915453.

[9] H. Herr, “Exoskeletons and orthoses: classification, design challenges and future directions,” *J. Neuroeng. Rehabil.*, vol. 6, p. 21, Jan. 2009, doi: 10.1186/1743-0003-6-21.

[10] S. J. Zaroodny, *Bumpusher - a powered aid to locomotion*. Defense Technical Information Center, 1963.

[11] *Hardiman i arm test - hardiman i prototype project*. Defense Technical Information Center, 1969.

[12] *Pitman, a powered exoskeletal suit for the infantryman*. Los Alamos National Laboratory, 1986.

[13] Y. Sarah, “UC Berkeley Researchers Developing Robotic Exoskeleton That Can Enhance Human Strength and Endurance,” *UC Berkeley*, 2004. https://www.berkeley.edu/news/media/releases/2004/03/03_exo.shtml (accessed Feb. 04, 2020).

[14] “Robotic exoskeleton replicates iron man - telegraph.” https://web.archive.org/web/20080501042247/http://www.telegraph.co.uk/earth/main.jhtml?view=DETAILS&grid=&xml=%2Fearth%2F2008%2F04%2F25%2Fsciiron125.xml (accessed Feb. 04, 2020).

[15] "Raytheon sarcos's exoskeleton nears production - ieee spectrum," *IEEE Spectrum*, 2011. https://spectrum.ieee.org/at-work/innovation/raytheon-sarcoss-exoskeleton-nears-production (accessed Feb. 04, 2020).

[16] "Sarcos achieves unprecedented power performance overcoming major obstacle to commercial deployment of full-body, powered industrial exoskeletons | sarcos robotics." https://www.sarcos.com/company/news/press-releases/power-performance-guardian-xo/ (accessed Apr. 13, 2021).

[17] S. Lee and Y. Sankai, "Power Assist Control for Walking Aid by HAL Based on Phase Sequence and EMG," in *International Conference on Control, Automation and System*, 2001, pp. 353–357.

[18] M. Vklbratovic and B. Borovac, "Zero moment point - thirthy five years of its life," *Int. J. Humanoid Robot.*, vol. 01, no. 01, pp. 157–173, Mar. 2004, doi: 10.1142/s0219843604000083.

[19] D. C. Johnson, D. W. Repperger, and G. Thompson, "Development of a mobility assist for the paralyzed, amputee, and spastic patient," in *Southern Biomedical Engineering Conference - Proceedings*, 1996, pp. 67–70, doi: 10.1109/sbec.1996.493115.

[20] Y. Saito, K. Kikuchi, H. Negoto, T. Oshima, and T. Haneyoshi, "Development of externally powered lower limb orthosis with bilateral-servo actuator," in *Proceedings of the 2005 IEEE 9th International Conference on Rehabilitation Robotics*, 2005, vol. 2005, pp. 394–399, doi: 10.1109/ICORR.2005.1501127.

[21] S. K. Banala *et al.*, "Gravity-balancing leg orthosis and its performance evaluation," *IEEE Trans. Robot.*, vol. 22, no. 6, pp. 1228–1239, Dec. 2006, doi: 10.1109/TRO.2006.882928.

[22] "Battery-powered, full-body exoskeleton lets users lift 200 pounds." https://newatlas.com/sarcos-robotics-guardian-xo-exoskeleton/57847/ (accessed Apr. 13, 2020).

[23] D. Shi, W. Zhang, W. Zhang, and X. Ding, "A Review on Lower Limb Rehabilitation Exoskeleton Robots," *J. Mech. Eng*, vol. 32, p. 74, 2019, doi: 10.1186/s10033-019-0389-8.

[24] H. Yano, S. Tamefusa, N. Tanaka, H. Saitou, and H. Iwata, "Gait rehabilitation system for stair climbing and descending," *2010 IEEE Haptics Symp.*, pp. 393–400, 2010, doi: 10.1109/HAPTIC.2010.5444627.

[25] I. Díaz, J. J. Gil, and E. Sánchez, "Lower-limb robotic rehabilitation: literature review and challenges," *J. Robot.*, vol. 2011, pp. 1–11, 2011, doi: 10.1155/2011/759764.

[26] P. Lum, D. Reinkensmeyer, R. Mahoney, W. Z. Rymer, and C. Burgar, "Robotic devices for movement therapy after stroke: current status and challenges to clinical acceptance," *Top. Stroke Rehabil.*, vol. 8, no. 4, pp. 40–53, 2002, doi: 10.1310/9KFM-KF81-P9A4-5WW0.

[27] M. Martins, A. Frizera, C. P. Santos, and R. Ceres, "Review and classification of human gait training and rehabilitation devices," in *Assistive Technology Research Series*, 2011, vol. 29, pp. 774–781, doi: 10.3233/978-1-60750-814-4-774.

[28] M. Dzahir and S. Yamamoto, "Recent trends in lower-limb robotic rehabilitation orthosis: control

scheme and strategy for pneumatic muscle actuated gait trainers," *Robotics*, vol. 3, no. 2, pp. 120–148, 2014, doi: 10.3390/robotics3020120.

[29] S. Hesse and C. Werner, "Connecting research to the needs of patients and clinicians," *Brain Res. Bull.*, vol. 78, no. 1, pp. 26–34, Jan. 2009, doi: 10.1016/j.brainresbull.2008.06.004.

[30] H. Schmidt, C. Werner, R. Bernhardt, S. Hesse, and J. Krüger, "Gait rehabilitation machines based on programmable footplates," *J. Neuroeng. Rehabil.*, vol. 4, p. 2, Jan. 2007, doi: 10.1186/1743-0003-4-2.

[31] A. Nilsson, K. S. Vreede, V. Häglund, H. Kawamoto, Y. Sankai, and J. Borg, "Gait training early after stroke with a new exoskeleton--the hybrid assistive limb: a study of safety and feasibility," *J. Neuroeng. Rehabil.*, vol. 11, p. 92, Jan. 2014, doi: 10.1186/1743-0003-11-92.

[32] J. K. Burgess, G. C. Weibel, and D. A. Brown, "Overground walking speed changes when subjected to body weight support conditions for nonimpaired and post stroke individuals," *J. Neuroeng. Rehabil.*, vol. 7, p. 6, Jan. 2010, doi: 10.1186/1743-0003-7-6.

[33] G. Chen, C. K. Chan, Z. Guo, and H. Yu, "A review of lower extremity assistive robotic exoskeletons in rehabilitation therapy," *Crit. Rev. Biomed. Eng.*, vol. 41, no. 4–5, pp. 343–63, Jan. 2013.

[34] L. Marchal-Crespo and D. J. Reinkensmeyer, "Review of control strategies for robotic movement training after neurologic injury," *J. Neuroeng. Rehabil.*, vol. 6, no. 1, p. 20, Jan. 2009, doi: 10.1186/1743-0003-6-20.

[35] G. J. Gelderblom, M. De Wilt, G. Cremers, and A. Rensma, "Rehabilitation robotics in robotics for healthcare; A roadmap study for the European Commission," in *2009 IEEE International Conference on Rehabilitation Robotics*, Jun. 2009, pp. 834–838, doi: 10.1109/ICORR.2009.5209498.

[36] R. Jiménez-Fabián and O. Verlinden, "Review of control algorithms for robotic ankle systems in lower-limb orthoses, prostheses, and exoskeletons," *Med. Eng. Phys.*, vol. 34, no. 4, pp. 397–408, 2012, doi: 10.1016/j.medengphy.2011.11.018.

[37] J. F. Veneman, R. Kruidhof, E. E. G. Hekman, R. Ekkelenkamp, E. H. F. Van Asseldonk, and H. van der Kooij, "Design and evaluation of the LOPES exoskeleton robot for interactive gait rehabilitation," *IEEE Trans. Neural Syst. Rehabil. Eng.*, vol. 15, no. 3, pp. 379–86, Sep. 2007, doi: 10.1109/TNSRE.2003.818185.

[38] A. Nassirharand, "Tracking and decoupling of multivariable nonlinear systems," in *2009 IEEE International Conference on Control Applications*, Jul. 2009, pp. 136–141, doi: 10.1109/CCA.2009.5281188.

[39] A. Nassirharand and H. Karimi, "Input/output characterization of highly nonlinear multivariable systems," *Adv. Eng. Softw.*, vol. 33, no. 11–12, pp. 825–830, 2002, doi: 10.1016/S0965-9978(02)00046-7.

[40] M. W. Whittle, *Gait analysis: an introduction*. Elsevier Science, 2014.

[41] R. W. Baker, *Measuring walking: a handbook of clinical gait analysis*. Wiley, 2013.

[42] M. Stalin, “Development of a smart insole system for real-time detection of temporal gait parameters and related deviations in unilateral lower-limb amputees,” University of Miami, 2012.

[43] M. Y. H. S M Nacy, S S Hassan, “A modified dynamic model of the human lower limb during complete gait cycle,” *Int. J. od Mech. Eng. Robot. Res.*, vol. 2, no. 2, pp. 9–19, 2013.

[44] R. L. A. N. R. Center, *Observational gait analysis*. Los Amigos Research and Education Institute, Rancho Los Amigos National Rehabilitation Center, 2001.

[45] J. Perry, *Gait analysis: normal and pathological function*. SLACK, 1992.

[46] C. J. M. M. Hasler JP, Molin M, Lentz K, Gerkens V, Oestergaard S, Scott E, Vazquez SL, delRio Nunez, “Observational gait analysis for evaluating the effectiveness of functional electrical stimulation enhanced gait,” *5th Annu. Conf. Int. Funct. Electr. Stimul. Soc.*, 2000.

[47] H. Sadeghi, P. Allard, F. Prince, and H. Labelle, “Symmetry and limb dominance in able-bodied gait: a review,” *Gait Posture*, vol. 12, no. 1, pp. 34–45, Sep. 2000, doi: 10.1016/S0966-6362(00)00070-9.

[48] B. Pietraszewski, S. Winiarski, and S. Jaroszczuk, “Three-dimensional human gait pattern - reference data for normal men,” *Acta Bioeng. Biomech. / Wrocław Univ. Technol.*, vol. 14, no. 3, pp. 9–16, Jan. 2012, doi: 10.5277/abb120302.

[49] B. Balaban and F. Tok, “Gait Disturbances in Patients With Stroke,” *Phys. Med. Rehabil.*, vol. 6, no. 7, pp. 635–642, Jul. 2014, doi: 10.1016/j.pmrj.2013.12.017.

[50] T. Rahman *et al.*, “Passive exoskeletons for assisting limb movement,” *J. Rehabil. Res. Dev.*, vol. 43, no. 5, pp. 583–90, Accessed: Oct. 22, 2018. [Online]. Available: http://www.ncbi.nlm.nih.gov/pubmed/17123200.

[51] S. K. Agrawal, S. K. Banala, and A. Fattah, “A gravity balancing passive exoskeleton for the human leg,” in *Robotics: Science and Systems*, 2006, no. 302, doi: 10.15607/RSS.2006.II.024.

[52] S. K. Banala *et al.*, “Gravity-balancing leg orthosis and its performance evaluation,” *IEEE Trans. Robot.*, vol. 22, no. 6, pp. 1228–1239, Dec. 2006, doi: 10.1109/TRO.2006.882928.

[53] M. F. W. Ng, R. K. Y. Tong, and L. S. W. Li, “A pilot study of randomized clinical controlled trial of gait training in subacute stroke patients with partial body-weight support electromechanical gait trainer and functional electrical stimulation: six-month follow-up,” *Stroke.*, vol. 39, no. 1, pp. 154–60, Jan. 2008, doi: 10.1161/STROKEAHA.107.495705.

[54] I. Schwartz *et al.*, “The effectiveness of locomotor therapy using robotic-assisted gait training in subacute stroke patients: a randomized controlled trial,” *PM R*, vol. 1, no. 6, pp. 516–23, Jun. 2009, doi: 10.1016/j.pmrj.2009.03.009.

[55] “LokoHelp | woodway.” http://www.woodway.com/products/lokohelp (accessed Jan. 17, 2016).

[56] “Gait trainer gt i,” *Reha-Stim Medtec GmbH & Co. KG*, 2014. http://www.reha-

stim.de/cms/index.php?id=76 (accessed Dec. 29, 2015).

[57] T. Ueba, O. Hamada, T. Ogata, T. Inoue, E. Shiota, and Y. Sankai, "Feasibility and safety of acute phase rehabilitation after stroke using the hybrid assistive limb robot suit," *Neurol. Med. Chir. (Tokyo).*, vol. 53, no. 5, pp. 287–90, Jan. 2013, doi: 10.2176/nmc.53.287.

[58] H. Watanabe, N. Tanaka, T. Inuta, H. Saitou, and H. Yanagi, "Locomotion improvement using a hybrid assistive limb in recovery phase stroke patients: a randomized controlled pilot study," *Arch. Phys. Med. Rehabil.*, vol. 95, no. 11, pp. 2006–12, Nov. 2014, doi: 10.1016/j.apmr.2014.07.002.

[59] K. Yamawaki *et al.*, *Application of robot suit hal to gait rehabilitation of stroke patients: a case study*, vol. 7383. Berlin, Heidelberg: Springer Berlin Heidelberg, 2012.

[60] J. Patton *et al.*, "Kineassist: design and development of a robotic overground gait and balance therapy device," *Top. Stroke Rehabil.*, vol. 15, no. 2, pp. 131–9, Jan. 2008, doi: 10.1310/tsr1502-131.

[61] "Gallery - rewalk – more than walking." http://rewalk.com/gallery-2/ (accessed Jan. 17, 2016).

[62] A. Roy *et al.*, "Measurement of human ankle stiffness using the anklebot," in *2007 IEEE 10th International Conference on Rehabilitation Robotics*, Jun. 2007, pp. 356–363, doi: 10.1109/ICORR.2007.4428450.

[63] A. M. Wong, M. Y. Lee, J. K. Kuo, and F. T. Tang, "The development and clinical evaluation of a standing biofeedback trainer," in *Journal of rehabilitation research and development*, Jul. 1997, vol. 34, no. 3, pp. 322–7.

[64] C. D. M. Simons, E. H. F. van Asseldonk, J. I. Folkersma, J. van den Hoek, M. Postma, and J. H. Buurke, "First clinical results with the new innovative robotic gait trainer lopes," *Gait Posture*, vol. 30, no. 2, p. s7, Nov. 2009, doi: 10.1016/j.gaitpost.2009.08.013.

[65] S. Freivogel, J. Mehrholz, T. Husak-Sotomayor, and D. Schmalohr, "Gait training with the newly developed 'lokohelp'-system is feasible for non-ambulatory patients after stroke, spinal cord and brain injury. a feasibility study," *Brain Inj.*, vol. 22, no. 7–8, pp. 625–32, Jul. 2008, doi: 10.1080/02699050801941771.

[66] "Motorika - enhanced patient specific rehabilitation solutions." http://motorika.com/ (accessed Feb. 18, 2020).

[67] S. Hesse, D. Uhlenbrock, and T. Sarkodie-Gyan, "Gait pattern of severely disabled hemiparetic subjects on a new controlled gait trainer as compared to assisted treadmill walking with partial body weight support," *Clin. Rehabil.*, vol. 13, no. 5, pp. 401–410, Oct. 1999, doi: 10.1191/026921599673896297.

[68] "ReWalk 6.0 – home." https://rewalk.com/ (accessed Feb. 18, 2020).

[69] "Hal - robots: your guide to the world of robotics." https://robots.ieee.org/robots/hal/ (accessed Feb. 18, 2020).

[70] S. K. Banala, A. Kulpe, and S. K. Agrawal, “A powered leg orthosis for gait rehabilitation of motor-impaired patients,” vol. 00, no. April, pp. 10–14, 2007, doi: 10.1109/ROBOT.2007.364115.

[71] H. Schmidt, “HapticWalker-A novel haptic device for walking simulation,” in *Proceedings of EuroHaptics 2004*, 2004, pp. 60–67.

[72] A. Veg and D. B. Popović, “Walkaround: Mobile balance support for therapy of walking,” *IEEE Trans. Neural Syst. Rehabil. Eng.*, vol. 16, no. 3, pp. 264–269, Jun. 2008, doi: 10.1109/TNSRE.2008.918424.

[73] A. Roy, H. I. Krebs, J. E. Barton, R. F. Macko, and L. W. Forrester, “Anklebot-assisted locomotor training after stroke: A novel deficit-adjusted control approach,” in *Proceedings - IEEE International Conference on Robotics and Automation*, 2013, pp. 2175–2182, doi: 10.1109/ICRA.2013.6630869.

[74] S. K. Banala, S. H. Kim, S. K. Agrawal, and J. P. Scholz, “Robot assisted gait training with active leg exoskeleton (alex),” *IEEE Trans. Neural Syst. Rehabil. Eng.*, vol. 17, no. 1, pp. 2–8, Feb. 2009, doi: 10.1109/TNSRE.2008.2008280.

[75] M. Bortole *et al.*, “The h2 robotic exoskeleton for gait rehabilitation after stroke: early findings from a clinical study,” *J. Neuroeng. Rehabil.*, vol. 12, p. 54, Jun. 2015, doi: 10.1186/s12984-015-0048-y.

[76] H. I. Krebs *et al.*, “Rehabilitation robotics: performance-based progressive robot-asssisted therapy,” *Auton. Robots*, vol. 15, no. 1, pp. 7–20, 2003, doi: 10.1023/A:1024494031121.

[77] P. S. Lum, C. G. Burgar, P. C. Shor, M. Majmundar, and M. Van der Loos, “Robot-assisted movement training compared with conventional therapy techniques for the rehabilitation of upper-limb motor function after stroke,” *Arch. Phys. Med. Rehabil.*, vol. 83, no. 7, pp. 952–959, Jul. 2002, doi: 10.1053/apmr.2001.33101.

[78] D. Chen, M. Ning, B. Zhang, and G. Yang, “Control strategy of the lower-limb exoskeleton based on the EMG signals,” *2014 IEEE Int. Conf. Robot. Biomimetics, IEEE ROBIO 2014*, pp. 2416–2420, 2015, doi: 10.1109/ROBIO.2014.7090701.

[79] C. Cao, L. Ma, Y. Xu, C. Cao, L. Ma, and Y. Xu, “Adaptive control theory and applications,” *J. Control Sci. Eng.*, vol. 2012, pp. 1–2, 2012, doi: 10.1155/2012/827353.

[80] R. Riener, L. Lünenburger, S. Jezernik, M. Anderschitz, G. Colombo, and V. Dietz, “Patient-cooperative strategies for robot-aided treadmill training: First experimental results,” *IEEE Trans. Neural Syst. Rehabil. Eng.*, vol. 13, no. 3, pp. 380–394, 2005, doi: 10.1109/TNSRE.2005.848628.

[81] A. Duschau-Wicke, T. Brunsch, L. Lunenburger, and R. Riener, “Adaptive support for patient-cooperative gait rehabilitation with the Lokomat,” in *2008 IEEE/RSJ International Conference on Intelligent Robots and Systems*, Sep. 2008, pp. 2357–2361, doi: 10.1109/IROS.2008.4650578.

[82] J. A. Blaya and H. Herr, “Adaptive control of a variable-impedance ankle-foot orthosis to assist drop-foot gait,” *IEEE Trans. Neural Syst. Rehabil. Eng.*, vol. 12, no. 1, pp. 24–31, Mar. 2004, doi: 10.1109/TNSRE.2003.823266.

[83] R. Lu, Z. Li, C.-Y. Su, and A. Xue, “Development and learning control of a human limb with a rehabilitation exoskeleton,” *IEEE Trans. Ind. Electron.*, vol. 61, no. 7, pp. 3776–3785, Jul. 2014, doi: 10.1109/TIE.2013.2275903.

[84] N. Koceska, S. Koceski, F. Durante, P. Beomonte, and T. Raparelli, “Control architecture of a 10 dof lower limbs exoskeleton for gait rehabilitation,” *Int. J. Adv. Robot. Syst.*, vol. 10, no. 1, p. 1, 2013, doi: 10.5772/55032.

[85] G. Mamani, J. Becedas, and V. Feliu Batlle, “Robust position control of a dc motor by sliding mode,” pp. 495–504, 2010.

[86] F. Cao, Y. Li, and J. Shi, “Adaptive sliding mode impedance control in lower limbs rehabilitation robotic,” *2013 Chinese Autom. Congr.*, pp. 310–315, 2013, doi: 10.1109/CAC.2013.6775749.

[87] V. I. Utkin, “Sliding mode control design principles and applications to electric drives,” *IEEE Trans. Ind. Electron.*, vol. 40, no. 1, pp. 23–36, 1993, doi: 10.1109/41.184818.

[88] J. Y. Hung, W. Gao, and J. C. Hung, “Variable structure control: a survey,” *IEEE Trans. Ind. Electron.*, vol. 40, no. 1, pp. 2–22, 1993, doi: 10.1109/41.184817.

[89] R. A. DeCarlo, S. H. Zak, and G. P. Matthews, “Variable structure control of nonlinear multivariable systems: a tutorial,” *Proc. IEEE*, vol. 76, no. 3, pp. 212–232, Mar. 1988, doi: 10.1109/5.4400.

[90] B. M. Patre, V. M. Panchade, and R. M. Nagarale, “Sliding mode control of dc drives,” in *Sliding Mode Control*, InTech, 2011.

[91] S. Mefoued, “A second order sliding mode control and a neural network to drive a knee joint actuated orthosis,” *Neurocomputing*, vol. 155, pp. 71–79, 2015, doi: 10.1016/j.neucom.2014.12.047.

[92] M. Aamir, “On replacing pid controller with ann controller for dc motor position control,” *Int. J. Res. Stud. Comput.*, vol. 2, no. 1, pp. 21–29, 2013, doi: 10.5861/ijrsc.2013.236.

[93] S. Zhang, M. Lei, Y. Dong, and W. He, “Adaptive neural network control of coordinated robotic manipulators with output constraint,” *IET Control Theory Appl.*, vol. 10, no. 17, pp. 2271–2278, 2016, doi: 10.1049/iet-cta.2016.0009.

[94] L. Liyang Wang, Z. Zhi Liu, C. L. P. Chen, Y. Yun Zhang, S. Sukhan Lee, and X. Xin Chen, “Energy-efficient svm learning control system for biped walking robots,” *IEEE Trans. Neural Networks Learn. Syst.*, vol. 24, no. 5, pp. 831–837, May 2013, doi: 10.1109/TNNLS.2013.2242486.

[95] Z. Li and C.-Y. Su, “Neural-adaptive sontrol of single-master-multiple-slaves teleoperation for coordinated multiple mobile manipulators with time-varying communication delays and input uncertainties,” *IEEE Trans. Neural Networks Learn. Syst.*, vol. 24, no. 9, pp. 1400–1413, Sep. 2013, doi: 10.1109/TNNLS.2013.2258681.

[96] W. He, Y. Dong, and C. Sun, “Adaptive neural impedance control of a robotic manipulator with input saturation,” vol. 46, no. 3, pp. 334–344, 2016, doi: 10.1109/TSMC.2015.2429555.

[97] S. Mefoued, “A robust adaptive neural control scheme to drive an actuated orthosis for assistance of knee movements,” *Neurocomputing*, vol. 140, pp. 27–40, 2014, doi: 10.1016/j.neucom.2014.03.038.

[98] W. He, A. O. David, Z. Yin, and C. Sun, “Neural network control of a robotic manipulator with input deadzone and output constraint,” *IEEE Trans. Syst. Man, Cybern. Syst.*, vol. 46, no. 6, pp. 759–770, Jun. 2016, doi: 10.1109/TSMC.2015.2466194.

[99] M. J. L. Orr, “Introduction to radial basis function networks,” 1996, Accessed: Dec. 12, 2016. [Online]. Available: www.anc.ed.ac.uk/mjo/papers/intro.ps.

[100] M. F. Wilkins, L. Boddy, C. W. Morris, and R. R. Jonker, “Identification of phytoplankton from flow cytometry data by using radial basis function neural networks,” *Appl Env. Microbiol*, vol. 65, no. 10, pp. 4404–4410, 1999.

[101] K. Kiguchi, T. Tanaka, and T. Fukuda, “Neuro-fuzzy control of a robotic exoskeleton with emg signals,” *IEEE Trans. Fuzzy Syst.*, vol. 12, no. 4, pp. 481–490, Aug. 2004, doi: 10.1109/TFUZZ.2004.832525.

[102] R. Fullér and D. Visiting, *Neural fuzzy systems*. Abo Akademi University, 1995.

[103] Y. H. Yin, Y. J. Fan, and L. D. Xu, “EMG and epp-integrated human-machine interface between the paralyzed and rehabilitation exoskeleton,” *IEEE Trans. Inf. Technol. Biomed.*, vol. 16, no. 4, pp. 542–549, 2012, doi: 10.1109/TITB.2011.2178034.

[104] A. Nassirharand, “Control system design of multivariable non-linear space robots,” *Aircr. Eng. Aerosp. Technol.*, vol. 80, no. 1, pp. 27–34, Jan. 2008, doi: 10.1108/00022660810841985.

[105] A. Nassirharand, J. H. Taylor, and K. N. Reid, “Controller design For nonlinear systems based on simultaneous stabilization theory and describing function models,” *J. Dyn. Syst. Meas. Control*, vol. 110, no. 2, p. 134, 1988, doi: 10.1115/1.3152663.

[106] J. H. Taylor and K. L. Strobel, “Nonlinear compensator synthesis via sinusoidal-input describing functions,” 1985, pp. 1242–1247.

[107] A. Nassirharand and H. Karimi, “Controller synthesis methodology for multivariable nonlinear systems with application to aerospace,” *J. Dyn. Syst. Meas. Control*, vol. 126, no. 3, p. 595, 2004, doi: 10.1115/1.1789975.

[108] A. Nassirharand, “Input/output characterization of highly-nonlinear systems,” *Adv. Eng. Softw.*, vol. 9, no. 3, pp. 129–133, Jul. 1987, doi: 10.1016/0141-1195(87)90002-7.

[109] S. H. Teh and A. Nassirharand, “Software for design of linear controllers for nonlinear systems,” in *2010 International Conference on Advance in Mechanical Engineering*, 2010, pp. 83–88.

[110] S. H. The and A. Nassirharand, “Idle speed control using a describing-function approach,” *Proc. Inst. Mech. Eng. Part D J. Automob. Eng.*, vol. 224, no. 4, pp. 533–545, Apr. 2010, doi: 10.1243/09544070JAUTO1327.

[111] Z. Wu, F. Li, W. Mi, and J. Lei, “Robust controller design for the cooperative control of lower

extremity rehabilitation robot," *Int. J. Control Autom.*, vol. 7, no. 4, pp. 313–328, 2014, doi: 10.14257/ijca.2014.7.4.28.

[112] F. C. Cao, C. F. Li, and Y. C. Li, "Robust sliding mode adaptive control for lower extremity exoskeleton," in *2015 Chinese Automation Congress (CAC)*, Nov. 2015, pp. 400–405, doi: 10.1109/CAC.2015.7382533.

[113] J. Zhang, Y. Dong, C. Yang, Y. Geng, Y. Chen, and Y. Yang, "5-Link model based gait trajectory adaption control strategies of the gait rehabilitation exoskeleton for post-stroke patients," *Mechatronics*, vol. 20, no. 3, pp. 368–376, 2010, doi: 10.1016/j.mechatronics.2010.02.003.

[114] K. H. Seo and J. J. Lee, "The development of two mobile gait rehabilitation systems," *IEEE Trans. Neural Syst. Rehabil. Eng.*, vol. 17, no. 2, pp. 156–166, Apr. 2009, doi: 10.1109/TNSRE.2009.2015179.

[115] "Maxon," *Maxon Motor*, 2016. http://www.maxonmotor.com/maxon/view/content/index (accessed Jan. 02, 2016).

[116] F. Salem, "Dynamic modeling, simulation and control of electric machines for mechatronics applications," *Int. J. Control. Autom. Syst.*, vol. 1, no. 2, pp. 30–42, 2013.

[117] A. Nassirharand and S. A. Hosseini, "Tracking and decoupling of multivariable non-linear systems," *Int. J. Model. Identif. Control*, vol. 6, no. 4, p. 341, 2009, doi: 10.1504/IJMIC.2009.024741.

[118] A. Gelb and W. E. Vander Velde, *Multiple-input describing functions and nonlinear system design - Arthur Gelb, Wallace E. Vander Velde - Google Books*. McGraw-Hill, 1968.

[119] G. M. Siouris, "Nonlinear conrol Engineering," *IEEE Trans. Syst. Man. Cybern.*, vol. 7, no. 7, pp. 567–568, 1977, doi: 10.1109/TSMC.1977.4309773.

[120] I. E. Kazakov, "Generalization of statistical linearization method to multidimensional systems," *Avtomat. i Telemekh.*, vol. 56, no. 7, pp. 1210–1215, 1965.

[121] A. Gelb and R. S. Warren, "Direct statistical analysis of nonlinear systems: cadet," *AIAA J.*, vol. 11, no. 5, pp. 689–694, May 1973, doi: 10.2514/3.50507.

[122] J. H. Taylor, "A new algorithmic state-space/describing function technique for limit cycle analysis," 1977.

[123] D. N. Hannebrink, H. S. H. Lee, H. Weinstock, and J. K. Hedrick, "Influence of axle load, track gage? And wheel profile on rail-vehicle hunting," *J. Manuf. Sci. Eng. Trans. ASME*, vol. 99, no. 1, pp. 186–195, Feb. 1977, doi: 10.1115/1.3439135.

[124] J. H. Taylor, "Describing functions," in *Wiley Encyclopedia of Electrical and Electronics Engineering*, John Wiley & Sons, Inc., 1999.

[125] M. Vidyasagar, *Nonlinear systems analysis second edition*. New Jersey: Prentice-Hall, 1993.

[126] Z. Úředníček, "Describing functions and prediction of limit cycles," *Wseas Trans. Syst. Control*, vol. 13, pp. 433–446, 2018.

[127] J. H. Taylor, “A systematic nonlinear controller design method based on quasilinear system models,” in *Proceedings of the American Control Conference*, 1983, p. 141.

[128] R. C. Dorf *et al.*, *Modern control systems*. Pearson (Addison-Wesley), 2011.

[129] T. Dogruer and N. Tan, “Lead and lag controller design in fractional-order control systems,” *Meas. Control*, vol. 52, no. 7–8, pp. 1017–1028, Sep. 2019, doi: 10.1177/0020294019858094.

[130] H. Nassirharan, Amir ; Karimi, “Closed-form solution for design of lead-lag compensators,” *Int. J. Electr. Eng. Educ.*, vol. 41, no. 2, pp. 172–180, 2004, doi: 10.7227/IJEEE.41.2.8.

[131] J. R. O’Donnell and J. H. Taylor, “CAE tools for nonlinear systems analysis and design based on sinusoidal-input describing functions,” *IFAC Proc. Vol.*, vol. 24, no. 4, pp. 89–94, Jul. 1991, doi: 10.1016/s1474-6670(17)54252-4.

[132] C. T. Chen, *Linear system theory and design*. New York: Oxford University Press, 1999.

[133] A. Nassirharand, “Computer-aided design of classical linear compensators with application to aerospace,” *J. Syst. Eng. Electron.*, vol. 20, no. 6, pp. 1373–1377, 2009.

Appendices

Appendix A

Parts Drawing

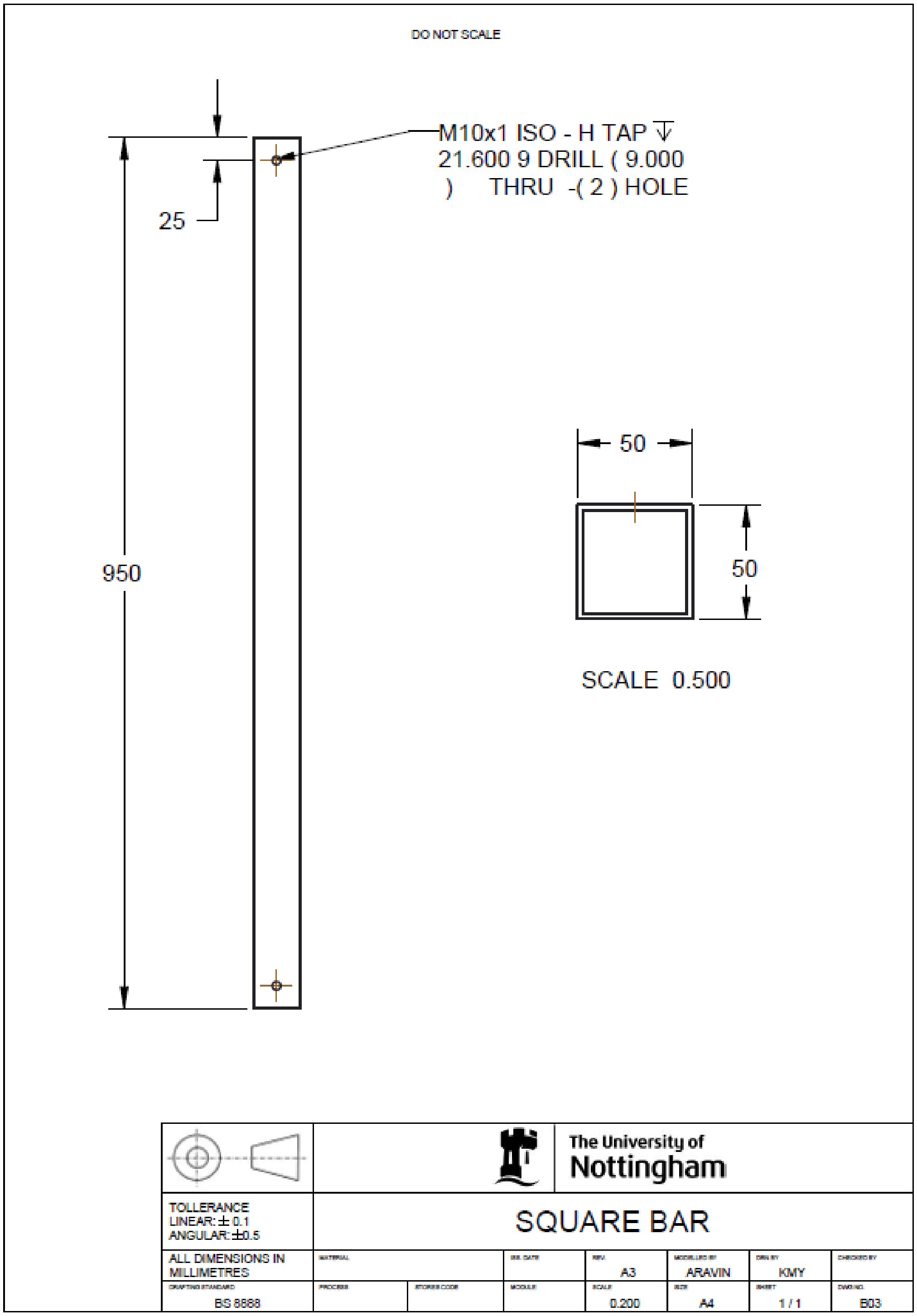

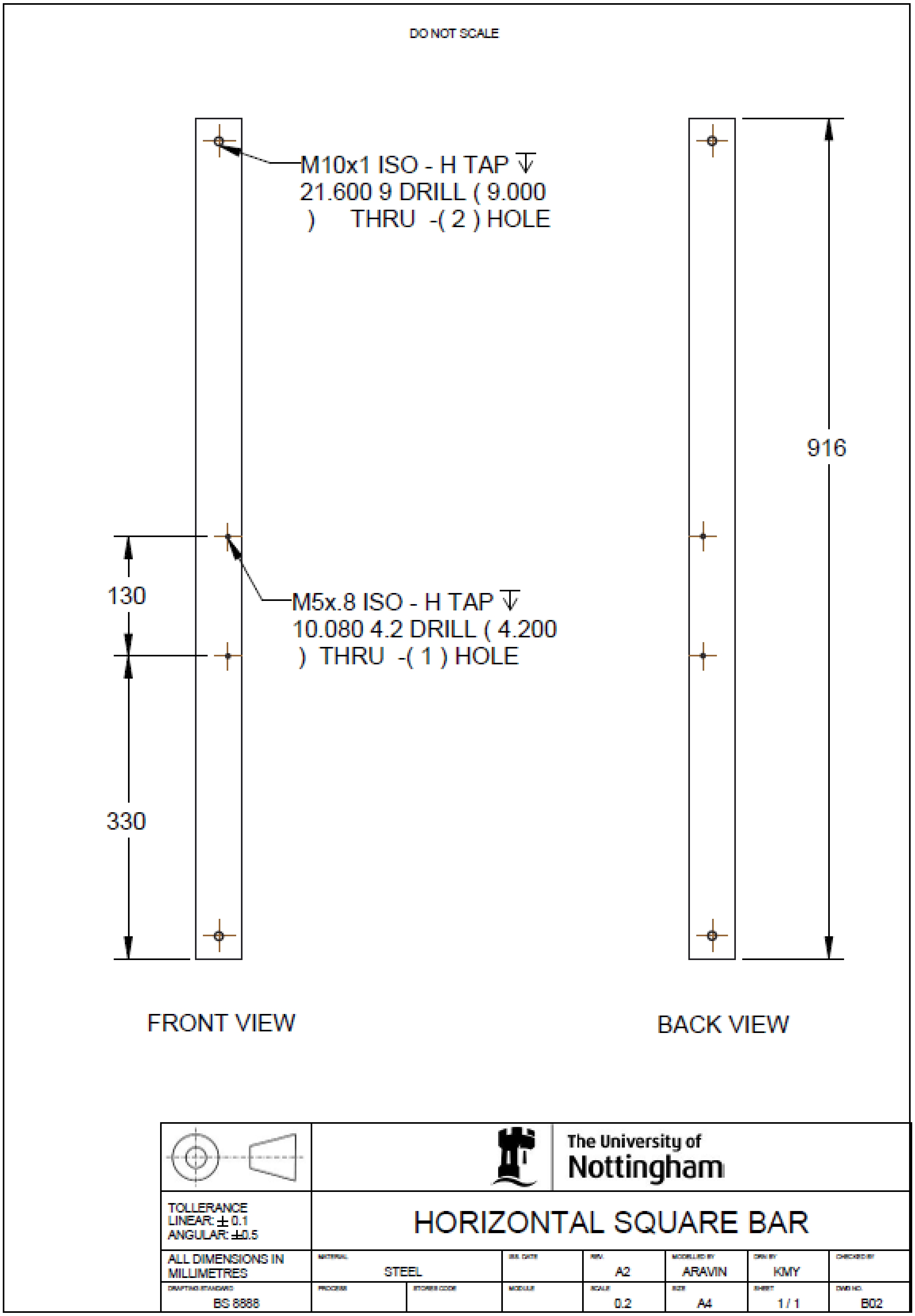
DO NOT SCALE
M10x1 ISO - H TAP
21.600 9 DRILL (9.000
) THRU -(2) HOLE
M5x.8 ISO - H TAP
10.080 4.2 DRILL (4.200
) THRU -(1) HOLE
130
330
916
FRONT VIEW
BACK VIEW
The University of Nottingham
TOLLERANCE
LINEAR: ± 0.1
ANGULAR: ±0.5
HORIZONTAL SQUARE BAR
ALL DIMENSIONS IN MILLIMETRES
STEEL
A2
ARAVIN
KMY
BS 8888
0.2
A4
1 / 1
B02

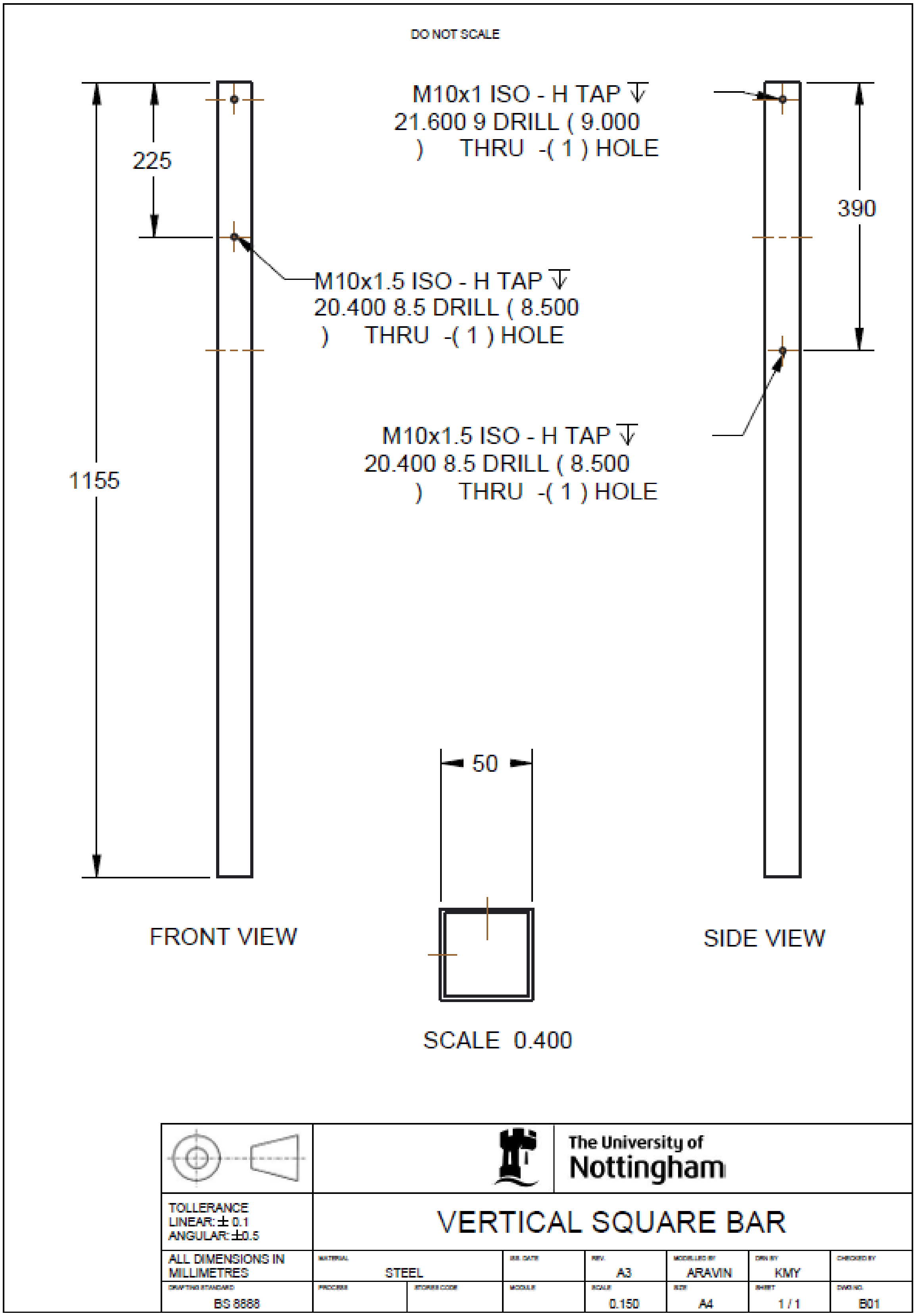
DO NOT SCALE
M10x1 ISO - H TAP 21.600 9 DRILL (9.000) THRU -(1) HOLE
225
1155
M10x1.5 ISO - H TAP 20.400 8.5 DRILL (8.500) THRU -(1) HOLE
390
M10x1.5 ISO - H TAP 20.400 8.5 DRILL (8.500) THRU -(1) HOLE
50
FRONT VIEW
SIDE VIEW
SCALE 0.400
The University of Nottingham
TOLLERANCE
LINEAR: ± 0.1
ANGULAR: ±0.5
VERTICAL SQUARE BAR
ALL DIMENSIONS IN MILLIMETRES
STEEL
A3
ARAVIN
KMY
BS 8888
0.150
A4
1 / 1
B01

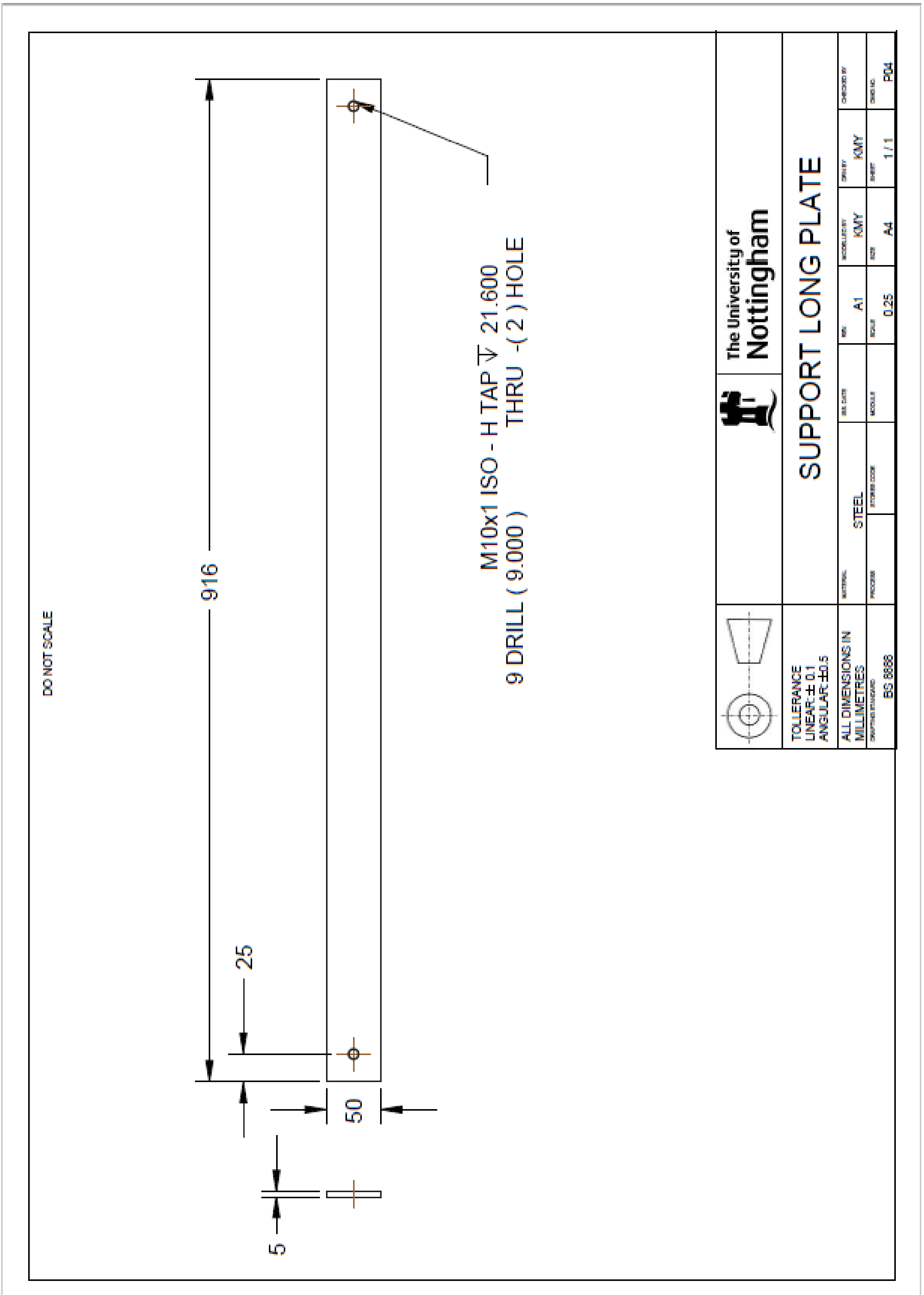
DO NOT SCALE
916
25
50
5
M10x1 ISO - H TAP ⊽ 21.600
9 DRILL (9.000) THRU -(2) HOLE
The University of Nottingham
SUPPORT LONG PLATE
TOLLERANCE
LINEAR: ± 0.1
ANGULAR: ±0.5
ALL DIMENSIONS IN MILLIMETRES
BS 8888
STEEL
A1
KMY
KMY
0.25
A4
1 / 1
P04

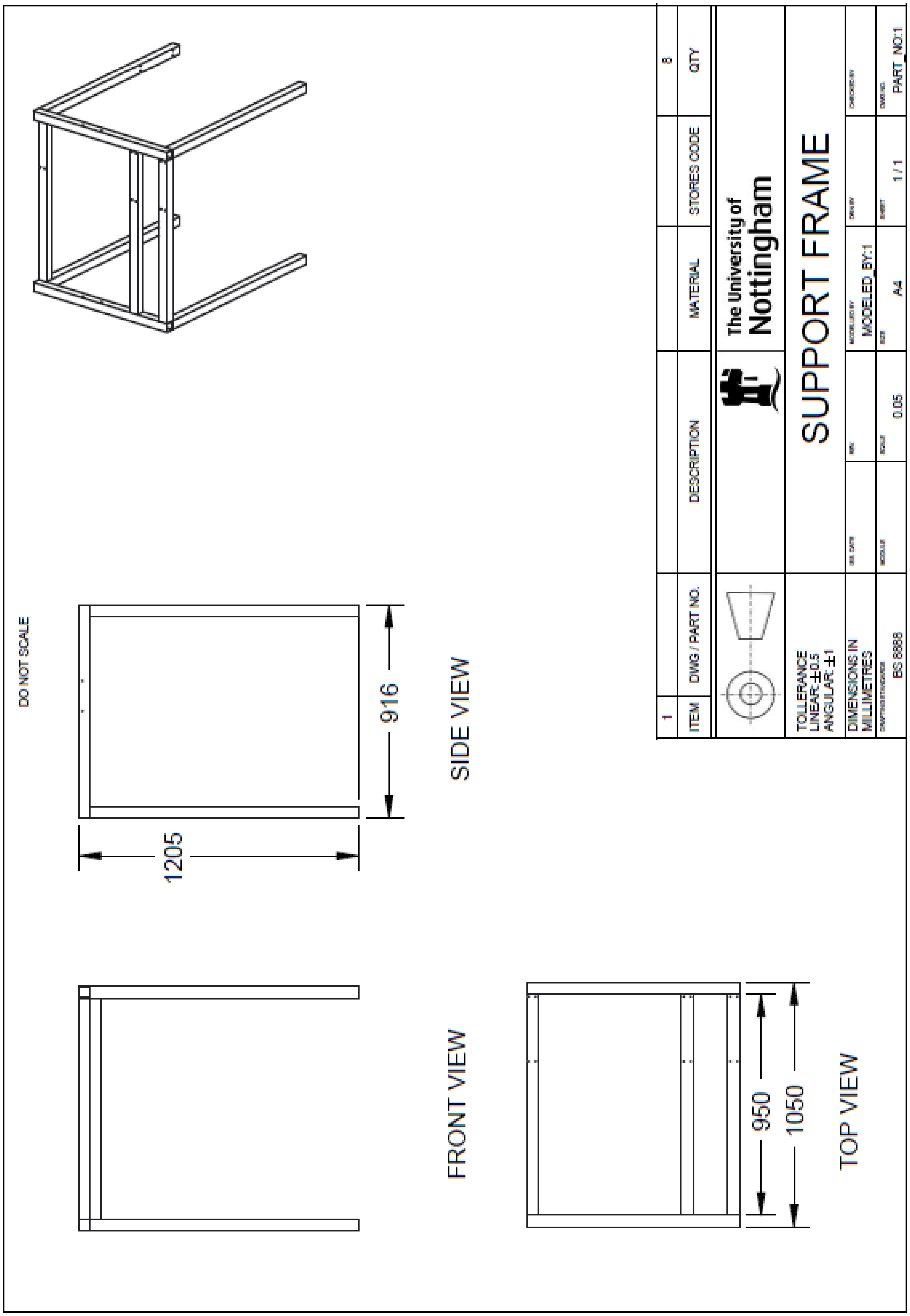
DO NOT SCALE
1205
916
SIDE VIEW
FRONT VIEW
950
1050
TOP VIEW
ITEM
1
DWG / PART NO.
DESCRIPTION
MATERIAL
STORES CODE
QTY
8
The University of Nottingham
SUPPORT FRAME
TOLLERANCE
LINEAR: ±0.5
ANGULAR: ±1
DIMENSIONS IN MILLIMETRES
BS 8888
0.05
MODELED_BY:1
A4
1 / 1
PART_NO:1

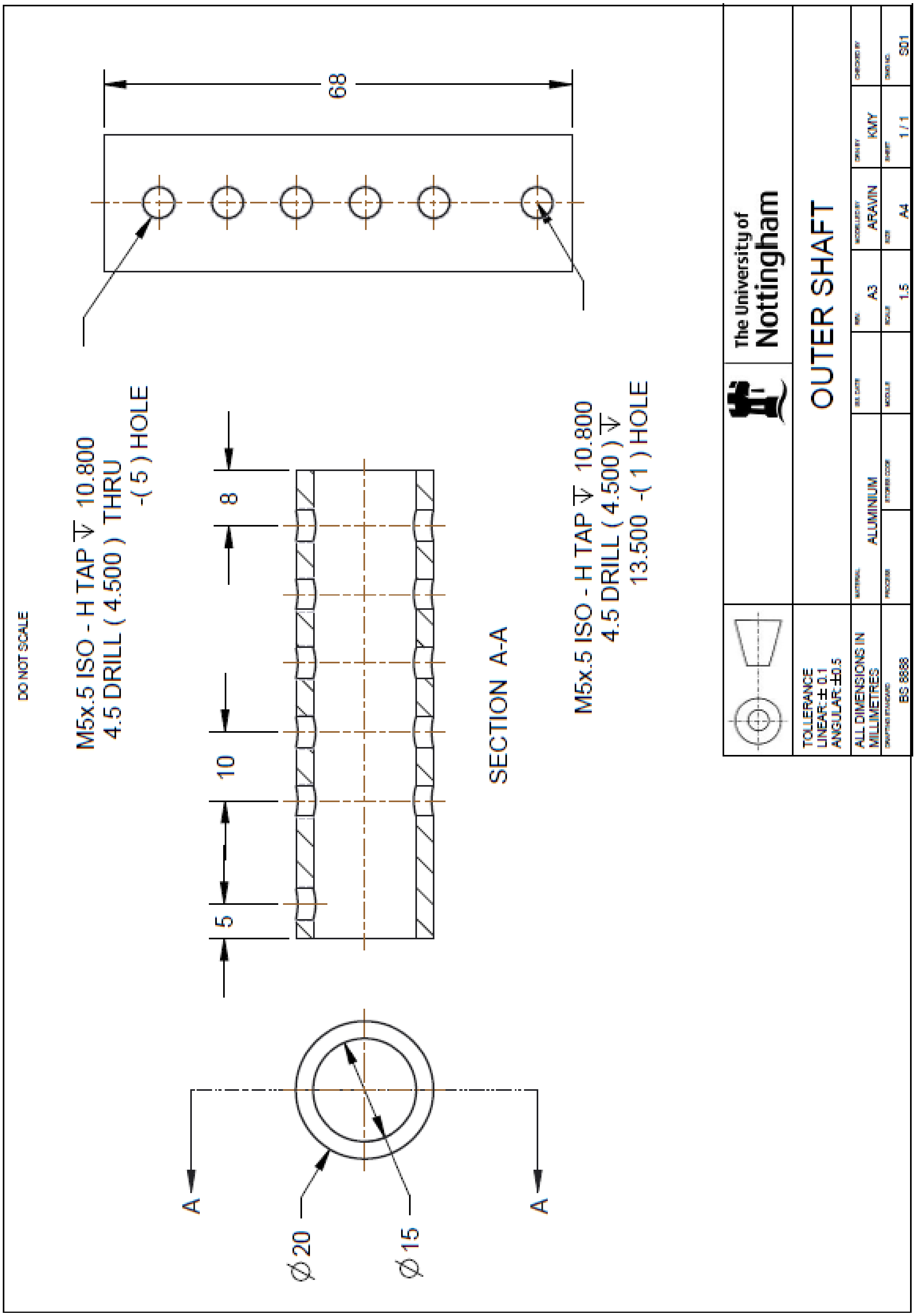
68
M5x.5 ISO - H TAP ⩔ 10.800
4.5 DRILL (4.500) THRU
-(5) HOLE
M5x.5 ISO - H TAP ⩔ 10.800
4.5 DRILL (4.500) ⩔
13.500 -(1) HOLE
DO NOT SCALE
8
10
5
SECTION A-A
A
A
Ø 20
Ø 15
The University of Nottingham
OUTER SHAFT
TOLLERANCE
LINEAR: ± 0.1
ANGULAR: ±0.5
ALL DIMENSIONS IN MILLIMETRES
BS 8888
ALUMINIUM
A3
ARAVIN
KMY
1:5
A4
1 / 1
S01

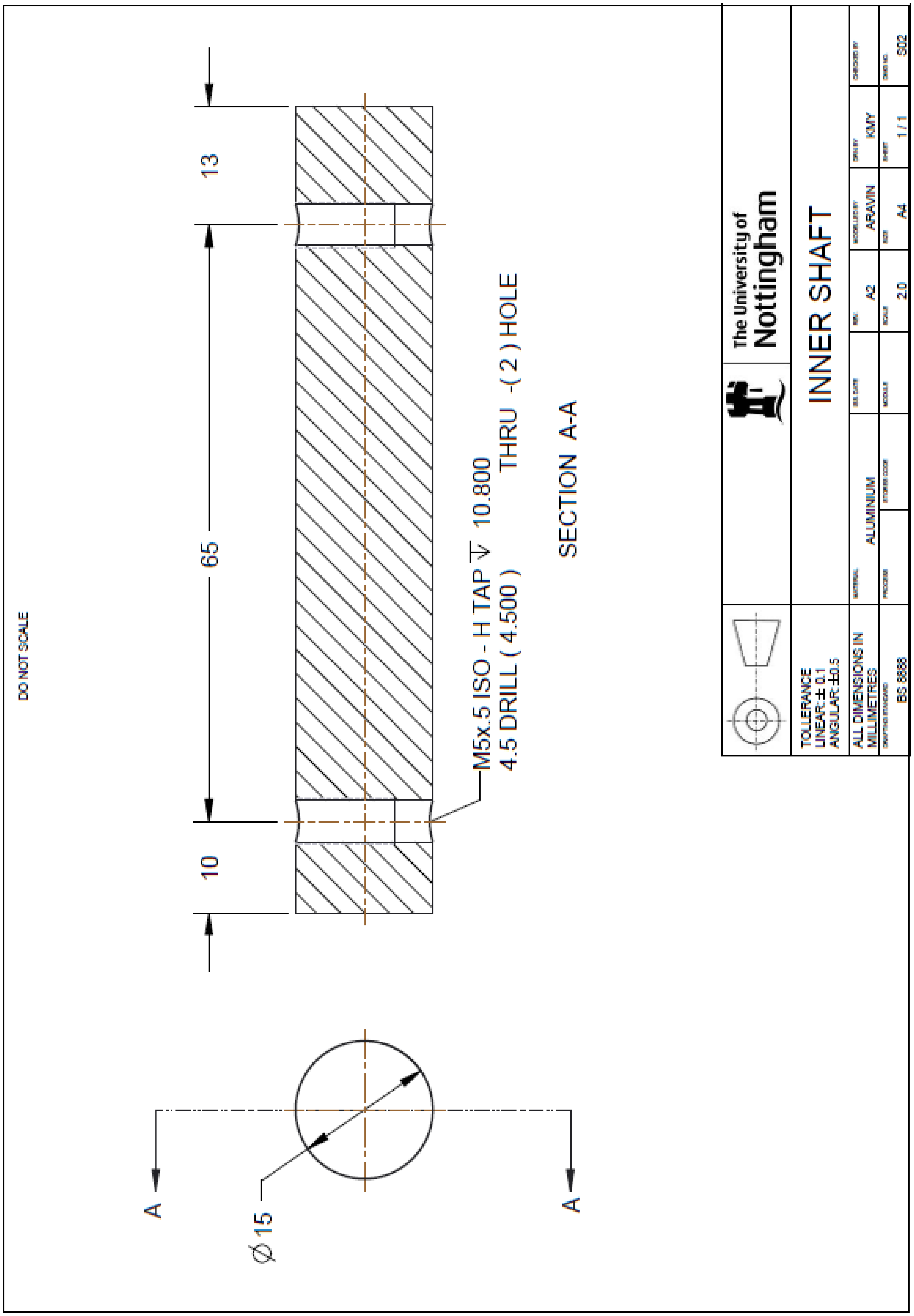
DO NOT SCALE
13
65
10
M5x.5 ISO - H TAP ⊽ 10.800
4.5 DRILL (4.500) THRU -(2) HOLE
SECTION A-A
A
A
Ø 15
The University of Nottingham
INNER SHAFT
TOLLERANCE
LINEAR: ± 0.1
ANGULAR: ±0.5
ALL DIMENSIONS IN MILLIMETRES
BS 8888
ALUMINIUM
A2
ARAVIN
KMY
2.0
A4
1 / 1
S02

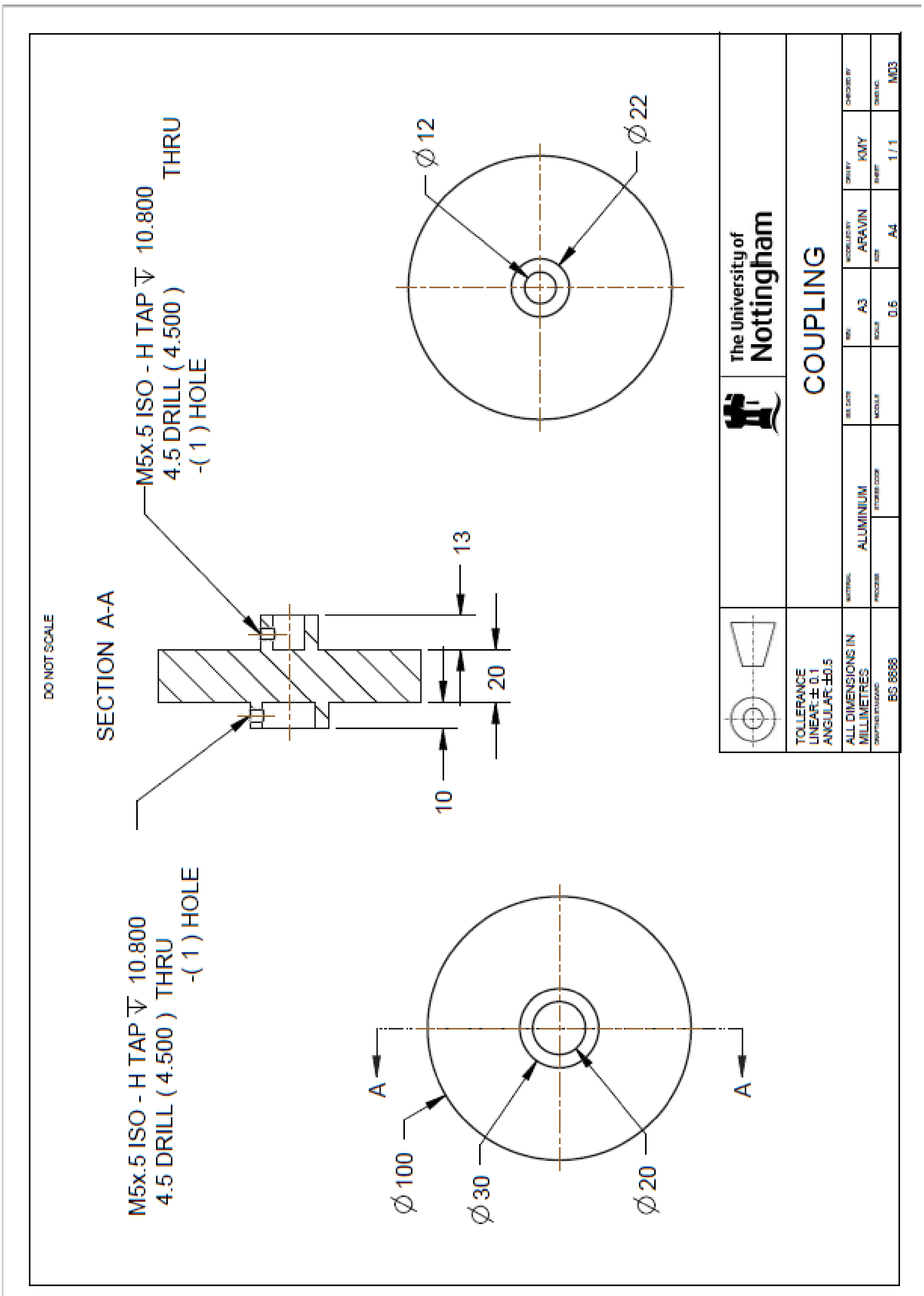

DO NOT SCALE
SECTION A-A
M5x.5 ISO - H TAP ⊽ 10.800
4.5 DRILL (4.500) THRU
-(1) HOLE
M5x.5 ISO - H TAP ⊽ 10.800
4.5 DRILL (4.500)
THRU
-(1) HOLE
13
20
10
⌀12
⌀22
A
A
⌀100
⌀30
⌀20
The University of Nottingham
COUPLING
TOLLERANCE
LINEAR: ± 0.1
ANGULAR: ±0.5
ALL DIMENSIONS IN MILLIMETRES
BS 8888
ALUMINIUM
A3
0.6
ARAVIN
A4
KMY
1 / 1
M03

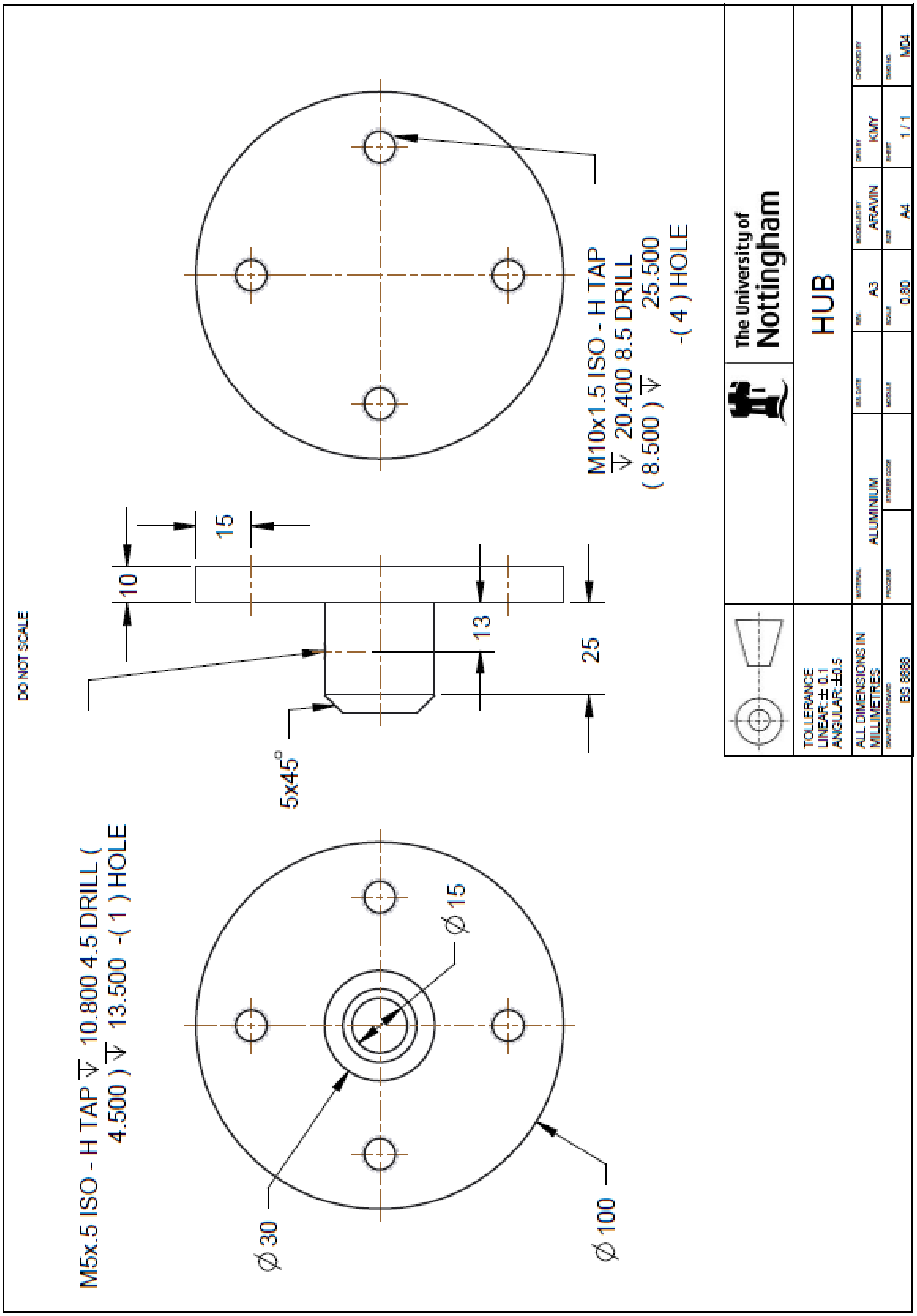
DO NOT SCALE
M5x.5 ISO - H TAP ⩔ 10.800 4.5 DRILL (
4.500) ⩔ 13.500 -(1) HOLE
Ø 30
Ø 100
Ø 15
5x45°
10
15
13
25
M10x1.5 ISO - H TAP
⩔ 20.400 8.5 DRILL
(8.500) ⩔ 25.500
-(4) HOLE
The University of
Nottingham
HUB
TOLLERANCE
LINEAR: ± 0.1
ANGULAR: ±0.5
ALL DIMENSIONS IN
MILLIMETRES
BS 8888
ALUMINIUM
A3
0.80
ARAVIN
A4
KMY
1 / 1
M04

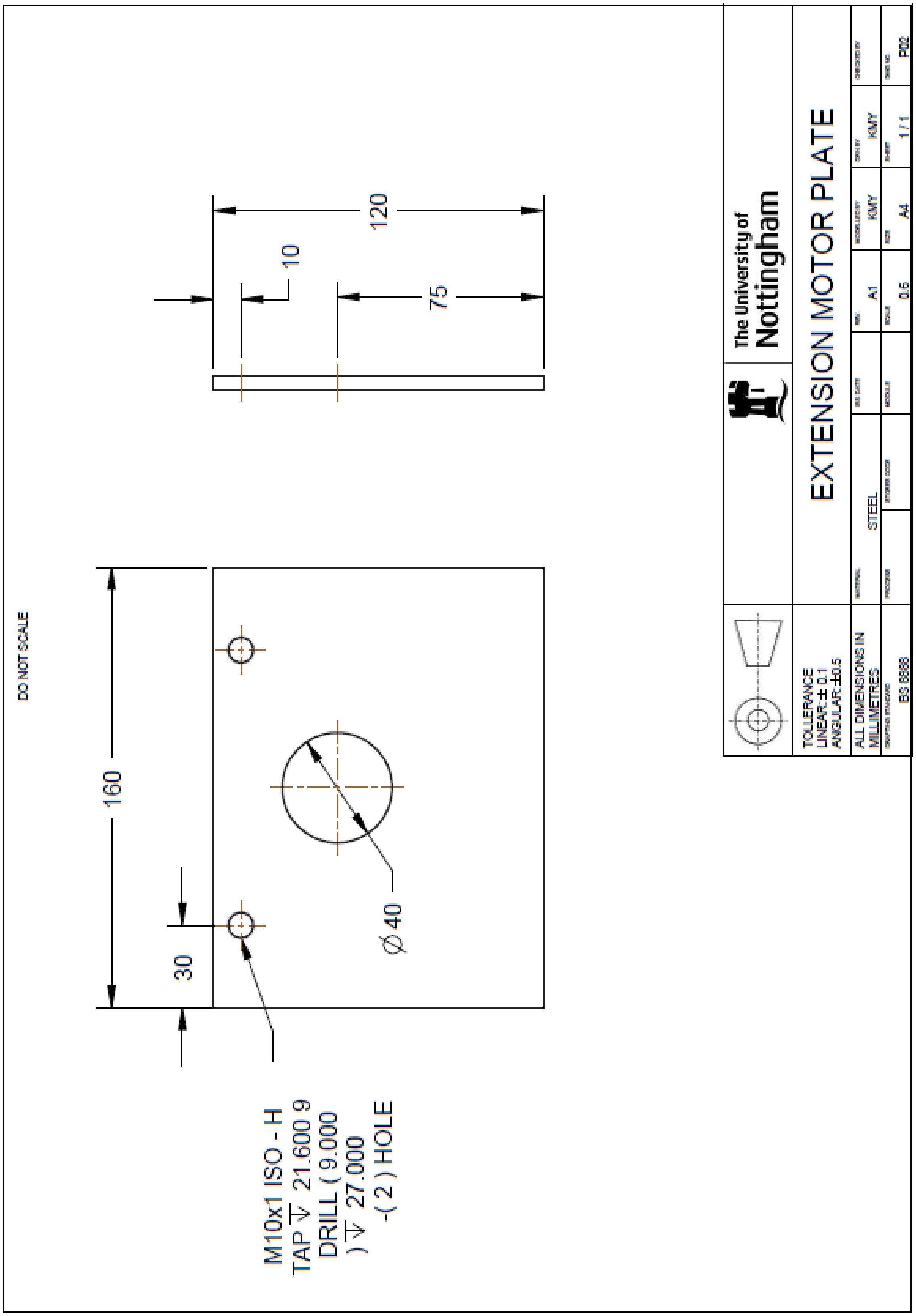
DO NOT SCALE
160
30
Ø 40
M10x1 ISO - H
TAP ↧ 21.600 9
DRILL (9.000
) ↧ 27.000
-(2) HOLE
120
10
75
TOLLERANCE
LINEAR: ± 0.1
ANGULAR: ±0.5
ALL DIMENSIONS IN
MILLIMETRES
BS 8888
STEEL
The University of
Nottingham
EXTENSION MOTOR PLATE
A1
KMY
KMY
0.6
A4
1 / 1
P02

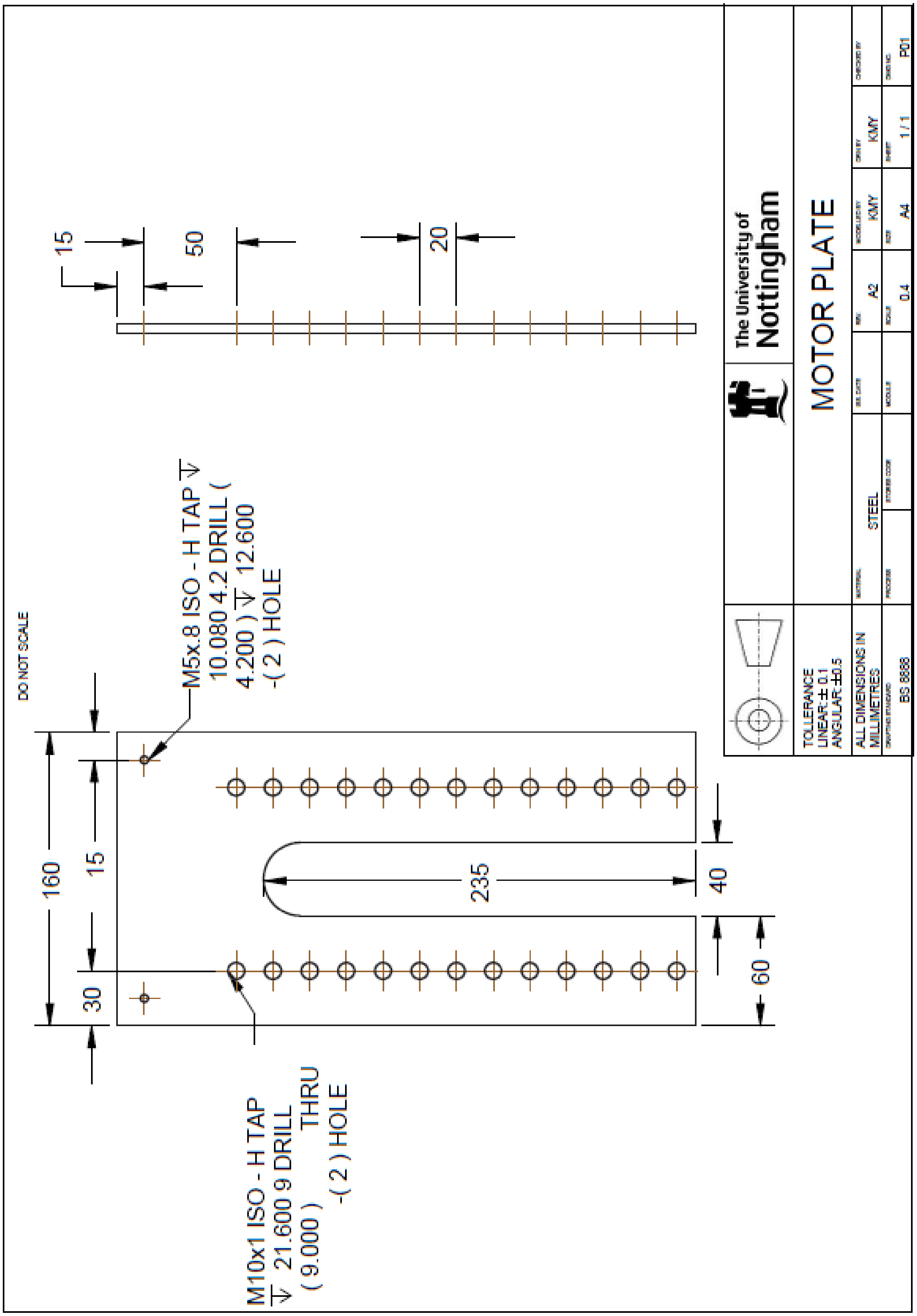
DO NOT SCALE
M5x.8 ISO - H TAP
10.080 4.2 DRILL (
4.200) 12.600
-(2) HOLE
M10x1 ISO - H TAP
21.600 9 DRILL
(9.000) THRU
-(2) HOLE
160
15
30
235
40
60
15
50
20
The University of Nottingham
MOTOR PLATE
TOLLERANCE
LINEAR: ± 0.1
ANGULAR: ±0.5
ALL DIMENSIONS IN MILLIMETRES
BS 8888
STEEL
A2
0.4
KMY
A4
KMY
1 / 1
P01

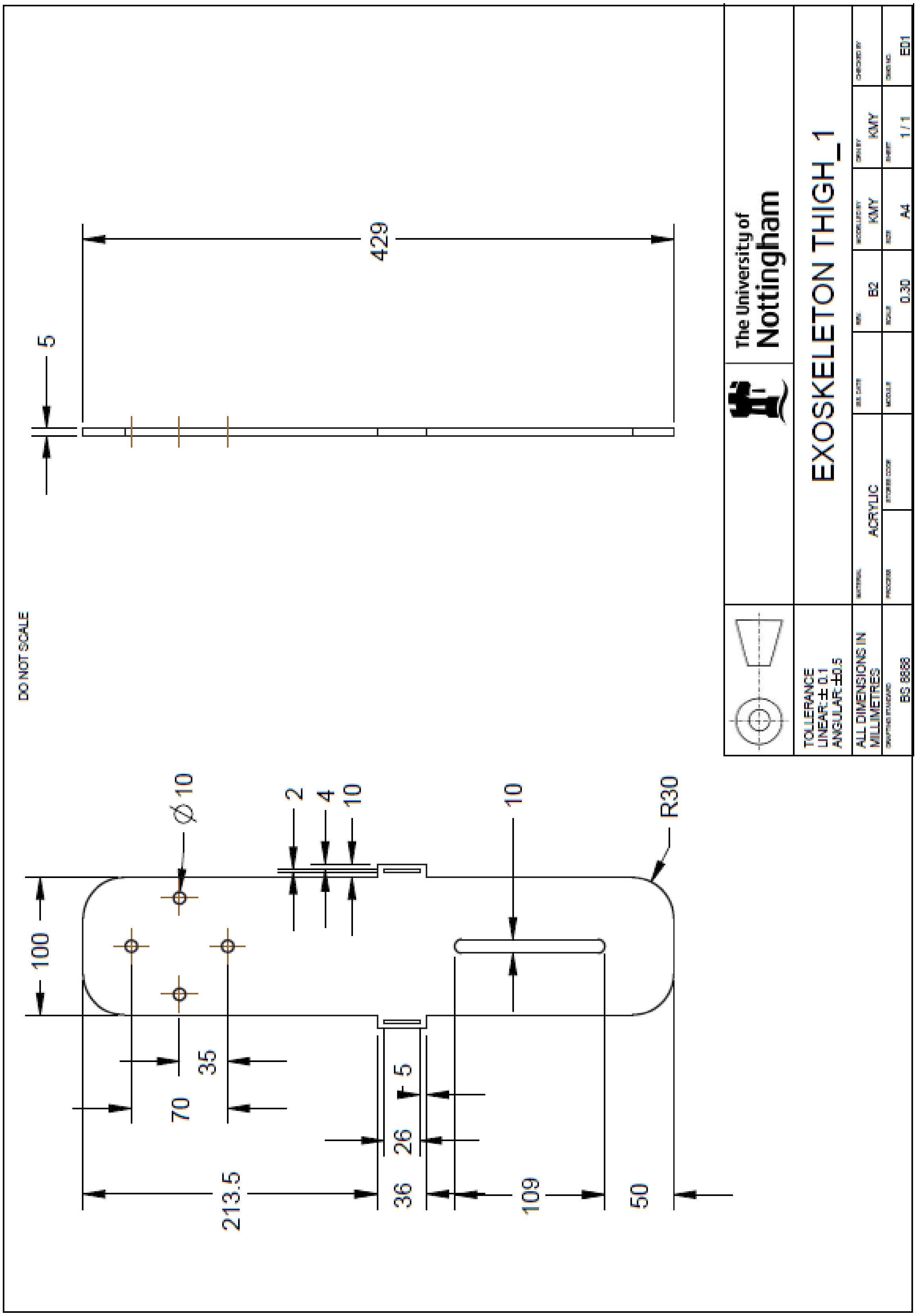
DO NOT SCALE
5
429
100
⌀10
2
4
10
10
R30
35
70
5
26
213.5
36
109
50
The University of Nottingham
EXOSKELETON THIGH_1
TOLLERANCE
LINEAR: ± 0.1
ANGULAR: ±0.5
ALL DIMENSIONS IN
MILLIMETRES
BS 8888
ACRYLIC
B2
KMY
KMY
0.30
A4
1 / 1
E01

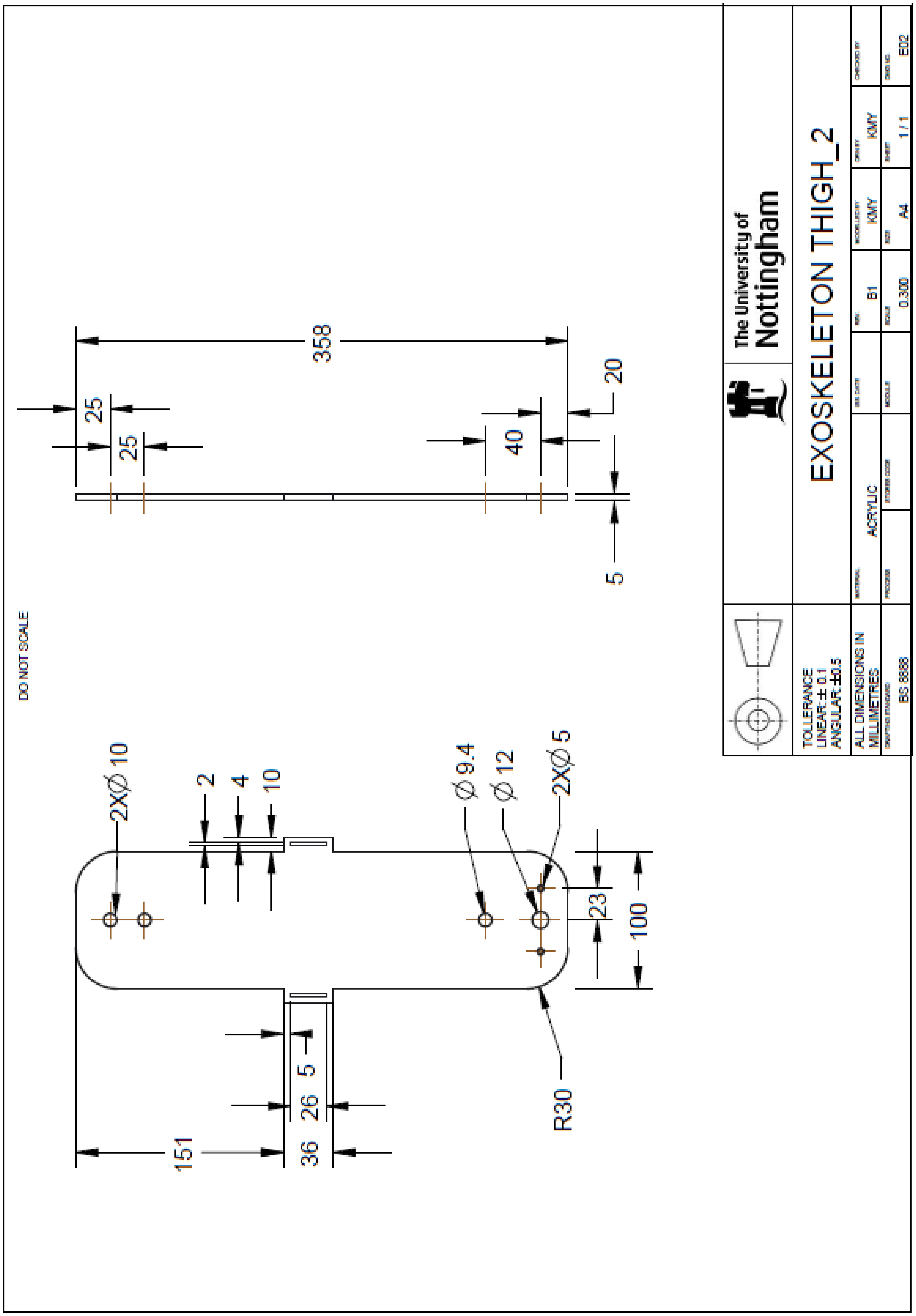
DO NOT SCALE
358
25
25
40
20
5
2X∅10
2
4
10
∅9.4
∅12
2X∅5
23
100
151
36
26
5
R30
The University of Nottingham
EXOSKELETON THIGH_2
TOLLERANCE
LINEAR: ± 0.1
ANGULAR: ±0.5
ALL DIMENSIONS IN MILLIMETRES
BS 8888
ACRYLIC
B1
0.300
KMY
A4
KMY
1 / 1
E02

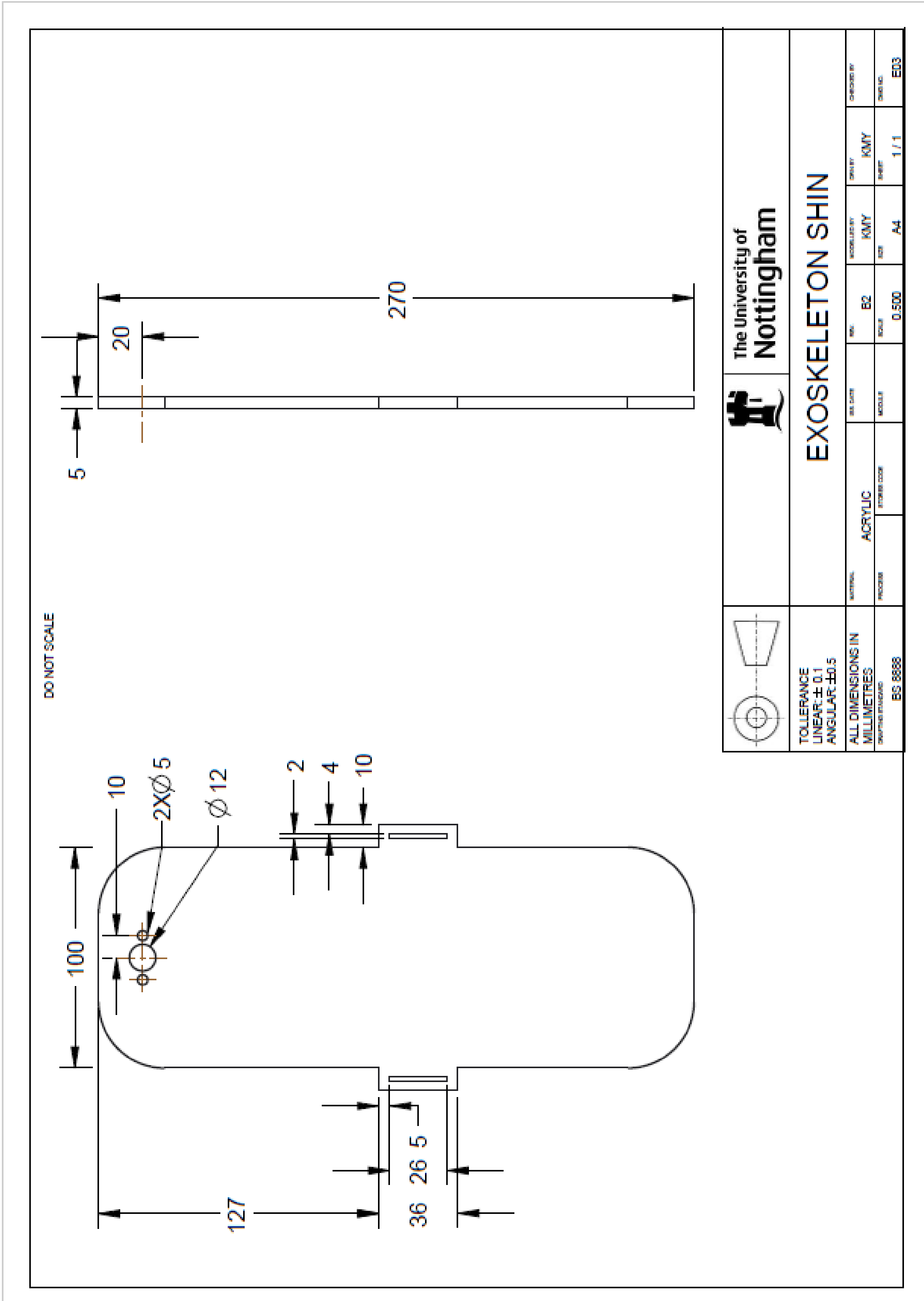

DO NOT SCALE
270
20
5
100
10
2XØ5
Ø12
2
4
10
127
36
26
5
TOLLERANCE
LINEAR: ± 0.1
ANGULAR: ±0.5
ALL DIMENSIONS IN MILLIMETRES
BS 8888
The University of Nottingham
EXOSKELETON SHIN
ACRYLIC
B2
KMY
KMY
0.500
A4
1 / 1
E03

Appendix B

Assembly Drawing

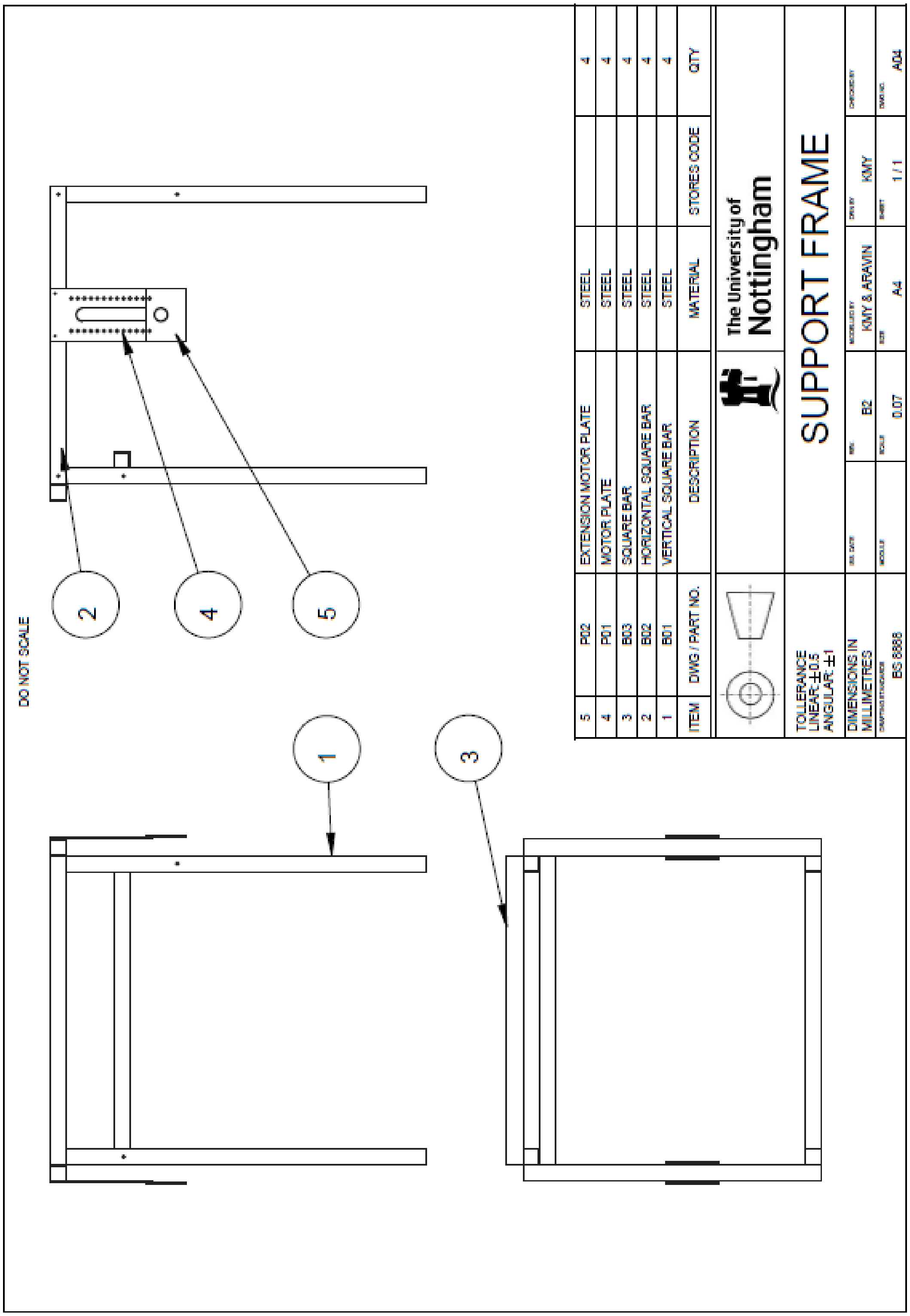

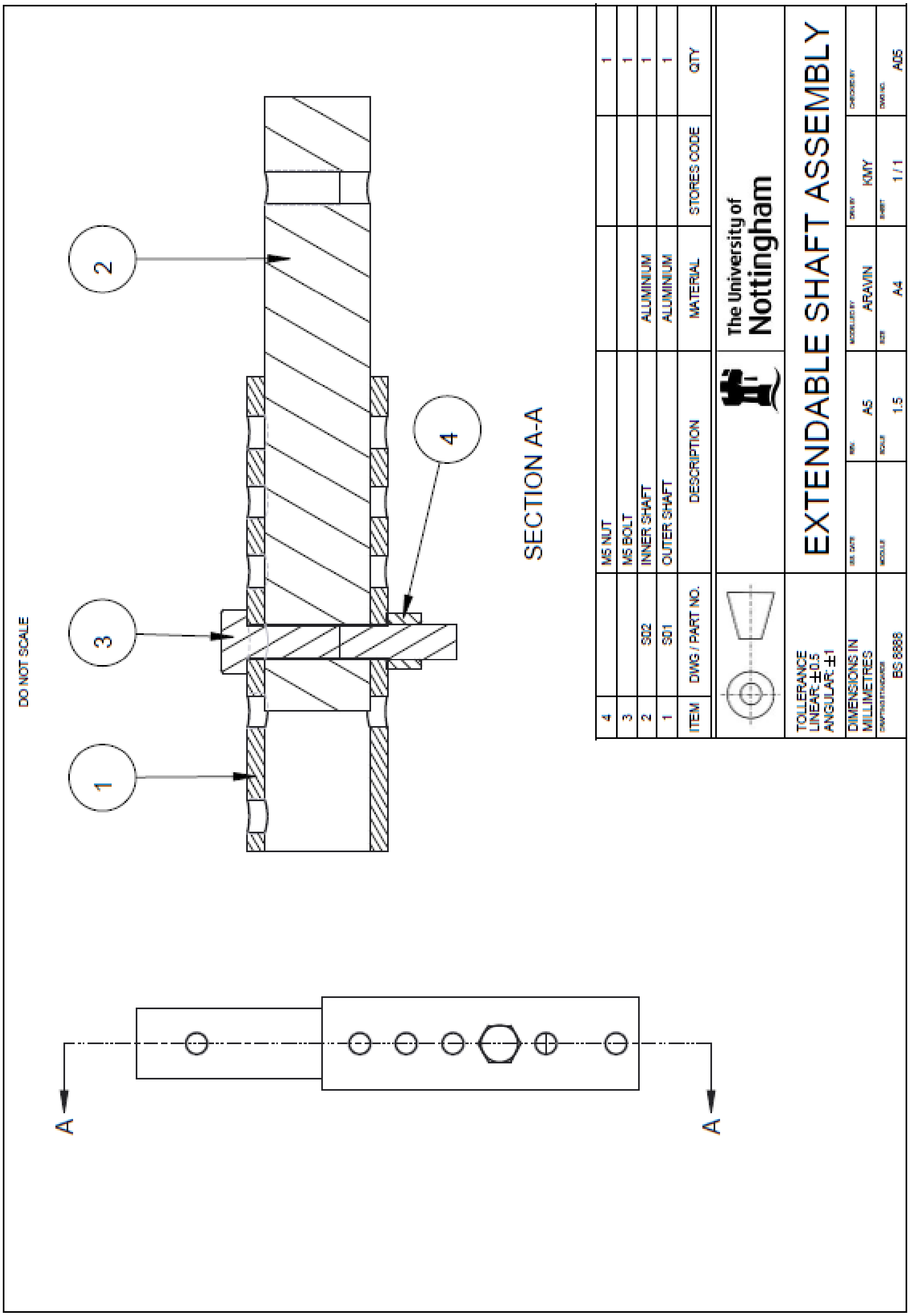
DO NOT SCALE
1
2
3
4
SECTION A-A
A
A
4 M5 NUT 1
3 M5 BOLT 1
2 S02 INNER SHAFT ALUMINIUM 1
1 S01 OUTER SHAFT ALUMINIUM 1
ITEM DWG / PART NO. DESCRIPTION MATERIAL STORES CODE QTY
The University of Nottingham
TOLLERANCE
LINEAR: ±0.5
ANGULAR: ±1
EXTENDABLE SHAFT ASSEMBLY
DIMENSIONS IN MILLIMETRES
A5
ARAVIN
KMY
BS 8888
1:5
A4
1 / 1
A05

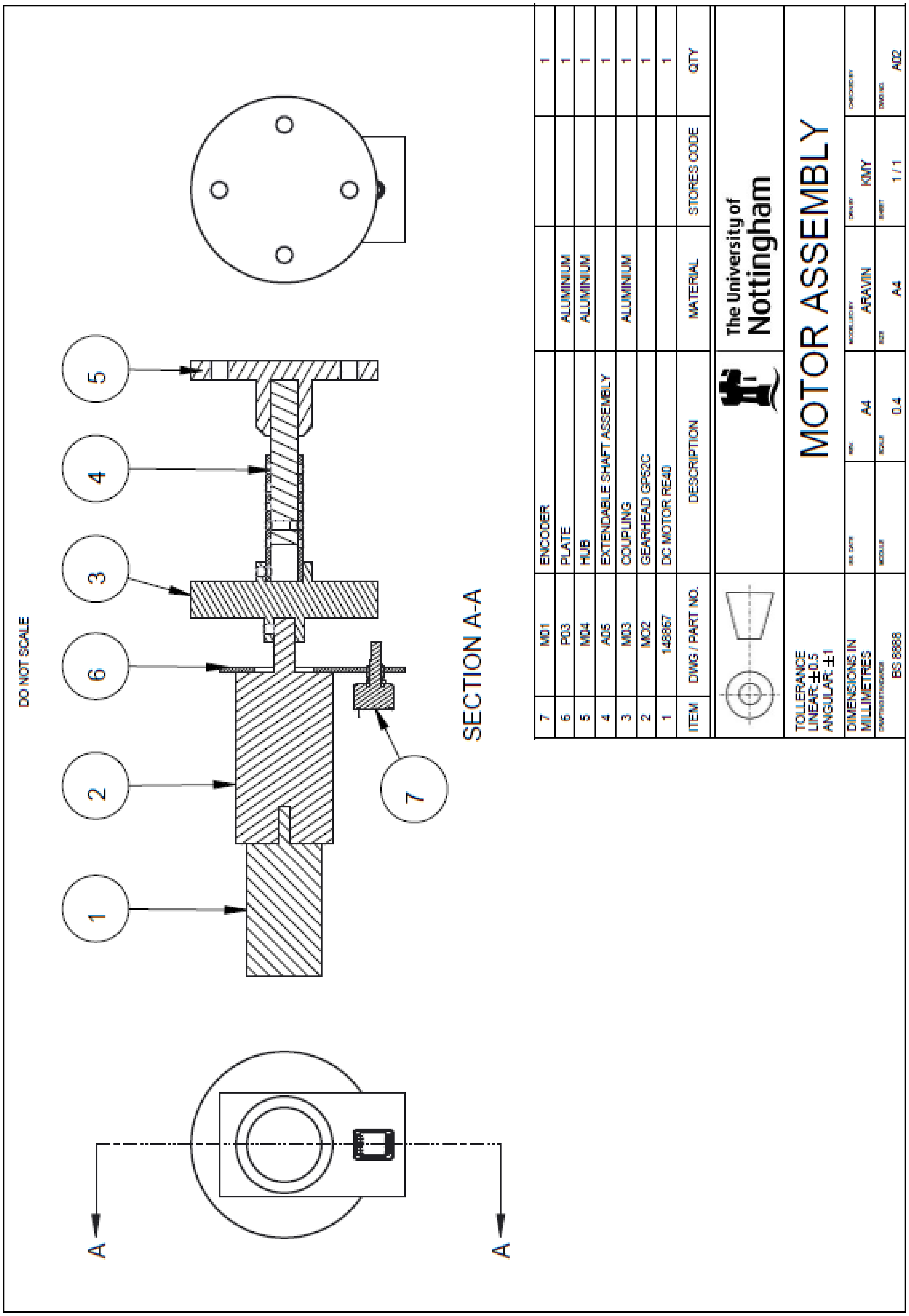
DO NOT SCALE
A
A
1
2
6
3
4
5
7
SECTION A-A
7 M01 ENCODER 1
6 P03 PLATE ALUMINIUM 1
5 M04 HUB ALUMINIUM 1
4 A05 EXTENDABLE SHAFT ASSEMBLY 1
3 M03 COUPLING ALUMINIUM 1
2 MO2 GEARHEAD GP52C 1
1 148867 DC MOTOR RE40 1
ITEM DWG / PART NO. DESCRIPTION MATERIAL STORES CODE QTY
The University of Nottingham
TOLLERANCE
LINEAR: ±0.5
ANGULAR: ±1
MOTOR ASSEMBLY
DIMENSIONS IN MILLIMETRES
A4
ARAVIN
KMY
BS 8888
0.4
A4
1 / 1
A02

DO NOT SCALE

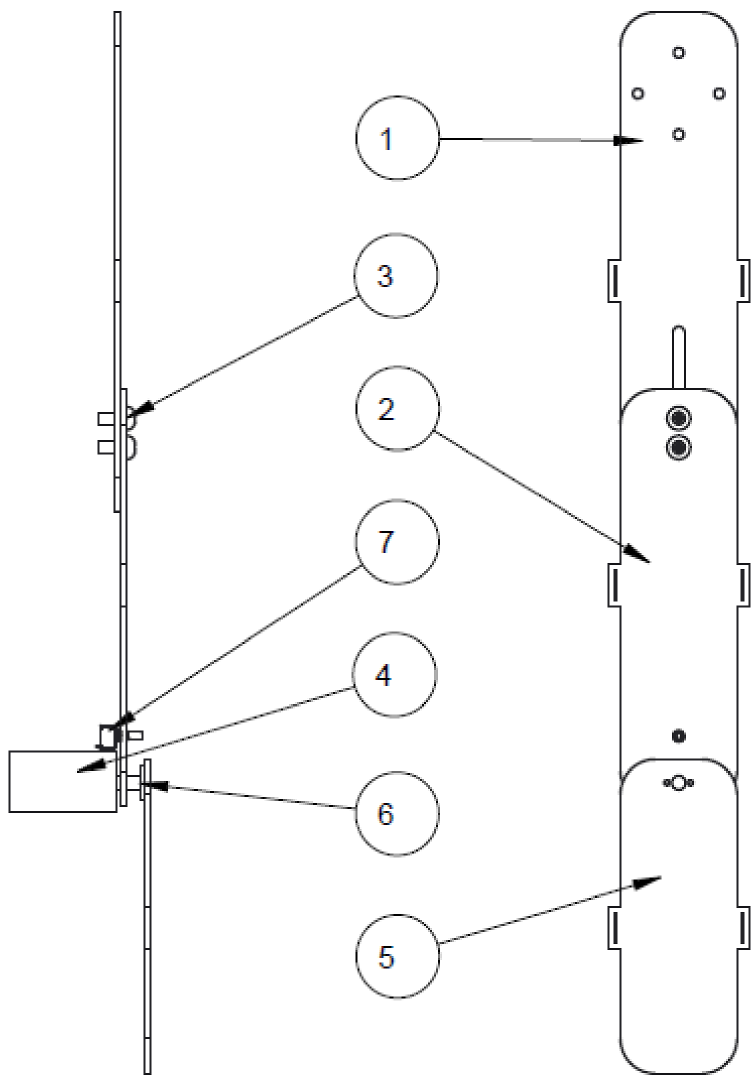

7	M01	ENCODER			1
6	M05	WASHER	ALUMINIUM		1
5	E03	EXOSKELETON SHIN	ACRYLIC		1
4	MO2	GEARHEAD GP52C			1
3	ICRPS0904	PAN HEAD SCREW			2
2	E02	EXOSKELETON THIGH_2	ACRYLIC		1
1	E01	EXOSKELETON THIGH_1	ACRYLIC		1
ITEM	DWG / PART NO.	DESCRIPTION	MATERIAL	STORES CODE	QTY

The University of Nottingham

TOLLERANCE
LINEAR: ±0.5
ANGULAR: ±1

EXOSKELETON ASSEMBLY

DIMENSIONS IN MILLIMETRES	ISS. DATE	REV. B2	MODELLED BY KMY	DRN BY KMY	CHECKED BY
DRAFTING STANDARDS BS 8888	MODULE	SCALE 0.2	SIZE A4	SHEET 1 / 1	DWG NO. A03

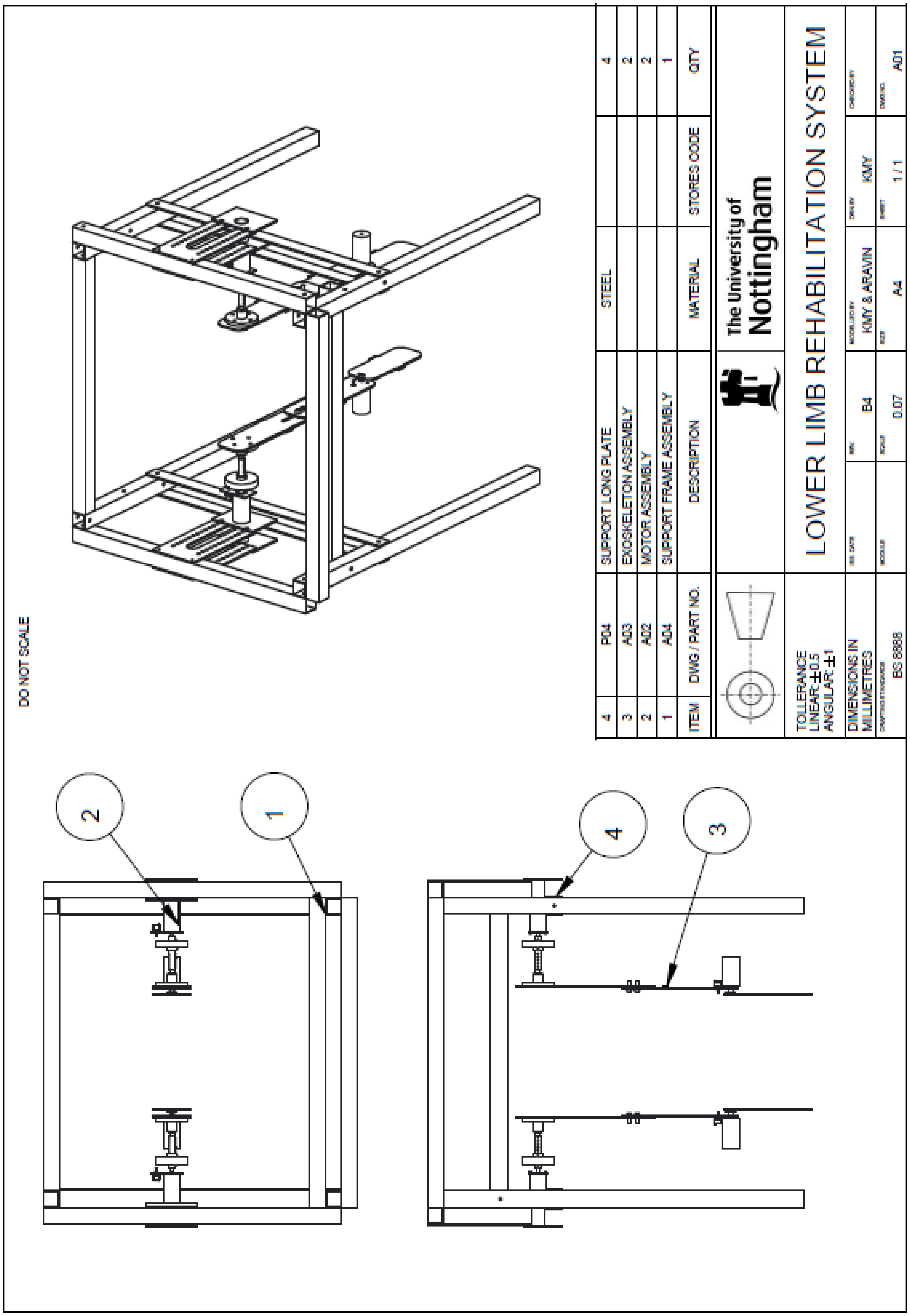
DO NOT SCALE
1
2
3
4
4 P04 SUPPORT LONG PLATE STEEL 4
3 A03 EXOSKELETON ASSEMBLY 2
2 A02 MOTOR ASSEMBLY 2
1 A04 SUPPORT FRAME ASSEMBLY 1
ITEM DWG / PART NO. DESCRIPTION MATERIAL STORES CODE QTY
The University of Nottingham
LOWER LIMB REHABILITATION SYSTEM
TOLLERANCE
LINEAR: ±0.5
ANGULAR: ±1
DIMENSIONS IN MILLIMETRES
BS 8888
B4
0.07
KMY & ARAVIN
A4
KMY
1 / 1
A01

Appendix C

Rehabilitation Circuit Diagram of Robotic Orthosis with Multifunction I/O Device

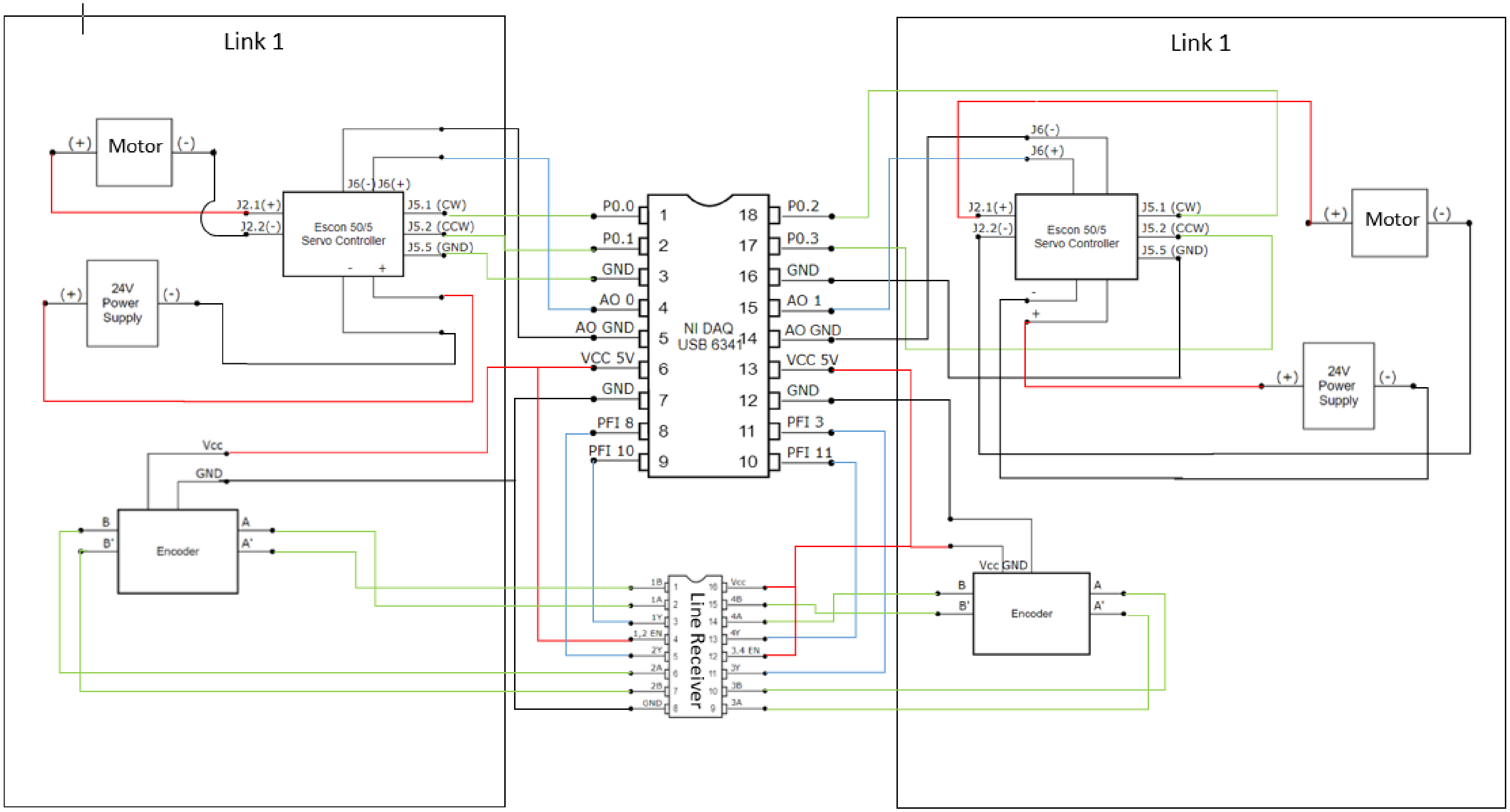

Appendix D

Circuit Diagram of Two-link Manipulator with Arduino Controller

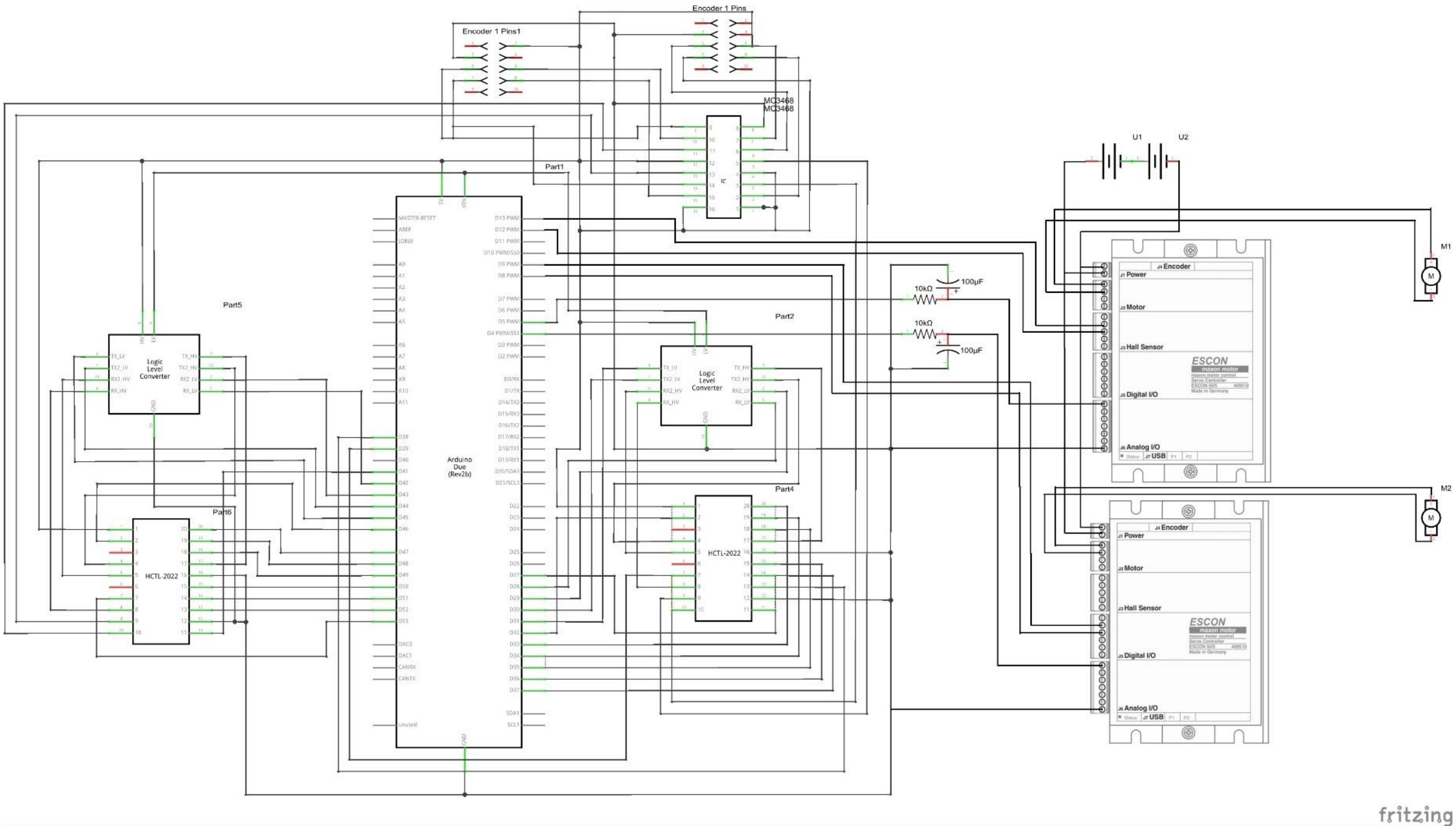

Appendix E

MATLAB Simulation Model of Lower Limb Robotic Orthosis

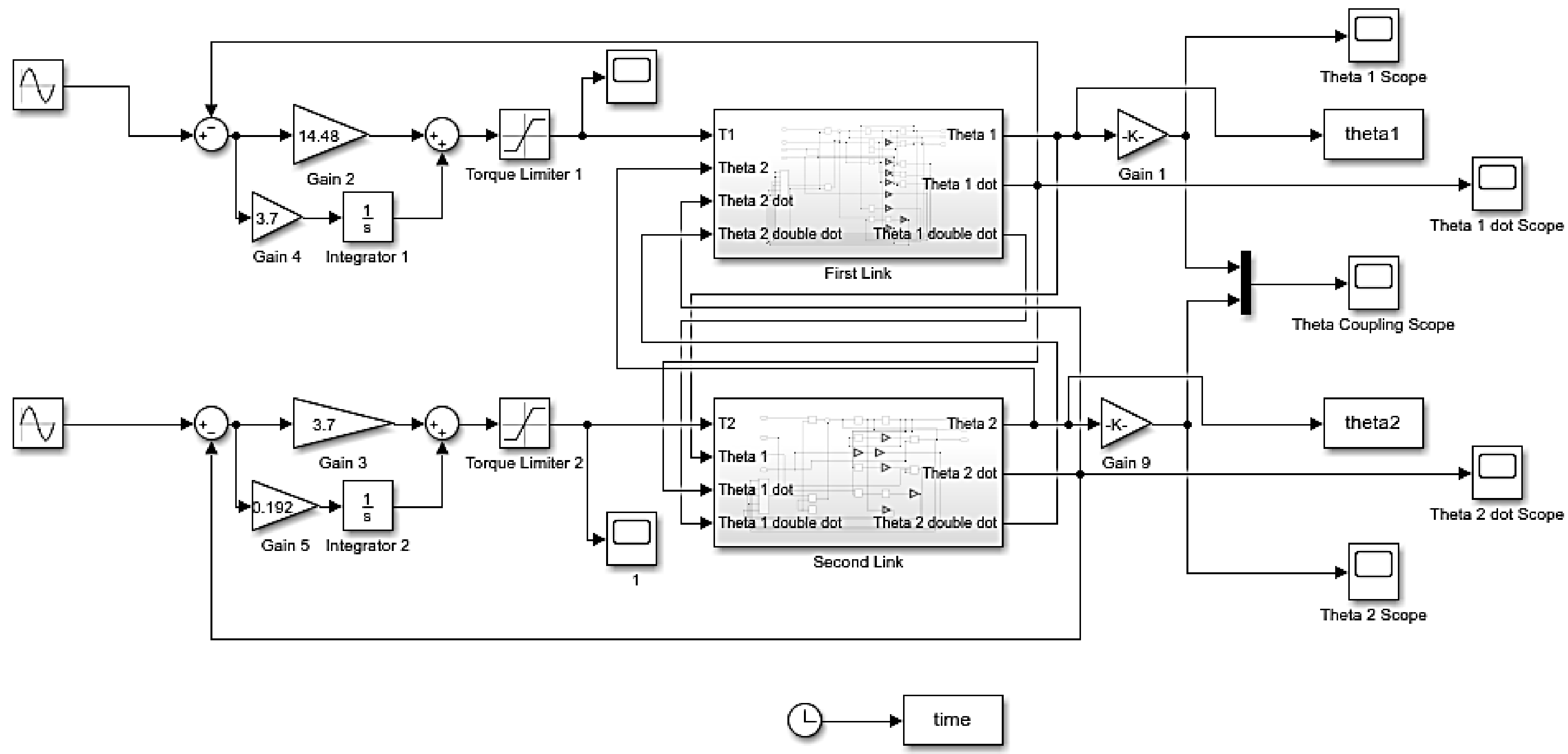

MATLAB SIDF Model of Lower Limb Robotic Orthosis

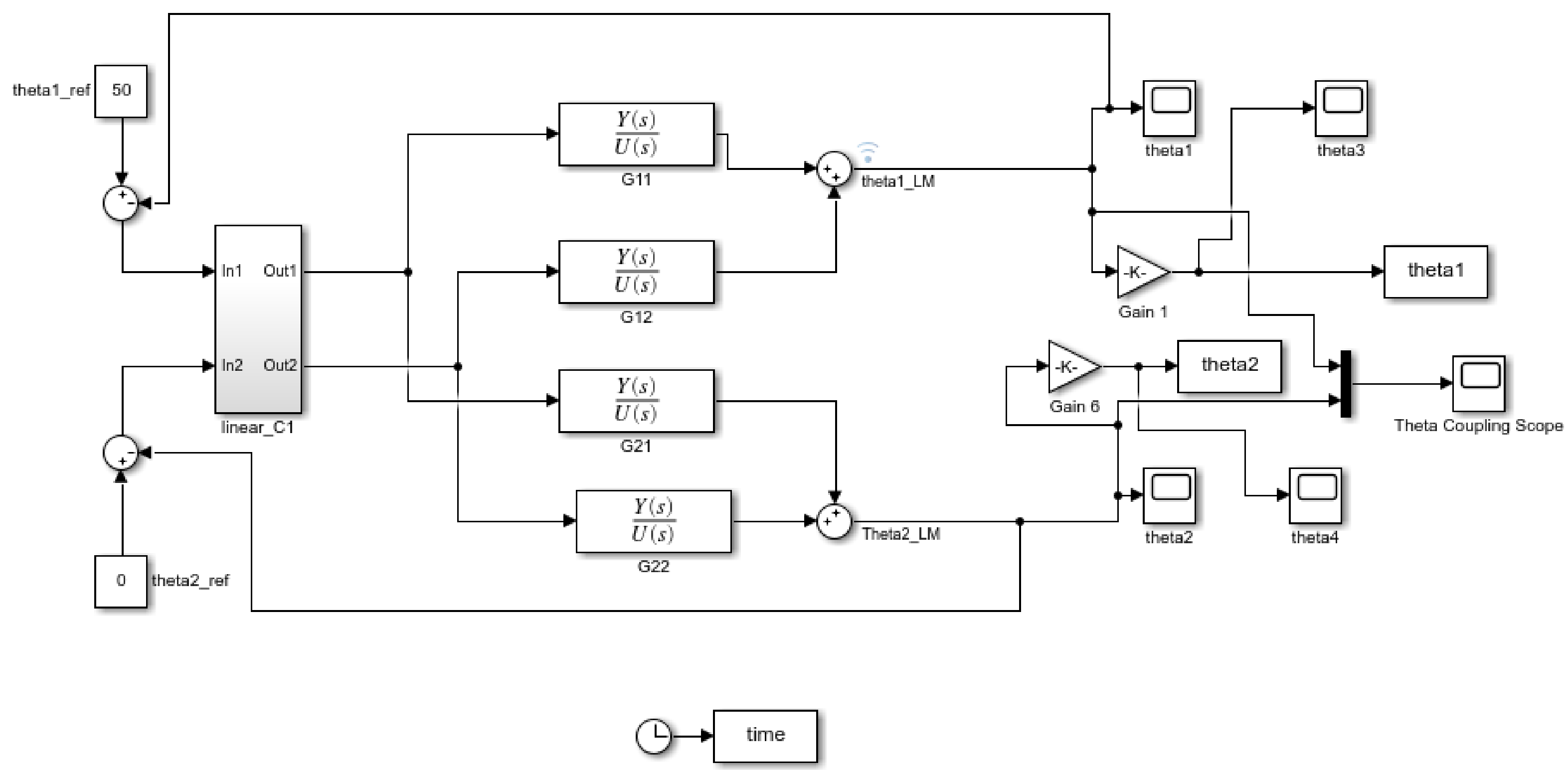

Appendix F

Coding of Lead-Lag Compensator in LABVIEW Interface

```
float32 u1_11, u2_11, y0_11, y1_11, y2_11;
float32 u0_12, u1_12, u2_12, u3_12, u4_12, u5_12, u6_12, y0_12, y1_12, y2_12, y3_12, y4_12, y5_12, y6_12;
float32 u0_21, u1_21, u2_21, u3_21, u4_21, u5_21, y0_21, y1_21, y2_21, y3_21, y4_21, y5_21, y6_21;
float32 u1_22, u2_22, u3_22, u4_22, y0_22, y1_22, y2_22, y3_22, y4_22;
float32 out1, out2;

u0_12 = u0_22;
u0_21 = u0_11;

y0_11 = 1.805* u0_11 - 1.575* u1_11 + 1.194*y1_11 - 0.2778* y2_11 ;
y0_12 = 0.000466*u0_12 + 0.03158*u1_12 - 0.06899*u2_12 + 0.0416*u3_12 - 0.004666*u4_12  +
0.000002409*u5_12 + 1.568*y1_12 - 0.6293*y2_12 +0.0604*y3_12 - 0.000483*y4_12 + 0.0000008515*y5_12 ;
y0_21 = 0.5774*u0_21 - 1.365*u1_21 + 1.037*u2_21 - 0.2497*u3_21 -  0.0000001466*u5_21 + 0.0003814*u4_21 +
1.782*y1_21 -1.037*y2_21+0.2314*y3_21- 0.01601*y4_21 +0.00005718*y5_21 -
0.000000000000000000000009277*y6_21;
y0_22 = 0.002885* u0_22 + 1.306* u1_22 -1.301* u2_22  +1.433*y1_22 -0.434* y2_22;
y0_11 = y0_11*0.3;
y0_12 = y0_12*0.001;
y0_21 = y0_21*0.02;
y0_22 = y0_22*85;

        y2_11 = y1_11;
        y1_11 = y0_11;
        u1_11 = u0_11;

y5_12 = y4_12;
y4_12 = y3_12;
y3_12 = y2_12;
y2_12 = y1_12;
y1_12 = y0_12;
u4_12 = u3_12;
u3_12 = u2_12;
u2_12 = u1_12;
u1_12 = u0_12;

y6_21 = y5_21;
y5_21 = y4_21;
 y4_21 = y3_21;
        y3_21 = y2_21;
        y2_21 = y1_21;
        y1_21 = y0_21;
        u4_21 = u3_21;
        u3_21 = u2_21;
        u2_21 = u1_21;
        u1_21 = u0_21;

        y2_22 = y1_22;
        y1_22 = y0_22;
        u2_22 = u1_22;
        u1_22 = u0_22;

out1 = y0_11 + y0_12;
out2 = y0_21 + y0_22;
```

LABVIEW Window of Experimental Setup with Lead-lag Compensator

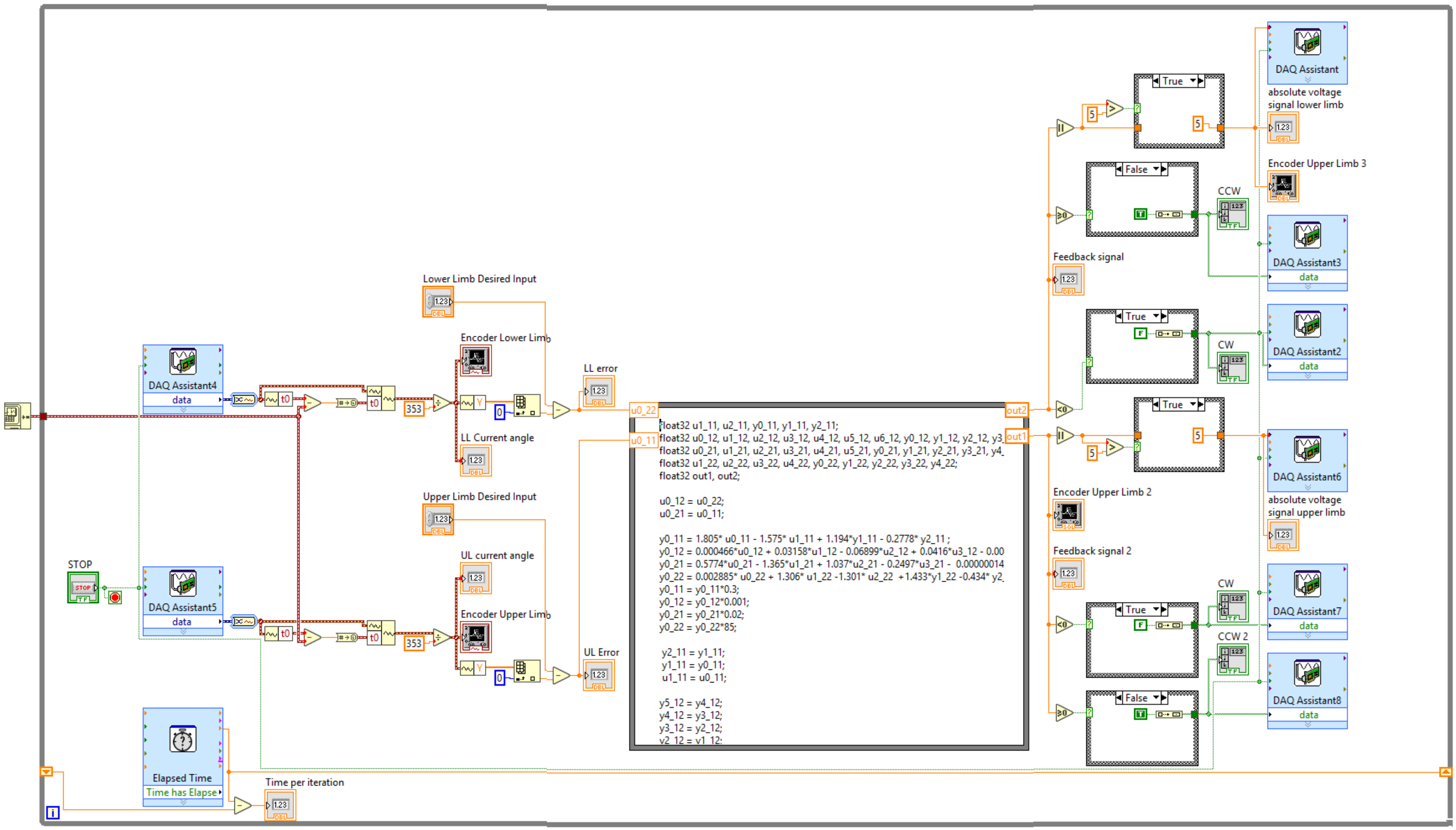

GUI of Experimental Setup with Lead-lag Compensator

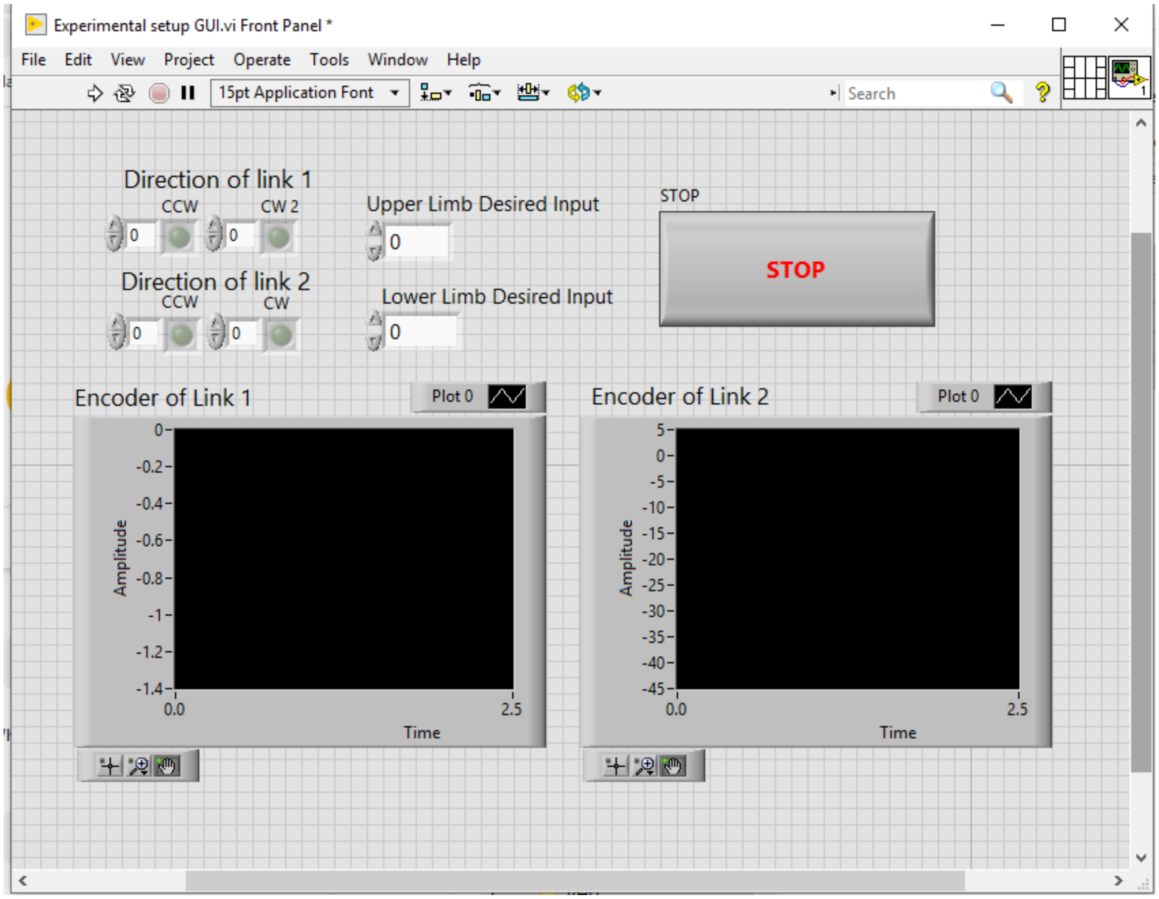

GUI of Step Response Testing in Experimental Setup

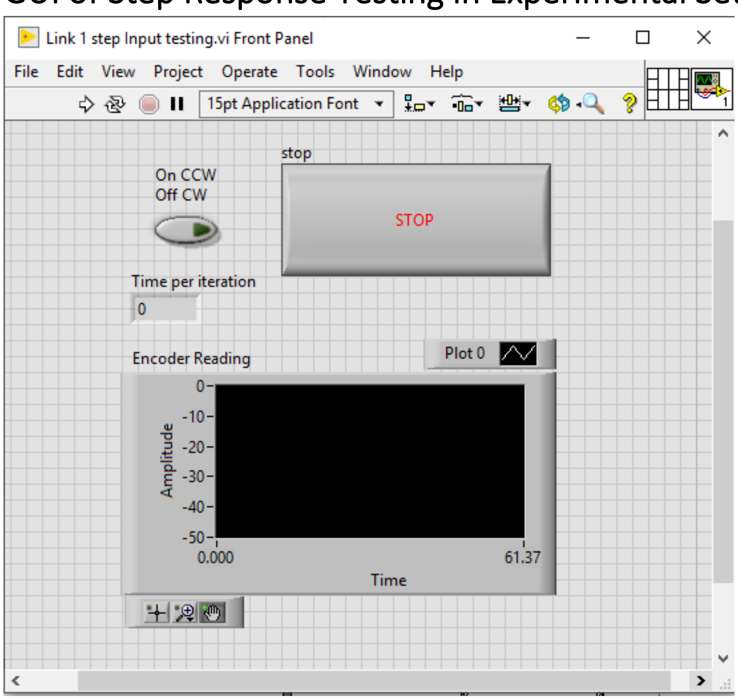

LABVIEW Window of Experimental Setup for Step Response Testing